HYDRODYNAMICS OF GAS SPOUTING AT HIGH TEMPERATURE

by

STANLEY W. M. WU

A THESIS SUBMITTED IN PARTIAL FULFILMENT OF

THE REQUIREMENTS FOR THE DEGREE OF

MASTER OF APPLIED SCIENCE

in

THE FACULTY OF GRADUATE STUDIES

Department of Chemical Engineering

We accept this thesis as conforming

to the required standard

THE UNIVERSITY OF BRITISH COLUMBIA

August 1986

In presenting this thesis in partial fulfilment of the requirements for an advanced degree at the The University of British Columbia, I agree that the Library shall make it freely available for reference and study. I further agree that permission for extensive copying of this thesis for scholarly purposes may be granted by the Head of my Department or by his or her representatives. It is understood that copying or publication of this thesis for financial gain shall not be allowed without my written permission.

Department of Chemical Engineering

The University of British Columbia
2075 Wesbrook Place
Vancouver, Canada
V6T 1W5

Date: August 1986

ABSTRACT

The spouted bed technique was developed for handling solids which were too coarse to fluidize well. In its early stages, it was primarily used for drying wheat. It was later found that spouting has potential application in high temperature operations such as coal combustion and gasification. However, literature review will show that there are very few reports on the hydrodynamics of spouted beds at high temperature and/or pressure. Most existing correlations or expressions are based upon experiments done at room conditions; they have not been tested with data from higher temperatures.

The goal of this study was to obtain experimental data at high temperatures, to examine the validity of existing equations and to modify the latter where appropriate. Spouting of sand particles (Ottawa sand) with preheated air, ranging from 20 to 420 °C, was conducted in a 156 mm stainless steel half-column, equipped with a glass panel. The transparent surface allowed one to measure spout diameter, fountain height, annulus height and other important parameters which otherwise are difficult to obtain in a full stainless steel column. In addition to air, helium and methane, at room conditions, were also used as spouting gases. With these two gases, it became possible to investigate the effect of changing gas density at constant

gas viscosity and the effect of changing gas viscosity at constant gas density.

The main experimental measurements were of minimum spouting velocities, spout diameters, maximum spoutable heights and bed pressure drops. For selected runs, additional measurements, such as of flow regime maps, particle circulation rates, radial and longitudinal pressure profiles, fountain heights and annular fluid velocities, were also obtained.

In general, it was found that the range of stable spouting decreased with decreasing gas density and increasing gas viscosity, hence with increasing air temperature. Some of the existing equations were found to be inadequate. The Mathur and Gishler (1955) equation was unsatisfactory when tested against the experimental values of U_{ms}. The expression of Epstein and Levine (1978) gave good prediction of the overall bed pressure drop for room conditions but overestimated the effect of temperature. The McNab (1972) equation for estimating spout diameter worked reasonably well for air spouting at room temperature but it underpredicted at higher temperatures. These equations were empirically modified to fit the new data obtained.

Table of Contents

LIST OF TABLES

LIST OF FIGURES

ACKNOWLEDGMENTS

I would like to express my appreciation to Dr. N. Epstein and Dr. J. Lim. Under their supervision, this research work was conducted. In addition, I am grateful to the Natural Sciences and Engineering Research Council for its financial support.

Finally, I would like to thank the staffs of the Chemical Engineering Department workshop and stores for their continuing assistance throughout this work.

1. INTRODUCTION

Many industrial processes require good contacting between fluid and solids to achieve optimum performance. Fluidization has been considered as one of the better techniques for this purpose. However, its application has been limited to relatively fine particulate solids in the case of gas-solid systems. For coarser materials, typically those with particle diameter greater than 1 mm, gas fluidization often gives rise to the formation of large bubbles and a tendency towards slugging which is undesirable. It was this limitation which led to the discovery and development of the spouted bed technique (Mathur and Gishler, 1955). The flow mechanisms of spouting are quite different from those of fluidization. However, the spouted bed technique appears to provide the same result for coarse particles as fluidization does for fine materials.

Figure 1.1 shows schematically a typical spouted bed in a cylindrical column with a conical base. The bed can be characterized by two distinct zones, the spout and the annulus. Under normal conditions of spouting, a fluid, usually a gas, enters vertically through an orifice opening at the bottom of the column. The resulting jet causes a stream of particles to move upwards rapidly through a central core. This diluted core is called the spout. The particles in the spout, after reaching to a height above the

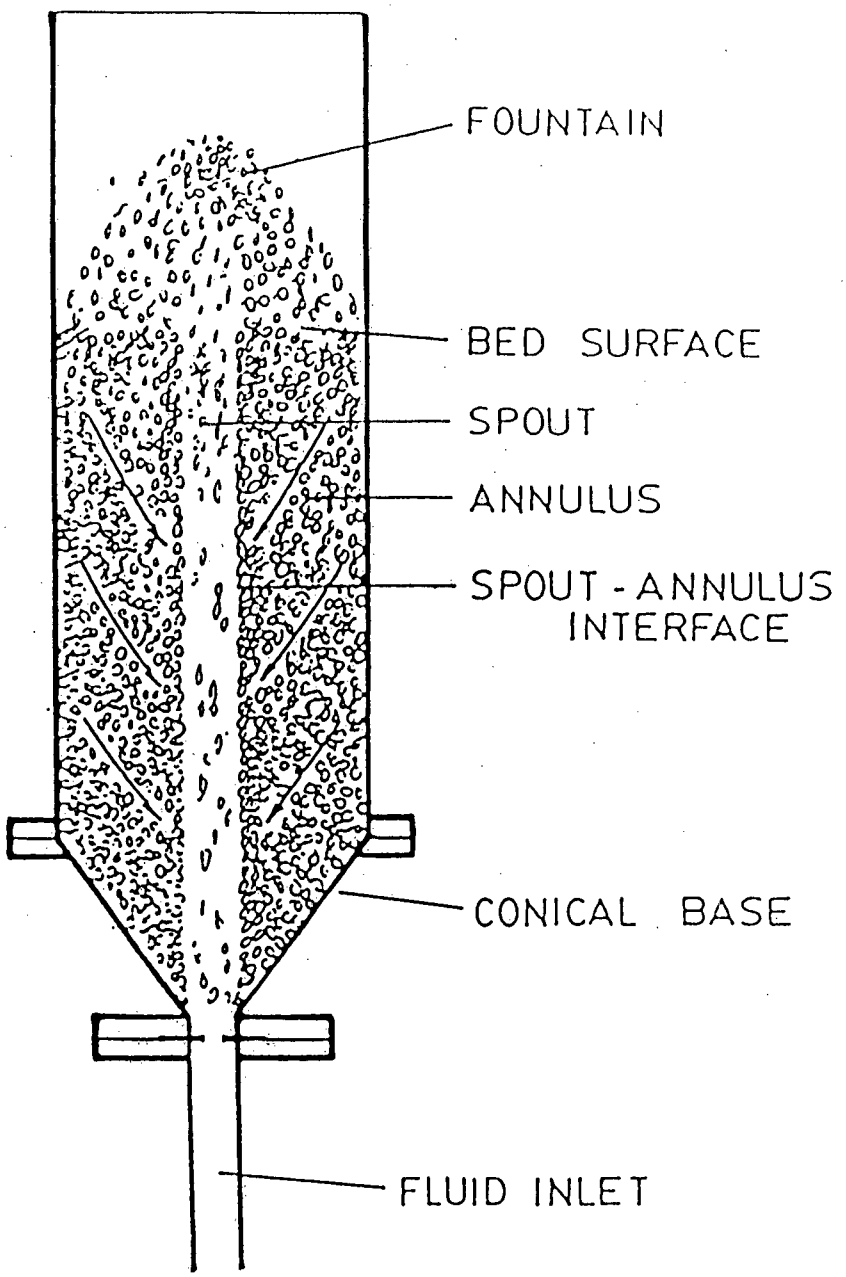

Figure 1.1 Schematic diagram of a spouted bed

bed surface, fall back as a fountain onto the surrounding packed bed, or the annulus, where they are transported downwards by gravity and, to some extent, radially inwards as a loosely packed bed. These particles are re-entrained into the spout through the spout wall over the entire bed height. The fluid from the spout seeps through these annular solids as it travels upwards. This systematic movement of the fluid and solids leads to effective contact between them.

Spouted beds exhibit some advantages (Bridgwater, 1982; Lim et al., 1984) over conventional fluidized beds. They have been used for various physical and chemical processes. Recently, high temperature spouting has attracted some attention because of its potential in the energy field. Successful operations include carbonization of caking coal (Barton et al., 1968, 1969; Ratcliffe and Rigby, 1969), gasification, pyrolysis and combustion of caking coal (Foong, et al., 1980, 1981; Jarallah and Watkinson, 1985; Lim et al., 1984) and combustion of low heating value fuels and wastes (Arbib et al., 1981; Arbib and Levy, 1982; Khoshnoodi and Weinberg, 1978). While the spouted bed technique has shown some future in these applications, there are still some questions to be answered.

One area which is still poorly understood is the hydrodynamic behaviour of spouted beds at high temperature.

A review of the published literature will indicate that most hydrodynamic information on gas spouting is for ambient conditions. The effect of temperature (as well as pressure) has not been well established. One other area of uncertainty is the heat transfer.

Although the effect of pressure and heat transfer are also important, the main concern of this work will be the effect of temperature. The primary objectives are to collect hydrodynamic data at high temperature and to test them against existing equations and correlations. It is important to point out here that many correlations have been obtained under ambient conditions and limited ranges of the relevant variables. Perhaps, by including the results from this work, more applicable equations can be developed from existing ones.

The dependent hydrodynamic parameters of interest are: regime maps, minimum spouting velocity, maximum spoutable bed height, spout shape and diameter, overall bed pressure drop, fountain height, fluid and particle velocities in the annulus, longitudinal and radial pressure profiles.

2. LITERATURE REVIEW

Gas spouting at ambient conditions has been well studied in most aspects. Many equations are available for predicting hydrodynamic parameters at room conditions. Mathur and Epstein (1974) and later Epstein and Grace (1984) have outlined some of these equations.

Information on high temperature spouting is somewhat scarce; there are only a few published articles. The emphasis of these articles has been mainly on performance characteristics, reaction kinetics (Ray and Sarkar, 1976; Ingle and Sarkar, 1976) and flow regimes (Khoe et al., 1983). The hydrodynamics have not been studied. Equations originally developed for room conditions are often used for high temperatures, with the assumption that these equations will give reasonable predictions if one uses values of gas physical properties appropriate to the actual operating conditions.

Since no equations have yet been proposed specifically for gas spouting at high temperature, the present review is confined to existing equations developed at room conditions, particularly the ones which contain gas properties as variables.

2.1 SPOUTABILITY OF PARTICLES

Applications of spouting have been limited to coarse particles (d_p > 1 mm). However, spouting of finer particles has also been reported. Chandnani (1984) gave a review of these published articles. He also conducted experiments in a 152-mm diameter, transparent conical-cylindrical half-column with particles ranging in size from 90 to 1000 μm and in density from 900 to 8900 kg/m^3. His findings lead to the conclusion that fine particles (d_p < 1 mm) can be spouted steadily if the fluid inlet diameter (orifice diameter) does not exceed 25.4 times the particle diameter. Observations by Mathur and Gishler (1955) and Ghosh (1965) also support his claim. Moreover, he has found that particle density has a negligible effect on spoutability. These results are all based on experiments with air at room temperature and atmospheric pressure.

2.2 MINIMUM SPOUTING VELOCITY

Figure 2.1 shows a typical pressure drop versus superficial velocity curve for spouting of coarse particles. The minimum (superficial) spouting velocity U_{ms} is represented by point B. This is obtained by first increasing the fluid flowrate until point C is reached. At this instant, the entire bed becomes mobile and steady spouting sets in. However, this point is bed-history dependent and is

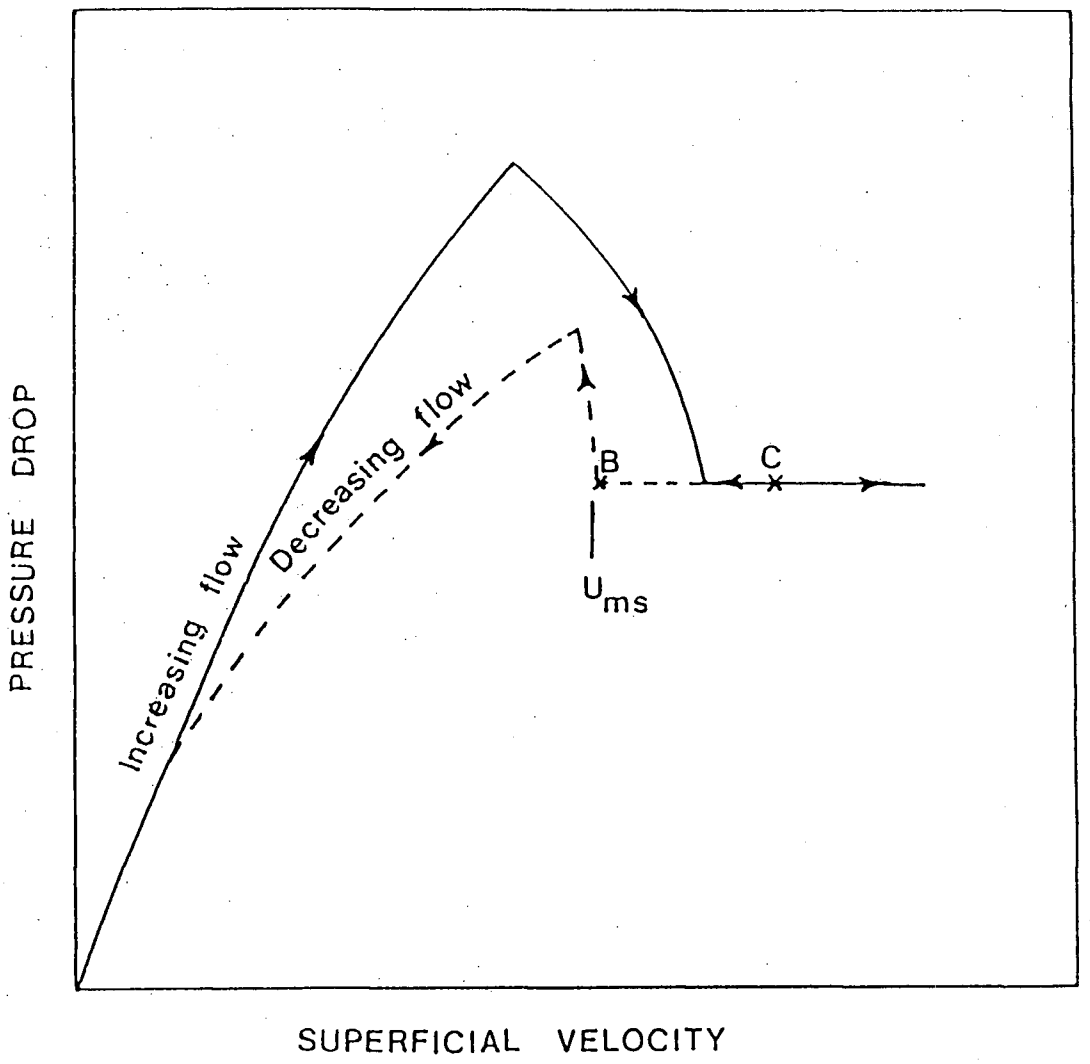

Figure 2.1 Typical pressure drop versus velocity curve for a spouted bed of coarse particles

not exactly reproducible. From point C, flowrate is decreased slowly till point B, at which further decrease of flowrate will cause the spout to collapse and the bed pressure to increase suddenly, as illustrated in this figure. For coarse particle spouting, it has been found that at this latter point (i.e., point B), the velocity is reproducible and hence taken as the minimum spouting velocity.

A number of correlations have been proposed for predicting this quantity, U_{ms} (Mathur and Epstein, 1974). The most widely used one seems to be the empirical equation of Mathur and Gishler (1955), which was derived from data for both gas- and liquid-spouted beds with diameters up to 0.6 m.

$$U_{ms} = \left[\frac{d_p}{D_c}\right]\left[\frac{D_i}{D_c}\right]^{1/3}\sqrt{\frac{2gH(\rho_p-\rho_f)}{\rho_f}} \qquad 2.1$$

The form of the above equation was developed using dimensional analysis; the value of the coefficient = 1 empirically.

A somewhat similar expression with a different value of the coefficient was derived by Ghosh (1965). The derivation was based on a momentum exchange between the entering fluid and the entrained particles.

$$U_{ms} = \sqrt{\frac{2\eta}{3\kappa}}\left[\frac{d_p}{D_c}\right]\left[\frac{D_i}{D_c}\right]\sqrt{\frac{2gH(\rho_p-\rho_f)}{\rho_f}} \qquad 2.2$$

Grbavcic et al. (1976), based on their flow model, derived the following correlation for U_{ms}:

$$\frac{\frac{U_{ms}}{U_{mf}} - a_s}{1 - a_s} = 1 - \left[1 - \frac{H}{H_m}\right]^3 \qquad 2.3$$

where a_s is defined as the ratio of the area of the spout to that of the bed. Since a_s is much smaller than 1 in most cases, Equation 2.3 can be further simplified to

$$U_{ms} = U_{mf}\left[1 - \left[1 - \frac{H}{H_m}\right]^3\right] \qquad 2.4$$

2.3 MAXIMUM SPOUTABLE BED HEIGHT

The maximum spoutable bed height, H_m, is the maximum height at which steady or stable spouting can be obtained. Mathur and Epstein (1974) suggested three distinct possible mechanisms for spout termination when the bed height exceeds H_m. They are:

1. Fluidization of Annular Solids
2. Choking of the Spout
3. Growth of Instability at the Spout-Annulus Interface

Most correlations for predicting H_m are based on the first mechanism or simply on empiricism.

The maximum value of the minimum spouting velocity is denoted U_m, i.e., the minimum spouting velocity at the maximum spoutable height. Grbavcic et al. reported that U_m

was very similar to U_{mf}. Although these quantities are approximately equal, there is some disagreement regarding the exact relationship between U_m and U_{mf}. In general,

$$\frac{U_m}{U_{mf}} = b = 1.0 \text{ to } 1.5 \qquad 2.5$$

Using the Mathur and Gishler equation, U_m can be determined from:

$$U_m = \left[\frac{d_p}{D_c}\right]\left[\frac{D_i}{D_c}\right]^{1/3}\sqrt{\frac{2gH_m(\rho_p-\rho_f)}{\rho_f}} \qquad 2.1a$$

U_{mf}, on the other hand, can be estimated from the Ergun (1952) equation, using the empirical approximations of Wen and Yu (1966):

$$\frac{1-\epsilon_{mf}}{\phi^2\epsilon_{mf}^3} = 11 \qquad 2.6a$$

$$\frac{1}{\phi\epsilon_{mf}^3} = 14 \qquad 2.6b$$

Substituting Equations 2.6a and 2.6b into Equation A.5 (Appendix A.1) yields the following:

$$Re_{mf} = \frac{d_p U_{mf}\rho_f}{\mu} = 33.7[\sqrt{1+35.9X10^{-6}Ar} - 1] \qquad 2.7$$

Combining Equations 2.5, 2.1a and 2.7, eliminating U_m and U_{mf}, the net result is

$$H_m = \left[\frac{D_c^2}{d_p}\right]\left[\frac{D_c}{D_i}\right]^{2/3}\left[\frac{568b^2}{Ar}\right][\sqrt{1+35.9X10^{-6}Ar} - 1]^2 \qquad A.7$$

McNab and Bridgwater (1977) further assumed that b was constant. Equation A.7 gave the best fit to existing experimental data by taking b = 1.11, that is, Equation A.7 became

$$H_m = \left[\frac{D_c^2}{d_p}\right]\left[\frac{D_c}{D_i}\right]^{2/3}\left[\frac{700}{Ar}\right]\left[\sqrt{1+35.9X10^{-6}Ar} - 1\right]^2 \qquad 2.8$$

This model, together with the experimental data available, were plotted as shown in Figure 2.2. One key feature of Equation 2.8 is that it predicts a critical value of d_p below which H_m increases with d_p and above which H_m decreases with d_p. This critical value is given by (see Appendix A.3)

$$(d_p)_{crit} = 60.6\left[\frac{\mu^2}{g(\rho_p-\rho_f)\rho_f}\right]^{1/3} \qquad A.14$$

Littman et al. (1979) developed the following correlation for spherical particles:

$$\frac{H_m D_i}{D_c^2} = 0.218 + \frac{0.00500}{A} \; ; \; A > 0.02 \qquad 2.9$$

where A is defined by

$$A = \frac{\rho_f U_{mf} U_t}{(\rho_p-\rho_f)gD_i} \qquad 2.10$$

U_{mf} is calculated from Equation A.5 and U_t is estimated from the following:

$$Ar = 18Re_t + 2.7Re_t^{1.687} \; ; \; Re_t \leq 1000 \qquad 2.11a$$

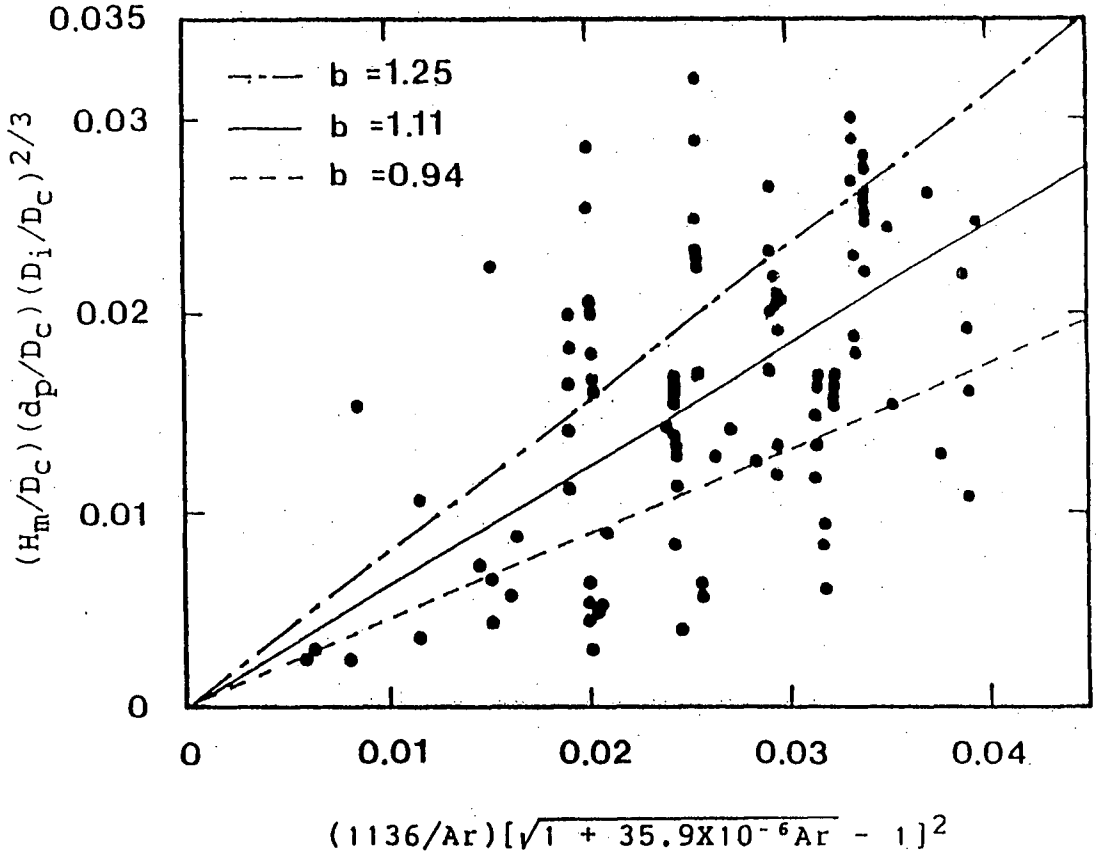

Figure 2.2 Comparison between experimental data and predictions by Equation 2.8 (McNab and Bridgwater, 1977). The solid line indicates the best fit. The other two lines show the 95% confidence limits.

$$Re_t = 1.745Ar^{0.5} \quad ; \quad Re_t > 1000 \qquad 2.11b$$

and

$$U_t = \frac{Re_t \mu}{\rho_f d_p} \qquad 2.11c$$

The parameter, A is a measure of the ratio of the inertial force of the jet entering the bed to the spouting pressure drop. For non-spherical particles, Morgan and Littman (1982) suggested the following expressions:

$$\frac{H_m D_i}{D_c^2} = 0.218 + \frac{5.13X10^{-3}}{A_\phi} + \frac{2.54X10^{-5}}{A_\phi^2}$$

$$\text{for } A_\phi > 0.014 \qquad 2.12a$$

$$= 175(A_\phi - 0.01)$$

$$\text{for } 0.010 \leq A_\phi \leq 0.014 \qquad 2.12b$$

Equations 2.12a and 2.12b apply for particles larger than $(d_p)_{crit}$ as given by Equation A.14. A_ϕ, like A, is defined by Equation 2.10. However, when calculating U_t and U_{mf}, the shape factor ϕ has to be taken into consideration. U_{mf} can again be estimated from Equation A.5 by using the appropriate values of ϕ and ϵ_{mf}. U_t for a spherical particle is first calculated using Equations 2.11a, 2.11b and 2.11c. The effect of ϕ on U_t is given by

$$\frac{U_t(\phi<1)}{U_t(\phi=1)} = 5\phi^3 - 7.57\phi^2 + 4.09\phi - 0.516 \qquad 2.13$$

Thus U_t for a non-spherical particle is obtained. Morgan and Littman reported that their expressions for H_m represented existing data reasonably well, with an average deviation of 24.2%.

Morgan and Littman also pointed out that $(d_p)_{crit}$ might depend on ϕ and ϵ_{mf} but still they used the value given by Equation A.14, which was slightly inconsistent with their expressions. To be more precise, their critical value should be defined by explicitly including the effect of ϕ and ϵ_{mf} (i.e., Equation A.16 in Appendix A.4), rather than by implicitly using the Wen and Yu approximations, Equations 2.6a and 2.6b (which are incorporated in Equation A.14).

2.4 AVERAGE SPOUT DIAMETER

There are many equations available for estimating the longitudinal average value of spout diameter, D_s (Mathur and Epstein, 1974; Littman, 1982). Bridgwater and Mathur (1972) proposed a simplified theoretical model which was derived from a force balance analysis. Their derived equation was

$$\frac{32f\rho_f Q_s^2}{\pi^2\psi(D_c-D_s)D_s^4} = 1 \qquad 2.14$$

Based on a number of approximations, Equation 2.14 was

reduced to a more manageable form:

$$D_s = 0.384\left[\frac{G^{0.5}D_c^{0.75}}{\rho_b^{0.25}}\right] \qquad 2.15$$

where all variables were expressed in SI units of m, kg and s. This equation is primarily restricted to air spouting. McNab and Bridgwater (1974) later pointed out that the model of Bridgwater and Mathur was oversimplified.

McNab (1972) applied statistical analysis to existing data and came up with the following expression:

$$D_s = 2.0\left[\frac{G^{0.49}D_c^{0.68}}{\rho_b^{0.41}}\right] \qquad 2.16$$

where all variables were again expressed in SI units. The coefficient, "2.0" should be replaced by "0.037" if British units are used instead.

Comparison of the above equation with that of Bridgwater and Mathur shows that the same variables have been included and that the dependence on each variable is of the same order of magnitude; the main difference is in the value of the fitting coefficient. In view of the simplifications introduced by Mathur and Bridgwater, the discrepancy between the two equations can be considered acceptable.

Littman et al. (1977) developed the following expression from a theory of flow in the annulus which used the vector form of the Ergun equation as its field equation:

$$\frac{H_m D_s^*}{(D_c^2 - D_s^{*2})} = 0.345 \left[\frac{D_s^*}{D_c}\right]^{-0.384} \qquad 2.17$$

Combining the above equation with Equation 2.9, Littman et al. (1979) came up with an analytical expression in the form of

$$\frac{D_s^*}{D_i} = \left[\frac{2.10\exp(-0.018/A)+1.0}{3.10}\right] \left[0.862 + 0.219\left[\frac{D_c}{D_i}\right] - 0.0053\left[\frac{D_c}{D_i}\right]^2\right] \qquad 2.18$$

The quantity, D_s^* is the spout diameter at the maximum spoutable bed height, under the minimum spouting condition. It is used as the reference value for other bed conditions. Littman (1982) also reported that under the minimum spouting condition

$$\frac{D_s(U_{ms})}{D_s^*} = 0.35\left[\frac{H}{H_m}\right] + 0.65 \qquad 2.19$$

and assuming the square root velocity relation of Equations 2.15 and 2.16, Equation 2.19 can be rewritten as

$$\frac{D_s(U)}{D_s^*} = \sqrt{\frac{U}{U_{ms}}}\left[0.35\left[\frac{H}{H_m}\right] + 0.65\right] \qquad 2.20$$

This procedure for estimating average spout diameter is

restricted to A > 0.02 and to spherical particles. Littman (1982) reported good agreement between experimental and calculated values. He also noted that for spouting of fine particles (0.275 to 0.995 mm) in water i.e., low A values, Equation 2.18 held but Equations 2.19 and 2.20 did not. Under the minimum spouting condition, Equation 2.19 was then to be replaced by

$$\frac{D_s(U_{ms})}{D_s^*} = 0.72\left[\frac{H}{H_m}\right] + 0.28 \qquad 2.21$$

2.5 FLUID AND PARTICLE VELOCITY IN THE ANNULUS

Mamuro and Hattori (1968) derived an expression for estimating the longitudinal annular fluid velocity. It was based on a force balance on a differential height dz of the annulus, with the following assumptions and boundary conditions:

1. Darcy's law applies
2. $z = 0$, $U_a = 0$
3. $z = H_m$, $U_a = U_{aH_m} = U_{mf}$

They came up with

$$\frac{U_a}{U_{mf}} = 1 - \left[1 - \frac{z}{H_m}\right]^3 \qquad 2.22$$

Equation 2.22 tends to overpredict U_a because $U_{mf} \geq U_{aH_m}$. If U_{mf} is replaced by the measured value of U_{aH_m}, the equation is found to work better.

An alternate equation for predicting longitudinal flow distribution is that of Lefroy and Davidson (1969)

$$\frac{U_a}{U_{aH_m}} = \sin\left[\frac{\pi z}{2H_m}\right] \qquad 2.23$$

Unlike the theoretical approach by Mamuro and Hattori, this equation was based on empirical findings. Epstein et al. (1978) recommended that Equation 2.23 should be modified to

$$\frac{U_a}{U_{aH_m}} = \sin\left[\frac{\pi z}{2H_m}\right]^{1/n} \qquad 2.24$$

where n is a flow regime index which varies from unity (Darcy's law) to a maximum value of 2 (inviscid flow).

Solid circulation rates for coarse particles were measured by Lim (1975). He reported that the particle velocity in the annulus was not constant at any fixed bed level; it was highest near the spout-annulus interface and decreased to a minimum at the bed wall. The solid circulation rate was found to increase linearly with bed level, except in the conical section of the column.

2.6 LONGITUDINAL PRESSURE PROFILE AND OVERALL BED PRESSURE DROP

The pressure gradient in the annulus of a spouted bed may be obtained from the Ergun (1952) equation,

$$-\frac{dP}{dz} = K_1 U_a + K_2 U_a^2 \qquad 2.25$$

Combining this expression with that of Mamuro and Hattori, it was shown (Epstein and Levine, 1978) that

$$\frac{P-P_H}{-\Delta P_f} = \frac{1}{h(2\beta-1)}[2(\beta-2)\{1.5(h^2 - x^2) - (h^3 - x^3) + 0.25(h^4 - x^4)\} + 3\{3(h^3 - x^3) - 4.5(h^4 - x^4) + 3(h^5 - x^5) - (h^6 - x^6) + 0.143(h^7 - x^7)\}] \qquad 2.26$$

where

$$h = H/H_m \qquad 2.27a$$

$$x = z/H_m \qquad 2.27b$$

$$\beta = 2 + \frac{3K_1}{2K_2 U_{mf}} \qquad 2.27c$$

and K_1 and K_2 are given in Appendix A (Equations A2.a and A.2b). The total bed pressure drop is thus determined by putting x = 0, i.e.,

$$\frac{-\Delta P_s}{-\Delta P_f} = \frac{2-(4/\beta)}{2-(1/\beta)}(1.5h - h^2 + 0.25h^3) + \frac{3}{2\beta-1}(3h^2 - 4.5h^3 + 3h^4 - h^5 + 0.143h^6) \qquad 2.28$$

At the maximum spoutable height, h = 1, this expression can be further reduced to

$$\left[\frac{-\Delta P_s}{-\Delta P_f}\right]_{max} = \frac{1.5(\beta-2)+1.929}{2\beta-1} \qquad 2.29a$$

$$= 0.75 \text{ when } \beta = \infty \text{(Darcy's Regime)} \qquad 2.29b$$

$$= 0.64 \text{ when } \beta = 2 \text{(Inviscid Regime)} \qquad 2.29c$$

or more generally

$$0.75 > \left[\frac{-\Delta P_s}{-\Delta P_f}\right]_{max} > 0.64 \qquad 2.30$$

A simpler empirical equation was proposed by Lefroy and Davidson (1969)

$$\frac{P-P_H}{-\Delta P_s} = \cos\left[\frac{\pi z}{2H}\right] \qquad 2.31$$

or

$$\frac{dP}{dz} = \frac{\Delta P_s \pi}{2H}\sin\left[\frac{\pi z}{2H}\right] \qquad 2.32$$

Assuming incipient fluidization at $z = H = H_m$, Equation 2.32 can be reduced to

$$\frac{\Delta P_f}{H_m} = \left(\frac{dP}{dz}\right)_{mf} = \frac{(\Delta P_s)_{max}\pi}{2H_m} \qquad 2.33$$

or

$$\left[\frac{\Delta P_s}{\Delta P_f}\right]_{max} = \frac{2}{\pi} = 0.637 \qquad 2.34$$

This constant ratio is in good agreement with the inviscid value of the previous model but differs from the Darcy Law value.

McNab and Bridgwater (1977) suggested a somewhat different correlation for estimating the overall spouted bed pressure drop:

$$\left[\frac{\Delta P_s}{\Delta P_f}\right] = \left[\frac{\Delta P_s}{\Delta P_f}\right]_{max} \left[\frac{H}{H_m}\right]^{\gamma} \qquad 2.35$$

where

$$\gamma = 0.1 \left[\frac{D_c}{D_i}\right]^{-0.6} \qquad 2.36$$

The main feature of this expression is the inclusion of D_i and D_c explicitly as variables, which the previous two models do not have except implicitly through H_m. The value of $(\Delta P_s/\Delta P_f)_{max}$ may be determined from the empirical equation of Pallai and Nemeth (1969)

$$\left[\frac{\Delta P_s}{\Delta P_f}\right]_{max} = 0.8 - 0.01 \left[\frac{D_c}{D_i}\right] \qquad 2.37$$

or it can be taken as one of the two limiting cases in the first model (Equation 2.30).

2.7 RADIAL PRESSURE PROFILE

The fluid pressure in the annulus generally does not vary radially at any given bed levels, except in the conical section where the pressure decreases towards the column wall (Mathur and Epstein, 1974; Littman et al., 1985). The vector Ergun equation has been applied to predict the fluid flow in the annulus by Rovero et al. (1983) and Littman et al. (1985). The radial pressure profiles generated from these two models are consistent with the reported observations.

2.8 FOUNTAIN HEIGHT

Grace and Mathur (1978) proposed the following expression for estimating the height of the fountain, H_F:

$$H_F = \epsilon_a^{1.46}\left[\frac{\rho_p V_{sH}^2}{2g(\rho_p-\rho_f)}\right] \qquad 2.38$$

2.9 REGIME MAP

A regime map or phase diagram gives a graphical description of how a potential spouted bed system behaves under the influence of increasing fluid flowrate and bed height. Typically, a complete regime map consists of the following regions:

1. Static (or Fixed) Bed
2. Coherent (or Stable) Spouting
3. Progressively Incoherent Spouting

4. Bubbling

5. Slugging

However, it is possible to have a regime map containing less than five regions. Figures 2.3 and 2.4 are examples of the the two (Chandnani 1984).

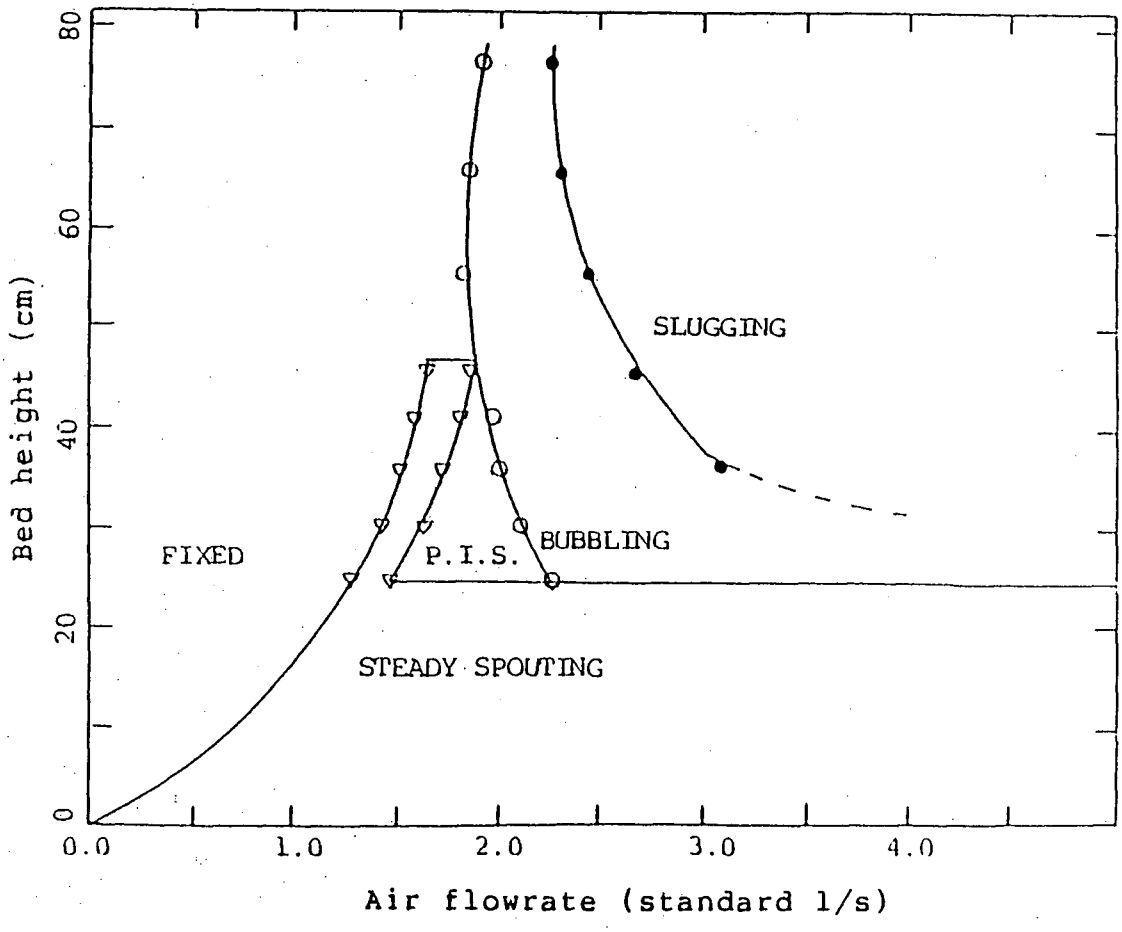

Figure 2.3 Regime map for sand, d_p = 0.516 mm,
D_i = 12.7 mm (Chandnani 1984)
P.I.S. = Progressively Incoherent Spouting

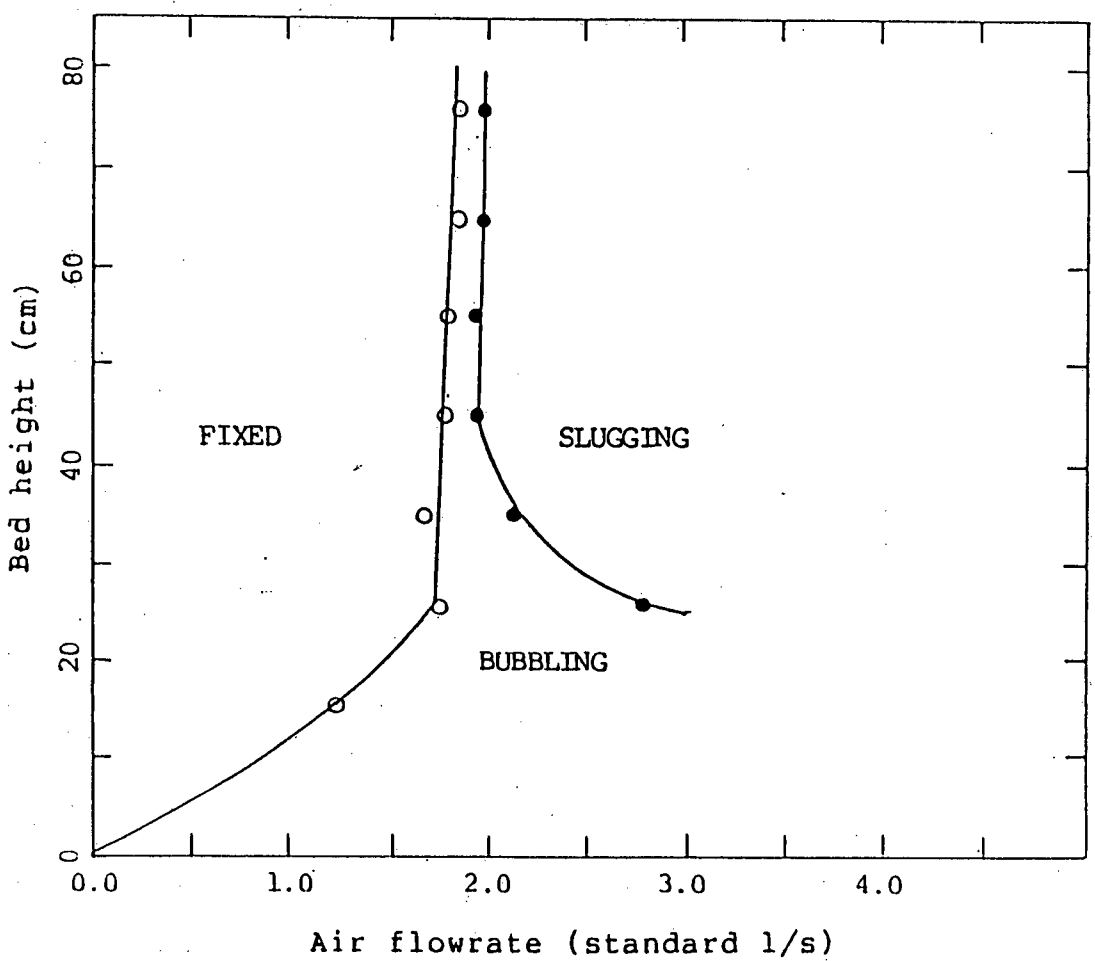

Figure 2.4 Regime map for sand, d_p = 0.516 mm, D_i = 19.05 mm (Chandnani, 1984)

3. APPARATUS, BED MATERIALS AND EXPERIMENTAL METHODS

3.1 CHOICE AND DESCRIPTION OF EQUIPMENT

A 156-mm inside diameter half column was built. The conical section at the bottom had an included angle of 60°. The main reason for using a half-column is that it allows visual observation, which is particularly important for measuring spout diameter and particle circulation rate. The validity of using half columns in spouted bed studies has been questioned and was investigated by Whiting and Geldart (1979) and Geldart et al. (1981). They reported that hydrodynamic data (such as U_{ms}, H_m and $V_p(R_c)$) obtained in a half column were similar to those in a full column. Rovero et al. (1985), however, have shown that the frictional effect caused by the flat wall cannot be overlooked when measuring the particle velocities. In the case of spout shapes, Lim (1975) has indicated that the flat wall in a half column has a negligible effect.

Due to the high temperature of the present experiments, the bed was constructed of 316 stainless steel. The vertical lengths of the conical and cylindrical sections were 89 and 1067 mm, respectively (Figure 3.1). The half column was furnished with a total of six measuring ports. The first one was in the conical section and was 38 mm above the orifice. This port was primarily used for measuring pressure. The

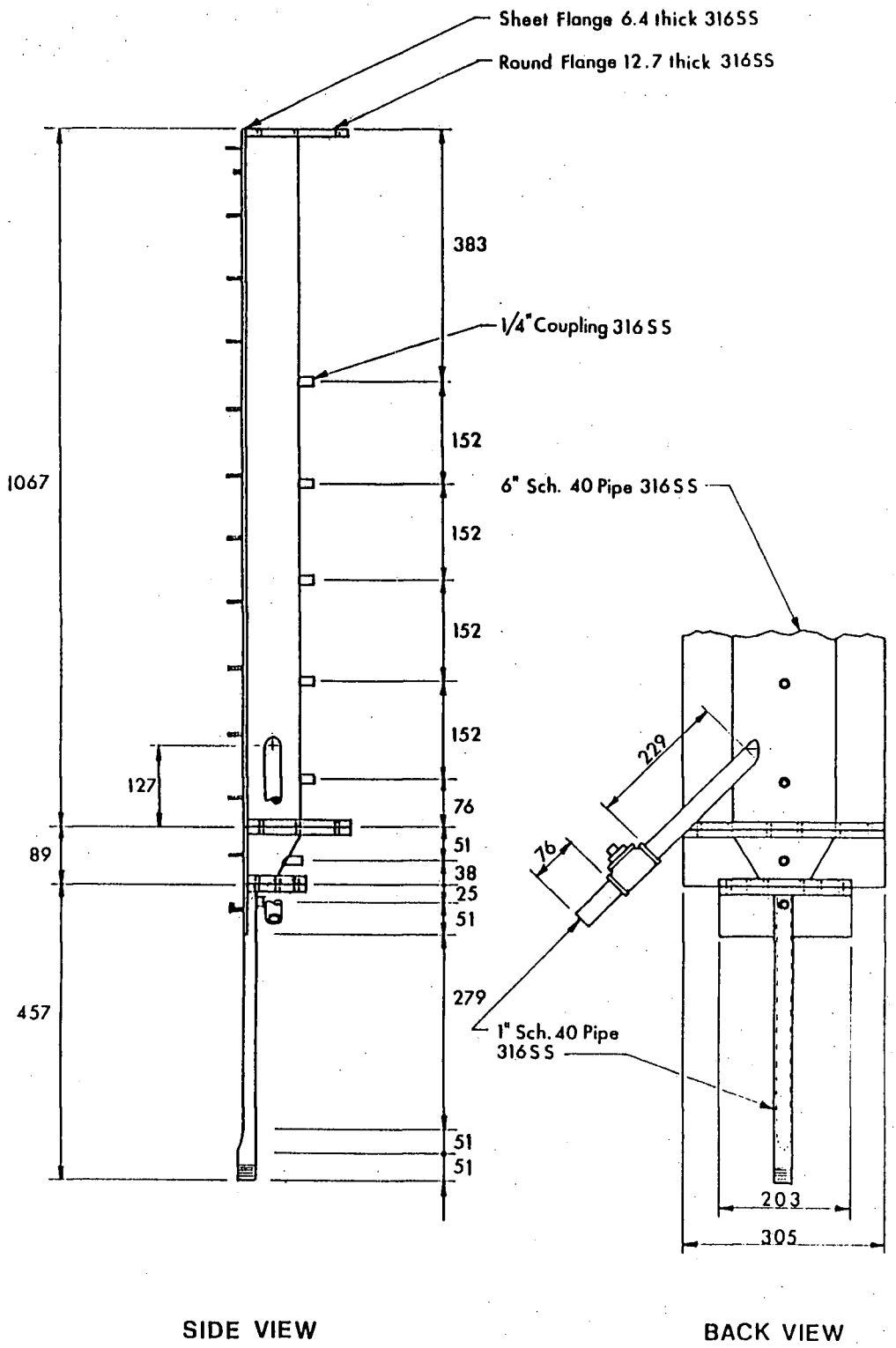

Figure 3.1 Details of the half spouted bed

(All dimensions in mm)

others were all in the cylindrical section with vertical separations of 152 mm. The position of the lowest one in this section was 165 mm above the orifice. These ports were all used for securing thermocouples. In addition to these five measuring ports, the cylindrical section was equipped with a solids discharge line which was 216 mm above the orifice. The bed, as described, was not long enough for handling bed heights close to 1 m. However, in some cold runs, H_m was found to exceed 1 m, making this column unsuitable in these cases. For this reason, another cylindrical section of 610 mm in length was constructed and added to the existing section, resulting in a total column height of 1.77 m. The fluid inlet section was a 26.64 mm ID half pipe with a straight vertical length of 355 mm, as shown in Figure 3.1.

Three orifice plates of different sizes were also made. Their openings were 12.7, 19.05 and 26.64 mm, respectively. An orifice collar on each plate extended 3 mm into the bed. For the 12.7 and 19.05 mm plates, the bottom face was machined so that the flow would converge smoothly. With this type of fluid inlet, the spouting action was more stable than for a simple orifice. A small indentation at the bottom of all three orifices plates allowed the insertion of wire screens which prevented particles from falling into the inlet pipe during shut-off. The key features of the orifice plates are shown in Figure 3.2.

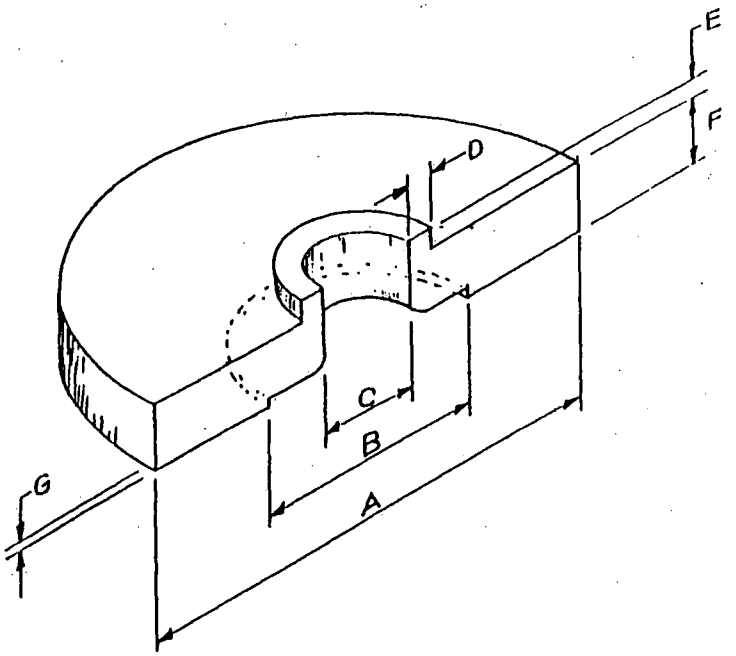

SIZE	Dimensions(mm)						
	A	B	C	D	E	F	G
S	76.2	41.0	12.70	3.2	3.2	9.5	1.6
M	76.2	41.0	19.05	3.2	3.2	9.5	1.6
L	76.2	41.0	26 64	3.2	3.2	9.5	1.6

Figure 3.2 Details of the orifice plates

The front panel of the bed was made of 6 mm 'Georgian polished wire-glass'. This type of glass could not in itself withstand the high temperatures required in this study. However, the wire inside the glass tended to hold the cracked pieces together. Any leaks were patched up using muffler cement (supplied by Holt Lloyd Limited of Canada). Although the cement reduced some of the visibility of the glass, frontal observation was still quite adequate. Quartz glasses were not used because they were expensive. Tempered glasses were tried, but they failed at high temperature (about 400 °C) and shattered into many pieces. The top of the column was located directly under an exhaust hood, which reduced the possibility of a high pressure buildup in the bed.

To reduce mechanical stress due to the different thermal expansion of glass and steel, the glass panel was assembled using a screw and plate device as indicated in Figure 3.3. The gasket material between the glass and the steel sheet flange was a compressible high temperature insulating material (970-J paper supplied by Plibrico Limited of Canada). This material worked well; however, it had to be replaced after each dismantling.

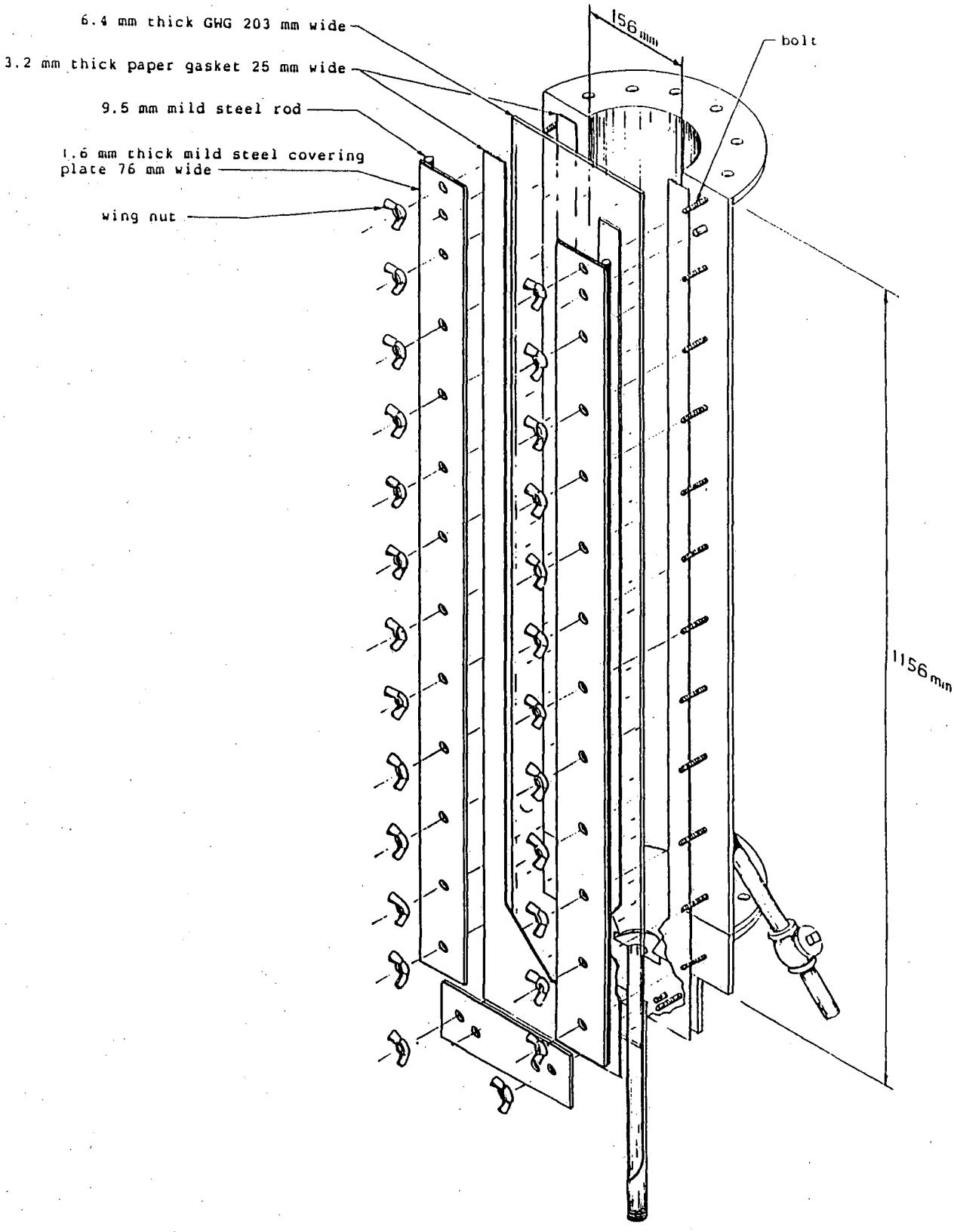

Figure 3.3 Isometric view of the half spouted bed

3.2 METHOD OF HEATING

Heating was provided by cylindrical electric heaters which were mounted on the outside of 2-inch Schedule-40 316 Stainless Steel pipes (heating sections). To enhance heat transfer, the heating sections were packed with ceramic rings. Three heating sections were used. Each heating unit had a power rating of 4.0 kW maximum and was controlled individually by monitoring the temperature in the gap between the outside wall of the pipe and the inside wall of the heater. Glass fibre insulation was used to blanket the piping and the back of the spouted bed to reduce heat loss to the surroundings. The front flat surface of the spouting column was used for observations and measurements, and it was therefore covered only during the heating up period. This heating set-up was capable of maintaining operating bed temperatures up to 420 °C. It was arbitrarily chosen to run at four temperature levels: 20, 170, 300 and 420 °C.

3.3 GAS FLOW AND INSTRUMENTATION

A schematic diagram of the apparatus is shown in Figure 3.4. Spouting air from the main air line flowed through either one of the rotameters (the smaller one was primarily used for low flowrate). From the rotameter, air went into the heating unit where it was raised to the desired temperature. This preheated air then entered the spouted bed

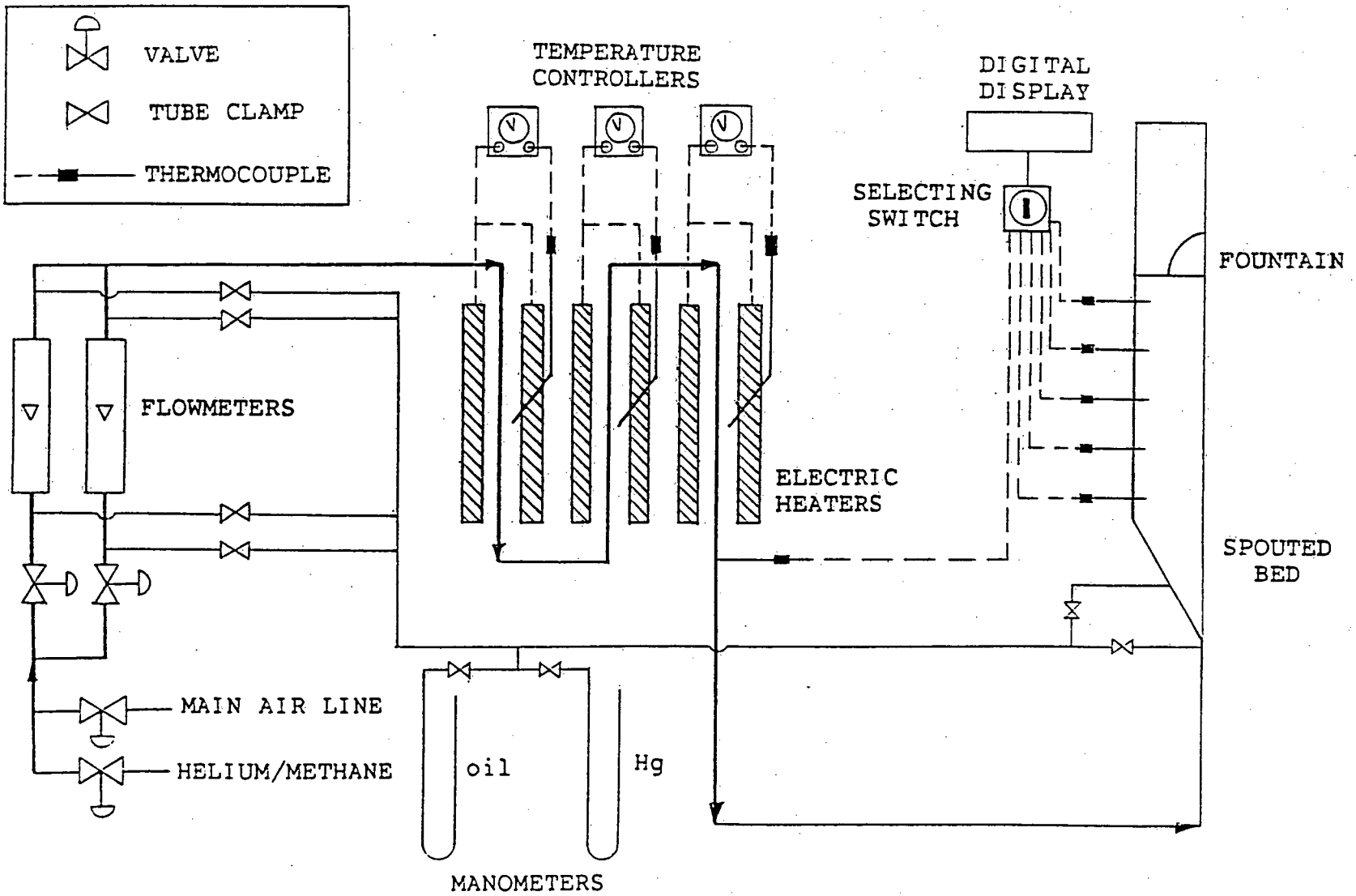

Figure 3.4 Schematic of the overall equipment layout

through the orifice. The spent air discharged into the exhaust hood where it was diluted with colder air from the adjacent surroundings. The mixed air, which was much cooler than the original discharge, was finally vented to the atmosphere.

Temperatures were measured and monitored with Chromel-Alumel (i.e., Type K) thermocouples at nine locations. Three of these thermocouples were positioned as described in Section 3.2 and the temperatures were indicated on the temperature controllers. The remaining thermocouples were all connected to a digital display through a selecting switch. One of them was located just after the heating unit. The others were mounted at the back of the cylindrical section of the half column, with the tips extended about 10 mm from the curved inner wall surface. These thermocouples measured the annular temperature along the bed in regular interval of 152 mm. The average of these values was taken as the overall bed temperature. Table 3.1 shows some typical temperature variations with bed levels together with other relevant information. These data were obtained while the experimental equipment was being debugged. During these trial runs, an additional thermocouple was inserted in the conical section (see Figure 3.1) in order to yield more complete temperature profiles. (During actual runs, this thermocouple in the conical section was replaced by a pressure port.) Preliminary measurements had also indicated

Table 3.1 Typical temperature profiles. Sand, ρ_p = 2600 kg/m^3, d_p = 1.25 mm

Bed Ht. (mm)	Desired Temp. (°C)	Controllers Setting (°C)	Air Temp. from heater (°C)	Time Req'd (hr)	At steady state Temperature profiles (°C) z = 38	165	317	469	621	773 mm
680	170	300	280	1.00	168	168	170	171	170	152
630	300	500	470	2.25	302	298	302	304	302	258
530	420	700	660	4.50	423	415	423	425	382	

that the radial temperature gradients in the annulus were insignificant. These observations were consistent with those reported by Zhao (1986).

The absolute pressure inside the rotameter was required when calculating the gas flowrate (Appendix C). This was achieved by measuring the gauge pressures before and after the rotameters using a mercury manometer. The average of the two manometer readings was assumed to be the gauge pressure inside the rotameter, from which the corresponding absolute pressure was determined. Two other pressure ports were positioned near the orifice; one was 38 mm above the orifice (i.e., in the conical section) whereas the other one was 25 mm below the orifice. The gauge pressures at these two locations were again measured with a manometer. These readings were used to determined the overall pressure drop across the bed and thus the absolute pressure in the bed as described in Sections 3.7.2 and 3.7.3. The mercury manometer had an uncertainty of ± 4 mm of Hg. For smaller readings which required better precision, an oil manometer was used instead. This oil had a specific gravity of 1.75 and the uncertainty of this oil manometer was equivalent to ± 0.6 mm of Hg.

3.4 BED MATERIAL

Only one type of particle was used in this study. It was Ottawa sand, suplied by Indusmin Limited of Montreal. This sand was mainly silica (>99%) with traces of Fe_2O_3, Al_2O_3 and CaO. The sand, as received, had a wide size range. Before it was used, it was first screened to narrow down the size distributions. Three sizes (small, medium and large) of sand were employed. The mean particle diameter of each size fraction was determined from sieve analysis as

$$d_{pj} = \frac{1}{\Sigma(x_i/d_{pi})} \qquad 3.1$$

where x_i is the weight fraction of particles within an average adjacent screen aperture size of d_{pi}. Several measurements were taken for each size before and after the given experiments. The average value of d_p was then used, i.e.,

$$d_p = (\Sigma d_{pj})/M \qquad 3.2$$

Table 3.2 summarizes such measurements. Apparently, there was only a small reduction in size during runs, thus justifying the use of Equation 3.2. The size distribution of each measurement is given in Appendix B.

The density of sand particles was determined by liquid displacement. Sand particles were first coated with a water

Table 3.2 Particle diameter

Size		Sample # 1	2	3	4	Average value	Overall average
S	Before	1.043	0.905	0.931	0.985	0.966	0.945 mm
	After*	0.946	0.879	0.910	0.960	0.924	
M	Before	1.281	1.300	1.232	1.255	1.267	1.250 mm
	After*	1.210	1.270	1.195	1.254	1.232	
L	Before	1.725	1.731	1.667	1.682	1.701	1.665 mm
	After*	1.672	1.647	1.514	1.678	1.628	

* Average duration : 6 - 8 hours

seal (Thompson's seal). A known weight of the coated particles was placed inside a 100 ml volumetric flask. The flask was then filled with water to the 100 ml mark. The additional weight measured was the weight of the water added, from which the corresponding volume of water was determined. The difference between the volume of water and 100 ml was the volume of the sand particles, from which the density could be calculated. Several measurements were made and the average particle density was found to be 2.60 gm/cm^3 with an uncertainty of less than 1%.

The "random loose" bulk density was determined using the procedure of Oman and Watson (1944). A graduated cylinder was partially filled with a known weight of particles. With the top end covered, the cylinder was inverted and returned quickly to the original upright position. The volume was then noted and the bulk density was thus determined. Such tests were repeated several times to produce an average value. The annulus of a spouted bed was considered to be a loosely packed bed and hence its bulk density ρ_b was assumed to be that obtained as just described. The voidage in the annulus could then be determined as

$$\epsilon_a = 1 - \rho_b/\rho_p \qquad 3.3$$

Table 3.3 summarizes the physical properties of the sand

Table 3.3 Physical properties of sand particles used

d_p (mm)	ρ_p (kg/m^3)	ρ_b (kg/m^3)	ϵ_a	δ (deg)	θ (deg)	Temp (^{o}C)	U_{mf}* (m/s)	U_t@ (m/s)
0.945	2600	1300	0.50	34.0	63.5	20	0.51	2.16
						170	0.48	2.38
						300	0.43	2.49
						420	0.40	2.59
1.250	2600	1300	0.50	34.0	63.5	20	0.70	2.73
						170	0.71	3.04
						300	0.67	3.21
						420	0.63	3.35
1.665	2600	1300	0.50	34.0	63.5	20	0.92	3.45
						170	0.99	3.86
						300	0.98	4.09
						420	0.97	4.30

* estimated from Equation 2.7

@ estimated from Equations 2.11 and 2.13

particles used in this study.

3.5 FLOWRATE MEASUREMENTS

Gas flowrates were measured by rotameters which were calibrated against a dry gas meter (model AL 425 by Canadian Meter Co. Ltd.). Pressure taps were located before and after the rotameters as described in Section 3.3. These pressure taps were connected to an assembly of two U-tube manometers, containing a blue oil (specific gravity = 1.75) and mercury (specific gravity = 13.6), respectively. These two manometers were also used for pressure measurements of the bed. The readings from the manometer allowed the conversion of a measured flowrate to a corresponding value at a standard condition of 20 °C and 1 atmosphere. The whole procedure and the resulting calibration curves are presented in Appendix C.1.

3.6 PROGRAM OF STUDY

In this study, there were three main independent variables, namely particle diameter, orifice opening and bed temperature. Table 3.4 gives the conditions of all the performed runs, while Table 3.5 lists the dependent variables actually measured in each run.

Table 3.4 Operating conditions

Run #	Spouting gas	d_p (mm)	D_i (mm)	Temp. (^oC)
1	Air	0.945	19.05	20
2	Air	0.945	19.05	170
3	Air	0.945	19.05	300
4	Air	0.945	19.05	420
5	Air	1.250	19.05	20
6	Air	1.250	19.05	170
7	Air	1.250	19.05	300
8	Air	1.250	19.05	420
9	Air	1.665	19.05	20
10	Air	1.665	19.05	170
11	Air	1.665	19.05	300
12	Air	1.665	19.05	420
13	Air	0.945	26.64	20
14	Air	0.945	26.64	170
15	Air	0.945	26.64	300
16	Air	0.945	26.64	420
17	Air	1.250	26.64	20
18	Air	1.250	26.64	170
19	Air	1.250	26.64	300
20	Air	1.250	26.64	420
21	Air	1.665	26.64	20
22	Air	1.665	26.64	170
23	Air	1.665	26.64	300
24	Air	1.665	26.64	420
25	Air	0.945	12.70	20
26	Air	0.945	12.70	170
27	Air	0.945	12.70	300
28	Air	0.945	12.70	420
29	Air	1.250	12.70	20
30	Air	1.250	12.70	170
31	Air	1.250	12.70	300
32	Air	1.250	12.70	420
33	Air	1.665	12.70	20
34	Air	1.665	12.70	170
35	Air	1.665	12.70	300
36	Air	1.665	12.70	420
37	Methane	1.250	19.05	20
38	Helium	1.250	19.05	20

Table 3.5 Dependent variables measured

Run #	H_m	D_s	U_{ms}	$-\Delta P_s$	U_a	V_p	H_F	P_z-P_H	Regime Map
1	x	x	x	x					
2	x	x	x	x					
3	x	x	x	x					
4	x	x	x	x					
5	x	x	x	x	x	x	x	x	x
6	x	x	x	x	x	x	x	x	x
7	x	x	x	x	x	x	x	x	x
8	x	x	x	x	x	x	x	x	x
9	x	x	x	x					
10	x	x	x	x					
11	x	x	x	x					
12	x	x	x	x					
13	x	x	x	x					
14	x	x	x	x					
15	x	x	x	x					
16	x	x	x	x					
17	x	x	x	x					
18	x	x	x	x					
19	x	x	x	x					
20	x	x	x	x					
21	x	x	x	x					
22	x	x	x	x					
23	x	x	x	x					
24	x	x	x	x					
25	x	x	x	x					
26	x	x	x	x					
27	x	x	x	x					
28	x	x	x	x					
29	x	x	x	x					
30	x	x	x	x					
31	x	x	x	x					
32	x	x	x	x					
33	x	x	x	x					
34	x	x	x	x					
35	x	x	x	x					
36	x	x	x	x					
37	x	x	x	x					
38	x	x	x	x					

For each run, if stable air spouting existed, the maximum spoutable bed height, the corresponding minimum spouting velocity and the overall bed pressure drop were measured. For this same bed height, the spout diameter was measured at $U \simeq 1.10\ U_{ms}$. Data were also collected at two other bed heights (0.50 H_m and 0.75 H_m approximately). Spouting gases other than air were also used (Runs # 37 and # 38), namely helium and methane. Runs # 5, # 6, # 7 and # 8 were repeated to ensure reproducibility of experimental data. It will be shown in later chapters that U_{ms}, $-\Delta P_s$, H_m and D_s are generally quite reproducible. Furthermore, for the repeated runs, additional measurements were made, namely of longitudinal and radial pressure profiles in the annulus, fluid and particle velocities in the annulus, regime maps and fountain heights. The actual experimental conditions in all the runs are listed in Appendix D, while the ranges of variables are summarized in Table 3.6.

3.7 METHODS OF MEASUREMENT

In the beginning of a typical hot run, the electric heaters were switched on with the temperature controllers all set at 500 °C. The heating sections and the ceramic packing inside them were pre-heated for about 20 minutes before air was turned on. The controllers were then set to the appropriate levels (see Table 3.1). Sands were poured slowly into the column from the open top. Bed heights could

Table 3.6 Ranges of variables studied

(ρ_p = 2600 kg/m^3, D_c = 156 mm)

d_p (mm)	0.945 — 1.665
D_i (mm)	12.70 — 26.64
H (m)	0.168 — 1.380
ρ_f (kg/m^3)	0.168 — 1.259
μ (10^{-5}kg/m·s)	1.09 — 3.20

be increased by adding more sands or decreased by opening the valve on the solids discharge line. The air flowrate was adjusted accordingly to maintain a steady spouting condition. When the bed reached the desired temperature within ± 5 °C, measurements were then taken as described in the next sub-sections. When all measurements were completed, the heaters were turned off and the valve was opened again to discharge the hot sand particles into a stainless steel bucket. The sands were drained mostly by gravity to the horizontal level of the discharge outlet. Further drainage was caused by maintaining a high air flowrate which subsequently yielded a high spout fountain. Some of the particles from the fountain fell through the discharge line into the receiving bucket. With this method, the column could be emptied in about 45 minutes. Air flow was kept on for an additional 90 minutes to cool off the whole apparatus.

3.7.1 MAXIMUM SPOUTABLE HEIGHT

H_m was determined by increasing the bed height until stable spouting could not be obtained for any gas flowrate. The corresponding loosely-packed bed height was then taken as H_m.

3.7.2 OVERALL BED PRESSURE DROP

A pressure tap was located about 25 mm below the orifice. According to Mathur and Epstein (1974), the pressure drop due to the bed should be determined as follows:

$$-\Delta P_S = \sqrt{P_B^2 - P_E^2 + P_{ATM}^2} - P_{ATM} \qquad 3.4$$

where P_B is the measured absolute upstream pressure for the bed and P_E is the corresponding value at the same flowrate for an empty column. It was found experimentally that $-\Delta P_S$ was reproducible when there were no screens under the orifice. When screens were in place, $-\Delta P_S$ could not be duplicated. It was later discovered that the ceramic packing in the heating section broke up into small pieces and randomly blocked the openings on the bottom side of the screens. Moreover, the top side of the screens was partially plugged by the sand particles in the bed. The combined effect of the two caused uncertainty in the measurements.

The screens had to be in place to prevent sand particles from entering into the inlet section during gas shut-off. To solve this problem, an alternate pressure tap was located 38 mm above the orifice, at which the measurement was independent of the screen conditions. A calibration curve was obtained by correlating $-\Delta P_S$ under no-screen conditions with the measured manometer value at

the pressure tap above the orifice. This curve, together with all the relevant data are presented in Appendix C.3. The overall bed pressure drops were then calculated from

$$-\Delta P_s = [0.171 + 0.976(-\Delta P_a)] \text{ cm Hg} \qquad 3.5$$

where $-\Delta P_a$ was the measured pressure drop above the orifice.

3.7.3 MINIMUM SPOUTING VELOCITY

The minimum spouting velocity was measured by observing the bed through the transparent front panel. The gas flowrate was first increased to a value above the minimum spouting condition and then decreased slowly until spouting ceased. The gas flowrate at which the fountain just collapsed was taken as the minimum spouting flowrate. This test was repeated at least twice to ensure reproducibility. The volumetric gas flowrate entering the half bed was calculated using Equation C.14 in Appendix C, assuming the absolute bed pressure was taken as

$$P_S = P_{ATM} + (-\Delta P_s)/2 \qquad 3.6$$

The superficial gas velocity was subsequently determined by dividing the volumetric flowrate by the cross-sectional area of the bed, i.e., $\pi D_c^2/8$ for a half column.

3.7.4 SPOUT DIAMETER AND SPOUT SHAPE

The spout diameter was measured by holding a ruler horizontally against the transparent front face of the column. Measurements were made at several bed levels to yield a full spout shape. The area-averaged spout diameter was calculated as follows:

$$D_S = \left[\frac{1}{H_a}\int_0^{H_a}\{D_S(z)\}^2 dz\right]^{1/2} \qquad 3.7$$

where $D_S(z)$ was the measured spout diameter at bed level, z. The numerical integration was done with "QINT4P", a routine described by Nicol (1982).

3.7.5 FLUID AND PARTICLE VELOCITIES IN THE ANNULUS

Before measuring the fluid velocity and pressure profiles (Section 3.7.6) in the annulus, the extension column was removed and replaced with a flanged cover (Figure 3.5). The fluid velocity was determined by means of a static pressure probe (Figure 3.6a) which consisted of two stainless steel tubes of 3.1 and 6.4 mm O.D., respectively. The smaller tube was placed inside the larger one, forming the main body. The bottom ends of the tubes were properly closed off with silver solder. Two sets of four holes (of 0.8 mm diameter) were also drilled. One set was located on

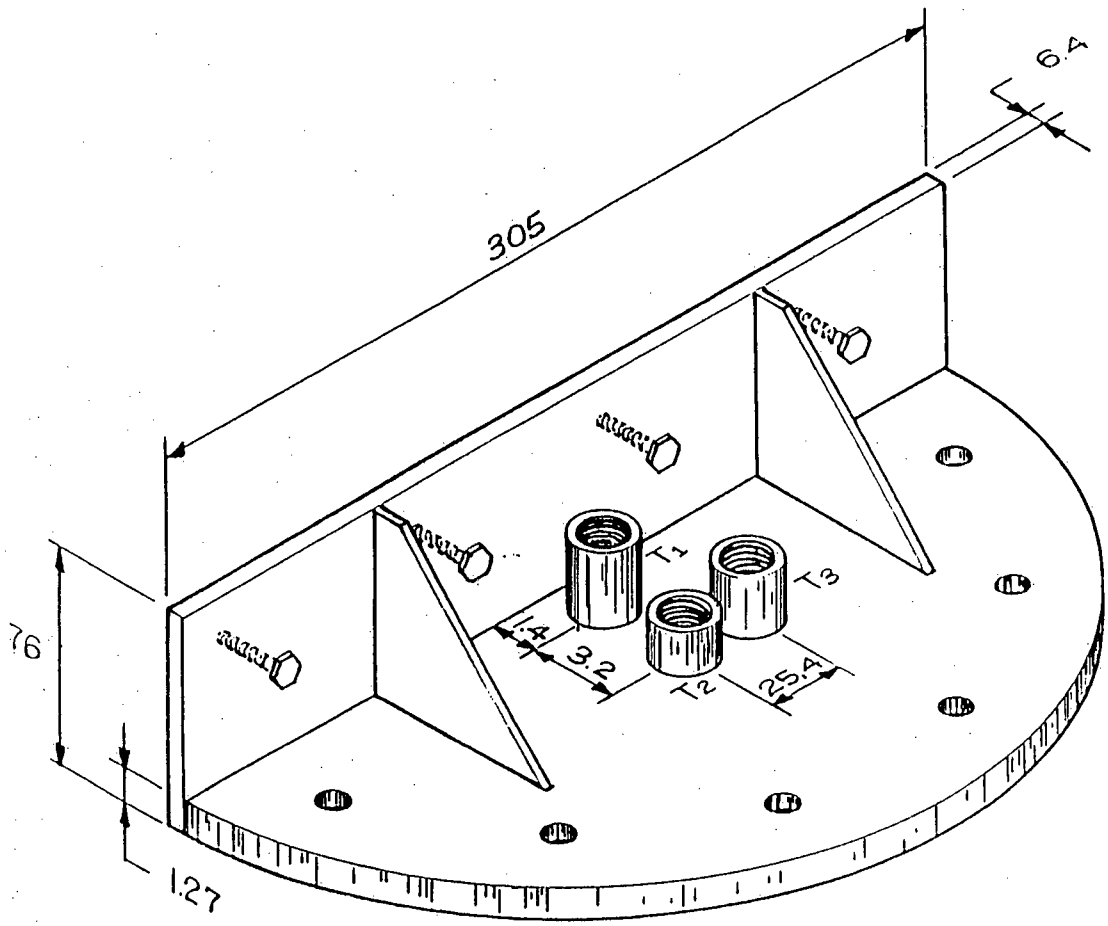

Figure 3.5 Details of the flanged cover

(All dimensions in mm)

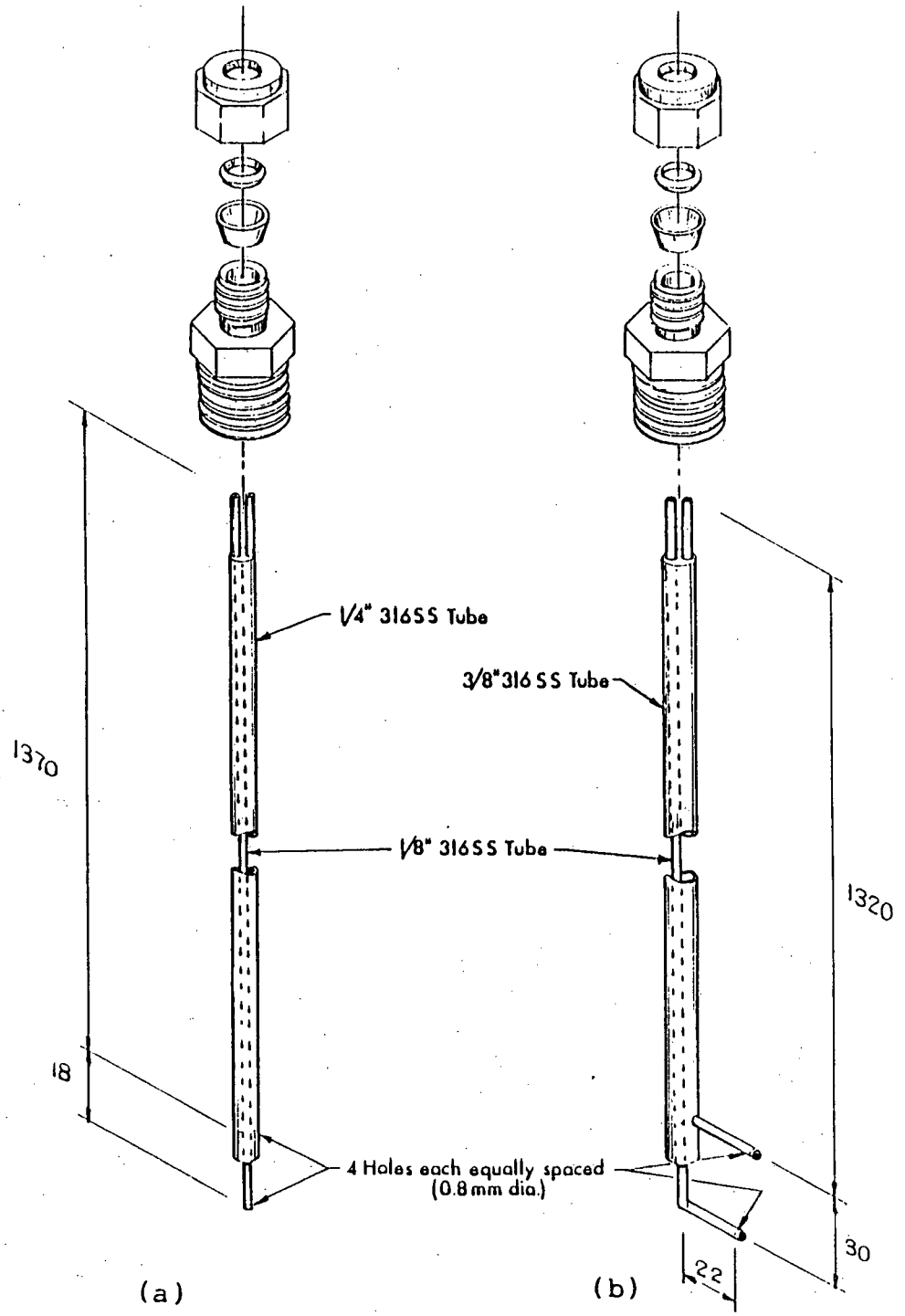

Figure 3.6 Details of the static pressure probes

(All dimensions in mm)

the small tube at the bottom part of the probe whereas the other set was on the outer shell with vertical separation of 18 mm between the two sets (of holes). Using a Swagelok® fitting, the probe was secured through port T2 in the flanged cover to restrict any lateral movement. The nut on the connector was only tightened slightly and could be loosened when adjusting the vertical position of the probe during measurements.

Static pressure gradients were measured at several bed levels. The small pressure drops were detected with a micromanometer (Model MM-3, made by Flow Corp. of Cambridge, Mass.) filled with butanol. These readings were converted to fluid velocities via a calibration curve. With the assumption that the annulus in a spouted bed behaves as a loosely packed bed of solids, the calibration was done in a loose bed of the same material. To ensure uniform (radial) distribution of fluid flow, the bed was set at a height well above the maximum spoutable bed height, H_m. Flowrates and pressure drops were recorded and a calibration of pressure drop versus superficial fluid velocity was thus obtained (see Appendix C.4).

The downward velocities of annular particles were determined at the flat wall of the half column by measuring with a stop watch the time taken for a tracer particle to move a small vertical distance of 4 cm. At any given bed

level, z, particle downward velocities were measured at five radial positions as illustrated in Figure 3.7. At each radial position, three measurements were taken on each side of the spout, resulting in a total of six readings, from which an average value was determined for this location. The volumetric solids flow in a full column annulus at this level was then given by

$$G_a(z) = \int_{R_s}^{R_c} [V_p(r)(1-\epsilon_a)(2\pi r)]dr \qquad 3.8$$

where $V_p(r)$ was the measured downward particle velocity at radial distance, r. The radial-averaged particle velocity was determined from the following equation:

$$\overline{V}_p = \frac{\int_{R_s}^{R_c} [V_p(r)(2\pi r)]dr}{\int_{R_s}^{R_c} (2\pi r)dr} \qquad 3.9$$

3.7.6 RADIAL AND LONGITUDINAL PRESSURE PROFILES

Another pressure probe (Figure 3.6b) was constructed. The main body consisted of two stainless tubes of 3.1 and 9.5 mm OD, respectively. The inner tube was sealed off at the bottom end and bent at an angle of 90°. A short piece of stainless steel tube of 3.1 mm OD was silver soldered perpendicularly onto a hole drilled on the outer shell, making a vertical separation of 3 cm with the bent section.

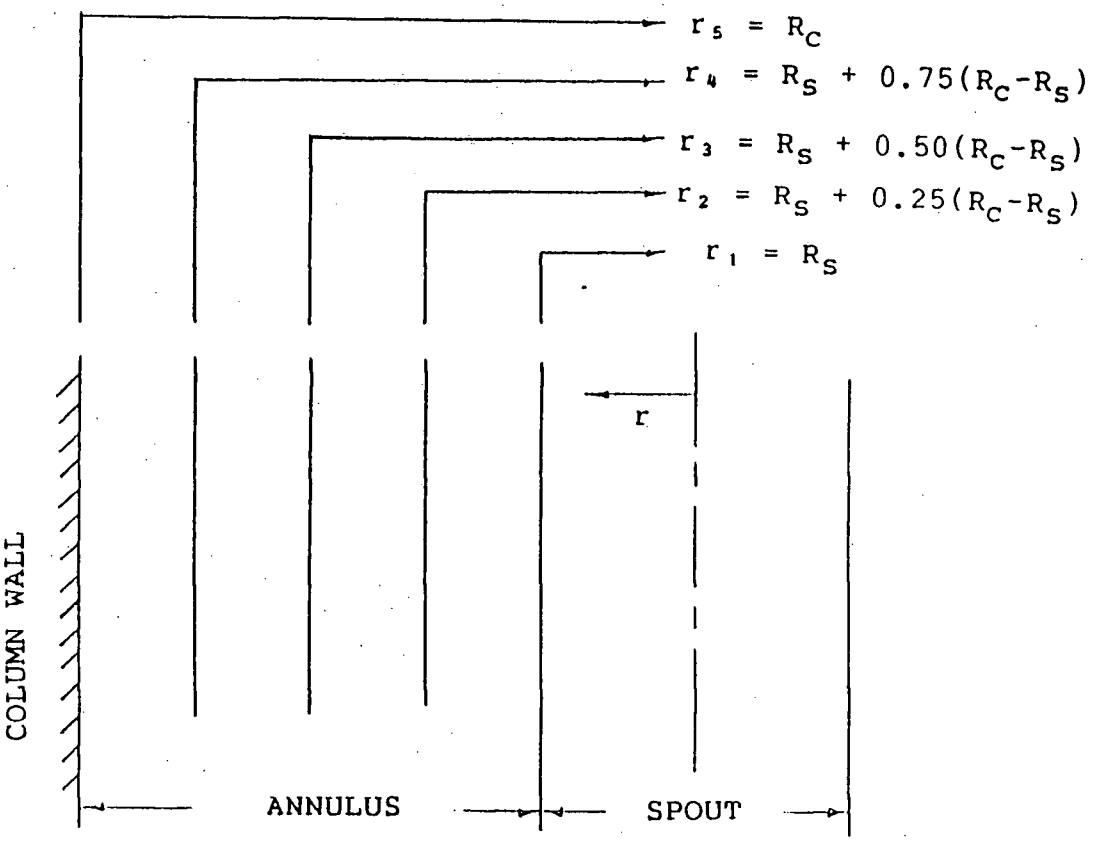

Figure 3.7 Radial position for particle velocity measurements

Holes of 0.8 mm were drilled on these two pieces. This probe could be used to measure the differential pressure drops. For the pressure profile studies, only the outlet corresponding to the bottom tip was connected to a manometer. This probe was inserted through port T3 of the top cover (Figure 3.5) in the same manner as described in Section 3.7.5. At any fixed bed level, z, the bed pressures were measured at five different radial positions in the annulus by rotating the probe. The average of these five measurements was taken as the average longitudinal value at the given level.

3.7.7 REGIME MAP

A regime map is a plot of bed height versus fluid flowrate for a given fluid-solid system. A typical regime map includes five regions. These are fixed bed, steady spouting, progressively incoherent spouting, bubbling and slugging. For bed heights ranging from zero to about 1.20 H_m, all the transitional points were located by varying the fluid flowrates. To be consistent with the method of measuring U_{ms}, all the transitional points were found with decreasing flow. At any given bed height, the fluid flowrate was first increased gradually during which the regime transformation was noted by means of visual observations. The flowrate was then decreased slowly and the transitional points were thus determined. This procedure of decreasing

flow was found to yield reproducible results.

3.7.8 FOUNTAIN HEIGHT

The fountain height is the distance from the annulus bed surface to the fountain top. It was measured directly against the front wall.

3.8 ERROR CALCULATION

When comparing experimental values with predicted values, the following definitions are used:

$$\% \text{ dev} = \frac{\text{CAL} - \text{EXP}}{\text{EXP}} \times 100\% \qquad 3.10$$

$$\text{RMS } \% \text{ ERROR} = \sqrt{[\Sigma(\% \text{ dev})^2]/M} \qquad 3.11$$

$$\text{AVE ERR} = [\Sigma(\% \text{ dev})]/M \qquad 3.12$$

where

EXP = experimental value

CAL = predicted value

M = number of data points

4. STABILITY OF SPOUTING

4.1 STABILITY

4.1.1 EFFECT OF TEMPERATURE ON SPOUTABILITY

Table 4.1 shows the spoutability of Ottawa sand under different combinations of d_p, D_i and T_s. The results obtained at room temperature are in excellent agreement with the criterion proposed by Chandnani (1984), that is, stable spouting will occur only if $D_i/d_p < 25.4$. This criterion does not predict any effect with bed temperature. In fact, it was derived from experiments carried out at room conditions with "only" air as spouting medium. However, it can be seen from Table 4.1 that the bed temperature does have some significant effect on the spoutability. For instance, stable spouting at $D_i/d_p = 20.2$ is obtainable at room temperature but not at 300 °C or higher. However, Table 4.1 also shows that stable spouting is achievable at D_i/d_p = 21.3 at all four temperature levels, which is slightly inconsistent with the observations in the previous case. These two values of D_i/d_p are so similar that the discrepancy may be due to the uncertainty in d_p. Another possible explanation is that the ratio, D_i/d_p, may not be sufficient to determine spoutability, especially for non-spherical particles.

Table 4.1 Spoutability of sand particles at different conditions

d_p (mm)	D_i (mm)	D_i/d_p	D_c/D_i	D_c/d_p	Stable Spouting Possible ? 20	170	300	420°C
1.665	12.70	7.6	12.3	93	YES	YES	YES	YES
1.250	12.70	10.2	12.3	124	YES	YES	YES	YES
1.665	19.05	11.4	8.2	93	YES	YES	YES	YES
0.945	12.70	13.4	12.3	165	YES	YES	YES	YES
1.250	19.05	15.2	8.2	124	YES	YES	YES	YES
1.665	26.64	16.0	5.8	93	YES	YES	YES	YES
0.945	19.05	20.2	8.2	165	YES	YES	NO	NO
1.250	26.64	21.3	5.8	124	YES	YES	YES	YES
0.945	26.64	28.2	5.8	165	NO	NO	NO	NO

Based on the results obtained at D_i/d_p = 20.2, the criterion proposed by Chandnani is not completely satisfactory at higher temperatures, at least for non-spherical particles. Modification by including the effect of bed temperature is necessary. Since both gas density and viscosity change with temperature, it may be more appropriate to use these two variables instead of temperature to develop a criterion of the form

$$f(D_i, d_p, \phi, \rho_f, \mu) < \lambda \qquad 4.1$$

where λ is some critical value or parameter. In this study, however, there were not sufficient data to derive such a criterion.

4.1.2 EFFECT OF TEMPERATURE ON SPOUTING CHARACTERISTICS

The obvious effect of increasing temperature is the decrease in H_m (Sections 4.2 and 4.3). When operating at bed heights well below H_m, increasing the bed temperature has no observable effect on the bed behaviour. However, as bed heights increased, the spout characteristics changed significantly with increasing temperature.

At room temperature, when $H \simeq H_m$, fluidization was observed at the top surface of the annulus. This was indicated by the upward particle entrainment at the annulus surface and the slightly higher voidage at the upper part of

the annulus. In addition, the spout diameter was found to expand at the bed surface and the resulting fountain height was relatively low (compared to the fountain height of a shallower bed at similar U/U_{ms} condition). Further increase in bed heights produced more annulus fluidization and also caused the spouting jet to submerge below the bed surface, discharging periodically as bubbles. Stable spouting subsequently became unachievable.

As the bed temperature increased, the spouting characteristics for bed heights near H_m were quite different from those observed at room conditions. For the high temperature cases (i.e., T_S = 420 °C), the spout-annulus interface near the bed surface was found to be slightly unstable. The interface followed a rippling motion. As bed heights approached H_m, the intensity of this instability increased which led to the tendency towards pulsing and choking in the spout. Just above H_m, the amplitude of these ripples became greater than the spout radius, resulting in a pinch point and the formation of a bubble. This regime transformation was obviously different from that at cold conditions. Though the spout and fountain shapes were similar to those at room temperature, fluidization in the annulus was not observed at all.

4.2 REGIME MAPS

Figure 4.1 shows the physical appearance of four different flow regimes in a typical spouted bed. Stable spouting can be characterized by two main features, a steady fountain with little fluctuation and a stable spout-annulus interface (Figure 4.1a). When rippling movement starts to appear at the spout-annulus interface near the bed surface, causing the fountain shape to get distorted and the fountain height to oscillate, the bed becomes less stable and this phenomenon is described as "progressively incoherent spouting" (Figure 4.1b). Bubbling sets in when the spouting jet cannot penetrate through the bed. Bubbles then form below the bed surface and discharge periodically (Figure 4.1c). If these bubbles grow to the size similar to that of the column diameter before they reach the bed surface, slugging will then occur (Figure 4.1d).

In the present study, regime maps for a fixed particle and a fixed orifice diameter (d_p = 1.25 mm, D_i = 19.05 mm) are presented at four different air temperatures in Figures 4.2, 4.3, 4.4 and 4.5, respectively. The effect of temperature was clearly demonstrated by the reduction of H_m with increasing temperature. Moreover, at higher temperatures, all other regime boundaries generally shift downwards, resulting in smaller regime areas for "Steady Spouting". Presumably, if the temperature were increased to

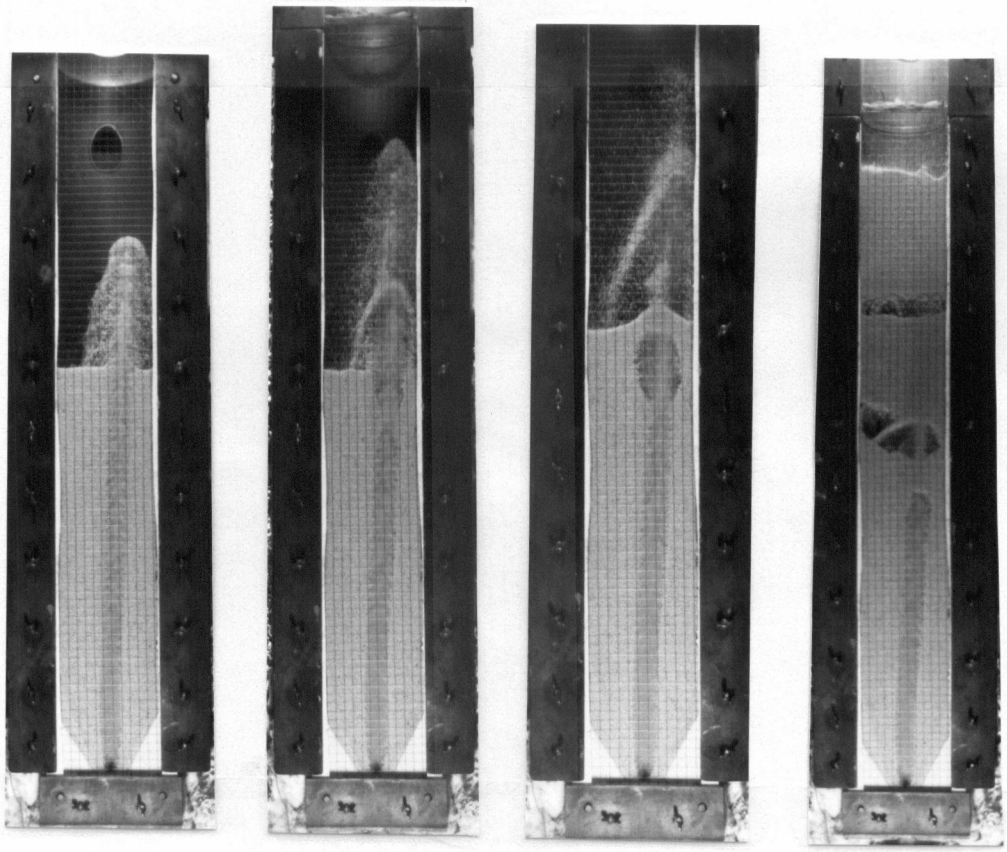

(a) (b) (c) (d)

Figure 4.1 Pictures of different regimes.

(a) steady spouting

(b) progressively incoherent spouting

(c) bubbling

(d) slugging

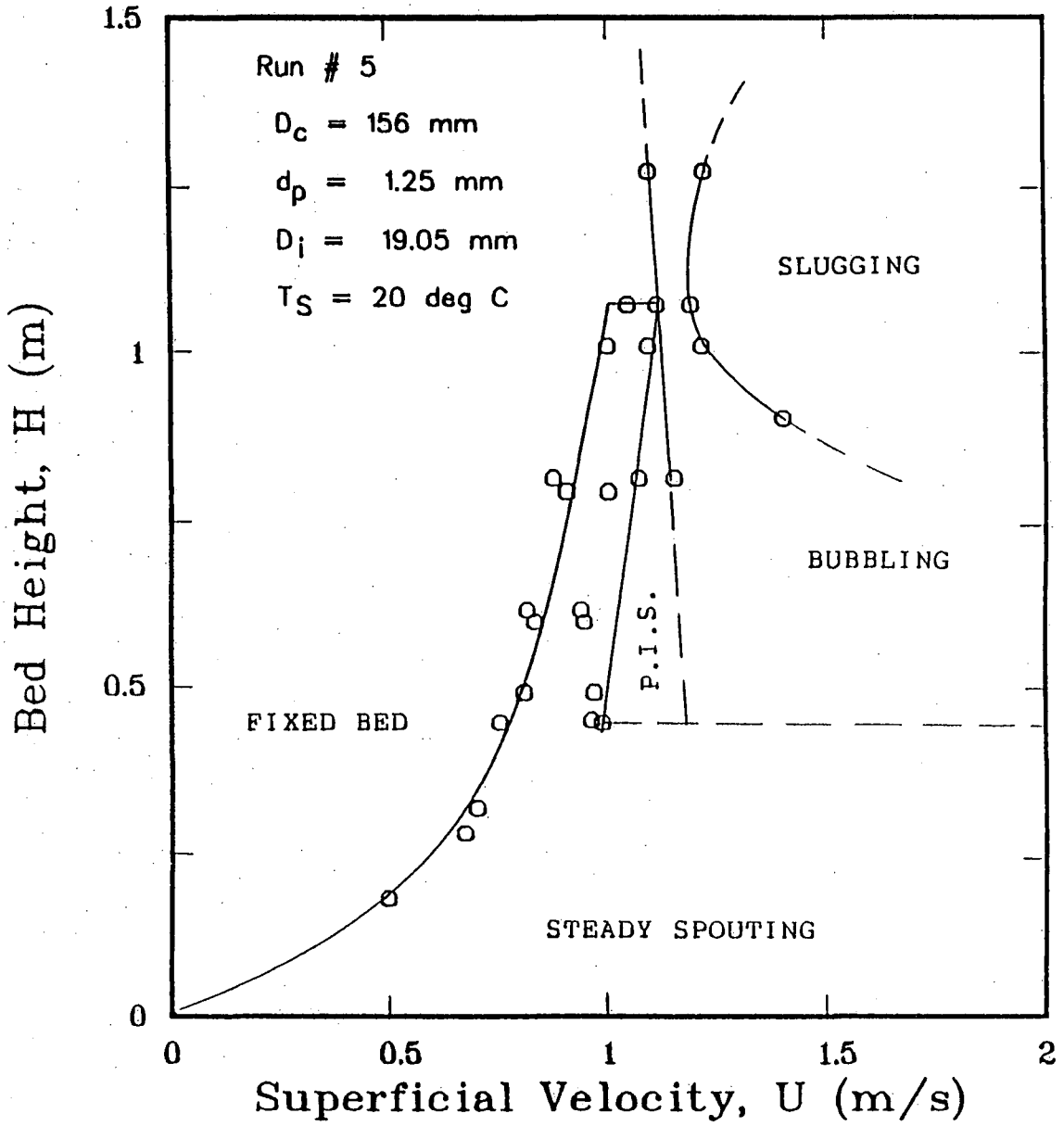

Figure 4.2 Regime map for air-sand system at 20 °C

P.I.S. = progressively incoherent spouting

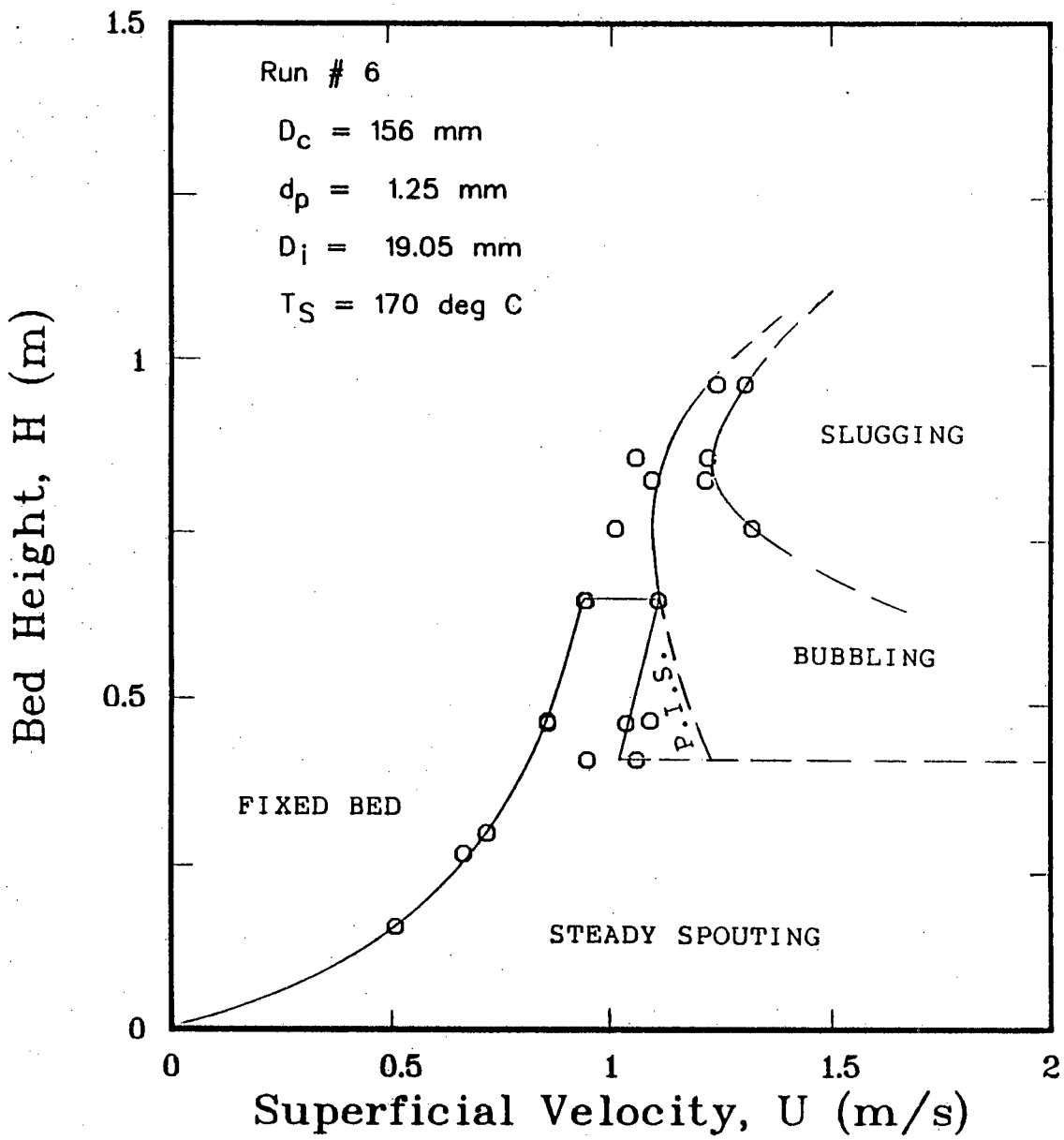

Figure 4.3 Regime map for air-sand system at 170 °C

P.I.S. = progressively incoherent spouting

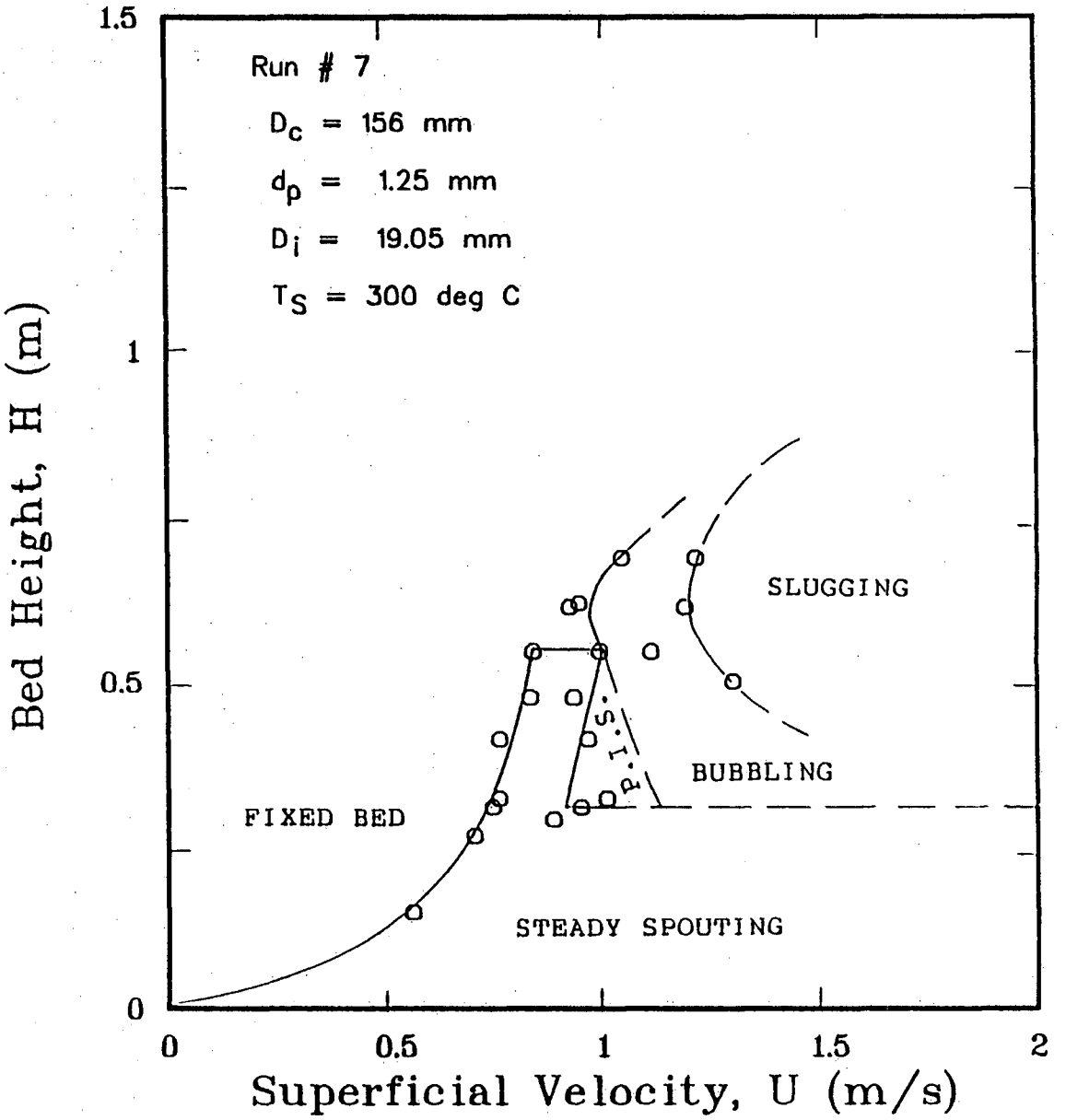

Figure 4.4 Regime map for air-sand system at 300 °C

P.I.S. = progressively incoherent spouting

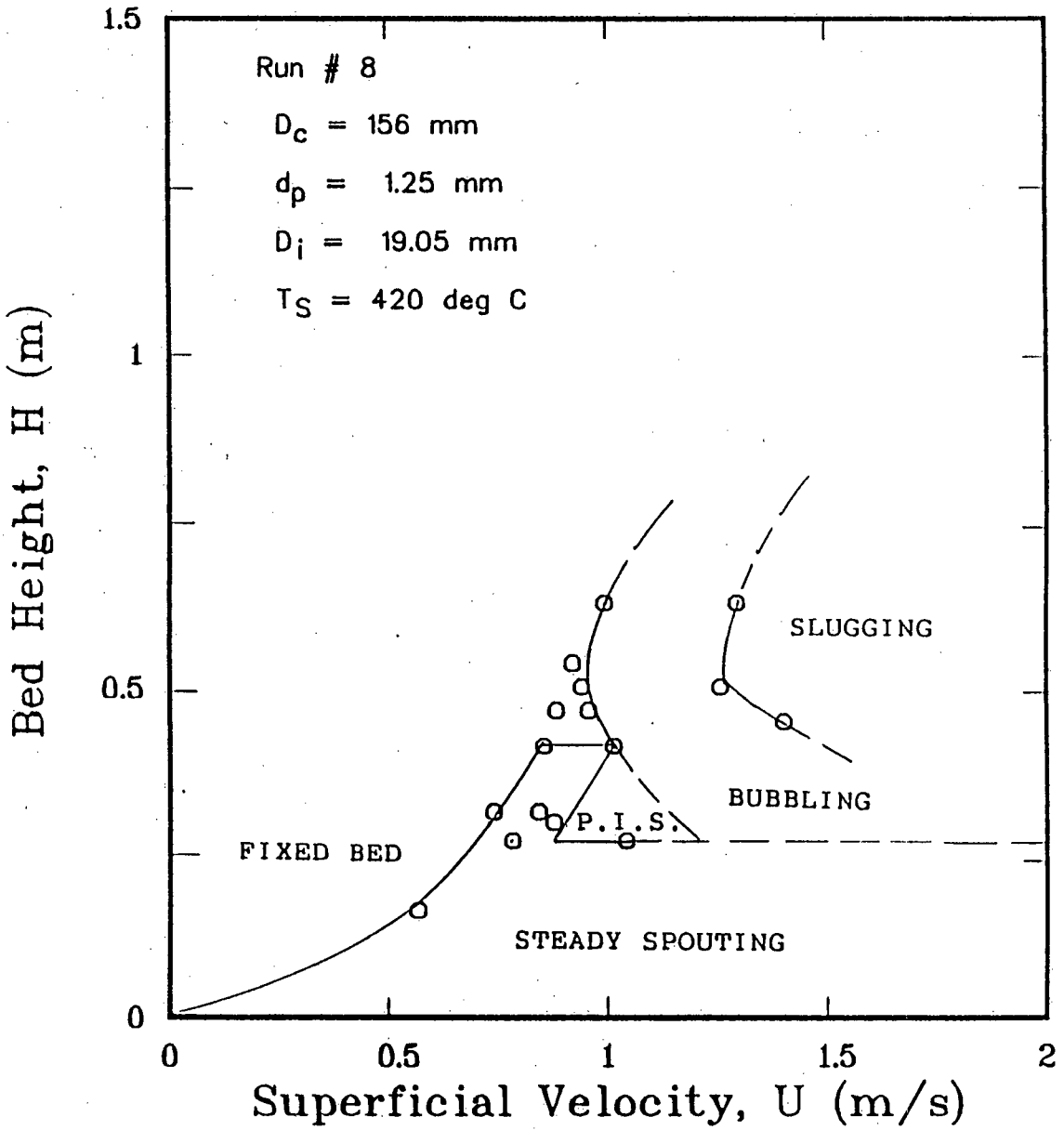

Figure 4.5 Regime map for air-sand system at 420 °C

P.I.S. = progressively incoherent spouting

still higher levels (i.e., > 420 °C), the region of "Steady Spouting" would eventually decrease to nil and the corresponding regime map would be similar to that of Figure 2.4 in Chapter 2.

4.3 MAXIMUM SPOUTABLE BED HEIGHT

4.3.1 EFFECT OF ORIFICE DIAMETER

Figure 4.6 illustrates the effect of orifice diameter on H_m at four different temperature levels. Increasing D_i produces lower values of H_m, provided that other operating parameters are fixed. This observed trend of H_m is consistent with that of Equation 2.8.

4.3.2 EFFECT OF PARTICLE DIAMETER

According to Equation 2.8, H_m goes through a maximum at

$$(d_p)_{crit} = 60.6\left[\frac{\mu^2}{g(\rho_p-\rho_f)\rho_f}\right]^{1/3} \qquad A.14$$

which was obtained by differentiating Equation 2.8 with respect to d_p, after substituting Ar from Equation A.4a, and then setting $dH_m/d(d_p)$ to zero. For air spouting of sand particles at atmospheric pressure, the critical values of d_p were calculated to be 1.3, 1.8, 2.3 and 2.6 mm at 20, 170, 300 and 420 °C, respectively. H_m increases with increasing d_p below the critical value and decreases with increasing d_p

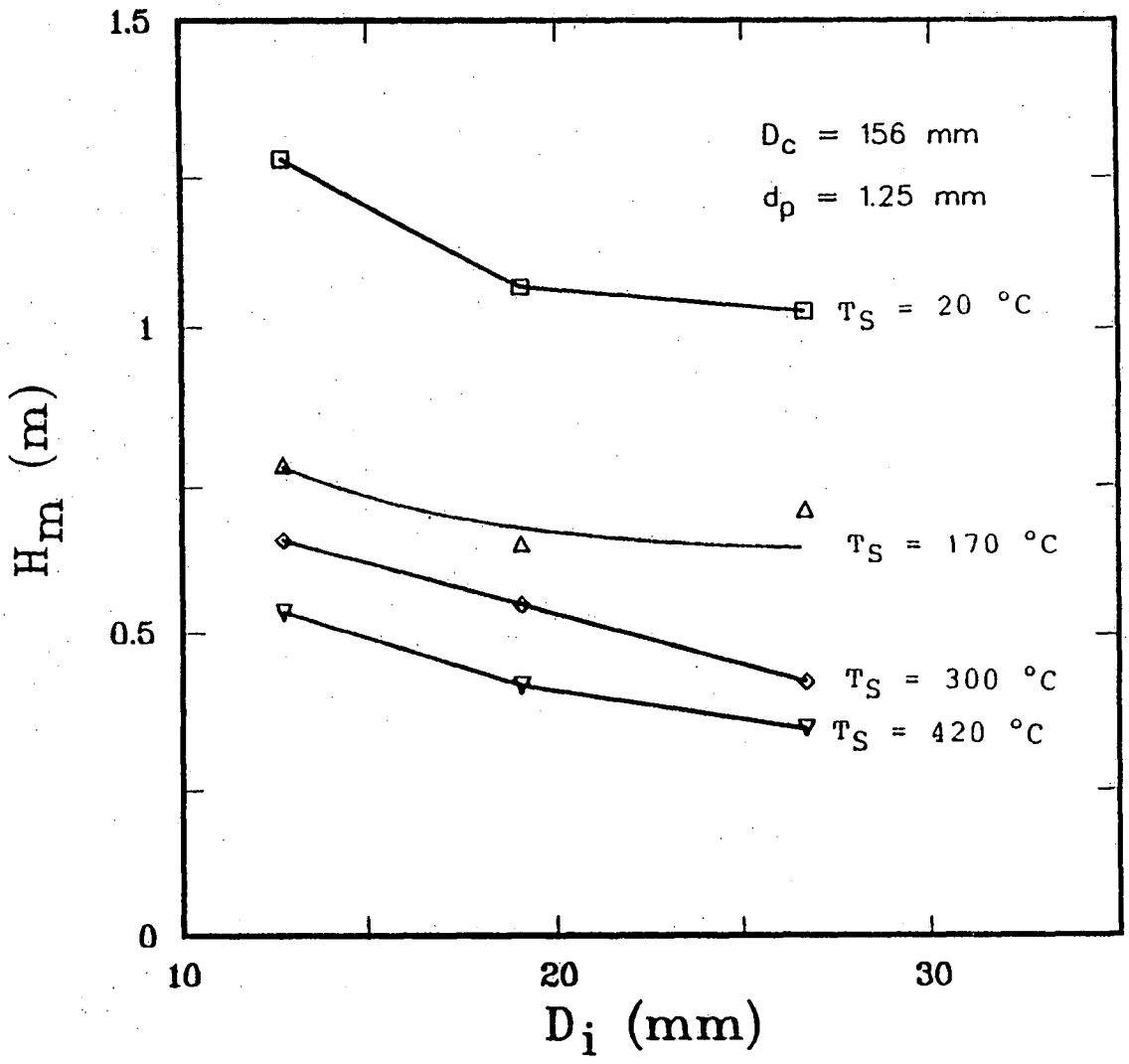

Figure 4.6 Effect of orifice diameter on maximum spoutable bed height for different temperatures

above it. The qualitative effect of increasing d_p as predicted by Equations 2.8 and A.14 was observed at 170, 300 and 420 °C but not consistently at room temperature (Figure 4.7). Equations 2.8 and A.14 are based on the approximation of Wen and Yu, ie., Equations 2.6a and 2.6b. The corresponding values of ϕ and ϵ_{mf} are 0.6689 and 0.4744 respectively. The more general form of Equation A.14, without the Wen-Yu approximation, is

$$(d_p)_{crit} = 29.52\left[\frac{(1-\epsilon_{mf})^2}{\epsilon_{mf}^3\phi^3}\right]^{1/3}\left[\frac{\mu^2}{g(\rho_p-\rho_f)\rho_f}\right]^{1/3} \qquad A.16$$

The above equation clearly indicates that $(d_p)_{crit}$ decreases with increasing ϕ. The effect of ϵ_{mf} is, however, less obvious. If Equation A.16 is differentiated with respect to ϵ_{mf} it can be shown that for $0 < \epsilon_{mf} < 1$, $d(d_p)_{crit}/d\epsilon_{mf} < 0$, implying that $(d_p)_{crit}$ decreases with increasing increasing ϵ_{mf} over this range. Experimentally ϵ_a was found to be 0.5 but ϕ, on the other hand, was not measured. If ϵ_{mf} is assumed equal to ϵ_a and ϕ equal to or greater than 0.6689 (which seems reasonable for sand), the resulting $(d_p)_{crit}$ would be smaller than the previously estimated values. This could partly explain the discrepancy at room temperature reported earlier. For instance, the combined effect of ϕ and ϵ_{mf} may lower the $(d_p)_{crit}$ to a value between 0.945 and 1.25 mm at room temperature and yet greater than 1.665 mm for temperatures of 170 °C and higher. In the room temperature case, experimental results suggest a

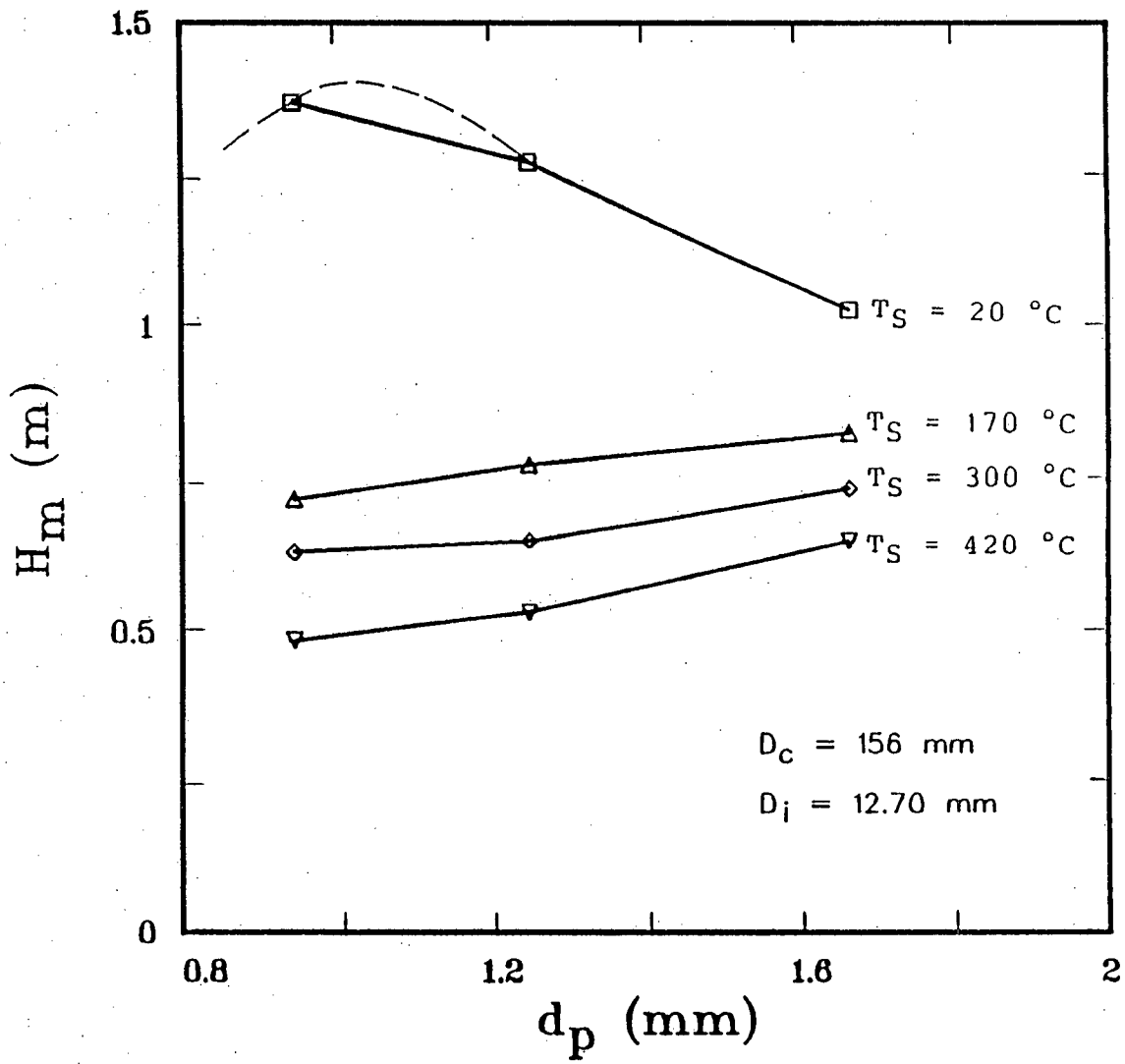

Figure 4.7 Effect of particle diameter on maximum spoutable bed height for different temperatures

decrease of H_m with increasing d_p. This trend could be interpreted here as: H_m increased with d_p to a maximum at $(d_p)_{crit}$ beyond which H_m decreased with increasing d_p. The dashed line in Figure 4.7 illustrates this interpretation. In the higher temperature cases, H_m simply increased with d_p because $d_p < (d_p)_{crit}$. This concept of $(d_p)_{crit}$ also helps to explain why the effect of temperature appears to be greater for smaller particles as shown in Figure 4.8.

4.3.3 EFFECT OF TEMPERATURE

The effect of temperature on H_m was examined by differentiating Equation 2.8 with respect to Ar while other variables, such as D_c, D_i and d_p were kept constant. It was found that $dH_m/dAr > 0$ for all values of Ar. This implies that H_m increases with Ar. For gas spouting, with increasing temperature, gas density decreases while viscosity increases, which results in a lower value of Ar and therefore a smaller value of H_m. This trend was supported qualitatively by the experimental results as shown in Figures 4.6, 4.7, 4.8 and 4.9. Equation 2.8 plus two other correlations are also included in the latter figure for direct comparison. Equation 2.9 (Littman et al., 1979) predicts increasing H_m with increasing temperature, which contradicts the experimental observations. It is important to point out here that under normal circumstances, Equations 2.12a and 2.12b (Morgan and Littman, 1982) should be used

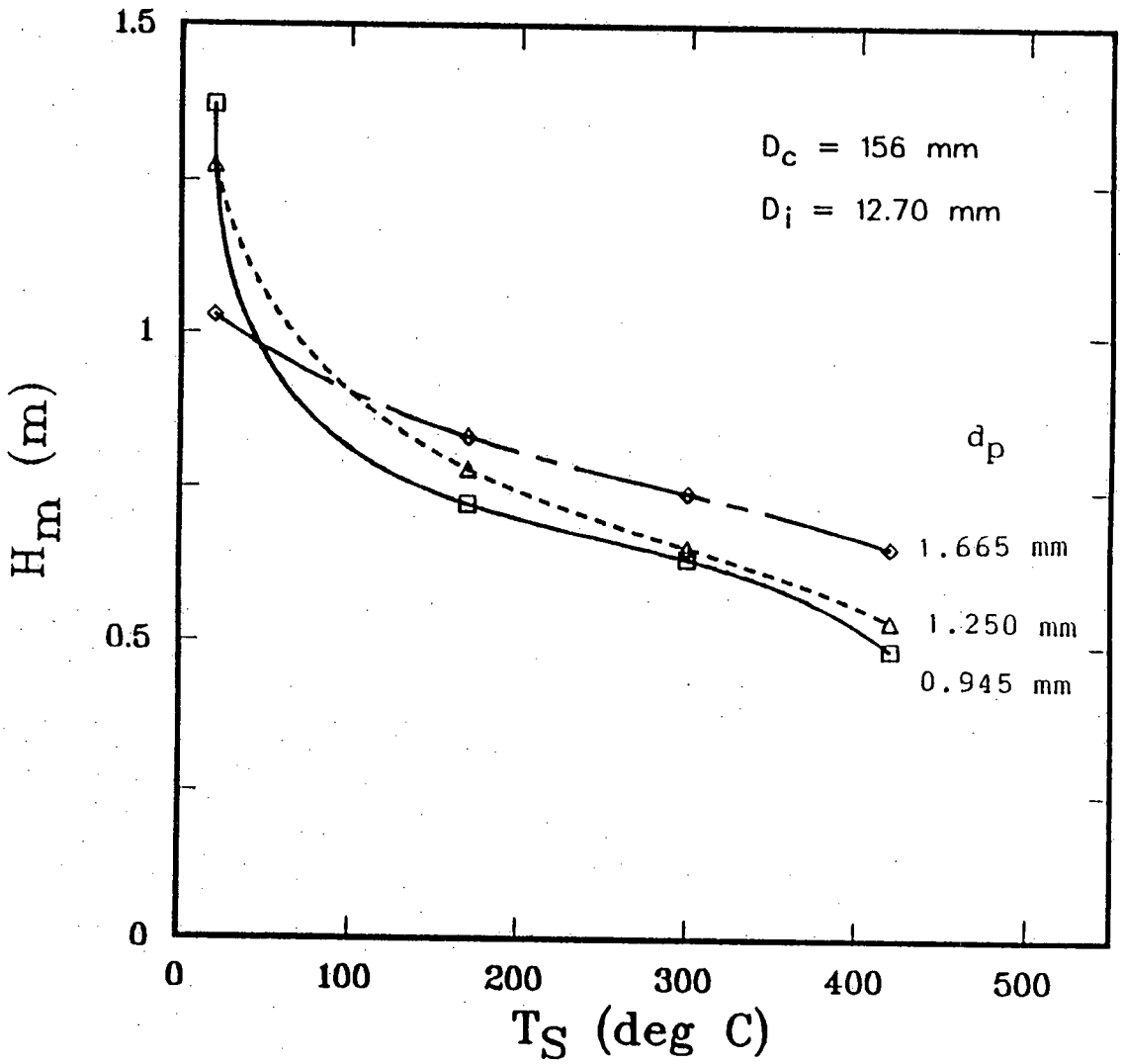

Figure 4.8 Effect of temperature on maximum spoutable bed height for different particle diameters

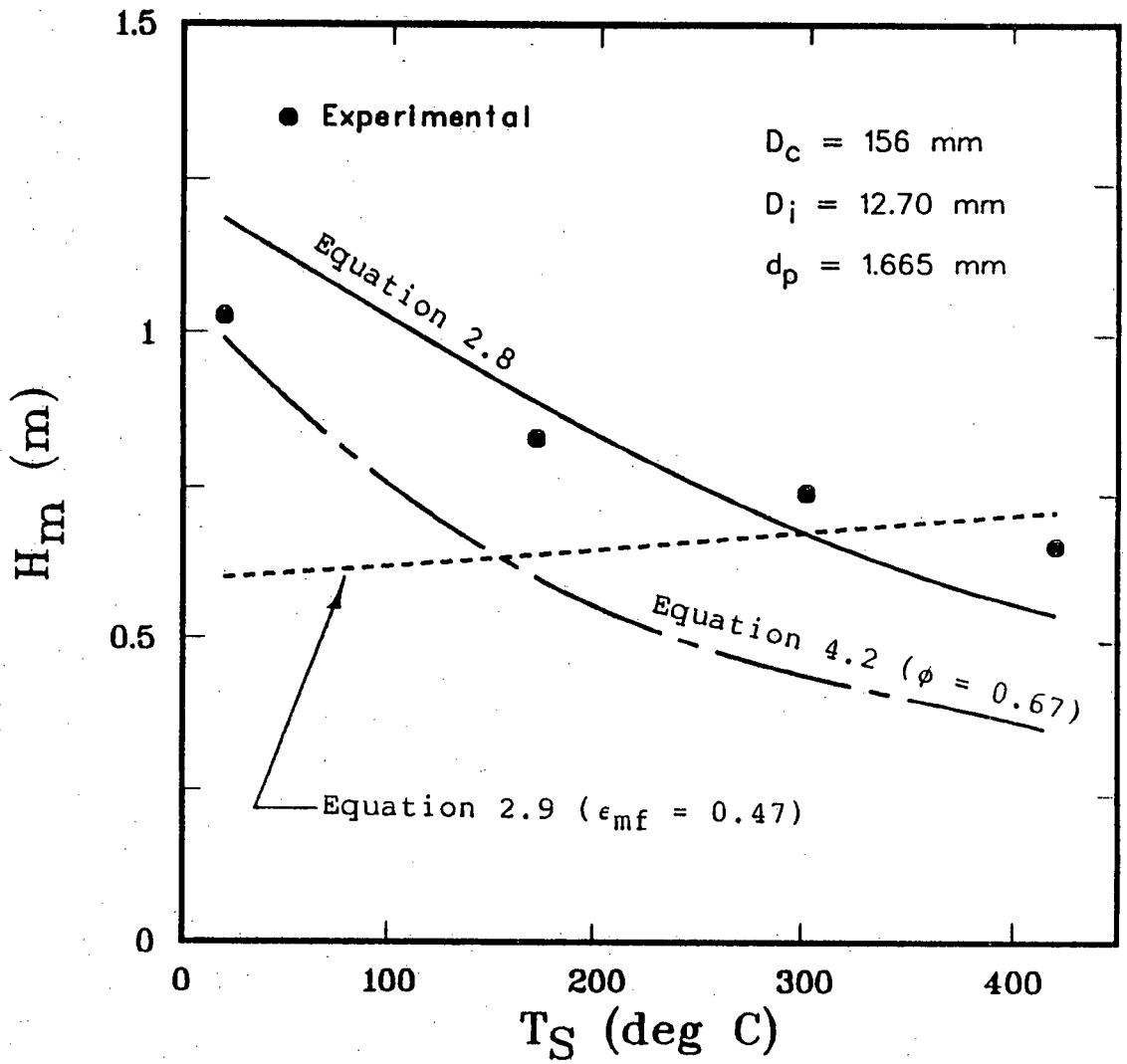

Figure 4.9 Effect of temperature on maximum spoutable bed height (Comparison between experimental data and predictions)

instead of Equation 2.9 because the latter is restricted to spherical particles only. Unfortunately, Equations 2.12a and 2.12b could not be applied since values of A_ϕ were outside the required ranges, while A was within the range of applicability of Equation 2.9. The third correlation in Figure 4.9 is that of Malek and Lu (1965), rendered fully dimensionless:

$$\frac{H_m}{D_c} = 336\left[\frac{D_c}{d_p}\right]^{0.75}\left[\frac{D_c}{D_i}\right]^{0.4}\left[\frac{\rho_f}{\rho_p}\right]^{1.2}\left[\frac{1}{\phi}\right]^2 \qquad 4.2$$

The shape factor, ϕ, in Equation 4.2 was arbitrarily taken as 0.6689, to be consistent with that implicitly in Equation 2.8. Although Equation 4.2 is entirely empirical, it manages to predict the correct trend of H_m with increasing temperature.

4.3.4 EFFECT OF FLUID DENSITY AND VISCOSITY

Table 4.2 shows how H_m varies with ρ_f and μ. At 20 °C, helium and air have similar μ but different ρ_f. By comparing the two experimental values of H_m, the effect of ρ_f at constant μ can be examined. H_m is higher for air spouting, implying that H_m increases with increasing ρ_f. On the other hand, the effect of μ at constant ρ_f can be seen from the remaining columns in Table 4.2. It is clear that H_m increased with decreasing μ. In other words, spouting will be more favorable if the spouting gas is more dense and less viscous. The effects of gas density and viscosity on

Table 4.2 Effects of μ and ρ_f on H_m. D_c = 156 mm, D_i = 19.05 mm and d_p = 1.25 mm

Spouting gas	He	Air	Air	Air	CH_4
T_S (°C)	20	20	170	300	20
ρ_f (kg/m^3)	0.170	1.259	0.815	0.624	0.707
μ (10^{-5}kg/m·s)	1.94	1.80	2.35	2.85	1.09
H_m (m)	0.533	1.067	0.648	0.546	1.380

H_m are consistent with the observed trend of H_m with temperature as reported in Section 4.3.3.

4.3.5 CORRELATION OF EXPERIMENTAL DATA

Table 4.3 lists all the experimental values of H_m versus the calculated values by Equation 2.8 (McNab and Bridgwater, 1977). The graphical comparison is shown in Figure 4.10 with the solid line (ie., b = 1.11) representing Equation 2.8. Although there is some scatter, it is not any worse, in fact is considerably better, than that of Figure 2.2. However, the experimental data of this study suggest a "b" value higher than 1.11. Appling a least squares fit to the present data yielded b = 1.23. The resulting equation is shown in Figure 4.10 as a dashed line.

4.4 MECHANISMS OF SPOUT TERMINATION AT MAXIMUM SPOUTABLE BED HEIGHT

Chandnani and Epstein (1986) suggested a procedure for estimating H_m if the mechanism for spout termination were due to choking. The spout was compared to a standpipe in which a fluid carried solids upwards. Choking occurred when the fluid velocity was reduced below a critical value, U_c. This critical velocity could be estimated from (Leung, 1980)

$$2gD_s(\epsilon_c^{-4.7}-1)/(U_c-U_t)^2 = 0.00874\rho_f^{0.77} \qquad 4.3$$

Table 4.3 Maximum spoutable bed height, experimental versus predictions. Sand, ρ_p = 2600 kg/m^3, D_c = 156 mm

Run #	Temp (°C)	d_p (mm)	D_i (mm)	ρ_f (kg/m^3)	ν (kg/ms)	Expt. H_m (m)	Pred. H_m e (m)	% dev
1-1	20	0.945	19.05	1.246	1.80E-05	1.168	0.866	-25.85
2-1	170	0.945	19.05	0.802	2.35E-05	0.419	0.485	15.85
5-1	20	1.250	19.05	1.259	1.80E-05	1.067	0.940	-11.88
6-1	170	1.250	19.05	0.815	2.35E-05	0.648	0.616	-4.91
7-1	300	1.250	19.05	0.624	2.85E-05	0.546	0.420	-23.06
8-1	420	1.250	19.05	0.514	3.20E-05	0.413	0.313	-24.10
9-1	20	1.665	19.05	1.244	1.80E-05	1.010	0.906	-10.25
10-1	170	1.665	19.05	0.824	2.35E-05	0.800	0.682	-14.81
11-1	300	1.665	19.05	0.629	2.85E-05	0.721	0.516	-28.49
12-1	420	1.665	19.05	0.515	3.20E-05	0.629	0.411	-34.64
17-1	20	1.250	26.64	1.252	1.80E-05	1.026	0.750	-26.86
18-1	170	1.250	26.64	0.816	2.35E-05	0.705	0.493	-30.07
19-1	300	1.250	26.64	0.623	2.85E-05	0.419	0.336	-19.91
20-1	420	1.250	26.64	0.511	3.20E-05	0.343	0.250	-27.23
21-1	20	1.665	26.64	1.254	1.80E-05	0.978	0.727	-25.64
22-1	170	1.665	26.64	0.822	2.35E-05	0.838	0.545	-35.02
23-1	300	1.665	26.64	0.631	2.85E-05	0.679	0.413	-39.19
24-1	420	1.665	26.64	0.517	3.20E-05	0.540	0.329	-38.98
25-1	20	0.945	12.70	1.276	1.80E-05	1.372	1.148	-16.29
26-1	170	0.945	12.70	0.814	2.35E-05	0.724	0.643	-11.25
27-1	300	0.945	12.70	0.622	2.85E-05	0.635	0.396	-37.67
28-1	420	0.945	12.70	0.511	3.20E-05	0.486	0.278	-42.83
29-1	20	1.250	12.70	1.261	1.80E-05	1.276	1.233	-3.39
30-1	170	1.250	12.70	0.818	2.35E-05	0.781	0.809	3.58
31-1	300	1.250	12.70	0.629	2.85E-05	0.654	0.553	-15.39
32-1	420	1.250	12.70	0.515	3.20E-05	0.533	0.411	-22.83
33-1	20	1.665	12.70	1.245	1.80E-05	1.029	1.188	15.46
34-1	170	1.665	12.70	0.820	2.35E-05	0.832	0.891	7.14
35-1	300	1.665	12.70	0.630	2.85E-05	0.743	0.676	-9.00
36-1	420	1.665	12.70	0.519	3.20E-05	0.654	0.541	-17.26
37-1	20	1.250	19.05	0.707	1.09E-05	1.380	1.079	-21.80
38-1	170	1.250	19.05	0.170	1.94E-05	0.533	0.290	-45.57

e by Equation 2.8

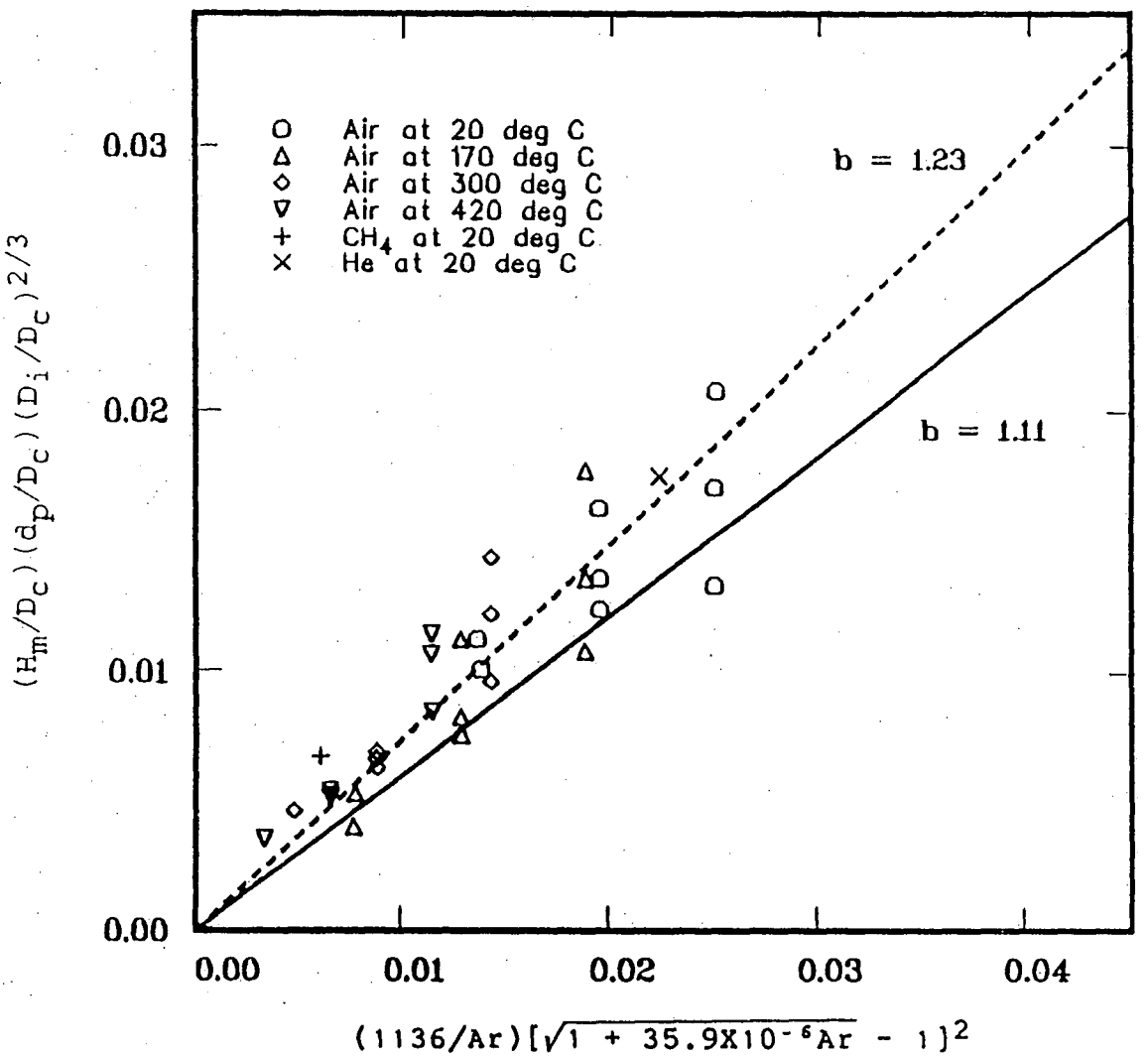

Figure 4.10 Comparison between experimental data and Equation 2.8

in which ϵ_c, the voidage at choking, could be calculated from the following equation (Smith, 1978):

$$(1-\epsilon_c)^{-2} = \left[\frac{2\rho_p}{\rho_p-\rho_f}\right](N\epsilon_c^{N-1})2\left[\frac{U_t^2}{gD_s}\right] \qquad 4.4$$

where N is the Richardson-Zaki index. If choking of spout occurred at H_m, then U_{sH_m} and D_{sH_m} would be equal to U_c and D_s, respectively. Knowing U_{sH_m}, U_{aH_m} and D_{sH_m}, the minimum spouting superficial velocity, U_m, could be determined and thus also H_m via Equation 2.1a.

The accuracy of this method depends very strongly on the value of D_{sH_m} and whether choking indeed occurs at H_m. Experimentally, D_s was found to be larger at $z = H_m$ than at lower levels. On the other hand, choking if it existed, generally occurred below the bed surface. Thus using the value of D_s at $z = H_m$ is somewhat inappropriate. This uncertainty of D_{sH_m} makes it difficult to apply the above method directly to estimate H_m for cases where choking has been observed. However, an attempt was made to compare some experimental values of U_{sH_m} with the corresponding calculated values of U_c. D_{sH_m} was arbitrarily taken as the average spout diameter (defined in Equation 3.7). These results are listed in Table 4.4. Fluidization of annular solids appears to be the spouting termination mechanism at room temperatures but it becomes less dominant at higher temperatures as indicated by the increasing difference between U_{aH_m} and U_{mf} (Figure 4.11). In addition, Figure

Table 4.4 Comparison between U_c and U_{sH_m}. Sand, d_p = 1.25 mm, D_c = 156 mm

Run #	TEMP (°C)	D_i (mm)	U_{ms} (m/s)	D_{sH_m} (m)	N	ϵ_c	U_c (m/s)	U_{sH_m} (m/s)	U_{mf} (m/s)	U_{aH_m} (m/s)
5-1	20	19.05	1.100	0.0342	2.5744	0.9353	7.60	9.00	0.702	0.70
6-1	170	19.05	1.009	0.0309	2.8201	0.9501	7.74	8.76	0.705	0.69
7-1	300	19.05	0.931	0.0296	2.9365	0.9559	7.95	8.44	0.666	0.65
8-1	420	19.05	0.871	0.0283	3.0163	0.9599	8.09	9.64	0.634	0.57
17-1	20	26.64	1.108	0.0344	2.5749	0.9351	7.64	9.03	0.702	0.70
18-1	170	26.64	1.048	0.0334	2.8199	0.9480	8.04	8.47	0.705	0.69
19-1	300	26.64	0.949	0.0300	2.9371	0.9556	8.01	8.69	0.666	0.65
20-1	420	26.64	0.947	0.0288	3.0174	0.9597	8.16	10.61	0.634	0.57
29-1	20	12.70	1.153	0.0331	2.5737	0.9364	7.47	10.72	0.701	0.70
30-1	170	12.70	0.959	0.0295	2.8195	0.9513	7.56	8.16	0.705	0.69
31-1	300	12.70	0.847	0.0292	2.9353	0.9561	7.89	6.26	0.665	0.65
32-1	420	12.70	0.801	0.0280	3.0159	0.9602	8.04	7.72	0.633	0.57

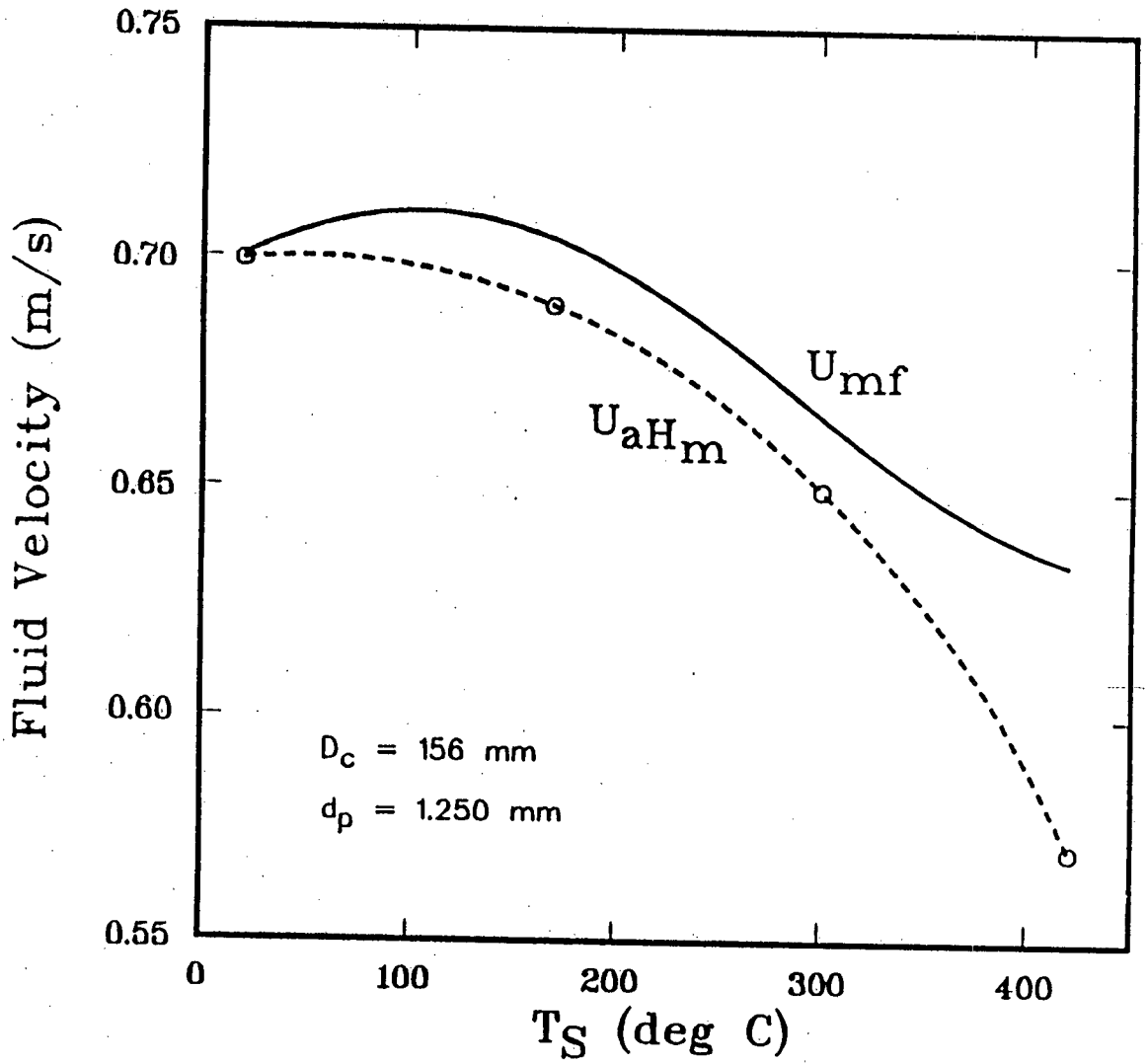

Figure 4.11 Effect of temperature on U_{mf} and U_{aH_m}
Sand, d_p = 1.25 mm, D_c = 156 mm

4.12a shows that U_{sH_m} approaches U_c at high temperatures and eventually becomes smaller than U_c. This means that as temperatures increases, the choking of the spout begins to overtake annular fluidization as the controlling factor. These results are consistent with experimental observations (Section 4.1.2). Figures 4.12b and 4.12c, however, do not show the same conclusion. In these two cases, U_{sH_m} was found to be greater than U_c even at high temperatures. The inconsistency is probably due to the fact that U_{sH_m} is very sensitive to the value of D_{sH_m}. A small change in D_{sH_m} can cause significant variation in U_{sH_m}. Additional discrepancy may also be attributed to the inexactness of Equations 4.3 and 4.4. An alternate way to interpret the results is to examine the ratios of D_i/d_p. These values are 10.2, 15.2 and 21.3, respectively, in Figures 4.12a, 4.12b and 4.12c. It appears that the choking of the spout at high temperatures only occurs at a low value of D_i/d_p as shown in Figure 4.12a. At higher ratios, spout termination (at high temperatures) may be due to the growth of instability at the spout-annulus interface.

This procedure of Chandnani and Epstein (1986) requires accurate values of D_{sH_m} in order to yield reasonable estimates of H_m for cases where choking is the termination mechanism. Unless there is a way of accurately determining D_{sH_m} without conducting an actual experiment, it is not very useful for design purposes.

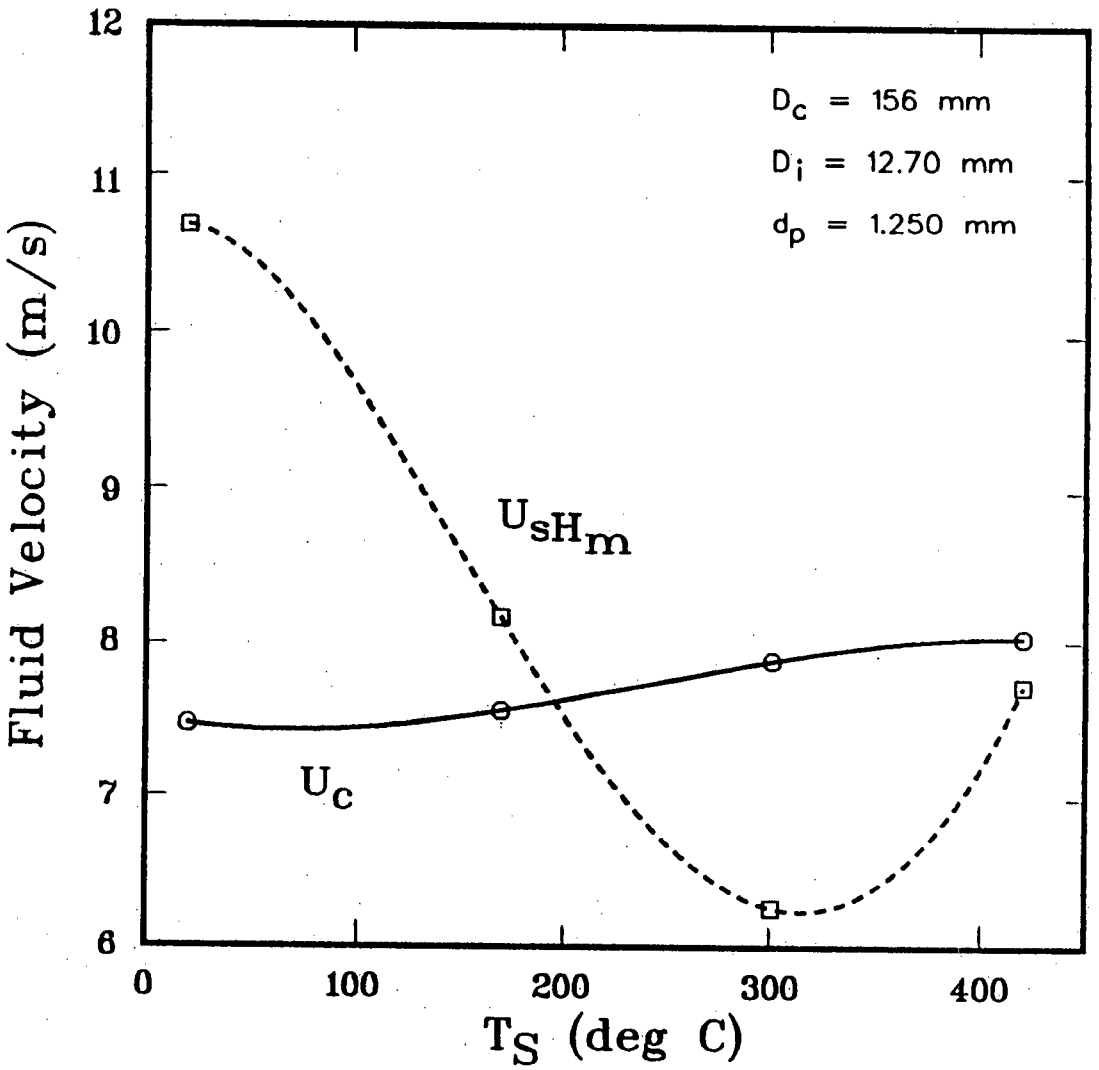

Figure 4.12a Effect of temperature on U_c and U_{sH_m}
Sand, d_p = 1.25 mm, D_c = 156 mm, D_i = 12.70 mm

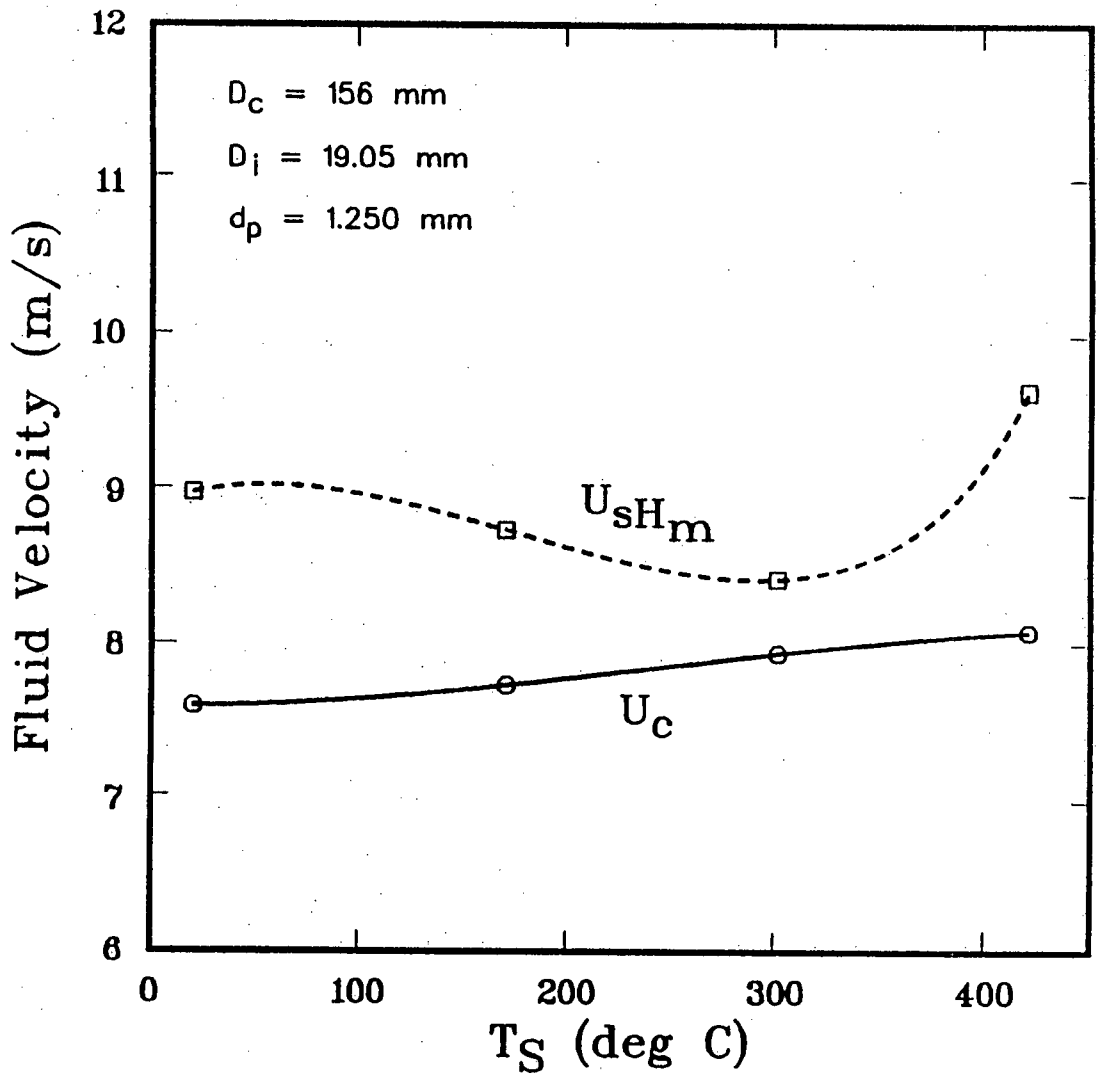

Figure 4.12b Effect of temperature on U_c and U_{sH_m}

Sand, d_p = 1.25 mm, D_c = 156 mm, D_i = 19.05 mm

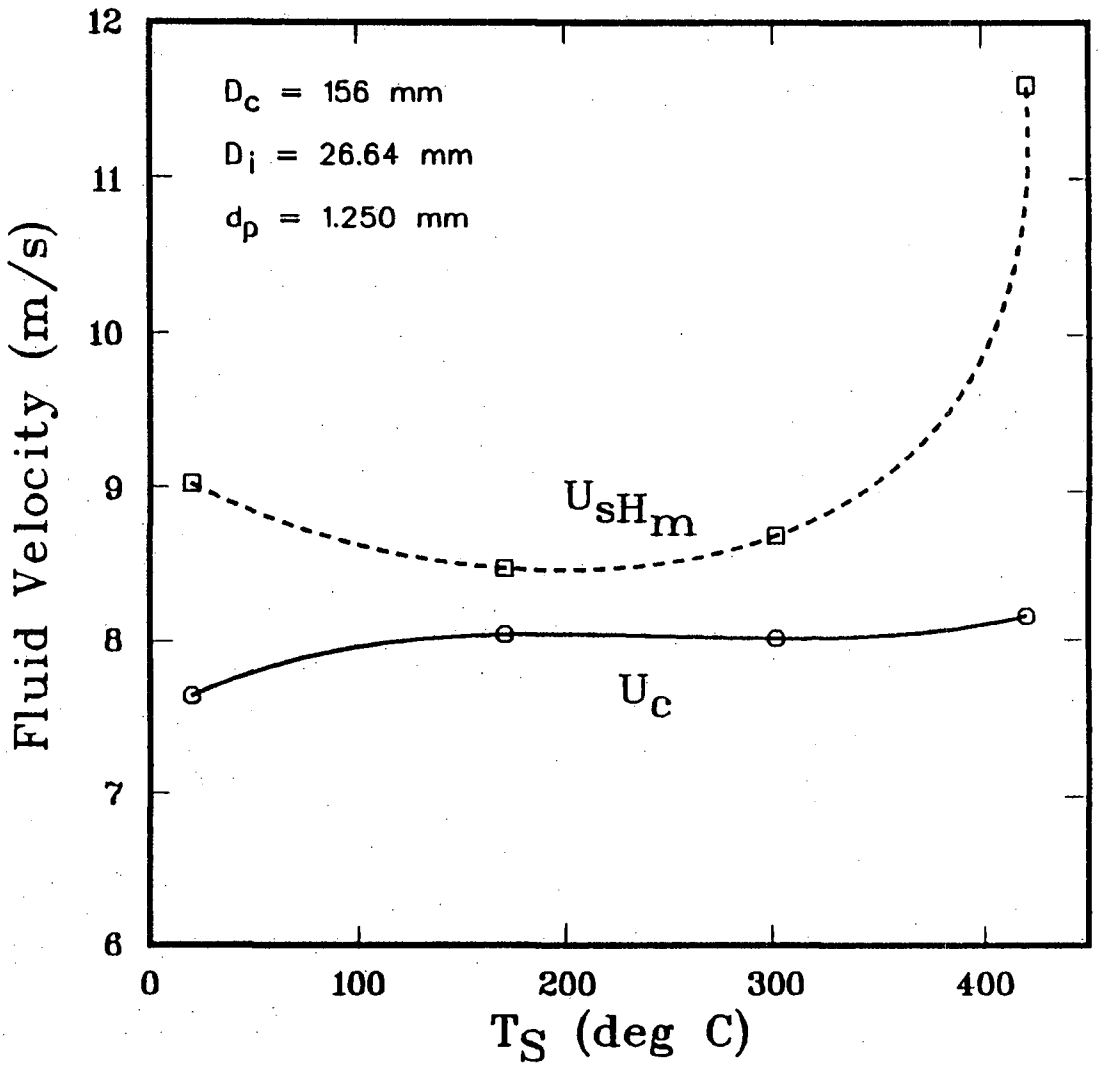

Figure 4.12c Effect of temperature on U_c and U_{sH_m}

Sand, d_p = 1.25 mm, D_c = 156 mm, D_i = 26.64 mm

5. MINIMUM SPOUTING VELOCITY AND OVERALL BED PRESSURE DROP

5.1 MINIMUM SPOUTING VELOCITY

Minimum spouting velocities were measured using the method described in Section 3.7.3. U_{ms} appeared to be more difficult to obtain at high temperatures. The main reason was that even a small adjustment of the flowmeter could amount to a significant change in the volumetric flowrate for a higher temperature condition because of the smaller fluid density. Thus, when measuring the air flowrates at higher temperatures, the smaller flowmeter (see Figure 3.4) was employed to yield a better precision. Tables 5.1a, 5.1b, 5.1c and 5.1d list all the experimental conditions and the corresponding results for U_{ms}.

5.1.1 EFFECT OF PARTICLE AND ORIFICE DIAMETERS

The effects of d_p and D_i on U_{ms} are shown in Figures 5.1 and 5.2, respectively. At room conditions, for any given bed heights, the values of U_{ms} are higher for bigger particles and larger orifice openings. The same trends also occur at high temperatures (420 °C). These observations are qualitatively consistent with Equation 2.1.

Table 5.1a Minimum spouting velocity, experimental versus prediction (T_s = 20 °C).

Sand, D_c = 156 mm and ρ_p = 2600 kg/m^3

Run #	d_p (mm)	D_i (mm)	H_m (m)	H (m)	ρ_f (kg/m^3)	U_{ms}* (m/s)	U_{ms} by Eq. 2.1 (m/s)	% dev	U_{ms} by Eq. 5.2 (m/s)	% dev
1-1	0.945	19.05	1.168	1.168	1.246	0.830	0.659	-20.6	0.832	0.2
1-2	0.945	19.05	1.168	0.889	1.233	0.685	0.578	-15.6	0.739	7.8
1-3	0.945	19.05	1.168	0.578	1.220	0.643	0.469	-27.1	0.612	-4.7
5-1	1.250	19.05	1.067	1.067	1.259	1.100	0.829	-24.6	1.065	-3.1
5-2	1.250	19.05	1.067	0.803	1.238	0.876	0.726	-17.1	0.943	7.8
5-3	1.250	19.05	1.067	0.518	1.222	0.782	0.586	-25.0	0.779	-0.4
9-1	1.665	19.05	1.010	1.010	1.244	1.314	1.081	-17.7	1.404	6.9
9-2	1.665	19.05	1.010	0.730	1.231	1.122	0.924	-17.7	1.220	8.7
9-3	1.665	19.05	1.010	0.502	1.218	0.960	0.770	-19.8	1.035	7.8
17-1	1.250	26.64	1.026	1.026	1.252	1.108	0.912	-17.7	1.129	1.9
17-2	1.250	26.64	1.026	0.832	1.241	0.957	0.825	-13.8	1.031	7.8
17-3	1.250	26.64	1.026	0.521	1.221	0.851	0.658	-22.7	0.841	-1.1
21-1	1.665	26.64	0.978	0.978	1.254	1.497	1.185	-20.9	1.488	-0.6
21-2	1.665	26.64	0.978	0.832	1.242	1.300	1.098	-15.6	1.388	6.8
21-3	1.665	26.64	0.978	0.559	1.223	1.138	0.907	-20.3	1.169	2.7
25-1	0.945	12.70	1.372	1.372	1.276	0.906	0.617	-32.0	0.811	-10.5
25-2	0.945	12.70	1.372	1.118	1.252	0.763	0.562	-26.3	0.745	-2.3
25-3	0.945	12.70	1.372	0.727	1.229	0.620	0.457	-26.2	0.618	-0.3
29-1	1.250	12.70	1.276	1.276	1.261	1.153	0.792	-31.4	1.054	-8.6
29-2	1.250	12.70	1.276	0.946	1.242	0.974	0.687	-29.5	0.927	-4.9
29-3	1.250	12.70	1.276	0.635	1.226	0.834	0.566	-32.1	0.779	-6.5
33-1	1.665	12.70	1.029	1.029	1.245	1.383	0.953	-31.1	1.294	-6.4
33-2	1.665	12.70	1.029	0.762	1.230	1.185	0.825	-30.4	1.136	-4.1
33-3	1.665	12.70	1.029	0.533	1.216	1.026	0.694	-32.3	0.973	-5.1
5-4	1.250	19.05	1.073	1.073	1.259	1.045	0.832	-20.4	1.068	2.2
5-5	1.250	19.05	1.073	1.010	1.254	0.998	0.808	-19.0	1.041	4.3
5-6	1.250	19.05	1.073	0.813	1.238	0.873	0.730	-16.4	0.948	8.6
5-7	1.250	19.05	1.073	0.597	1.227	0.831	0.628	-24.4	0.829	-0.2
5-8	1.250	19.05	1.073	0.444	1.217	0.750	0.544	-27.5	0.729	-2.9
5-9	1.250	19.05	1.073	0.279	1.209	0.670	0.433	-35.4	0.594	-11.3
37-1	1.250	19.05	1.380	1.380	0.707	1.537	1.258	-18.1	1.394	-9.3
37-2	1.250	19.05	1.380	1.067	0.695	1.454	1.116	-23.2	1.250	-14.0
37-3	1.250	19.05	1.380	0.705	0.683	1.168	0.915	-21.7	1.045	-10.6
37-4	1.250	19.05	1.380	0.254	0.670	0.855	0.555	-35.1	0.668	-21.9
38-1	1.250	19.05	0.533	0.533	0.170	1.362	1.596	17.2	1.342	-1.5
38-2	1.250	19.05	0.533	0.403	0.169	1.178	1.392	18.2	1.187	0.8
38-3	1.250	19.05	0.533	0.273	0.168	1.043	1.149	10.1	1.000	-4.2

* experimental value

Table 5.1b Minimum spouting velocity, experimental versus prediction (T_s = 170 °C)

Sand, D_c = 156 mm and ρ_p = 2600 kg/m^3

Run #	d_p (mm)	D_i (mm)	H_m (m)	H (m)	ρ_f (kg/m^3)	U_{ms}* (m/s)	U_{ms} by Eq. 2.1 (m/s)	% dev	U_{ms} by Eq. 5.2 (m/s)	% dev
2-1	0.945	19.05	0.419	0.419	0.802	0.576	0.492	-14.5	0.594	3.2
2-2	0.945	19.05	0.419	0.292	0.799	0.548	0.412	-24.8	0.507	-7.5
2-3	0.945	19.05	0.419	0.203	0.797	0.415	0.344	-17.1	0.432	4.1
6-1	1.250	19.05	0.648	0.648	0.815	1.009	0.803	-20.4	0.960	-4.9
6-2	1.250	19.05	0.648	0.451	0.806	0.868	0.674	-22.4	0.819	-5.6
6-3	1.250	19.05	0.648	0.292	0.801	0.731	0.544	-25.6	0.677	-7.4
10-1	1.665	19.05	0.800	0.800	0.824	1.263	1.182	-6.4	1.415	12.0
10-2	1.665	19.05	0.800	0.597	0.814	1.157	1.027	-11.2	1.247	7.7
10-3	1.665	19.05	0.800	0.400	0.805	1.034	0.846	-18.2	1.047	1.2
18-1	1.250	26.64	0.705	0.705	0.816	1.048	0.936	-10.6	1.073	2.4
18-2	1.250	26.64	0.705	0.568	0.809	0.951	0.844	-11.2	0.977	2.8
18-3	1.250	26.64	0.705	0.356	0.802	0.824	0.671	-18.5	0.796	-3.4
22-1	1.665	26.64	0.838	0.838	0.822	1.567	1.355	-13.5	1.557	-0.6
22-2	1.665	26.64	0.838	0.625	0.813	1.319	1.177	-10.8	1.371	4.0
22-3	1.665	26.64	0.838	0.422	0.805	1.177	0.972	-17.4	1.155	-1.8
26-1	0.945	12.70	0.724	0.724	0.814	0.600	0.561	-6.5	0.690	14.9
26-2	0.945	12.70	0.724	0.549	0.807	0.532	0.491	-7.8	0.611	14.9
26-3	0.945	12.70	0.724	0.356	0.801	0.452	0.396	-12.3	0.505	11.8
30-1	1.250	12.70	0.781	0.781	0.818	0.959	0.769	-19.8	0.952	-0.7
30-2	1.250	12.70	0.781	0.565	0.809	0.797	0.658	-17.4	0.827	3.8
30-3	1.250	12.70	0.781	0.387	0.801	0.674	0.547	-18.8	0.701	4.1
34-1	1.665	12.70	0.832	0.832	0.820	1.569	1.056	-32.7	1.318	-16.0
34-2	1.665	12.70	0.832	0.619	0.810	1.305	0.916	-29.8	1.160	-11.1
34-3	1.665	12.70	0.832	0.406	0.802	1.056	0.746	-29.3	0.965	-8.6
6-4	1.250	19.05	0.648	0.648	0.813	0.978	0.804	-17.8	0.960	-1.8
6-5	1.250	19.05	0.648	0.464	0.806	0.860	0.683	-20.6	0.830	-3.6
6-6	1.250	19.05	0.648	0.267	0.799	0.689	0.520	-24.5	0.651	-5.6

* experimental value

Table 5.1c Minimum spouting velocity, experimental versus prediction (T_s = 300 °C)

Sand, D_c = 156 mm and ρ_p = 2600 kg/m^3

Run #	d_p (mm)	D_i (mm)	H_m (m)	H (m)	ρ_f (kg/m^3)	U_{ms}* (m/s)	U_{ms} by Eq. 2.1 (m/s)	% dev	U_{ms} by Eq. 5.2 (m/s)	% dev
7-1	1.250	19.05	0.546	0.546	0.624	0.931	0.843	-9.5	0.956	2.6
7-2	1.250	19.05	0.546	0.413	0.621	0.875	0.734	-16.1	0.845	-3.4
7-3	1.250	19.05	0.546	0.279	0.618	0.773	0.606	-21.7	0.712	-8.0
11-1	1.665	19.05	0.721	0.721	0.629	1.348	1.284	-4.7	1.452	7.8
11-2	1.665	19.05	0.721	0.521	0.624	1.159	1.096	-5.4	1.260	8.7
11-3	1.665	19.05	0.721	0.359	0.620	0.991	0.912	-7.9	1.070	8.0
19-1	1.250	26.64	0.419	0.419	0.623	0.949	0.826	-12.9	0.916	-3.5
19-2	1.250	26.64	0.419	0.324	0.620	0.896	0.728	-18.7	0.818	-8.7
19-3	1.250	26.64	0.419	0.219	0.617	0.782	0.600	-23.3	0.688	-12.0
23-1	1.665	26.64	0.679	0.679	0.631	1.528	1.392	-8.8	1.523	-0.3
23-2	1.665	26.64	0.679	0.508	0.625	1.307	1.209	-7.4	1.342	2.7
23-3	1.665	26.64	0.679	0.343	0.620	1.166	0.998	-14.4	1.130	-3.1
27-1	0.945	12.70	0.635	0.635	0.622	0.581	0.601	3.5	0.699	20.4
27-2	0.945	12.70	0.635	0.476	0.620	0.495	0.521	5.3	0.616	24.5
27-3	0.945	12.70	0.635	0.311	0.618	0.451	0.422	-6.4	0.511	13.2
31-1	1.250	12.70	0.654	0.654	0.629	0.847	0.803	-5.3	0.945	11.5
31-2	1.250	12.70	0.654	0.495	0.623	0.736	0.702	-4.7	0.837	13.7
31-3	1.250	12.70	0.654	0.311	0.618	0.580	0.558	-3.8	0.683	17.6
35-1	1.665	12.70	0.743	0.743	0.630	1.403	1.139	-18.8	1.346	-4.1
35-2	1.665	12.70	0.743	0.543	0.625	1.178	0.977	-17.1	1.173	-0.5
35-3	1.665	12.70	0.743	0.365	0.619	1.010	0.805	-20.3	0.986	-2.4
7-4	1.250	19.05	0.546	0.546	0.626	0.892	0.841	-5.6	0.955	7.1
7-5	1.250	19.05	0.546	0.413	0.622	0.852	0.734	-13.8	0.845	-0.8
7-6	1.250	19.05	0.546	0.311	0.619	0.787	0.639	-18.8	0.746	-5.2
7-7	1.250	19.05	0.546	0.267	0.618	0.740	0.592	-20.0	0.697	-5.8

* experimental value

Table 5.1d Minimum spouting velocity, experimental versus prediction (T_s = 420 °C).

Sand, D_c = 156 mm and ρ_p = 2600 kg/m^3

Run #	d_p (mm)	D_i (mm)	H_m (m)	H (m)	ρ_f (kg/m^3)	U_{ms}* (m/s)	U_{ms} by Eq. 2.1 (m/s)	% dev	U_{ms} by Eq. 5.2 (m/s)	% dev
8-1	1.250	19.05	0.413	0.413	0.514	0.871	0.807	-7.3	0.889	2.1
8-2	1.250	19.05	0.413	0.267	0.511	0.813	0.651	-19.9	0.734	-9.7
8-3	1.250	19.05	0.413	0.206	0.510	0.670	0.573	-14.4	0.655	-2.1
12-1	1.665	19.05	0.629	0.629	0.515	1.311	1.326	1.1	1.443	10.0
12-2	1.665	19.05	0.629	0.457	0.512	1.235	1.134	-8.2	1.254	1.5
12-3	1.665	19.05	0.629	0.305	0.510	1.001	0.928	-7.3	1.049	4.8
20-1	1.250	26.64	0.343	0.343	0.511	0.947	0.826	-12.8	0.884	-6.6
20-2	1.250	26.64	0.343	0.241	0.510	0.843	0.693	-17.8	0.756	-10.3
20-3	1.250	26.64	0.343	0.168	0.509	0.695	0.579	-16.7	0.645	-7.2
24-1	1.665	26.64	0.540	0.540	0.517	1.473	1.371	-7.0	1.450	-1.6
24-2	1.665	26.64	0.540	0.406	0.513	1.322	1.194	-9.7	1.282	-3.1
24-3	1.665	26.64	0.540	0.254	0.511	1.147	0.946	-17.5	1.042	-9.2
28-1	0.945	12.70	0.486	0.486	0.511	0.573	0.580	1.2	0.655	14.3
28-2	0.945	12.70	0.486	0.362	0.510	0.516	0.501	-3.0	0.575	11.3
28-3	0.945	12.70	0.486	0.229	0.509	0.419	0.399	-4.8	0.469	12.0
32-1	1.250	12.70	0.533	0.533	0.515	0.801	0.801	-0.0	0.911	13.7
32-2	1.250	12.70	0.533	0.400	0.513	0.707	0.695	-1.7	0.802	13.5
32-3	1.250	12.70	0.533	0.232	0.510	0.559	0.531	-5.1	0.631	12.8
36-1	1.665	12.70	0.654	0.654	0.519	1.321	1.176	-10.9	1.339	1.4
36-2	1.665	12.70	0.654	0.486	0.515	1.131	1.018	-10.0	1.176	4.0
36-3	1.665	12.70	0.654	0.311	0.511	0.952	0.818	-14.0	0.967	1.6
8-4	1.250	19.05	0.413	0.413	0.514	0.860	0.807	-6.1	0.889	3.4
8-5	1.250	19.05	0.413	0.270	0.511	0.801	0.655	-18.2	0.738	-7.9

* experimental value

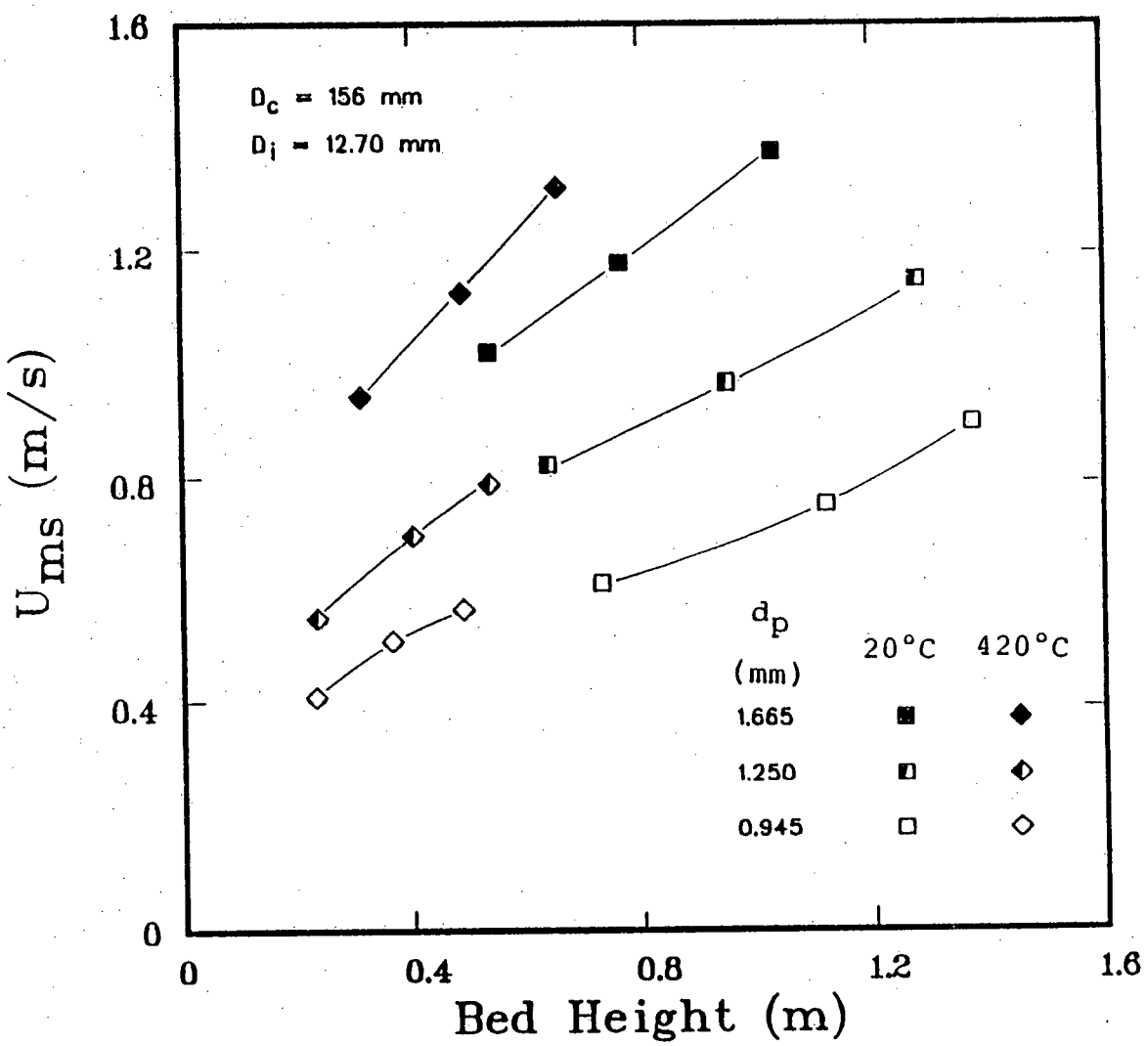

Figure 5.1 Effect of particle diameter on U_{ms}

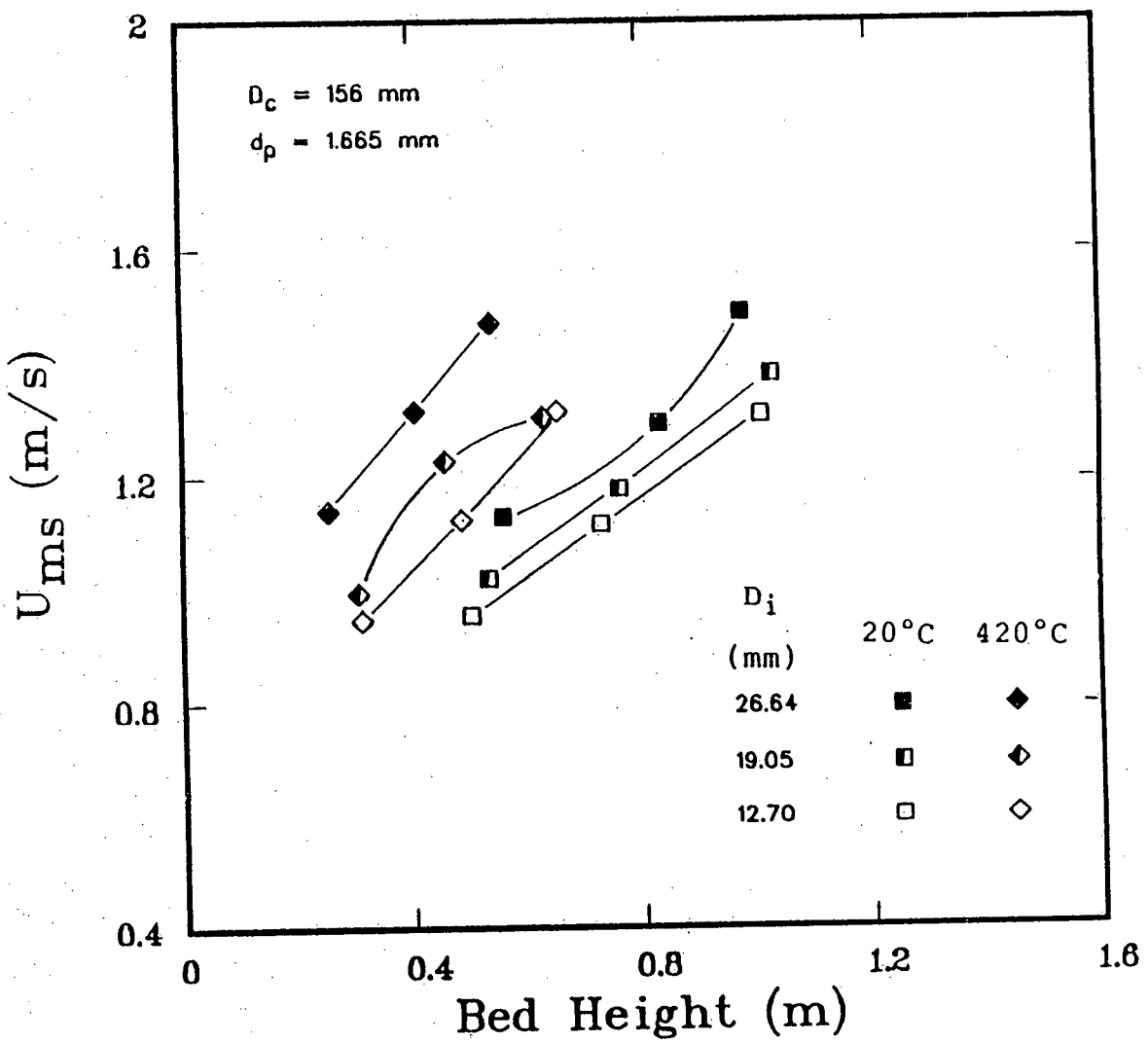

Figure 5.2 Effect of orifice diameter on U_{ms}

5.1.2 EFFECT OF TEMPERATURE

Figure 5.3 illustrates the effect of bed temperatures on U_{ms} for a fixed particle size and orifice diameter. Though there is some overlapping among the data points, this figure generally indicates that for a given bed height, U_{ms} increases with increasing temperature as predicted by Equation 2.1. Supporting evidence is also given in Figures 5.1 and 5.2.

5.1.3 DATA CORRELATION

Experimental values of U_{ms} were compared with the values calculated by Equation 2.1. For air spouting at room temperature, Equation 2.1 underpredicted U_{ms} by about 30% for the smallest orifice diameter (Table 5.1a). The deviation decreased to around 20% for the largest D_i. This equation appeared to work better with increasing temperature (Tables 5.1b, 5.1c and 5.1d). Equation 2.1 reportedly gives good predictions of U_{ms} at room conditions but not in the present case. One possible explanation may be the inadequate knowledge of how to specify d_p for use in Equation 2.1 in the case of non-spherical particles.

Using Equation 2.1 as a base, assuming $\rho_p >> \rho_f$ while d_p, D_c and D_i are fixed, the effect of H/ρ_f on U_{ms} can be examined. Figure 5.4 illustrates a typical example. For this

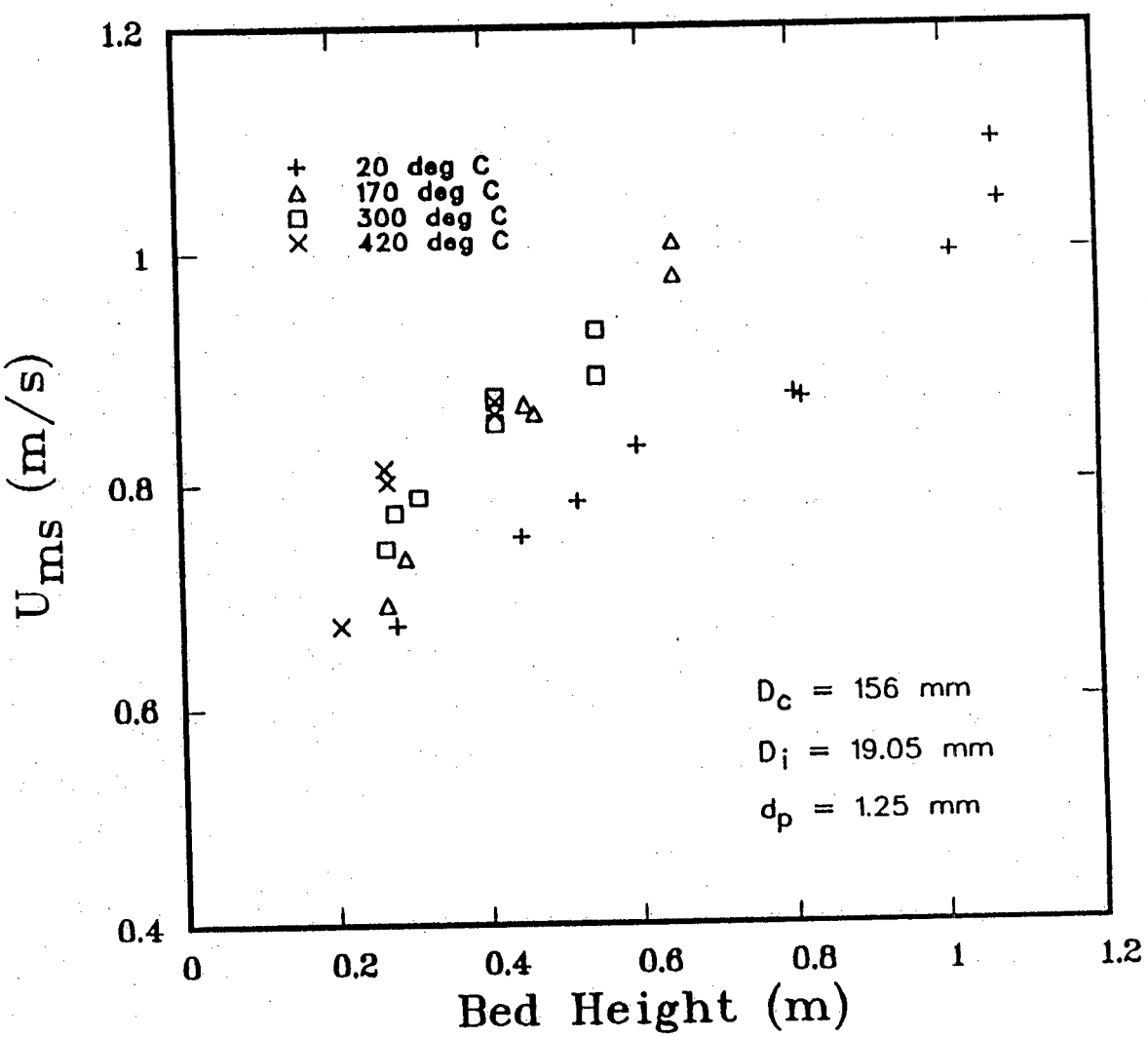

Figure 5.3 Effect of bed temperature on U_{ms}

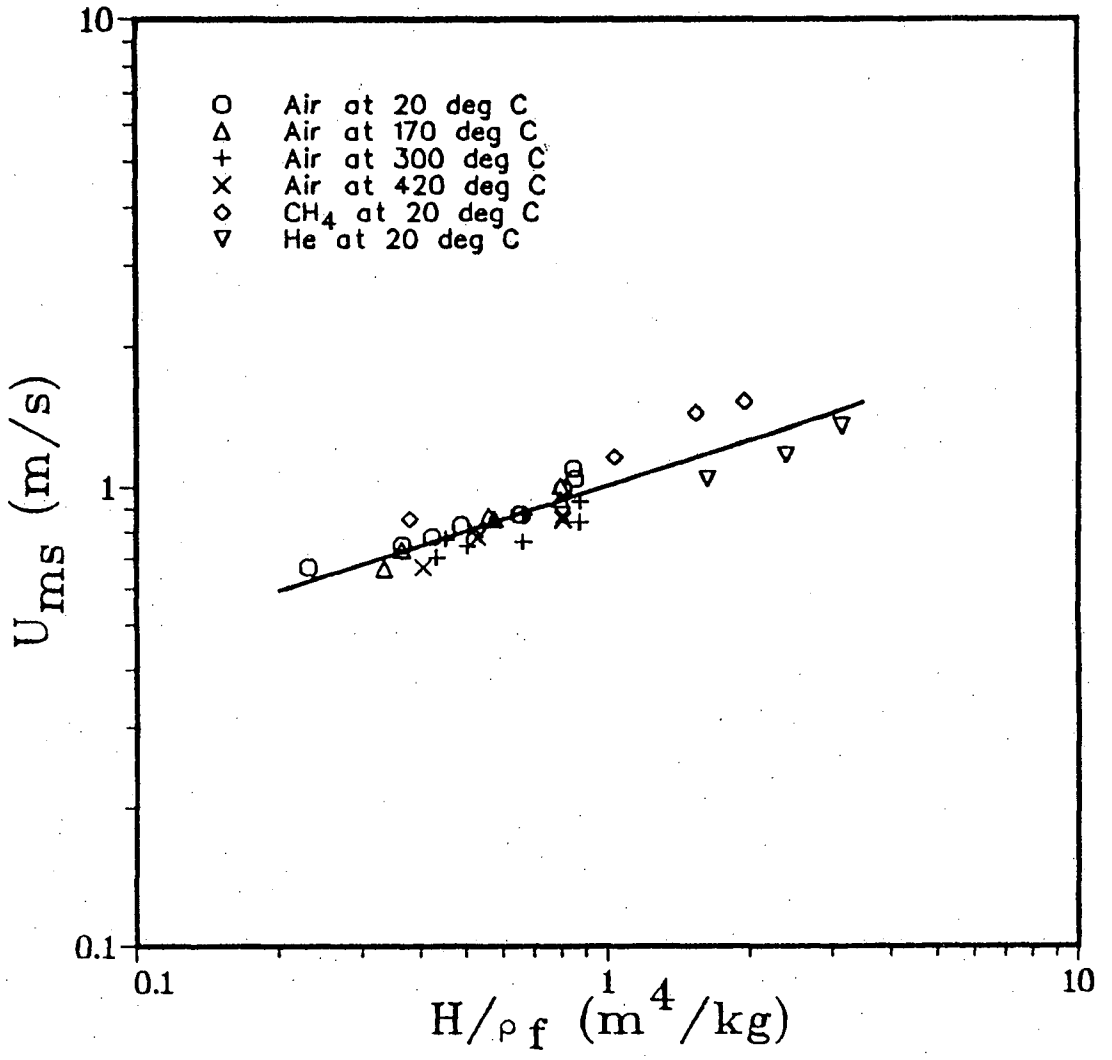

Figure 5.4 Effect of H/ρ_f on U_{ms}. Sand, d_p = 1.25 mm, D_i = 19.05 mm, D_c = 156 mm and ρ_p = 2600 kg/m^3 The solid line indicates the best fit.

plot, a least squares fit produced a slope of 0.33. The slopes for other conditions were also calculated (Table 5.2). Although the experimental data did not always fit well, there was a clear indication that the slope (based on this work) was less than 0.50 (i.e., the value in Equation 2.1). Manurung (1964) has reported similar findings. He noted that Equation 2.1 overestimates the effect of bed height on U_{ms}.

The effects of d_p and D_i were not investigated individually because H/ρ_f was not fixed. However, it was possible to fit the experimental data to the following expression:

$$U_{ms} = K\left[\frac{d_p}{D_c}\right]^{\sigma}\left[\frac{D_i}{D_c}\right]^{\tau}(2gH)^{\omega}\left[\frac{\rho_p-\rho_f}{\rho_f}\right]^{\xi} \qquad 5.1$$

where K, σ, τ, ω and ξ were found by applying the least squares method to experimental data. In this case, H and $(\rho_p-\rho_f)/\rho_f$ were treated as two separate variables. The best fit resulted when K, σ, τ, ω and ξ were equal to 8.452, 1.038, 0.2213, 0.4437 and 0.2688 respectively. Based on these results, the effects of d_p, D_i, H and $(\rho_p-\rho_f)/\rho_f$ on U_{ms} have not been adequately described by Equation 2.1. Moreover, the values of ω and ξ are quite different from each other, indicating that H and $(\rho_p-\rho_f)/\rho_f$ should not be grouped as one single parameter. The calculated values of U_{ms} from this curve-fit model are tabulated alongside those

Table 5.2 Slopes of U_{ms} versus (H/ρ_f) plot at different conditions. Sand, ρ_p = 2600 kg/m^3 and D_c = 156 mm

d_p (mm)	D_i (mm)	Slope of $\ln(U_{ms})$ versus $\ln(H/\rho_f)$
0.945	12.70	0.54
0.945	19.05	0.48
1.250	12.70	0.44
1.250	19.05	0.33 **
1.250	26.64	0.38
1.665	12.70	0.35
1.665	19.05	0.33
1.665	26.64	0.37

** see Figure 5.4

by Equation 2.1 in Tables 5.1a, 5.1b, 5.1c and 5.1d.

More curve fittings were done by forcing some of the coefficients in Equation 5.1 to equal those in Equation 2.1. The results are summarized in Table 5.3, with the best fit identified as I. First of all, there is some theoretical justification to assume $\omega = 0.5$ (Ghosh, 1965). The resulting expression (curve-fit II) is dimensionally consistent. Based on the values in the first two curve-fits, σ is not very different from unity and it is therefore set to 1.0 in addition to making $\omega = 0.5$ in curve-fit III. Finally, results from III suggest that it is reasonable to take τ as 1/3. With $\omega = 0.5$, $\sigma = 1.0$ and $\tau = 1/3$, a least squares fit produces IV. Equation 2.1 is also included in this table for comparison. The second, third and fourth curve-fits are barely worse than the first one but Equation 2.1 is clearly inferior. If one assumes that Equation 2.1 correctly predicts the quantitative effects of d_p, D_i and H on U_{ms}, curve-fit IV will be recommended over the other three.

5.2 OVERALL BED PRESSURE DROP

Tables 5.4a, 5.4b, 5.4c and 5.4d summarize all the experimental conditions and the corresponding values of $-\Delta P_s$. These experimental values of $-\Delta P_s$ were obtained using the method outlined in Section 3.7.2. When measuring U_{ms}, it was noticed that $-\Delta P_s$ did not change significantly with

Table 5.3 Comparison between various versions of Equation 5.1

Curve-Fit	K	σ	τ	ω	ξ	AVE ERR (%)	RMS % ERR	$\Sigma(EXP-CAL)^2$
I	8.452	1.038	0.2213	0.4437	0.2688	1.04	8.31	0.610
II	5.694	1.008	0.2854	0.5000*	0.3004	0.78	8.49	0.686
III	6.208	1.000*	0.3343	0.5000*	0.2979	0.65	8.44	0.749
IV	6.665	1.000*	0.3333*	0.5000*	0.2890	0.71	8.45	0.751
Eq. 2.1	1.000	1.000	0.3333	0.5000	0.5000	-15.14	18.31	3.823

EXP = experimantal value

CAL = calculated value

* Exponent fixed at this value

Table 5.4a Overall pressure drop, experimental data and prediction by Equation 2.28 (T_s = 20 °C).

Sand, D_c = 156 mm and ρ_p = 2600 kg/m^3

Run #	H (m)	H/H_m	d_p (mm)	D_i (cm)	$-\Delta P_s$* (kN/m^2)	$-\Delta P_s$@ (kN/m^2)	% dev
1-1	1.168	1.000	0.945	1.905	7.80	10.64	36.45
1-2	0.889	0.761	0.945	1.905	5.67	7.10	25.21
1-3	0.578	0.495	0.945	1.905	3.44	3.44	-0.12
5-1	1.067	1.000	1.250	1.905	10.01	9.51	-4.99
5-2	0.803	0.753	1.250	1.905	6.49	6.16	-4.98
5-3	0.518	0.485	1.250	1.905	3.82	2.86	-25.29
9-1	1.010	1.000	1.665	1.905	7.46	8.81	18.20
9-2	0.730	0.723	1.665	1.905	5.27	5.28	0.08
9-3	0.502	0.497	1.665	1.905	3.11	2.66	-14.40
17-1	1.026	1.000	1.250	2.664	8.86	9.14	3.21
17-2	0.832	0.811	1.250	2.664	6.95	6.68	-3.86
17-3	0.521	0.508	1.250	2.664	3.60	2.99	-17.11
21-1	0.978	1.000	1.665	2.664	9.24	8.53	-7.68
21-2	0.832	0.851	1.665	2.664	7.24	6.67	-7.86
21-3	0.559	0.572	1.665	2.664	3.97	3.36	-15.36
25-1	1.372	1.000	0.945	1.270	12.98	12.49	-3.82
25-2	1.118	0.815	0.945	1.270	8.90	9.26	4.05
25-3	0.727	0.530	0.945	1.270	5.03	4.56	-9.46
29-1	1.276	1.000	1.250	1.270	10.43	11.37	8.98
29-2	0.946	0.741	1.250	1.270	7.20	7.19	-0.11
29-3	0.635	0.498	1.250	1.270	4.52	3.58	-20.88
33-1	1.029	1.000	1.665	1.270	7.75	8.98	15.79
33-2	0.762	0.741	1.665	1.270	5.20	5.60	7.64
33-3	0.533	0.518	1.665	1.270	2.78	2.94	5.71
5-4	1.073	1.000	1.250	1.905	9.97	9.56	-4.06
5-5	1.010	0.941	1.250	1.905	9.24	8.76	-5.23
5-6	0.813	0.758	1.250	1.905	6.52	6.27	-3.89
5-7	0.597	0.556	1.250	1.905	4.61	3.69	-19.91
5-8	0.444	0.414	1.250	1.905	2.95	2.12	-28.05
5-9	0.279	0.260	1.250	1.905	1.57	0.84	-46.27
37-1	1.380	1.000	1.250	1.905	12.77	12.12	-5.13
37-2	1.067	0.773	1.250	1.905	8.90	8.15	-8.49
37-3	0.705	0.511	1.250	1.905	5.37	3.90	-27.35
37-4	0.254	0.184	1.250	1.905	1.29	0.48	-62.51
38-1	0.533	1.000	1.250	1.905	4.14	4.99	20.47
38-2	0.403	0.756	1.250	1.905	2.95	3.34	13.11
38-3	0.273	0.512	1.250	1.905	1.72	1.78	3.93

* experimental value @ calculated value

Table 5.4b Overall pressure drop, experimental data and prediction by Equation 2.28 (T_S = 170 °C).

Sand, D_c = 156 mm and ρ_p = 2600 kg/m^3

Run #	H (m)	H/H_m	d_p (mm)	D_i (cm)	$-\Delta P_s$* (kN/m^2)	$-\Delta P_s$@ (kN/m^2)	% dev
2-1	0.419	1.000	0.945	1.905	2.12	3.90	84.16
2-2	0.292	0.697	0.945	1.905	1.43	2.29	60.57
2-3	0.203	0.484	0.945	1.905	0.89	1.25	40.78
6-1	0.648	1.000	1.250	1.905	5.41	5.91	9.21
6-2	0.451	0.696	1.250	1.905	3.26	3.43	4.98
6-3	0.292	0.451	1.250	1.905	1.88	1.62	-13.78
10-1	0.800	1.000	1.665	1.905	7.77	7.14	-8.13
10-2	0.597	0.746	1.665	1.905	5.27	4.57	-13.33
10-3	0.400	0.500	1.665	1.905	2.99	2.27	-24.09
18-1	0.705	1.000	1.250	2.664	5.67	6.43	13.47
18-2	0.568	0.806	1.250	2.664	4.06	4.69	15.72
18-3	0.356	0.505	1.250	2.664	2.12	2.16	2.14
22-1	0.838	1.000	1.665	2.664	7.33	7.48	2.05
22-2	0.625	0.746	1.665	2.664	5.06	4.78	-5.47
22-3	0.422	0.504	1.665	2.664	2.95	2.41	-18.25
26-1	0.724	1.000	0.945	1.270	5.33	6.73	26.30
26-2	0.549	0.758	0.945	1.270	3.59	4.51	25.75
26-3	0.356	0.492	0.945	1.270	1.87	2.22	18.95
30-1	0.781	1.000	1.250	1.270	6.18	7.13	15.30
30-2	0.565	0.723	1.250	1.270	3.97	4.39	10.67
30-3	0.387	0.496	1.250	1.270	2.01	2.32	14.97
34-1	0.832	1.000	1.665	1.270	6.82	7.43	8.92
34-2	0.619	0.744	1.665	1.270	4.35	4.73	8.66
34-3	0.406	0.488	1.665	1.270	2.23	2.26	1.46
6-4	0.648	1.000	1.250	1.905	5.12	5.91	15.58
6-5	0.464	0.716	1.250	1.905	3.25	3.59	10.47
6-6	0.267	0.412	1.250	1.905	1.42	1.37	-3.06

* experimental value @ calculated value

Table 5.4c Overall pressure drop, experimental data and prediction by Equation 2.28 (T_s = 300 °C).

Sand, D_c = 156 mm and ρ_p = 2600 kg/m^3

Run #	H (m)	H/H_m	d_p (mm)	D_i (cm)	$-\Delta P_s$* (kN/m^2)	$-\Delta P_s$@ (kN/m^2)	% dev
7-1	0.546	1.000	1.250	1.905	3.59	5.06	41.03
7-2	0.413	0.756	1.250	1.905	2.68	3.37	25.92
7-3	0.279	0.511	1.250	1.905	1.55	1.78	14.81
11-1	0.721	1.000	1.665	1.905	5.22	6.55	25.41
11-2	0.521	0.723	1.665	1.905	3.65	4.02	9.87
11-3	0.359	0.498	1.665	1.905	2.32	2.13	-8.34
19-1	0.419	1.000	1.250	2.664	3.20	3.88	21.17
19-2	0.324	0.773	1.250	2.664	2.14	2.68	24.97
19-3	0.219	0.523	1.250	2.664	1.31	1.42	8.28
23-1	0.679	1.000	1.665	2.664	5.84	6.16	5.56
23-2	0.508	0.748	1.665	2.664	3.93	4.00	1.78
23-3	0.343	0.505	1.665	2.664	2.06	2.06	-0.05
27-1	0.635	1.000	0.945	1.270	2.99	5.97	99.50
27-2	0.476	0.750	0.945	1.270	2.13	3.95	85.22
27-3	0.311	0.490	0.945	1.270	1.44	1.99	37.86
31-1	0.654	1.000	1.250	1.270	5.07	6.06	19.38
31-2	0.495	0.757	1.250	1.270	3.28	4.04	23.17
31-3	0.311	0.476	1.250	1.270	1.45	1.88	29.22
35-1	0.743	1.000	1.665	1.270	5.33	6.75	26.56
35-2	0.543	0.731	1.665	1.270	3.80	4.21	10.91
35-3	0.365	0.491	1.665	1.270	2.01	2.14	6.69
7-4	0.546	1.000	1.250	1.905	4.18	5.06	20.93
7-5	0.413	0.756	1.250	1.905	2.80	3.37	20.21
7-6	0.311	0.570	1.250	1.905	1.84	2.14	15.86
7-7	0.267	0.489	1.250	1.905	1.51	1.64	8.78

* experimental value @ calculated value

Table 5.4d Overall pressure drop, experimental data and prediction by Equation 2.28 (T_s = 420 °C).

Sand, D_c = 156 mm and ρ_p = 2600 kg/m^3

Run #	H (m)	H/H_m	d_p (mm)	D_i (cm)	$-\Delta P_s$* (kN/m^2)	$-\Delta P_s$e (kN/m^2)	% dev
8-1	0.413	1.000	1.250	1.905	2.73	3.86	41.49
8-2	0.267	0.646	1.250	1.905	1.42	2.02	42.62
8-3	0.206	0.499	1.250	1.905	1.04	1.32	27.05
12-1	0.629	1.000	1.665	1.905	2.98	5.78	93.66
12-2	0.457	0.727	1.665	1.905	1.94	3.60	85.78
12-3	0.305	0.485	1.665	1.905	1.04	1.82	74.69
20-1	0.343	1.000	1.250	2.664	1.38	3.21	133.00
20-2	0.241	0.703	1.250	2.664	1.25	1.92	53.48
20-3	0.168	0.490	1.250	2.664	0.87	1.06	22.37
24-1	0.540	1.000	1.665	2.664	4.01	4.96	23.60
24-2	0.406	0.752	1.665	2.664	2.35	3.26	38.46
24-3	0.254	0.470	1.665	2.664	1.44	1.48	2.71
28-1	0.486	1.000	0.945	1.270	1.67	4.59	174.85
28-2	0.362	0.745	0.945	1.270	1.23	3.02	144.53
28-3	0.229	0.471	0.945	1.270	0.85	1.45	70.59
32-1	0.533	1.000	1.250	1.270	2.99	4.98	66.49
32-2	0.400	0.750	1.250	1.270	2.31	3.29	42.51
32-3	0.232	0.435	1.250	1.270	0.99	1.34	36.18
36-1	0.654	1.000	1.665	1.270	4.90	6.01	22.43
36-2	0.486	0.743	1.665	1.270	3.08	3.88	25.96
36-3	0.311	0.476	1.665	1.270	1.50	1.83	21.86
8-4	0.413	1.000	1.250	1.905	2.82	3.86	36.78
8-5	0.270	0.654	1.250	1.905	1.53	2.06	34.65

* experimental value e calculated value

flowrates if $U/U_{ms} > 1$. Therefore, $-\Delta P_s$ was arbitrarily taken as the value measured at $U \simeq 1.05\ U_{ms}$.

5.2.1 EFFECT OF ORIFICE AND PARTICLE DIAMETERS

The effects of D_i and d_p on $-\Delta P_s$ are illustrated in Figures 5.5 and 5.6, respectively. The results indicate that $-\Delta P_s$ does not depend strongly on either D_i or d_p. In addition, the data points in these two figures tend to suggest that $-\Delta P_s$ is also independent of bed temperature.

5.2.2 EFFECT OF TEMPERATURE

The results of $-\Delta P_s$ versus H obtained at different temperatures and with different spouting gases are shown in Figure 5.7. All the data points appear to lie on the same curve. This means that the bed temperature and gas properties have only negligible effects and $-\Delta P_s$ mainly depends on H.

5.2.3 DATA CORRELATION

The experimental values of $-\Delta P_s$ were compared with the calculated values by Equation 2.28 (see Tables 5.4a, 5.4b, 5.4c and 5.4d). $-\Delta P_f$ in Equation 2.28 was estimated from $(\rho_p-\rho_f)g(1-\epsilon_a)H$. At room temperature, predicted values of $-\Delta P_s$ were generally in good agreement with experimental

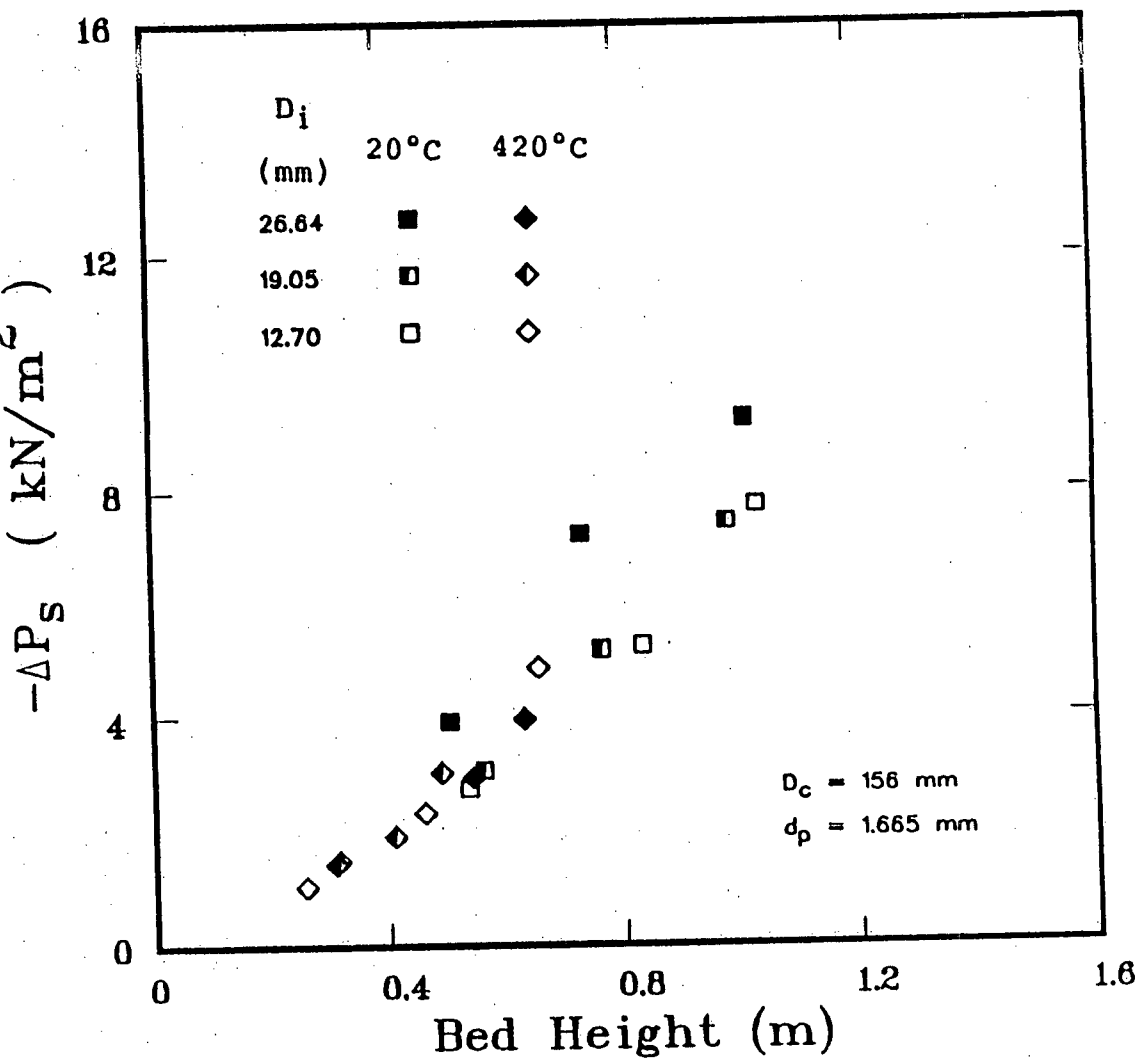

Figure 5.5 Effect of orifice diameter on $-\Delta P_s$

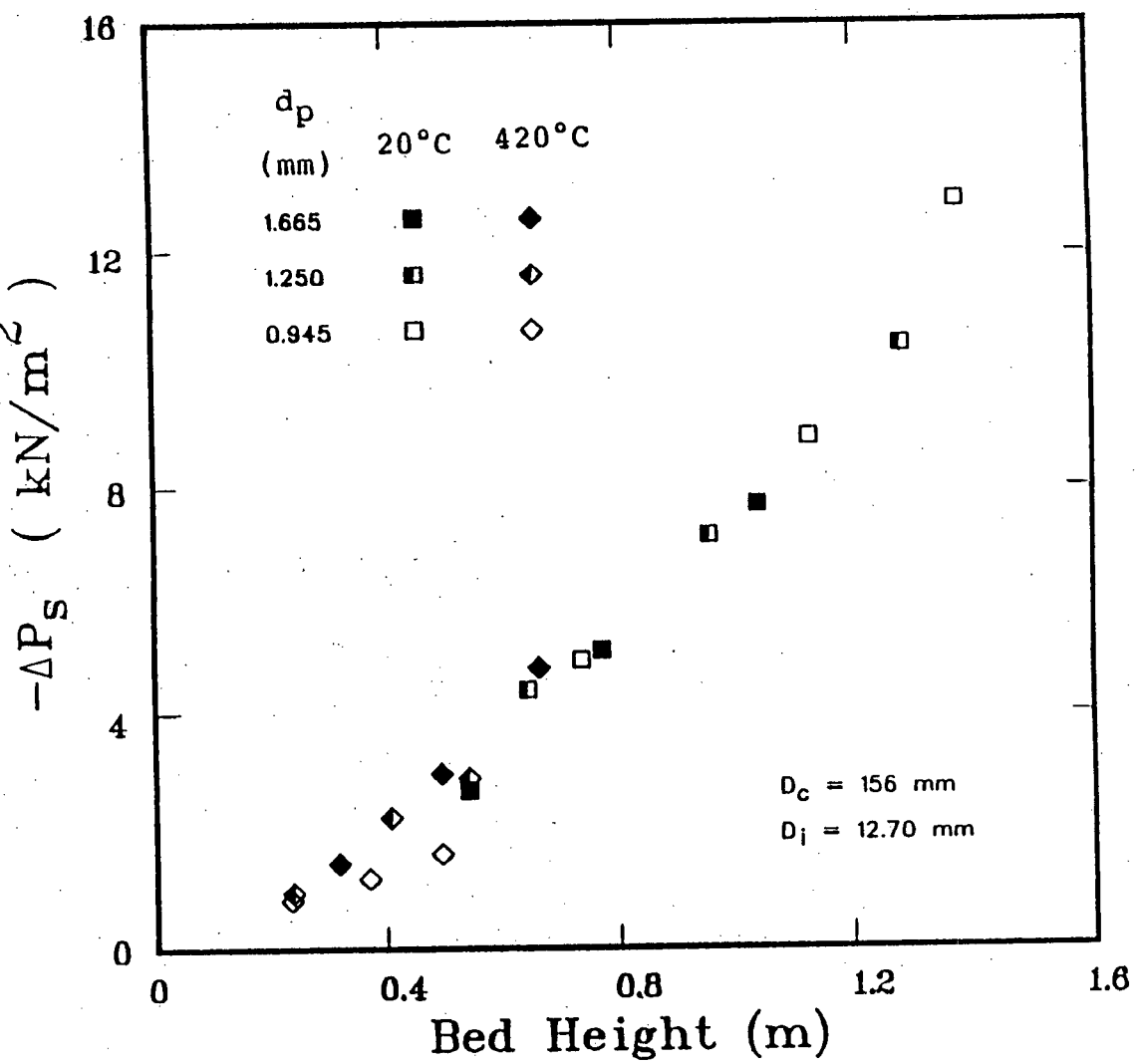

Figure 5.6 Effect of particle diameter on $-\Delta P_s$

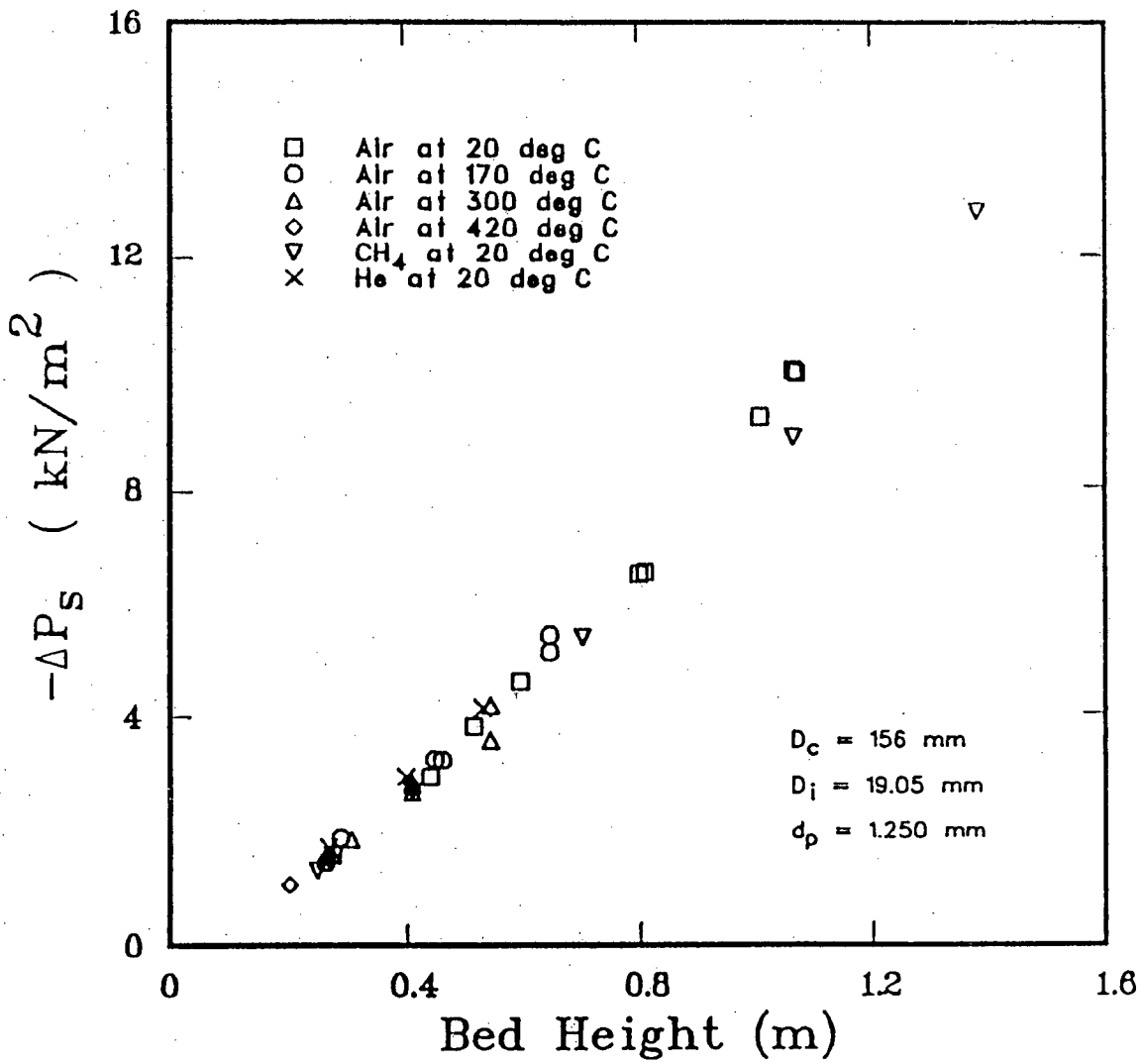

Figure 5.7 Effect of bed temperature on $-\Delta P_s$

values. As temperature increased, however, Equation 2.28 overestimated $-\Delta P_s$, particularly for the smallest orifice. This equation also predicts that $-\Delta P_s/-\Delta P_f$ increases slightly with temperature at fixed H/H_m (Figure 5.8) but this does not agree with the experimental data. In fact, it was found that at a fixed bed height, the measured value of $-\Delta P_s$ at 420 °C was similar to that at room temperature (see Figure 5.7) but the values of H/H_m for these two cases were quite different because of the higher H_m in the latter case. Equation 2.28 was therefore not suitable for predicting $-\Delta P_s$ at high temperature. Figure 5.9 shows how Equation 2.28 compares with experimental results.

Equation 2.28 was derived with the following assumptions:

1. $U_{aH_m} = U_{mf}$ and
2. $-dP/dz = (\rho_p-\rho_f)(1-\epsilon_a)g$ at H_m

If the annular solids are not completely fluidized at H_m, these assumptions would not apply and some modifications would be required. Table 5.5 illustrates how U_{aH_m} and $(-dP/dz)_{H_m}$ varied as temperature changed. The values of U_{aH_m} were determined by extrapolation of experimental data (see Chapter 7). $(-dP/dz)_{H_m}$, on the other hand, was determined from the calibration curve of $(-\Delta P)$ versus U_a. The pressure drop at U_{aH_m} was divided by the vertical distance between the two measuring points of the static pressure probe (Figure 3.6a) to yield the pressure gradient. There is

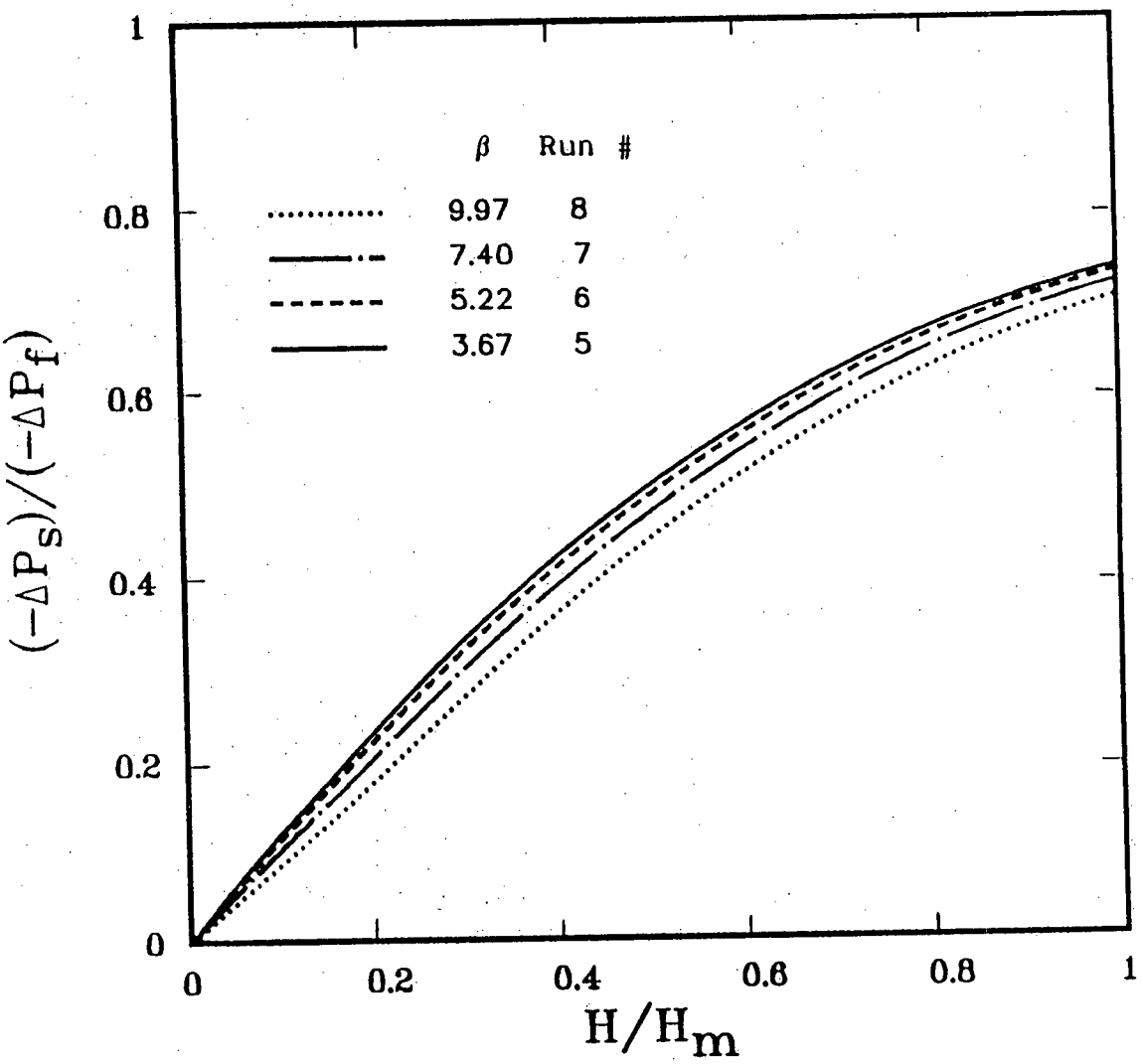

Figure 5.8 Effect of β and H/H_m on $(-\Delta P_s)/(-\Delta P_f)$ as predicted by Equation 2.28

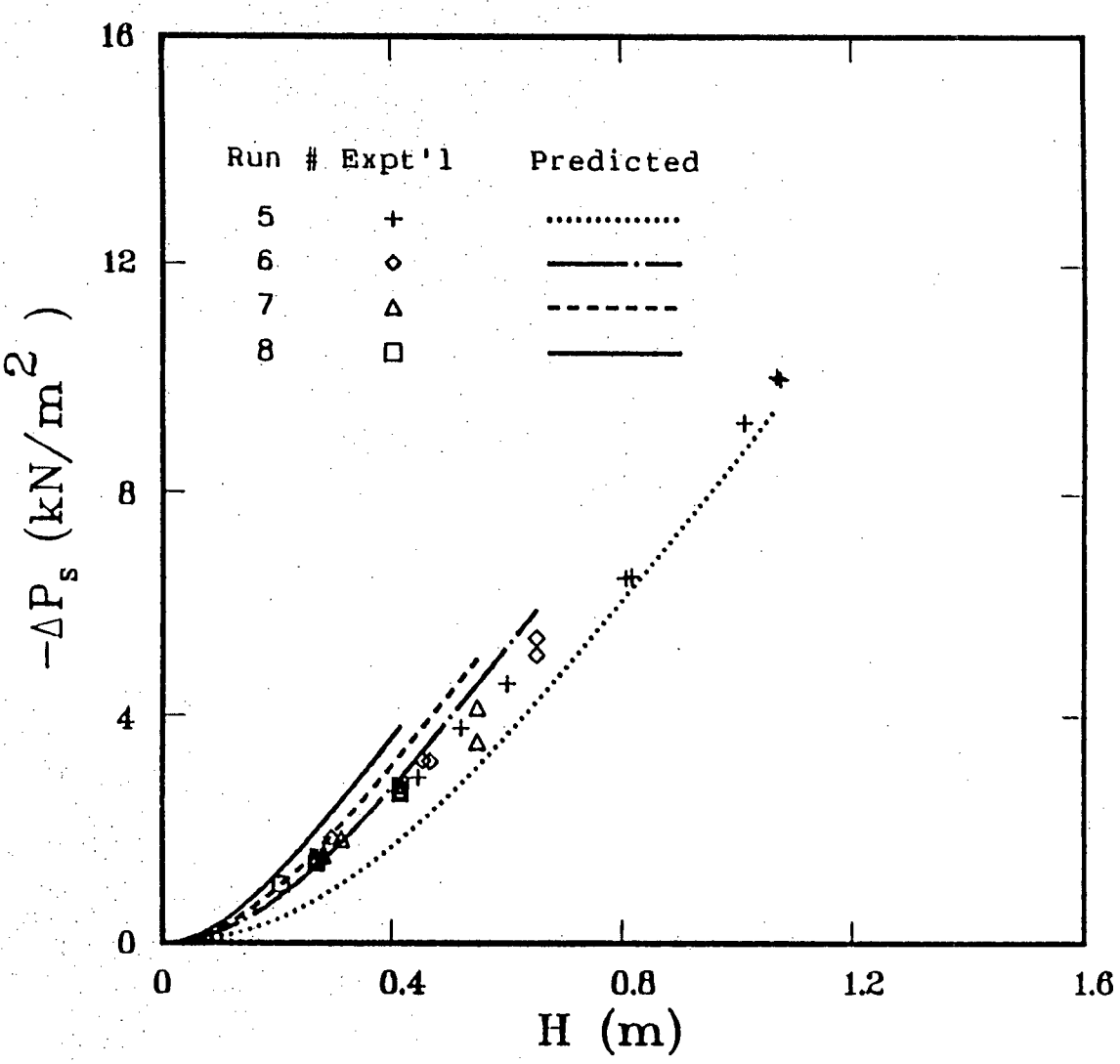

Figure 5.9 Comparison between experimental ($-\Delta P_s$) and prediction by Equation 2.28

Table 5.5 Comparison between experimental and predicted values of U_a and $-dP/dz$ at $z = H = H_m$

D_i = 19.05 mm and d_p = 1.25 mm

Run #	Temp (°C)	H_m (m)	U_{aH_m}@ (m/s)	U_{mf}* (m/s)	$-(dP/dz)_{H_m}$@ (kN/m^3)	$-(dP/dz)_{mf}$** (kN/m^3)
5-4	20	1.073	0.70	0.70	11.741	12.753
6-4	170	0.648	0.69	0.71	11.380	12.753
7-4	300	0.546	0.65	0.67	9.730	12.753
8-4	420	0.413	0.57	0.63	8.397	12.753

@ experimental value

* calculated value by Equation 2.7

** calculated value by $(\rho_p-\rho_f)(1-\epsilon_a)g$

strong evidence that with increasing temperature, assumtions 1 and 2 would fail. If U_{mf} were replaced by U_{aH_m}, β would change but its effect would be small, as shown in Figure 5.8. Using an experimental rather than a calculated value of $-\Delta P_f$ would show some slight improvement for results at high temperature but at the same time might create larger deviations for those at room conditions. Hence this kind of modification is still unsatisfactory.

Experimental results indicated that the effect of temperature on spouted bed pressure drop was not significant. The distribution of data points as shown in Figures 5.7 and 5.9 could be well described by the simpler expression of Manurung (1964),

$$-\Delta P_s = \rho_b g H/[1+(t/H)] \qquad 5.2$$

where

$$t = \left[\frac{0.81(\tan\theta)^{1.5}}{\phi^2}\right](D_c)\left[\frac{D_c d_p}{D_i{}^2}\right]^{0.78} \qquad 5.3$$

and θ is the angle of internal friction. If ϕ is taken as 0.6689 (to be consistent with the Wen and Yu approximations), the two extreme values of t which bracket all the conditions of the present experiments are 1.1578 and 0.2343 respectively. Putting these constants into Equation 5.2 produced the curves shown in Figure 5.10. Almost all the

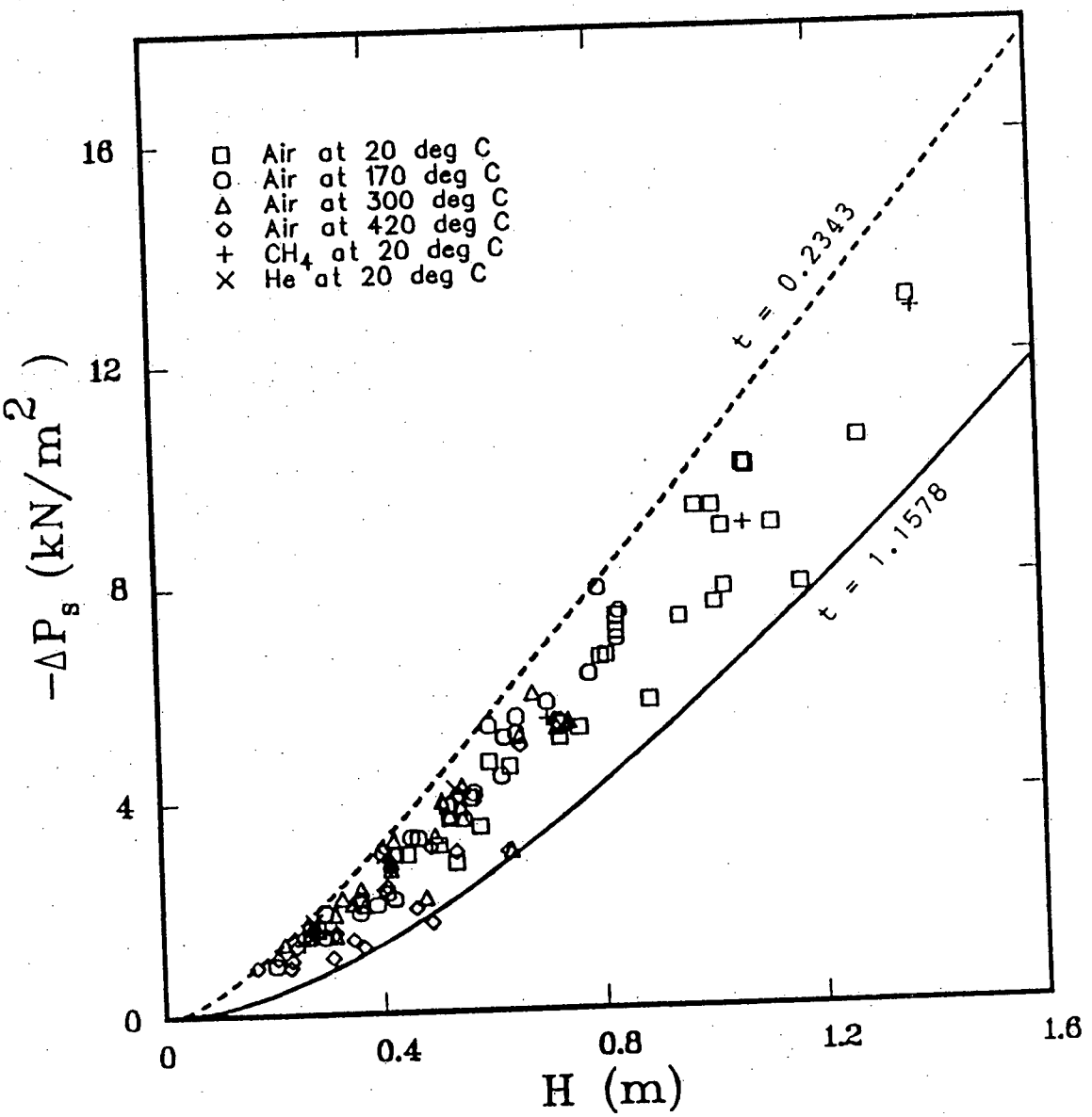

Figure 5.10 Overall bed pressure drop versus bed height

The two lines represent Equation 5.2

data points were well within these two boundaries. Equation 5.2 can be rearranged to yield the following expression

$$H = \left[\frac{-\Delta P_s}{\rho_b g}\right]\left[1 + \frac{t}{H}\right] \qquad 5.4$$

Using the specific value of t which applies to each run, all the experimental data are replotted as $[(-\Delta P_s)/(\rho_b g)][1+(t/H)]$ versus H in Figure 5.11. Equation 5.4 is represented by the 45° straight line through the origin. Apparently, the fit is poor. The reason for this could be the arbitrary definition of t given by Equation 5.3, an empirical correlation which may be limited in scope.

Although the Manurung equations did not compare well with the present data on an absolute basis, they did show some consistency with the experimental observations, that is, the effects of temperature and fluid properties on $-\Delta P_s$ were correctly indicated as insignificant.

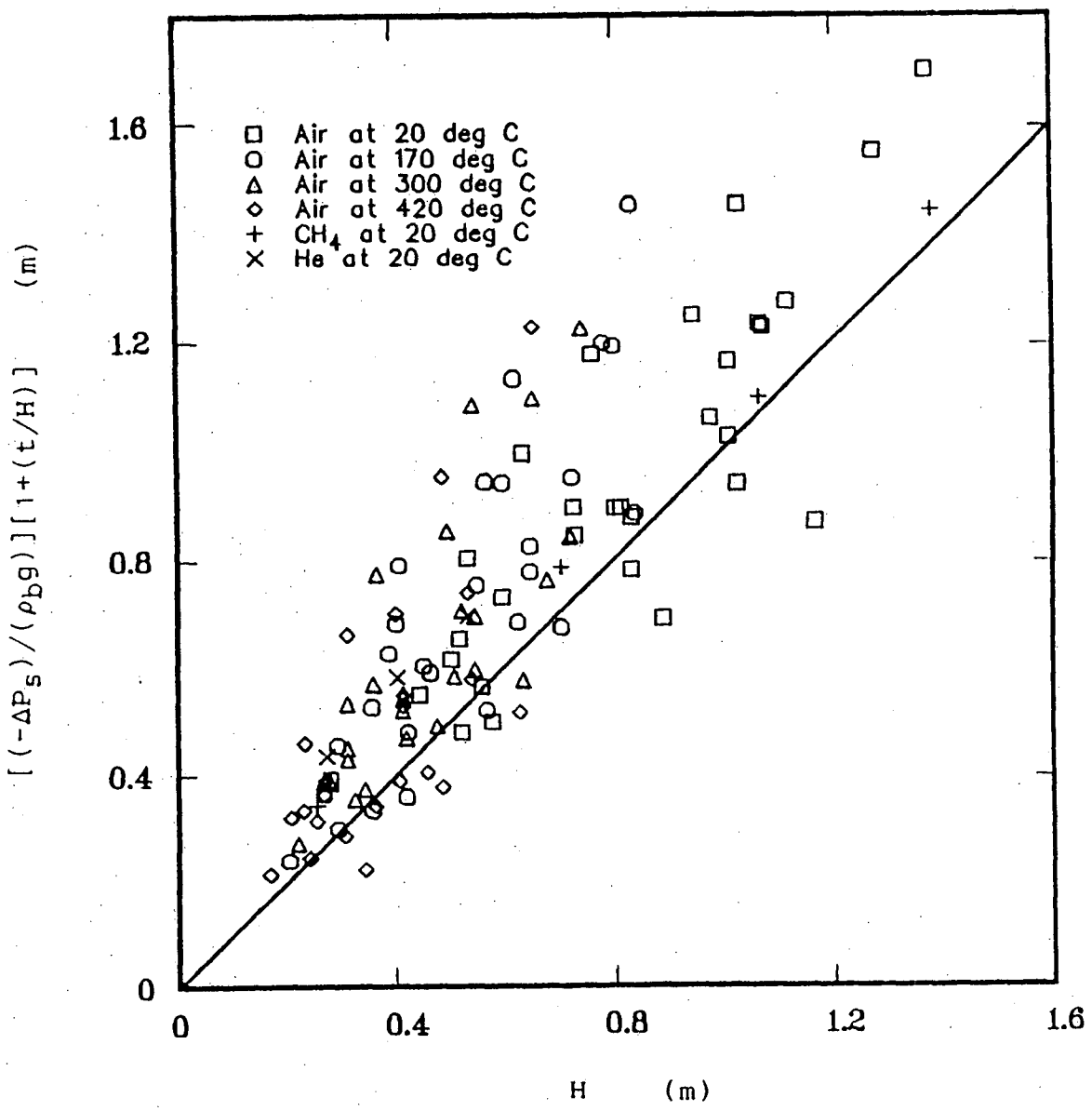

Figure 5.11 Comparison between experimental results and prediction by Equations 5.3 and 5.4
The prediction is indicated by the 45° line.

6. SPOUT SHAPE, SPOUT DIAMETER AND FOUNTAIN HEIGHT

6.1 SPOUT SHAPE AND DIAMETER

In this work, two general types of spout shapes were observed (Figure 6.1). In both cases, the spout diameter expanded in the conical region and then converged slightly. Above the conical region, the spout diameter remained constant for type (b) whereas for type (a), the spout diameter was primarily constant but diverged near the bed surface. The bed temperature had a negligible effect on the spout shape. The only significant factor affecting the spout shape appeared to be the dimensionless bed height, namely H/H_m (Figure 6.2). Type (a) was found at bed heights close to H_m. As bed heights became lower, the spout shape approached type (b).

The average spout diameter was determined using Equation 3.7. Tables 6.1a, 6.1b, 6.1c and 6.1d summarize all the experimental conditions and the corresponding results while the experimental values of spout diameter versus bed level are given in Appendix D.

The variation of the average spout diameter (D_s) with bed height and bed temperature is shown in Figure 6.3. At a given temperature, D_s increased with increasing bed height. On the other hand, at a fixed bed height, the trend of D_s

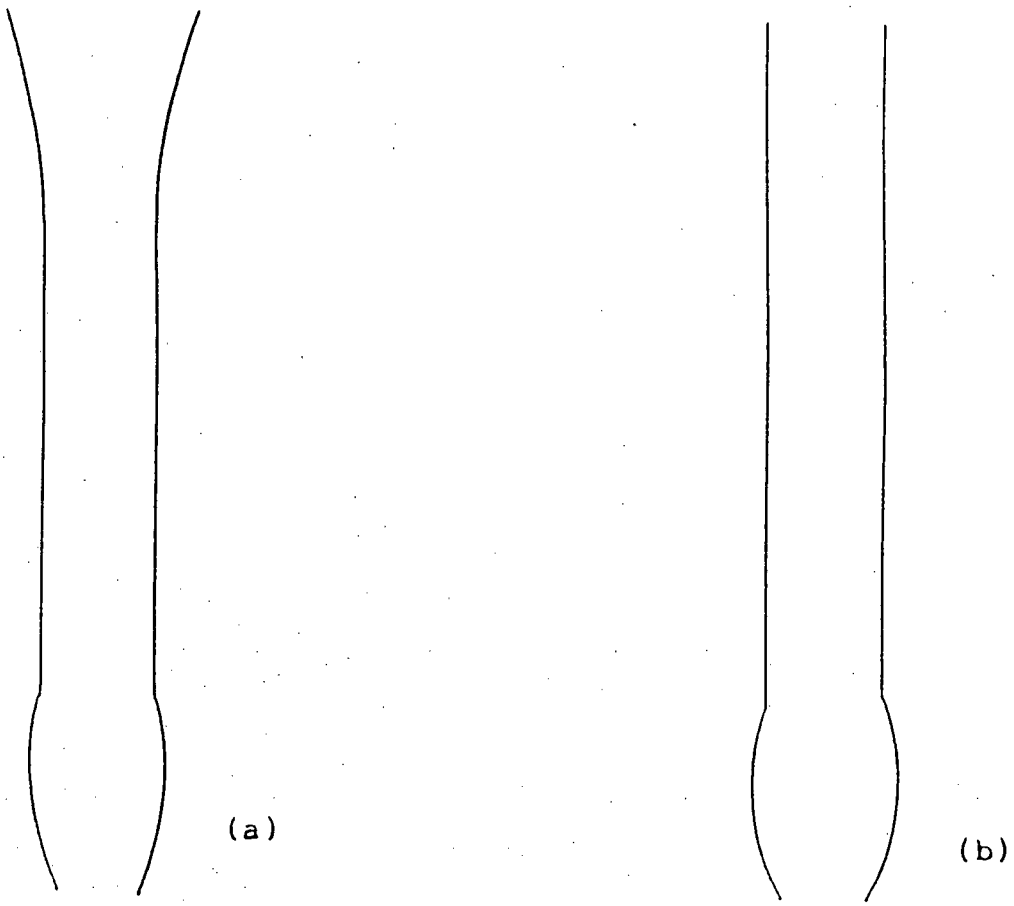

Figure 6.1 Observed spout shapes

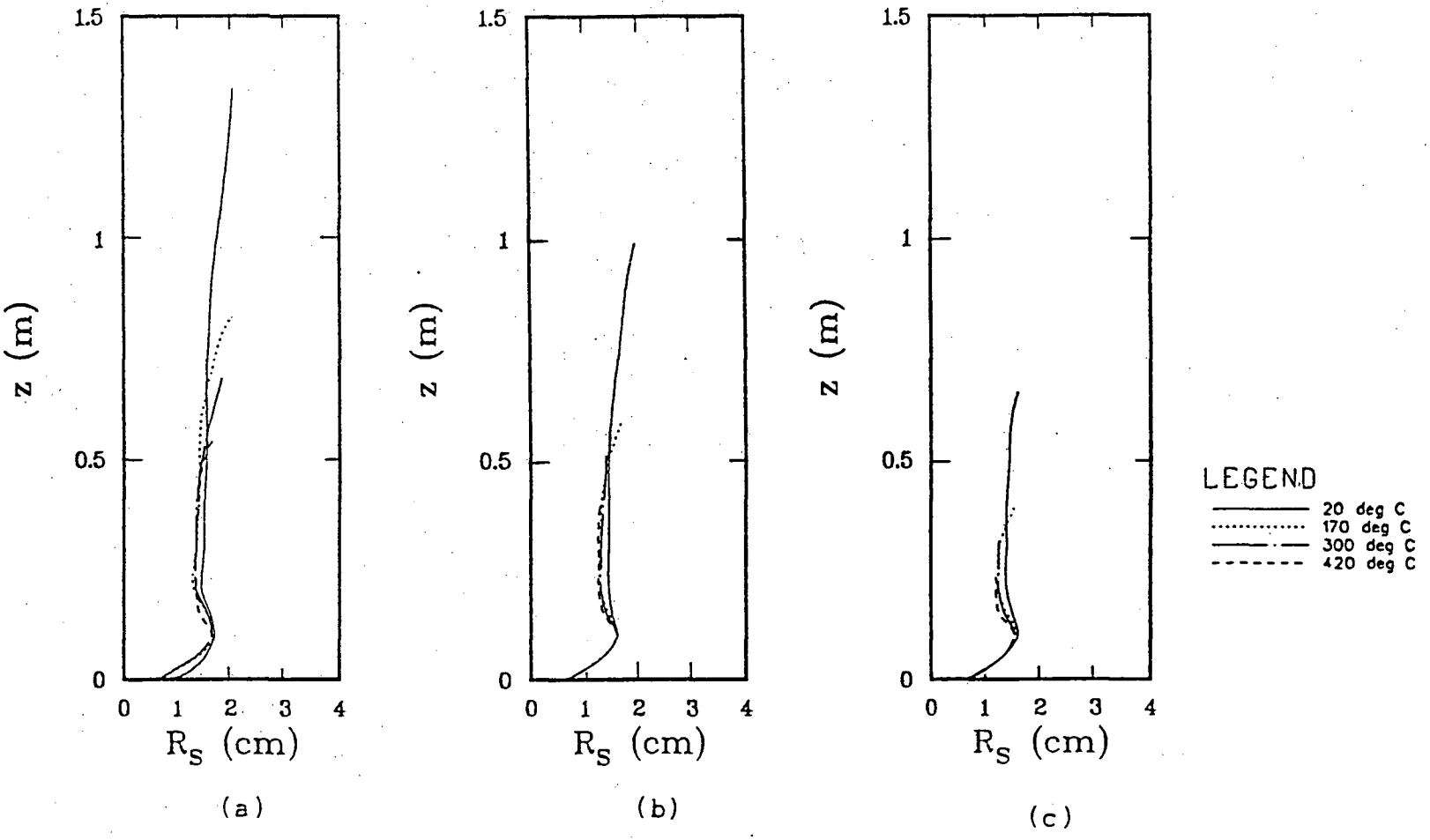

Figure 6.2 Effect of bed height and bed temperature on spout shape. Sand, d_p = 1.25 mm, D_i = 12.70 mm, $U/U_{ms} \simeq 1.10$.
(a) $H = H_m$, (b) $H \simeq 0.75\ H_m$ and (c) $H \simeq 0.50\ H_m$

Table 6.1a Average spout diameters and corresponding experimental conditions (bed temperature = 20 °C)

Run #	H/H_m	U/U_{ms}	G (kg/m^2s)	d_p (mm)	D_i (mm)	ρ_f (kg/m^3)	ν (kg/ms)	$D_{s\&}$ (cm)	D_{sP} (cm)	% dev	$D_{s\#}$ (cm)	% dev
1-1-a	1.000	1.075	1.112	0.945	19.05	1.246	1.80E-05	3.179	3.144	-1.10	2.978	-6.34
1-2-a	0.761	1.095	0.925	0.945	19.05	1.234	1.80E-05	2.876	2.873	-0.11	2.757	-4.14
1-3-a	0.495	1.124	0.882	0.945	19.05	1.220	1.80E-05	2.834	2.806	-0.97	2.709	-4.40
5-1-a	1.000	1.085	1.499	1.250	19.05	1.256	1.80E-05	3.416	3.639	6.54	3.381	-1.02
5-2-a	0.753	1.121	1.217	1.250	19.05	1.239	1.80E-05	3.062	3.286	7.32	3.101	1.28
5-3-a	0.485	1.110	1.062	1.250	19.05	1.223	1.80E-05	2.917	3.074	5.38	2.934	0.59
9-1-a	1.000	1.053	1.721	1.665	19.05	1.244	1.80E-05	3.694	3.894	5.42	3.600	-2.56
9-2-a	0.723	1.044	1.439	1.665	19.05	1.229	1.80E-05	3.444	3.567	3.58	3.342	-2.95
9-3-a	0.497	1.123	1.312	1.665	19.05	1.217	1.80E-05	3.284	3.409	3.82	3.220	-1.94
17-1-a	1.000	1.026	1.424	1.250	26.64	1.252	1.80E-05	3.443	3.549	3.08	3.310	-3.87
17-2-a	0.811	1.119	1.328	1.250	26.64	1.240	1.80E-05	3.272	3.430	4.82	3.220	-1.59
17-3-a	0.508	1.122	1.166	1.250	26.64	1.221	1.80E-05	3.042	3.218	5.78	3.057	0.49
21-1-a	1.000	1.011	1.900	1.665	26.64	1.261	1.80E-05	3.848	4.088	5.27	3.749	-3.46
21-2-a	0.850	1.109	1.792	1.665	26.64	1.242	1.80E-05	3.719	3.972	6.80	3.665	-1.46
21-3-a	0.572	1.148	1.596	1.665	26.64	1.224	1.80E-05	3.418	3.753	9.80	3.501	2.42
25-1-a	1.000	1.029	1.188	0.945	12.70	1.275	1.80E-05	3.033	3.247	7.07	3.044	0.37
25-2-a	0.815	1.110	1.060	0.945	12.70	1.252	1.80E-05	2.857	3.071	7.49	2.912	1.94
25-3-a	0.530	1.124	0.857	0.945	12.70	1.229	1.80E-05	2.623	2.767	5.50	2.670	1.80
29-1-a	1.000	1.047	1.523	1.250	12.70	1.261	1.80E-05	3.308	3.668	10.88	3.401	2.80
29-2-a	0.741	1.081	1.308	1.250	12.70	1.242	1.80E-05	3.094	3.404	10.03	3.197	3.34
29-3-a	0.498	1.124	1.149	1.250	12.70	1.226	1.80E-05	2.843	3.195	12.37	3.034	6.72
33-1-a	1.000	1.045	1.799	1.665	12.70	1.245	1.80E-05	3.577	3.980	11.26	3.669	2.56
33-2-a	0.741	1.108	1.616	1.665	12.70	1.230	1.80E-05	3.311	3.776	14.04	3.514	6.13
33-3-a	0.518	1.110	1.385	1.665	12.70	1.216	1.80E-05	3.115	3.501	12.39	3.297	5.86
5-6-a	0.758	1.075	1.163	1.250	19.05	1.238	1.80E-05	2.974	3.214	8.06	3.042	2.27
5-6-b	0.758	1.128	1.220	1.250	19.05	1.238	1.80E-05	3.091	3.290	6.44	3.105	0.46
5-6-c	0.758	1.190	1.286	1.250	19.05	1.237	1.80E-05	3.124	3.376	8.07	3.178	1.72
5-9-a	0.260	1.058	0.857	1.250	19.05	1.209	1.80E-05	2.876	2.767	-3.78	2.683	-6.72
5-9-b	0.260	1.118	0.905	1.250	19.05	1.209	1.80E-05	2.930	2.842	-3.00	2.747	-6.26
5-9-c	0.260	1.179	0.955	1.250	19.05	1.209	1.80E-05	3.006	2.918	-2.93	2.811	-6.47

continued

Run #	H/H_m	U/U_{ms}	G (kg/m^2s)	d_p (mm)	D_t (mm)	ρ_f (kg/m^3)	ν (kg/ms)	D_s& (cm)	D_s● (cm)	% dev	D_s# (cm)	% dev
37-1-a	1.000	1.064	1.157	1.250	19.05	0.707	1.09E-05	3.646	3.206	-12.08	3.289	-9.80
37-2-a	0.773	1.075	1.086	1.250	19.05	0.695	1.09E-05	3.368	3.108	-7.73	3.215	-4.54
37-3-a	0.511	1.093	0.872	1.250	19.05	0.683	1.09E-05	3.142	2.791	-11.18	2.938	-6.49
37-4-a	0.184	1.075	0.616	1.250	19.05	0.670	1.09E-05	2.497	2.354	-5.73	2.541	1.77
37-4-b	0.184	1.117	0.639	1.250	19.05	0.670	1.09E-05	2.547	2.396	-5.91	2.582	1.36
37-4-c	0.184	1.170	0.670	1.250	19.05	0.669	1.09E-05	2.642	2.453	-7.16	2.636	-0.21
38-1-a	1.000	1.129	0.261	1.250	19.05	0.170	1.94E-05	2.732	1.545	-43.43	2.815	3.02
38-2-a	0.756	1.068	0.212	1.250	19.05	0.169	1.94E-05	2.585	1.396	-46.01	2.576	-0.33
38-2-b	0.756	1.112	0.221	1.250	19.05	0.169	1.94E-05	2.629	1.424	-45.82	2.623	-0.22
38-2-c	0.756	1.174	0.233	1.250	19.05	0.169	1.94E-05	2.663	1.462	-45.11	2.684	0.79
38-3-a	0.512	1.050	0.184	1.250	19.05	0.168	1.94E-05	2.457	1.302	-47.00	2.427	-1.22
38-3-b	0.512	1.095	0.192	1.250	19.05	0.168	1.94E-05	2.595	1.330	-48.77	2.472	-4.73
38-3-c	0.512	1.178	0.206	1.250	19.05	0.168	1.94E-05	2.641	1.376	-47.89	2.549	-3.49

& experimental value

● calculated value by Equation 2.16 (McNab equation)

calculated value by Equation 6.5

Table 6.1b Average spout diameters and corresponding experimental conditions (bed temperature = 170 °C)

Run #	H/H_m	U/U_{ms}	G (kg/m^2s)	d_p (mm)	D_i (mm)	ρ_f (kg/m^3)	ν (kg/ms)	D_s& (cm)	D_s@ (cm)	% dev	D_s# (cm)	% dev
2-1-a	1.000	1.101	0.508	0.945	19.05	0.802	2.35E-05	2.928	2.142	-26.86	2.482	-15.22
2-2-a	0.697	1.104	0.483	0.945	19.05	0.799	2.35E-05	2.499	2.089	-16.39	2.431	-2.71
2-3-a	0.484	1.099	0.363	0.945	19.05	0.797	2.35E-05	2.470	1.816	-26.46	2.150	-12.96
6-1-a	1.000	1.089	0.896	1.250	19.05	0.815	2.35E-05	3.094	2.828	-8.59	3.160	2.13
6-2-a	0.696	1.114	0.779	1.250	19.05	0.806	2.35E-05	3.001	2.641	-12.00	2.983	-0.59
6-3-a	0.451	1.100	0.644	1.250	19.05	0.801	2.35E-05	2.836	2.406	-15.17	2.752	-2.96
10-1-a	1.000	1.071	1.114	1.665	19.05	0.823	2.35E-05	3.496	3.147	-9.99	3.463	-0.94
10-2-a	0.746	1.115	1.050	1.665	19.05	0.814	2.35E-05	3.289	3.057	-7.06	3.386	2.94
10-3-a	0.500	1.092	0.909	1.665	19.05	0.805	2.35E-05	3.225	2.848	-11.68	3.191	-1.06
18-1-a	1.000	1.098	0.939	1.250	26.64	0.816	2.35E-05	3.337	2.894	-13.28	3.224	-3.40
18-2-a	0.806	1.134	0.873	1.250	26.64	0.809	2.35E-05	3.161	2.792	-11.66	3.131	-0.95
18-3-a	0.505	1.117	0.737	1.250	26.64	0.802	2.35E-05	3.054	2.570	-15.85	2.917	-4.50
22-1-a	1.000	1.050	1.352	1.665	26.64	0.822	2.35E-05	3.536	3.460	-2.15	3.767	6.54
22-2-a	0.746	1.123	1.204	1.665	26.64	0.813	2.35E-05	3.399	3.269	-3.83	3.594	5.74
22-3-a	0.504	1.131	1.071	1.665	26.64	0.805	2.35E-05	3.300	3.087	-6.47	3.426	3.81
26-1-a	1.000	1.108	0.541	0.945	12.70	0.814	2.35E-05	2.632	2.209	-16.08	2.540	-3.48
26-2-a	0.758	1.102	0.473	0.945	12.70	0.807	2.35E-05	2.402	2.068	-13.90	2.403	0.02
26-3-a	0.492	1.091	0.395	0.945	12.70	0.801	2.35E-05	2.294	1.893	-17.47	2.227	-2.93
30-1-a	1.000	1.086	0.851	1.250	12.70	0.818	2.35E-05	2.952	2.758	-6.58	3.087	4.57
30-2-a	0.723	1.099	0.709	1.250	12.70	0.809	2.35E-05	2.748	2.522	-8.23	2.861	4.11
30-3-a	0.496	1.104	0.596	1.250	12.70	0.801	2.35E-05	2.676	2.316	-13.45	2.661	-0.55
34-1-a	1.000	1.052	1.353	1.665	12.70	0.820	2.35E-05	3.456	3.461	0.15	3.771	9.12
34-2-a	0.744	1.088	1.152	1.665	12.70	0.811	2.35E-05	3.302	3.199	-3.12	3.528	6.85
34-3-a	0.488	1.093	0.926	1.665	12.70	0.802	2.35E-05	3.141	2.874	-8.49	3.220	2.51
6-5-a	0.716	1.079	0.748	1.250	19.05	0.806	2.35E-05	2.978	2.589	-13.07	2.931	-1.57
6-5-b	0.716	1.162	0.806	1.250	19.05	0.806	2.35E-05	3.048	2.685	-11.90	3.028	-0.67
6-5-c	0.716	1.208	0.837	1.250	19.05	0.806	2.35E-05	3.175	2.735	-13.85	3.078	-3.07
6-6-a	0.412	1.039	0.572	1.250	19.05	0.799	2.35E-05	2.781	2.270	-18.38	2.616	-5.93
6-6-b	0.412	1.122	0.618	1.250	19.05	0.799	2.35E-05	2.838	2.358	-16.93	2.705	-4.68
6-6-c	0.412	1.180	0.650	1.250	19.05	0.799	2.35E-05	2.890	2.417	-16.38	2.765	-4.32

& experimental value

@ calculated value by Equation 2.16 (McNab equation)

calculated value by Equation 6.5

Table 6.1c Average spout diameters and corresponding experimental conditions (bed temperature = 300 °C)

Run #	H/H_m	U/U_{ms}	G (kg/m^2s)	d_p (mm)	D_i (mm)	ρ_f (kg/m^3)	μ (kg/ms)	D_s& (cm)	D_se (cm)	% dev	D_s# (cm)	% dev
7-1-a	1.000	1.105	0.643	1.250	19.05	0.625	2.85E-05	2.955	2.404	-18.65	3.029	2.50
7-2-a	0.756	1.113	0.605	1.250	19.05	0.621	2.85E-05	2.810	2.333	-16.97	2.955	5.18
7-3-a	0.510	1.106	0.529	1.250	19.05	0.618	2.85E-05	2.803	2.185	-22.06	2.792	-0.38
11-1-a	1.000	1.064	0.902	1.665	19.05	0.629	2.85E-05	3.438	2.837	-17.47	3.501	1.84
11-2-a	0.723	1.179	0.855	1.665	19.05	0.626	2.85E-05	3.260	2.764	-15.21	3.426	5.08
11-3-a	0.498	1.126	0.693	1.665	19.05	0.620	2.85E-05	3.058	2.494	-18.45	3.136	2.55
19-1-a	1.000	1.093	0.646	1.250	26.64	0.623	2.85E-05	3.000	2.409	-19.69	3.038	1.26
19-2-a	0.773	1.090	0.605	1.250	26.64	0.620	2.85E-05	2.946	2.333	-20.80	2.957	0.37
19-3-a	0.523	1.106	0.534	1.250	26.64	0.617	2.85E-05	2.829	2.195	-22.42	2.805	-0.85
23-1-a	1.000	1.080	1.042	1.665	26.64	0.631	2.85E-05	3.500	3.045	-12.99	3.724	6.39
23-2-a	0.748	1.113	0.910	1.665	26.64	0.625	2.85E-05	3.275	2.850	-12.98	3.521	7.51
23-3-a	0.505	1.124	0.813	1.665	26.64	0.620	2.85E-05	3.238	2.697	-16.72	3.361	3.79
27-1-a	1.000	1.046	0.378	0.945	12.70	0.622	2.85E-05	2.468	1.853	-24.92	2.409	-2.37
27-2-a	0.750	1.083	0.332	0.945	12.70	0.620	2.85E-05	2.278	1.739	-23.67	2.280	0.08
27-3-a	0.490	1.100	0.306	0.945	12.70	0.618	2.85E-05	2.031	1.671	-17.74	2.203	8.45
31-1-a	1.000	1.105	0.589	1.250	12.70	0.629	2.85E-05	2.916	2.303	-21.03	2.911	-0.18
31-2-a	0.757	1.096	0.503	1.250	12.70	0.623	2.85E-05	2.686	2.131	-20.65	2.726	1.48
31-3-a	0.476	1.103	0.395	1.250	12.70	0.618	2.85E-05	2.596	1.893	-27.07	2.460	-5.23
35-1-a	1.000	1.071	0.948	1.665	12.70	0.631	2.85E-05	3.395	2.907	-14.36	3.574	5.28
35-2-a	0.730	1.117	0.822	1.665	12.70	0.624	2.85E-05	3.251	2.711	-16.60	3.371	3.68
35-3-a	0.491	1.104	0.690	1.665	12.70	0.619	2.85E-05	2.898	2.488	-14.13	3.132	8.06
7-5-a	0.756	1.055	0.559	1.250	19.05	0.622	2.85E-05	2.831	2.244	-20.72	2.855	0.83
7-5-b	0.756	1.112	0.589	1.250	19.05	0.622	2.85E-05	2.874	2.303	-19.88	2.920	1.60
7-5-c	0.756	1.160	0.614	1.250	19.05	0.622	2.85E-05	2.977	2.350	-21.06	2.973	-0.13
7-7-a	0.489	1.049	0.479	1.250	19.05	0.618	2.85E-05	2.757	2.081	-24.52	2.675	-2.98
7-7-b	0.489	1.111	0.508	1.250	19.05	0.618	2.85E-05	2.805	2.142	-23.65	2.744	-2.18
7-7-c	0.489	1.162	0.531	1.250	19.05	0.618	2.85E-05	2.848	2.189	-23.15	2.797	-1.80

& experimental value

e calculated value by Equation 2.16 (McNab equation)

calculated value by Equation 6.5

Table 6.1d Average spout diameters and corresponding experimental conditions (bed temperature = 420 °C)

Run #	H/H_m	U/U_{ms}	G (kg/m^2s)	d_p (mm)	D_i (mm)	ρ_f (kg/m^3)	μ (kg/ms)	D_s& (cm)	D_s@ (cm)	% dev	D_s# (cm)	% dev
8-1-a	1.000	1.101	0.493	1.250	19.05	0.514	3.20E-05	2.834	2.110	-25.53	2.905	2.50
8-2-a	0.646	1.105	0.458	1.250	19.05	0.511	3.20E-05	2.796	2.036	-27.19	2.818	0.80
8-3-a	0.499	1.100	0.375	1.250	19.05	0.510	3.20E-05	2.616	1.846	-29.45	2.586	-1.15
12-1-a	1.000	1.103	0.744	1.665	19.05	0.515	3.20E-05	3.514	2.582	-26.52	3.470	-1.26
12-2-a	0.727	1.127	0.713	1.665	19.05	0.512	3.20E-05	3.233	2.529	-21.79	3.412	5.54
12-3-a	0.485	1.120	0.571	1.665	19.05	0.510	3.20E-05	2.957	2.268	-23.30	3.103	4.92
20-1-a	1.000	1.027	0.497	1.250	26.64	0.511	3.20E-05	2.876	2.119	-26.33	2.920	1.52
20-2-a	0.703	1.106	0.476	1.250	26.64	0.510	3.20E-05	2.811	2.074	-26.20	2.867	2.00
20-3-a	0.490	1.114	0.394	1.250	26.64	0.509	3.20E-05	2.740	1.891	-30.99	2.643	-3.53
24-1-a	1.000	1.124	0.857	1.665	26.64	0.517	3.20E-05	3.449	2.767	-19.77	3.685	6.85
24-2-a	0.752	1.124	0.762	1.665	26.64	0.513	3.20E-05	3.386	2.612	-22.85	3.510	3.66
24-3-a	0.470	1.112	0.652	1.665	26.64	0.511	3.20E-05	3.053	2.420	-20.73	3.284	7.57
28-1-a	1.000	1.101	0.323	0.945	12.70	0.510	3.20E-05	2.478	1.715	-30.77	2.422	-2.24
28-2-a	0.745	1.077	0.284	0.945	12.70	0.509	3.20E-05	2.059	1.611	-21.77	2.292	11.33
28-3-a	0.471	1.126	0.240	0.945	12.70	0.508	3.20E-05	1.941	1.483	-23.59	2.132	9.86
32-1-a	1.000	1.095	0.452	1.250	12.70	0.515	3.20E-05	2.796	2.023	-27.66	2.796	-0.00
32-2-a	0.750	1.103	0.400	1.250	12.70	0.513	3.20E-05	2.591	1.905	-26.48	2.655	2.46
32-3-a	0.435	1.104	0.315	1.250	12.70	0.510	3.20E-05	2.562	1.695	-33.86	2.398	-6.42
36-1-a	1.000	1.086	0.746	1.665	12.70	0.519	3.20E-05	3.312	2.585	-21.94	3.466	4.66
36-2-a	0.743	1.108	0.645	1.665	12.70	0.515	3.20E-05	3.212	2.407	-25.05	3.262	1.55
36-3-a	0.476	1.108	0.539	1.665	12.70	0.511	3.20E-05	2.880	2.205	-23.45	3.024	5.01
8-5-a	0.654	1.041	0.426	1.250	19.05	0.511	3.20E-05	2.714	1.965	-27.61	2.731	0.63
8-5-b	0.654	1.094	0.448	1.250	19.05	0.511	3.20E-05	2.809	2.014	-28.31	2.791	-0.63
8-5-c	0.654	1.191	0.488	1.250	19.05	0.511	3.20E-05	2.908	2.100	-27.79	2.897	-0.39

& experimental value

@ calculated value by Equation 2.16 (McNab equation)

calculated value by Equation 6.5

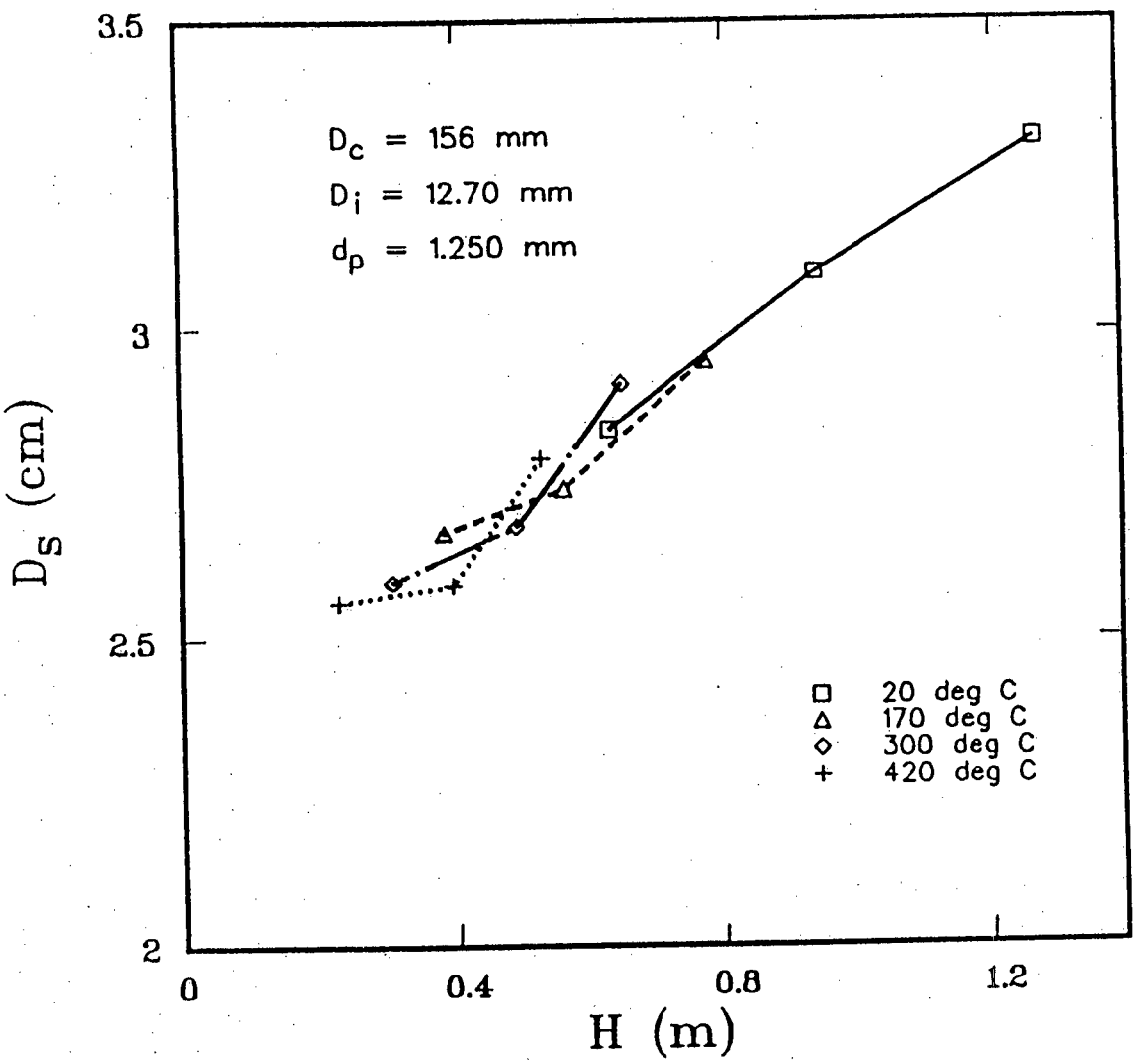

Figure 6.3 Effect of bed height and bed temperature on D_s. Sand, d_p = 1.25 mm, D_i = 12.70 mm, $U/U_{ms} \simeq 1.10$.

with T_s was somewhat inconclusive based on this figure. The effect of the bed temperature is best illustrated in Figure 6.4. At a constant bed height (i.e., H ≃ 27 cm) and a constant value of U/U_{ms}, D_s was observed to decrease only slightly with increasing bed temperature. Thus the effect of the bed temperature was not significant. Figure 6.4 also shows the trend of D_s with the bed temperature as predicted by McNab's correlation, Equation 2.16. It clearly demonstrates that this equation is not suitable for estimating D_s at high bed temperature.

In general, McNab's correlation worked fairly well for air spouting at room conditions (see Table 6.1a). As temperature increased, however, it underpredicted the average diameter (Tables 6.1b, 6.1c and 6.1d). It can be seen from Table 6.1a that the McNab equation was also unsatisfactory for Run # 38 in which helium gas was the spouting medium. The method of Littman (1982) was not applicable because it was restricted to spherical particles.

Based on the theoretical model of Bridgwater and Mathur (1972), an alternate equation was developed. Starting with their model,

$$\frac{32 f \rho_f Q_s^2}{\pi^2 \psi (D_c - D_s) D_s^4} = 1 \qquad 2.14$$

the following assumptions were made:

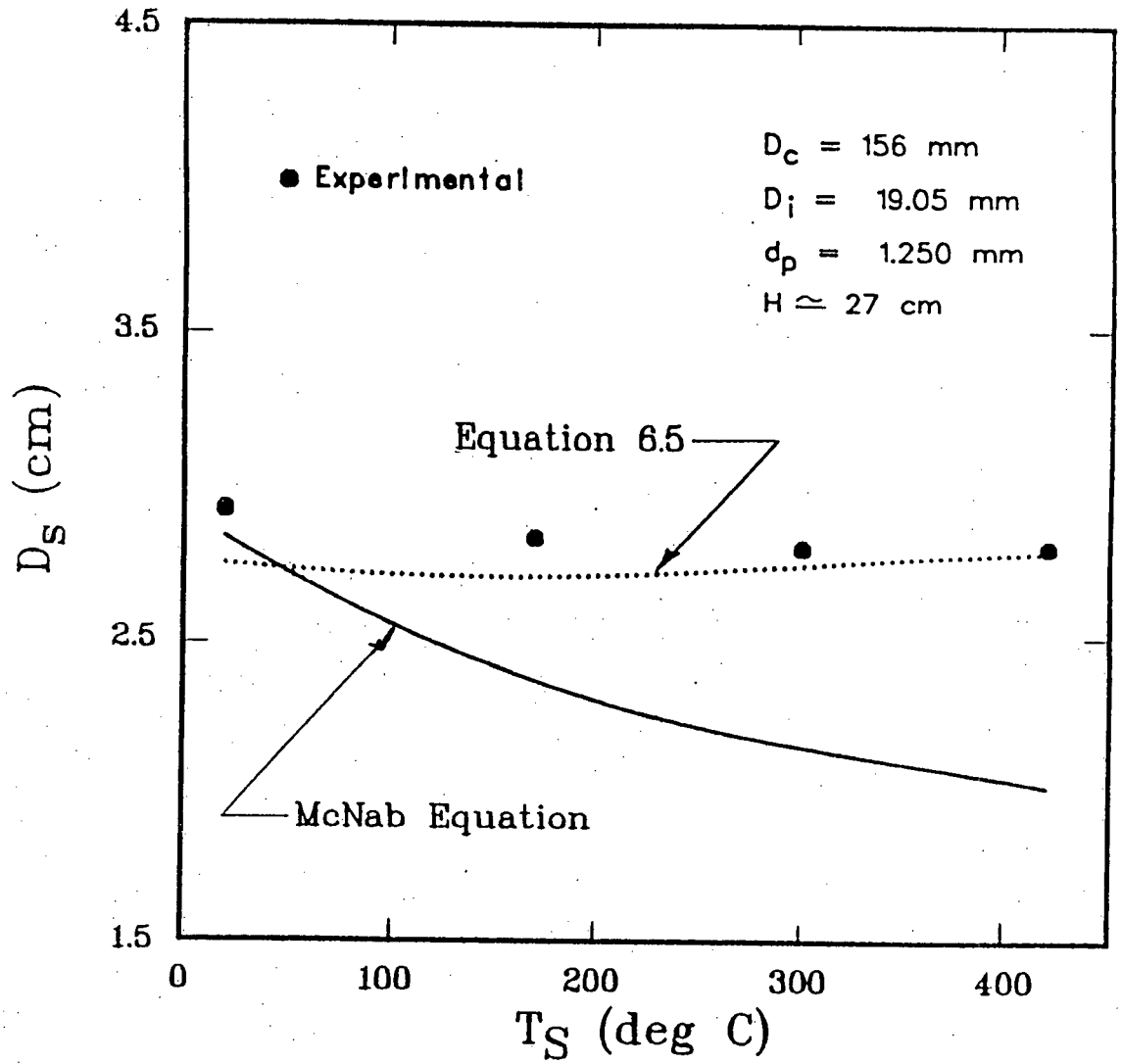

Figure 6.4 Effect of bed temperature on D_s. Sand, d_p = 1.25 mm, D_i = 19.05 mm, $U/U_{ms} \simeq 1.10$

1. $f = k_1 Re_s^{\,a} = k_1[4Q_s\rho_f/\mu\pi D_s]^a$

2. $Q_s = k_2 Q_t = 0.25k_2\pi D_c^{\,2}G/\rho_f$

3. $\psi = k_3\rho_b g$

4. $(D_c - D_s) = k_4 D_c$

Equation 2.14 then becomes

$$k\left[\frac{G^{2+a}D_c^{\,3+2a}}{\mu^a(\rho_b\rho_f g)D_s^{\,4+a}}\right] = 1 \qquad 6.1$$

where

$$k = \frac{32k_1(4/\pi)^a(k_2\pi/4)^{2+a}}{\pi^2(k_3k_4)} \qquad 6.2$$

Equation 6.1 can be reduced to

$$\left[\frac{D_s^{\,4}\rho_f\rho_b g}{G^2D_c^{\,3}}\right] = k\left[\frac{GD_c^{\,2}}{\mu D_s}\right]^a \qquad 6.3$$

In the above expression, k, a and both groups are dimensionless. Applying a least squares fit to all the experimental data yielded k = 438.8 and a = -0.4708. Equation 6.1 can also be rewritten as

$$D_s = \left[k\left[\frac{G^{2+a}D_c^{\,3+2a}}{\mu^a(\rho_b\rho_f g)}\right]\right]^{1/(4+a)} \qquad 6.4$$

The equation of Bridgwater and Mathur (Equation 2.15) can be recovered with the following conditions:

1. $k_1 = 0.08$; $a = 0$

2. $k_2 = 0.5$

3. $k_3 = 0.5$

4. $k_4 = 1.0$

5. $g = 9.81\ m/s^2$

6. $\rho_f = 1.20\ kg/m^3$

Substituting k = 438.8 and a = -0.4708 into Equation 6.4 gives

$$D_s = 5.606\left[\frac{G^{0.4333}D_c^{0.5832}\mu^{0.1334}}{(\rho_b\rho_f g)^{0.2834}}\right] \qquad 6.5$$

As seen in Figure 6.4, Equation 2.16 overpredicts the effect of temperature on the average spout diameter whereas Equation 6.5 provides better agreement. Table 6.2 summarizes the average deviations between the experimental values and the calculated values by these two equations for different fluid conditions. The deficiency of Equation 2.16 is clearly demonstrated . Equation 6.5, on the other hand, shows excellent agreement with the experimental results in each of the six conditions. Figures 6.5a and 6.5b illustrate the overall applicability of Equation 6.5 as compared to Equation 2.16. This proposed expression (i.e., Equation 6.5) appears to work better than McNab's. It is also dimensionally consistent, which is another advantage over the McNab expression. D_c and ρ_b were not varied in this study. Hence Equation 6.5 has not been tested for the effects of these two parameters.

Table 6.2 Comparison between experimental and calculated values of D_s

Spouting gas	Temp (°C)	McNab Equation		Equation 6.5	
		AVERAGE ERROR (%)	RMS % ERROR	AVERAGE ERROR (%)	RMS % ERROR
Air	20	5.6	7.3	-0.4	3.7
Air	170	-12.2	13.6	-0.8	5.3
Air	300	-19.5	19.9	1.8	3.9
Air	420	-25.8	26.0	2.3	4.7
Methane	20	-8.3	8.7	-3.0	5.2
Helium	20	-46.3	46.3	-0.9	2.6

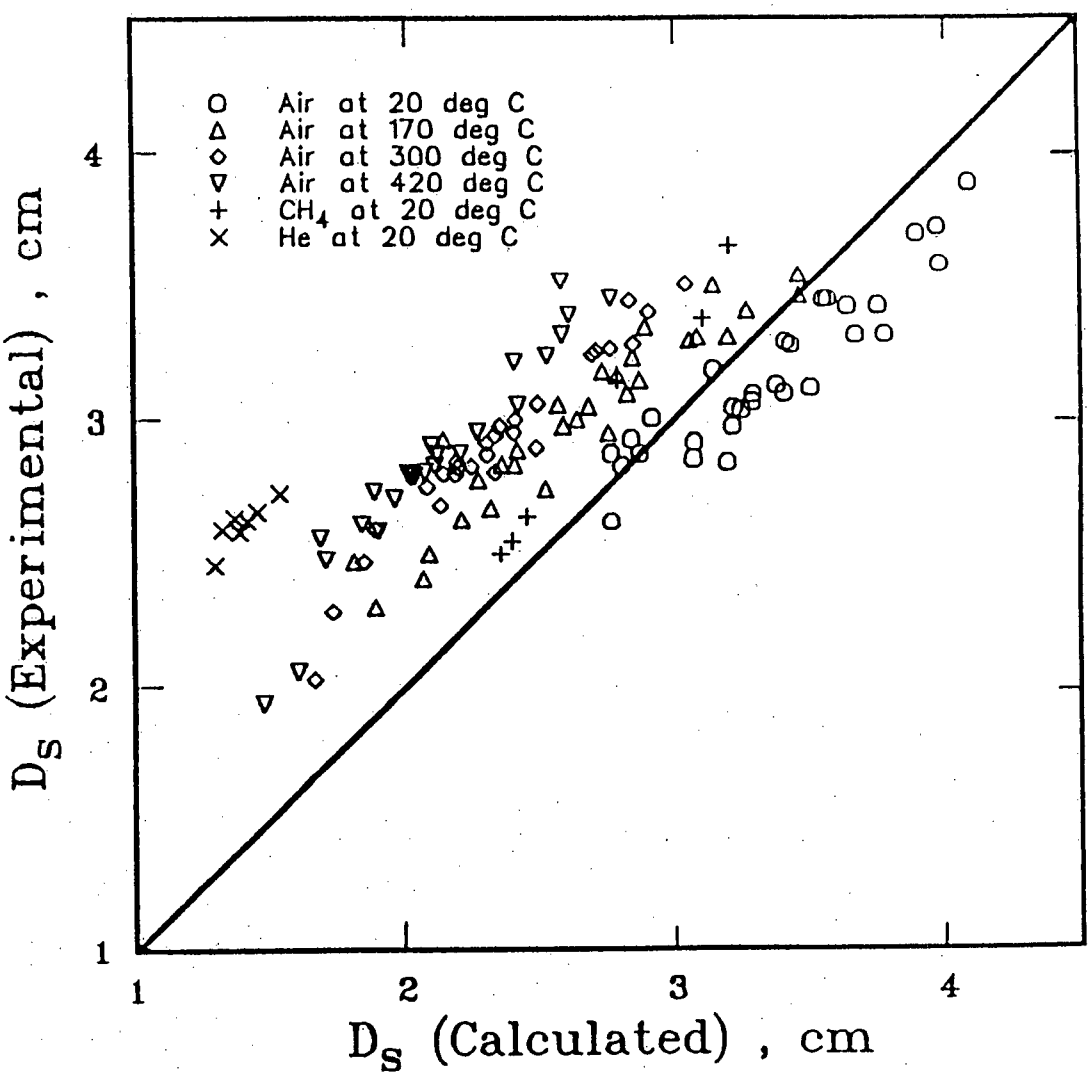

Figure 6.5a Comparison between experimental average spout diameter and prediction by Equation 2.16

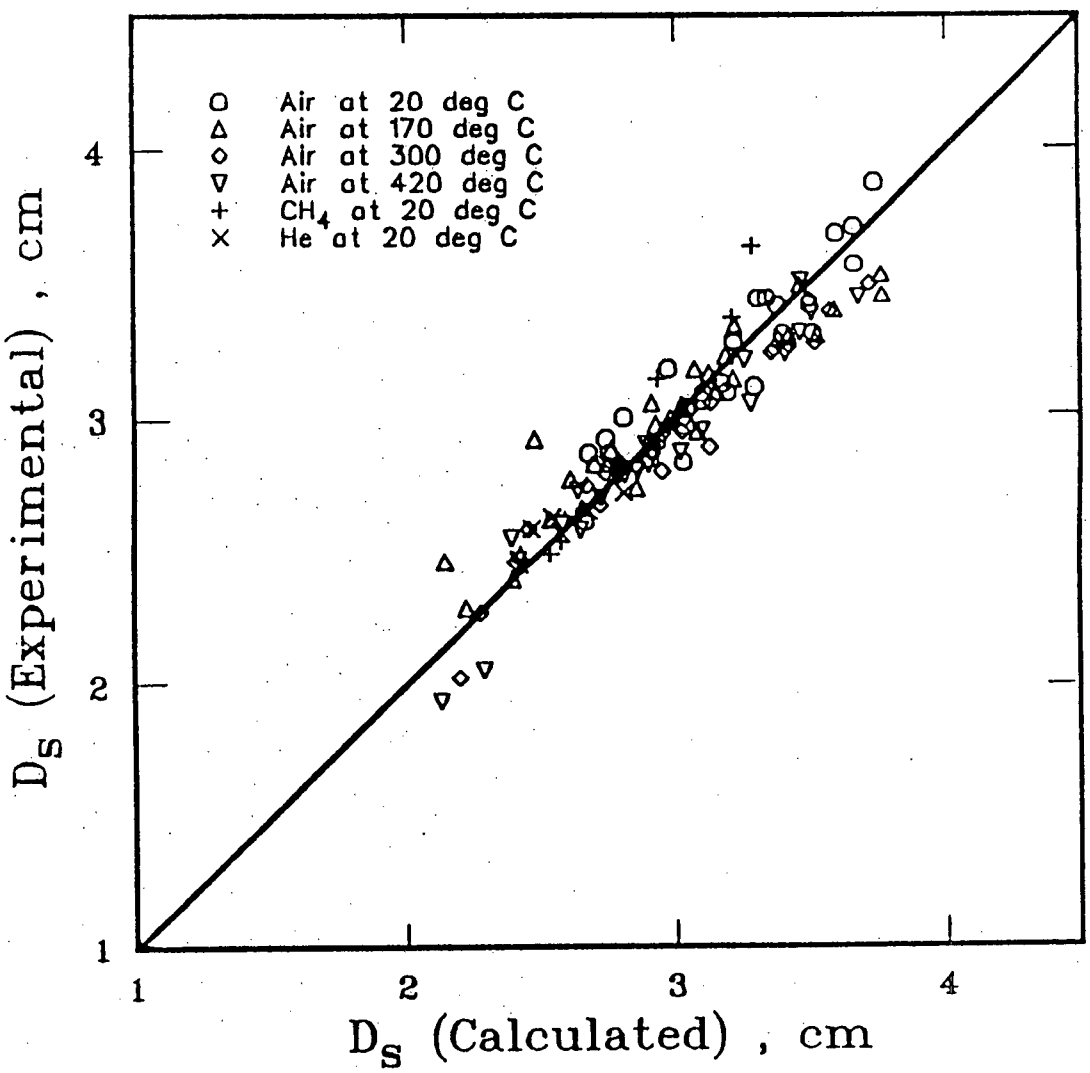

Figure 6.5b Comparison between experimental average spout diameter and prediction by Equation 6.5

6.2 FOUNTAIN HEIGHT

At steady spouting, all observed fountain shapes were basically parabolic. Fountain heights increased with U/U_{ms} but decreased with increasing bed height (Table 6.3 and Figure 6.6). Chandnani (1984) reported similar findings for fine particle spouting. The data reported by Grace and Mathur (1978) indicate the same trend with increasing U/U_{ms} but the effect of the bed height is not completely clear. However, in most cases, fountain heights were indeed smaller for higher bed heights. The effect of U/U_{ms} and bed height on spout particle velocity (Figures 6.7 and 6.8) has been reported by Lim (1975). Figure 6.7 illustrates that V_{sH} increases with U/U_{ms}, which explains the effect of U/U_{ms} on H_F in Figure 6.6, via Equation 2.38. Figure 6.8, on the other hand, does not clearly indicate any effect of bed height on V_{sH}, and hence provides no obvious explanation for the effect of H in Figure 6.6.

The fluid velocity in the spout at the bed surface, U_{sH}, was estimated from measured values of U_{aH} and D_{sH} (Table 6.4). For smaller bed heights, U_{sH} was found to be higher than for larger bed heights. With the assumption that higher U_{sH} produces higher V_{sH} and since H_F is directly proportional to V_{sH}^2 as indicated in Equation 2.38, higher fountain heights will be expected from higher U_{sH}. These results are consistent with those shown in Figure 6.6

Table 6.3 Experimental values of fountain height

Run #	Temp (°C)	H (m)	U/U_{ms}	H_F (cm)
5-6-a	20	0.813	1.076	13.74
5-6-b	20	0.813	1.128	21.54
5-6-c	20	0.813	1.190	26.88
5-9-a	20	0.279	1.058	17.88
5-9-b	20	0.279	1.118	24.02
5-9-c	20	0.279	1.179	28.64
6-5-a	170	0.464	1.079	12.22
6-5-b	170	0.464	1.162	16.93
6-5-c	170	0.464	1.208	22.86
6-6-a	170	0.267	1.039	16.18
6-6-b	170	0.267	1.122	21.45
6-6-c	170	0.267	1.180	25.29
7-5-a	300	0.413	1.055	10.24
7-5-b	300	0.413	1.112	15.98
7-5-c	300	0.413	1.160	20.58
7-7-a	300	0.267	1.049	14.34
7-7-b	300	0.267	1.111	19.02
7-7-c	300	0.267	1.162	23.80
8-5-a	420	0.270	1.041	10.00
8-5-b	420	0.270	1.094	13.08
8-5-c	420	0.270	1.191	17.88

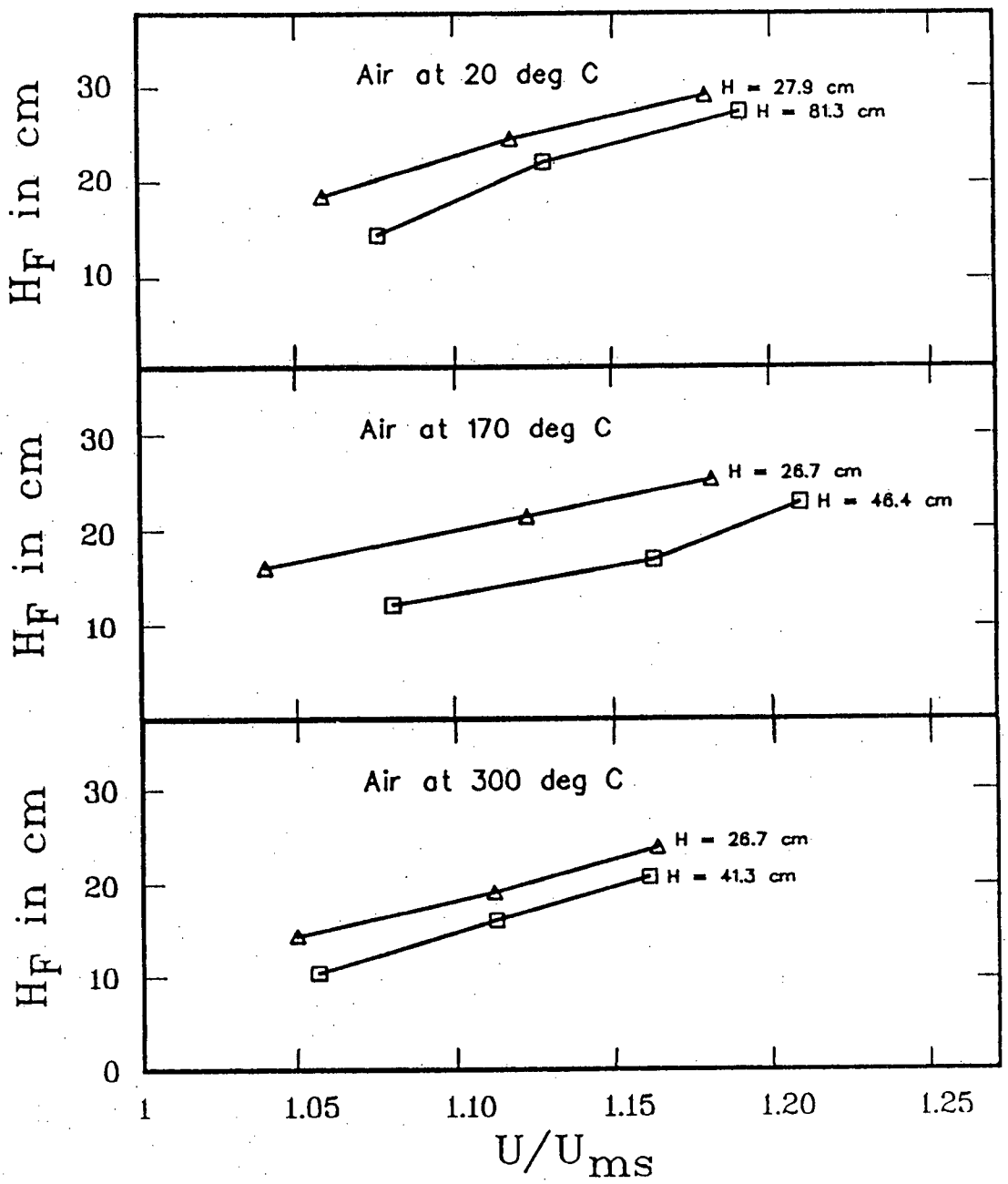

Figure 6.6 Effect of bed height and U/U_{ms} on fountain height. Sand, d_p = 1.25 mm, D_i = 19.05 mm

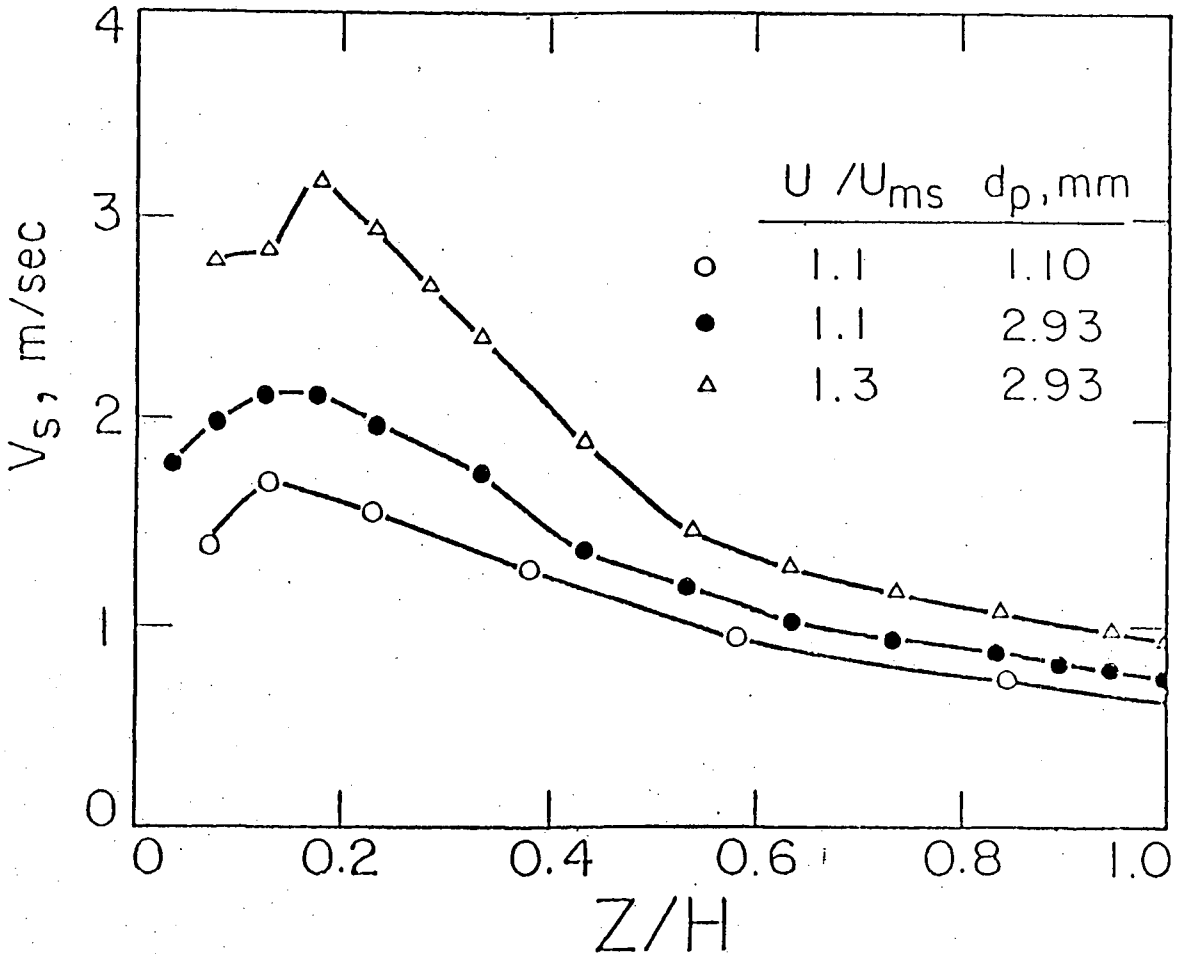

Figure 6.7 Effect of spouting velocity and particle diameter on spout particle velocity. Glass beads, D_c = 152 mm, H/D_c =3.0, D_i/D_c = 0.125 (Lim, 1975)

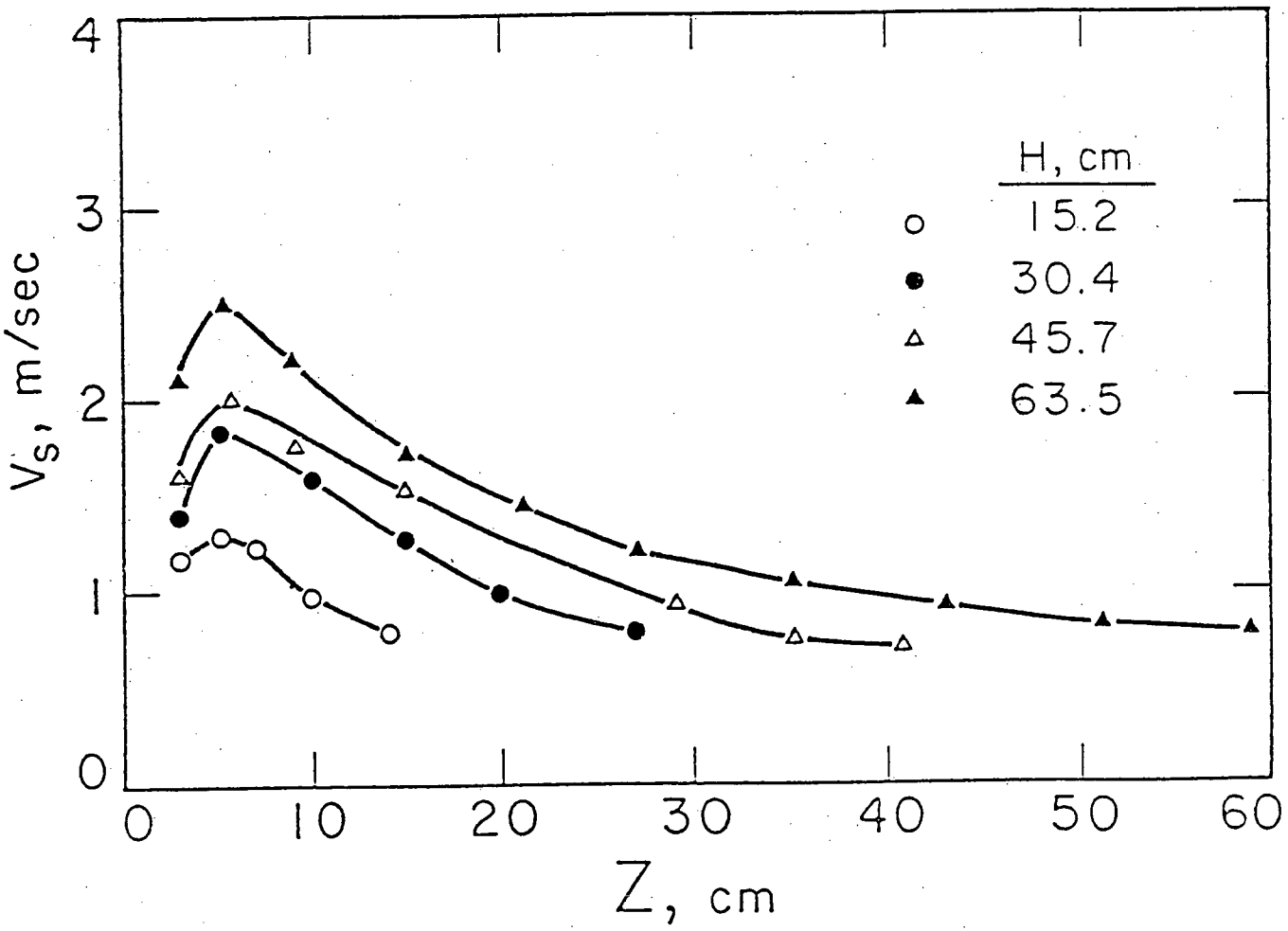

Figure 6.8 Effect of bed height on spout particle velocity.

D_c = 152 mm, D_i/D_c = 0.125, U/U_{ms} = 1.1 (Lim, 1975)

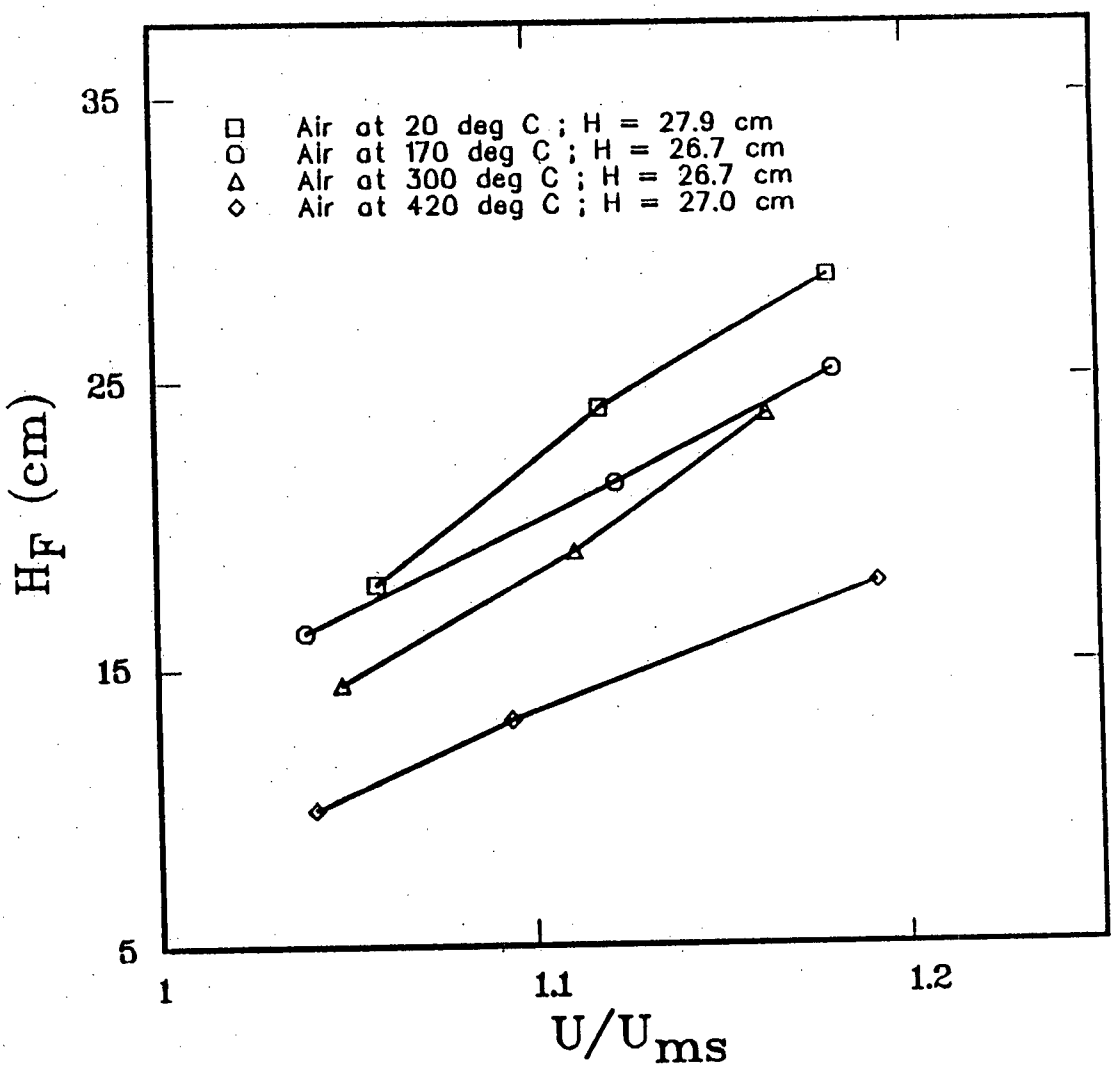

Figure 6.9 Effect of bed temperature on fountain height.

Sand, d_p = 1.25 mm, D_i = 19.05 mm

All the observed fountains were general quite stable regardless of bed temperatures but they started to fluctuate up and down as U/U_{ms} increased. At an approximately fixed bed height, the fountain height decreased with increasing bed temperature (Figure 6.9 and Table 6.3). This can be explained in terms of momentum transfer. At a lower temperature, the higher mass flow rate of gas at a given velocity causes higher spout particle velocities which produce higher fountain heights as predicted by Equation 2.38.

Table 6.4 U_{sH} at selected conditions

Run #	H (m)	U/U_{ms}	H_F (cm)	D_{sH} (m)	U (m/s)	Ua_H * (m/s)	U_{sH} ⊕ (m/s)
5-6-b	0.813	1.128	21.54	0.038	0.985	0.687	5.68
5-9-b	0.279	1.118	24.02	0.029	0.749	0.560	6.00
6-5-b	0.464	1.162	16.93	0.038	0.999	0.675	6.11
6-6-b	0.267	1.122	21.45	0.028	0.773	0.551	7.41
7-5-b	0.413	1.112	15.98	0.033	0.947	0.639	7.49
7-7-b	0.267	1.111	19.02	0.029	0.822	0.528	8.99

* determined from experimental data

⊕ $U_{sH} = [UD_c^2 - U_{aH}(D_c^2 - D_{sH}^2)] / D_{sH}^2$

7. PRESSURE PROFILES AND FLUID AND PARTICLE VELOCITIES IN THE ANNULUS

7.1 RADIAL PRESSURE PROFILES

Radial pressure profiles in the annulus were measured as described in Section 3.7.6. The results are listed in Table 7.1 and plotted in Figures 7.1a, 7.1b, 7.1c and 7.1d. The radial pressure profiles above the conical section for all four runs were essentially flat but for Run # 5-6-b, there were some slight decreases near the column wall. This can be explained in terms of the wall effect, that is, the volume adjacent to the wall has a higher voidage than the rest of the annulus, thus provides an easier passage for gas flow and subsequently produces the observed drops towards the column wall as shown in Figure 7.1a. For the other three runs (i.e., Runs # 6-5-b, # 7-5-b and # 8-5-b) in which the bed heights were much lower than that of Run # 5-6-b (see Table 7.1), there was no decrease in pressure at the wall. This means that the wall effect becomes less significant for lower bed heights. In general, the results indicate constant radial pressure in the annulus for any given bed levels above the conical region. This is in good agreement with the previously reported results (Mathur and Epstein, 1974). In addition, the bed temperature had no observable effect on the shape of the pressure profiles.

Table 7.1 Experimental values of annular pressure, d_p = 1.25 mm, D_1 = 19.05 mm

Run #	Temp (°C)	H (m)	H_a (m)	U/U_{ms}	z (m)	P_z-P_H in diff. rad. posit. (kN/m^2) r=3.8	5.2	6.4	7.3	7.7 cm	Mean (kN/m^2)
5-6-b	20	0.813	0.840	1.128	0.70	1.67	1.63	1.63	1.60	1.48	1.60
					0.50	3.84	3.80	3.76	3.76	3.73	3.78
					0.30	5.69	5.68	5.69	5.74	5.66	5.69
					0.10	6.18	6.18	6.18	6.18	6.10	6.16
					0.05	6.49	6.45				6.47
					0.00						6.52
6-5-b	170	0.464	0.480	1.162	0.40	0.67	0.67	0.67	0.65	0.65	0.66
					0.30	1.71	1.67	1.69	1.68	1.68	1.67
					0.15	2.80	2.76	2.76	2.77	2.77	2.77
					0.05	3.21	3.24				3.23
					0.00						3.25
7-5-b	300	0.413	0.430	1.112	0.35	0.69	0.69	0.69	0.68	0.67	0.68
					0.25	1.52	1.52	1.52	1.52	1.51	1.52
					0.15	2.20	2.20	2.20	2.17	2.17	2.19
					0.05	2.68	2.68				2.68
					0.00						2.77
8-5-b	420	0.270	0.285	1.094	0.25	0.19	0.19	0.19	0.19	0.19	0.19
					0.20	0.57	0.57	0.57	0.55	0.56	0.56
					0.15	0.81	0.81	0.80	0.80	0.80	0.80
					0.10	1.11	1.09	1.09	1.07	1.05	1.08
					0.05	1.37	1.37				1.37
					0.00						1.52

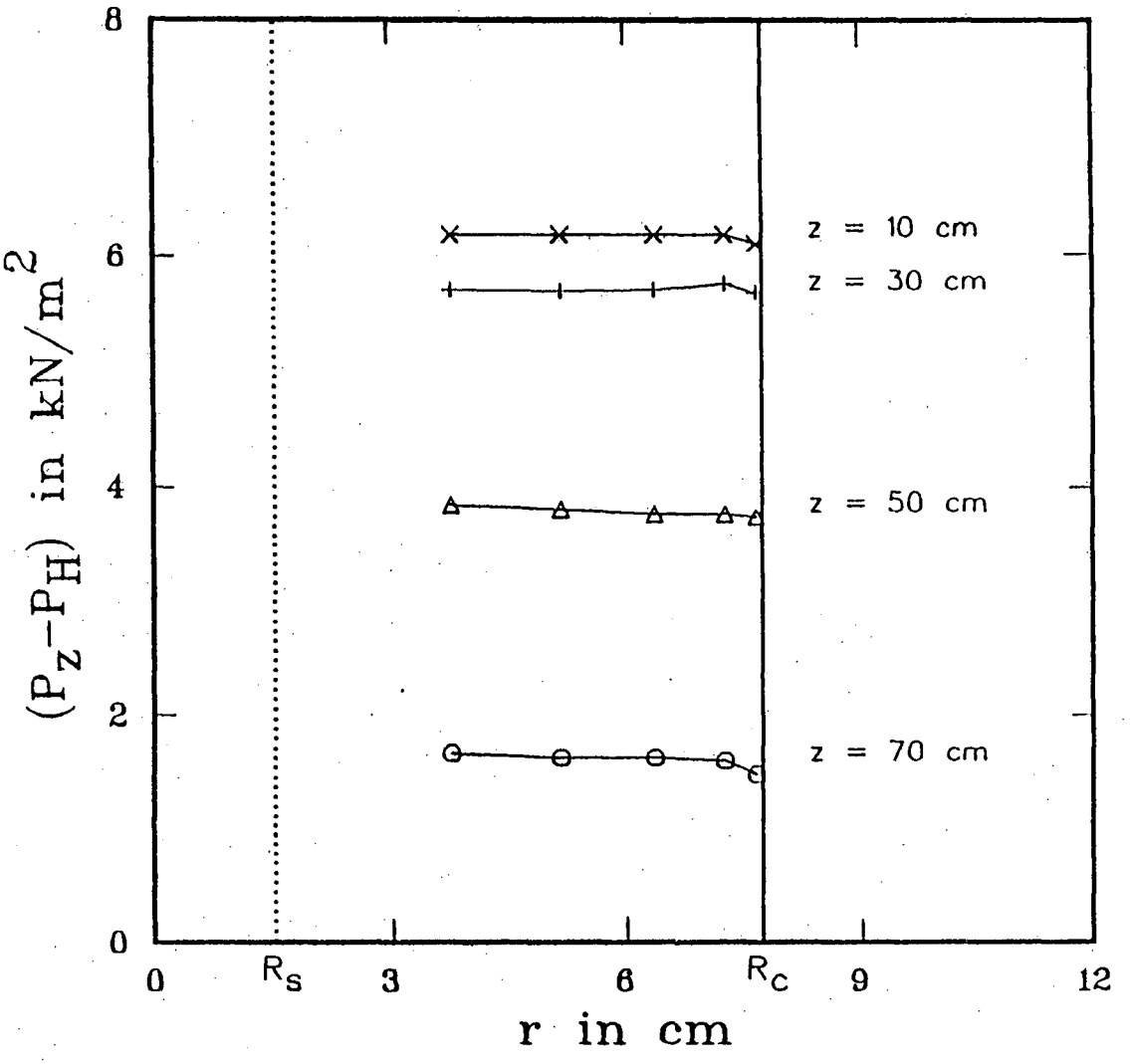

Figure 7.1a Radial pressure profiles in the cylindrical section (T_S = 20 °C)

R_c = column radius; R_s = average spout radius

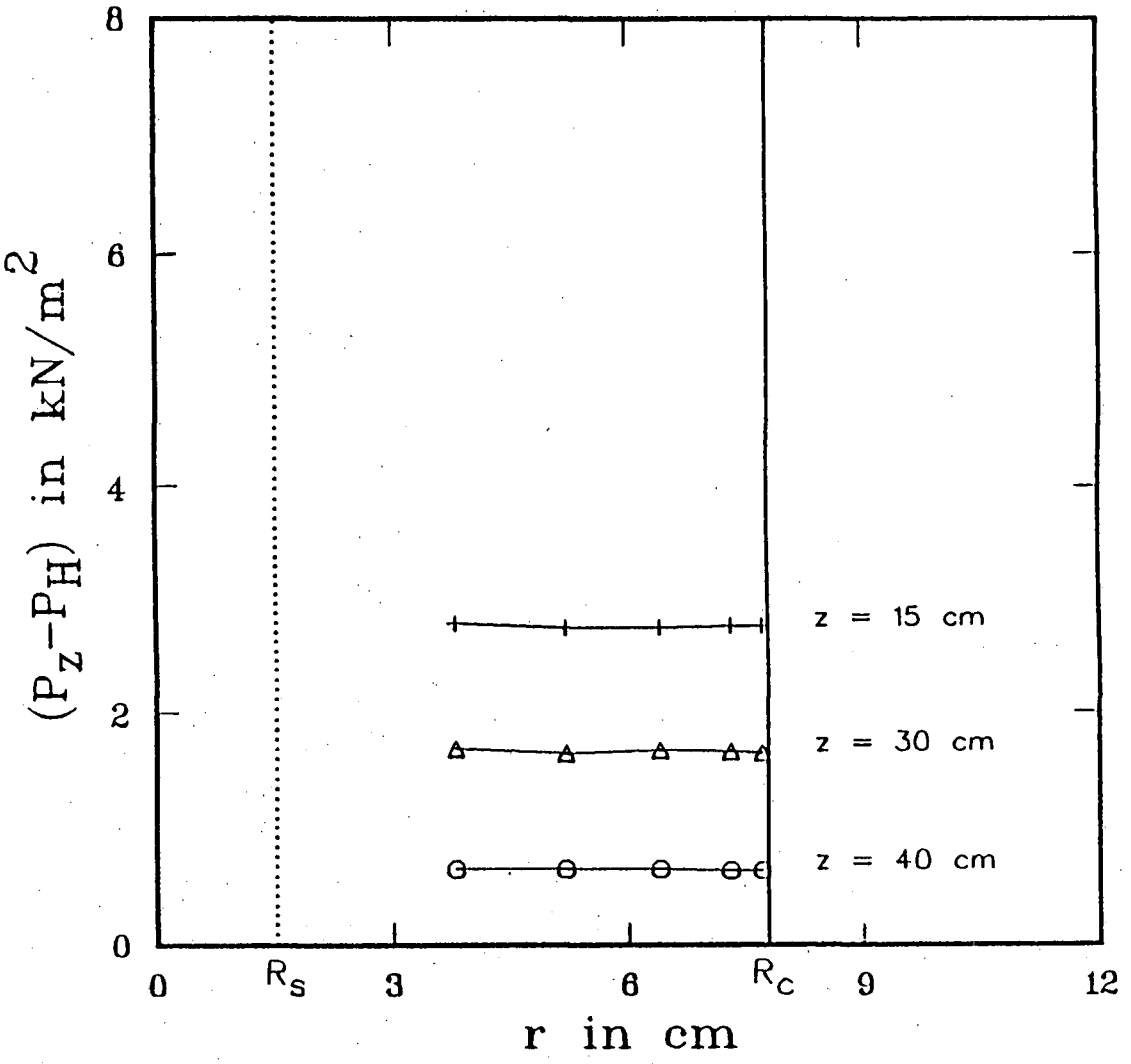

Figure 7.1b Radial pressure profiles in the cylindrical section (T_S = 170 °C)

R_c = column radius; R_s = average spout radius

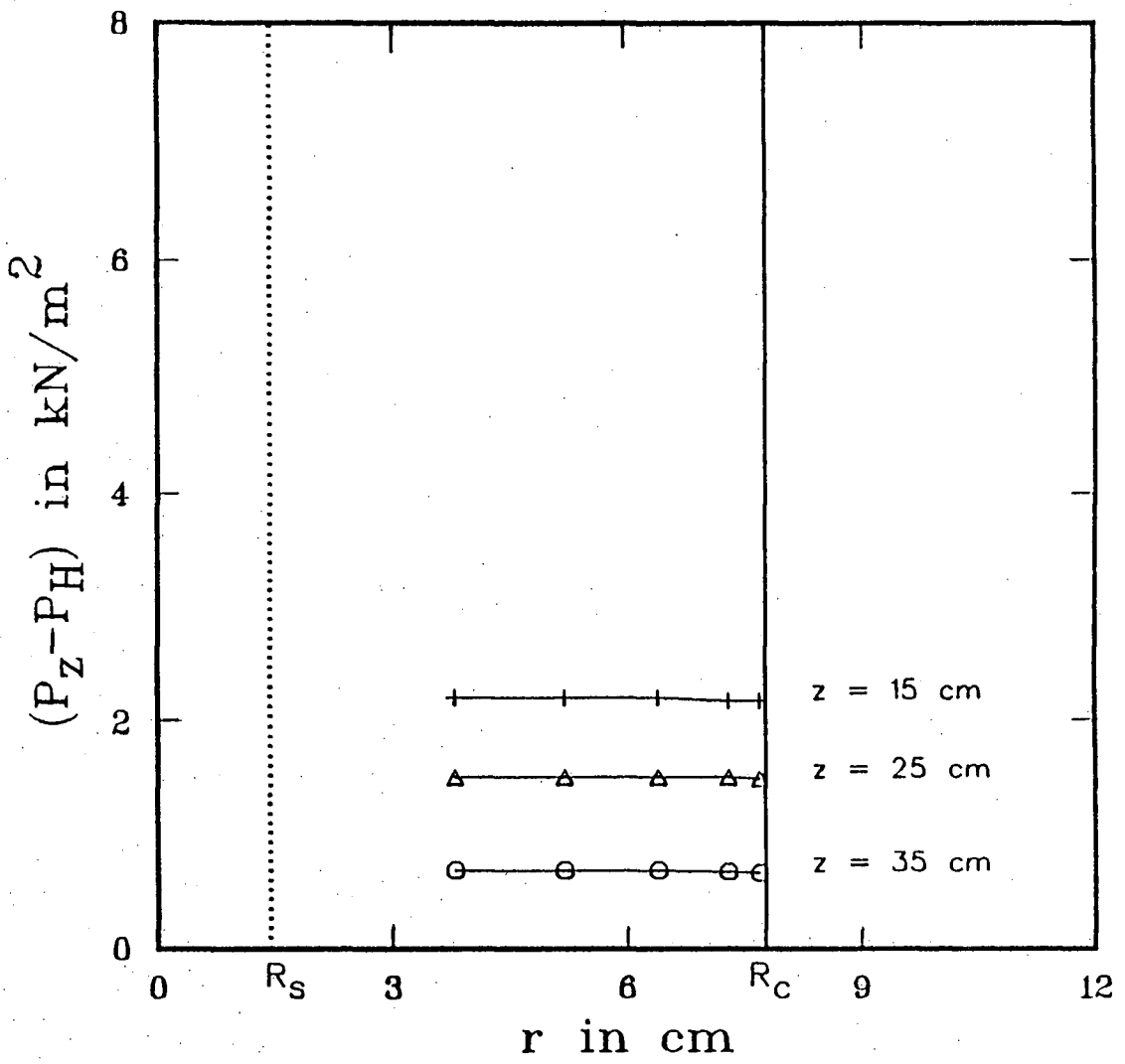

Figure 7.1c Radial pressure profiles in the cylindrical section (T_S = 300 °C)

R_C = column radius; R_S = average spout radius

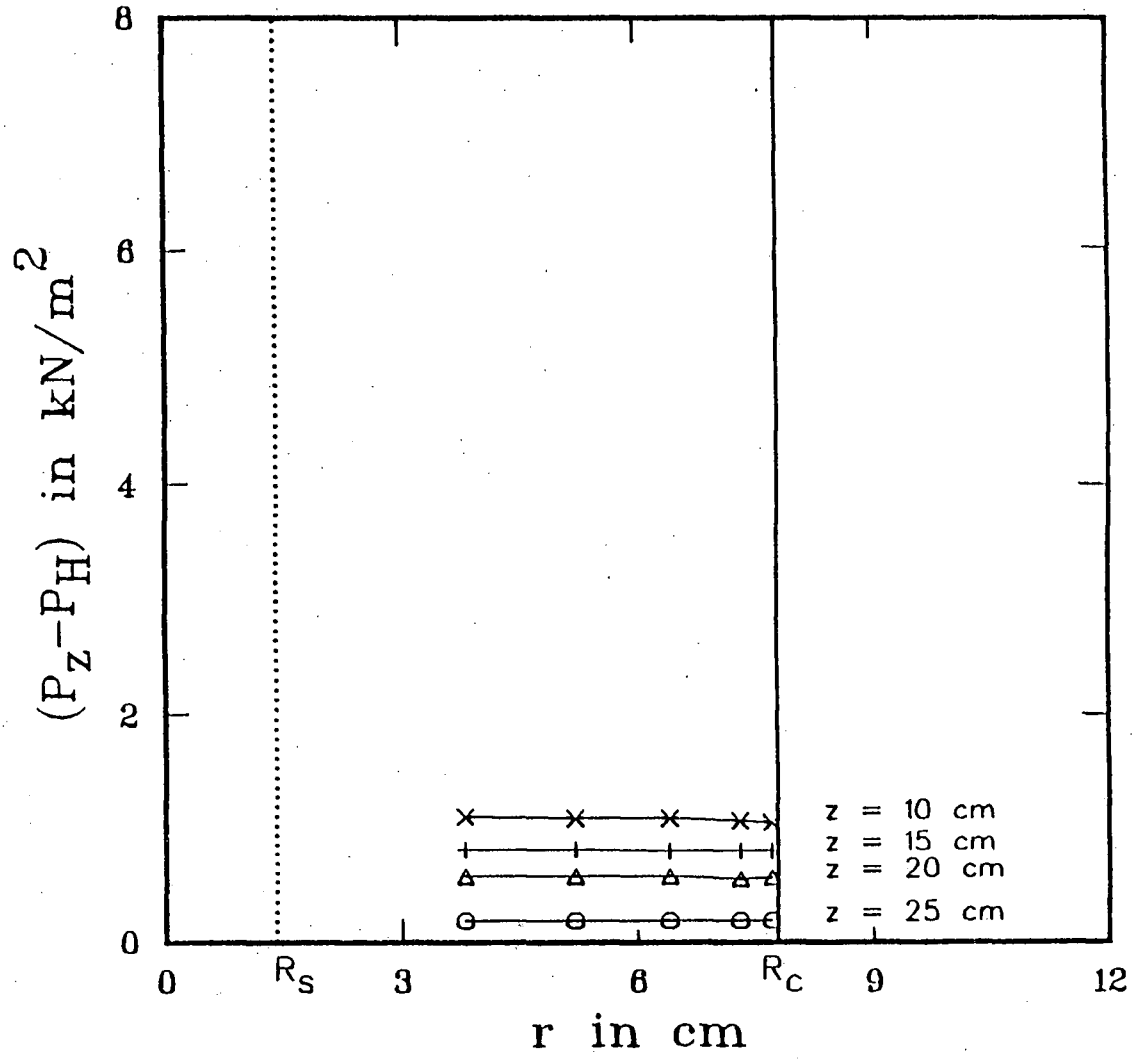

Figure 7.1d Radial pressure profiles in the cylindrical section (T_S = 420 °C)

R_c = column radius; R_s = average spout radius

7.2 LONGITUDINAL PRESSURE PROFILES

Dividing Equation 2.26 by Equation 2.28 yields an expression which describes the longitudinal pressure profiles in the annulus, ie.,

$$\frac{P-P_H}{-\Delta P_s} = 1 - \frac{(2\beta-4)f(x)+3g(x)}{(2\beta-4)f(h)+3g(h)} \qquad 7.1$$

where

$$f(\chi) = 1.5\chi^2 - \chi^3 + 0.25\chi^4 \qquad 7.2a$$

$$g(\chi) = 3\chi^3 - 4.5\chi^4 + 3\chi^5 - \chi^6 + 0.143\chi^7 \qquad 7.2b$$

The variation of $(P-P_H)/(-\Delta P_s)$ with z depends on two parameters, namely h (i.e., H/H_m) and β. These parameters are, in turn, related to the particle and fluid properties. Equation 2.31, on the other hand, is independent of these two parameters. Figures 7.2a, 7.2b, 7.2c and 7.2d show the difference between these two expressions under four chosen conditions (Runs # 5-6-b, # 6-5-b, # 7-5-b and # 8-5-b), together with the experimental results. In each case, Equations 7.1 and 2.31 produce almost identical profiles with very small deviation. Both equations work well at room temperature (Figure 7.2a) but overpredict at higher temperatures (Figures 7.2b, 7.2c and 7.2d).

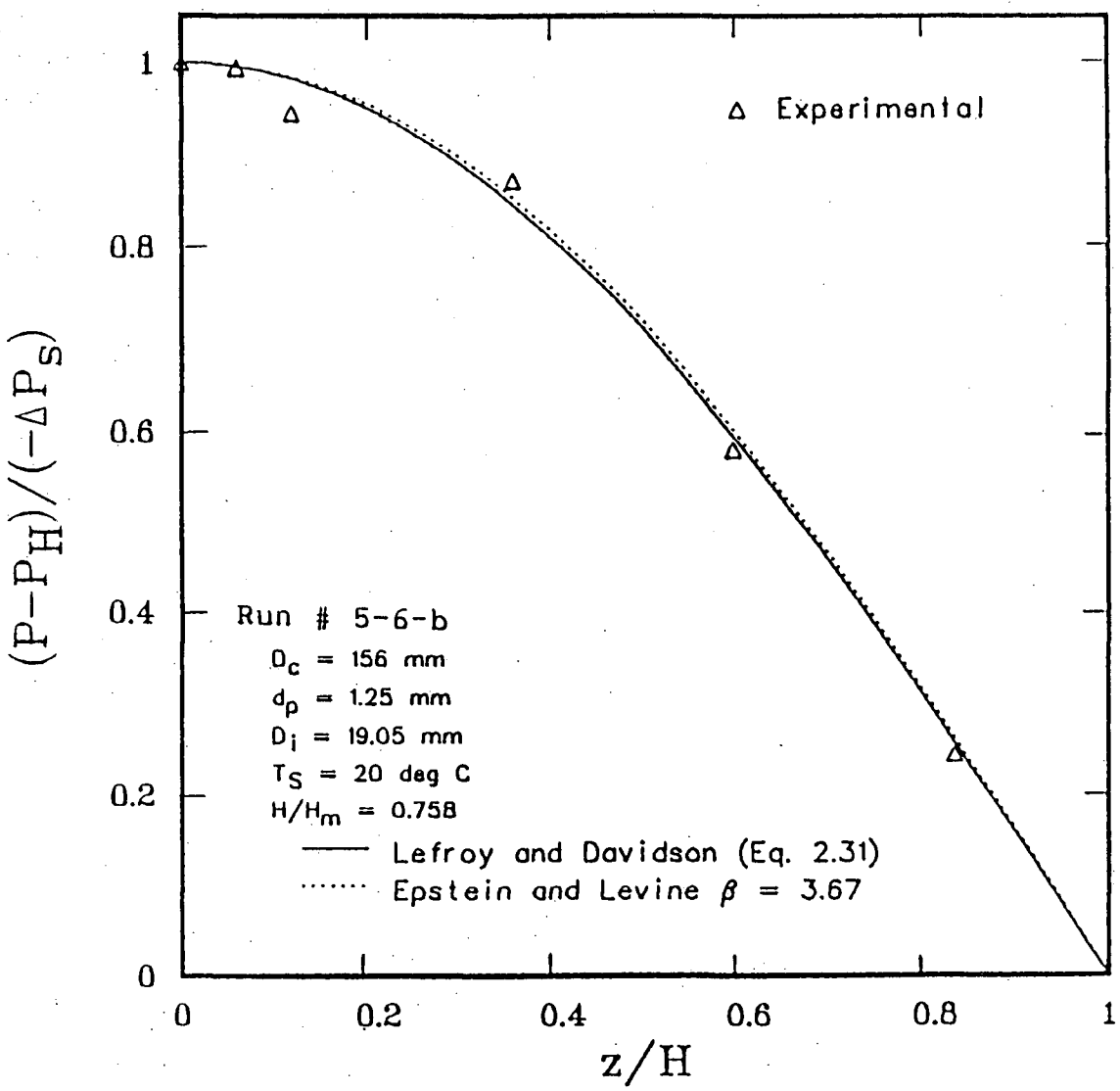

Figure 7.2a Longitudinal pressure profiles, experimental versus predicted (T_S = 20 °C)

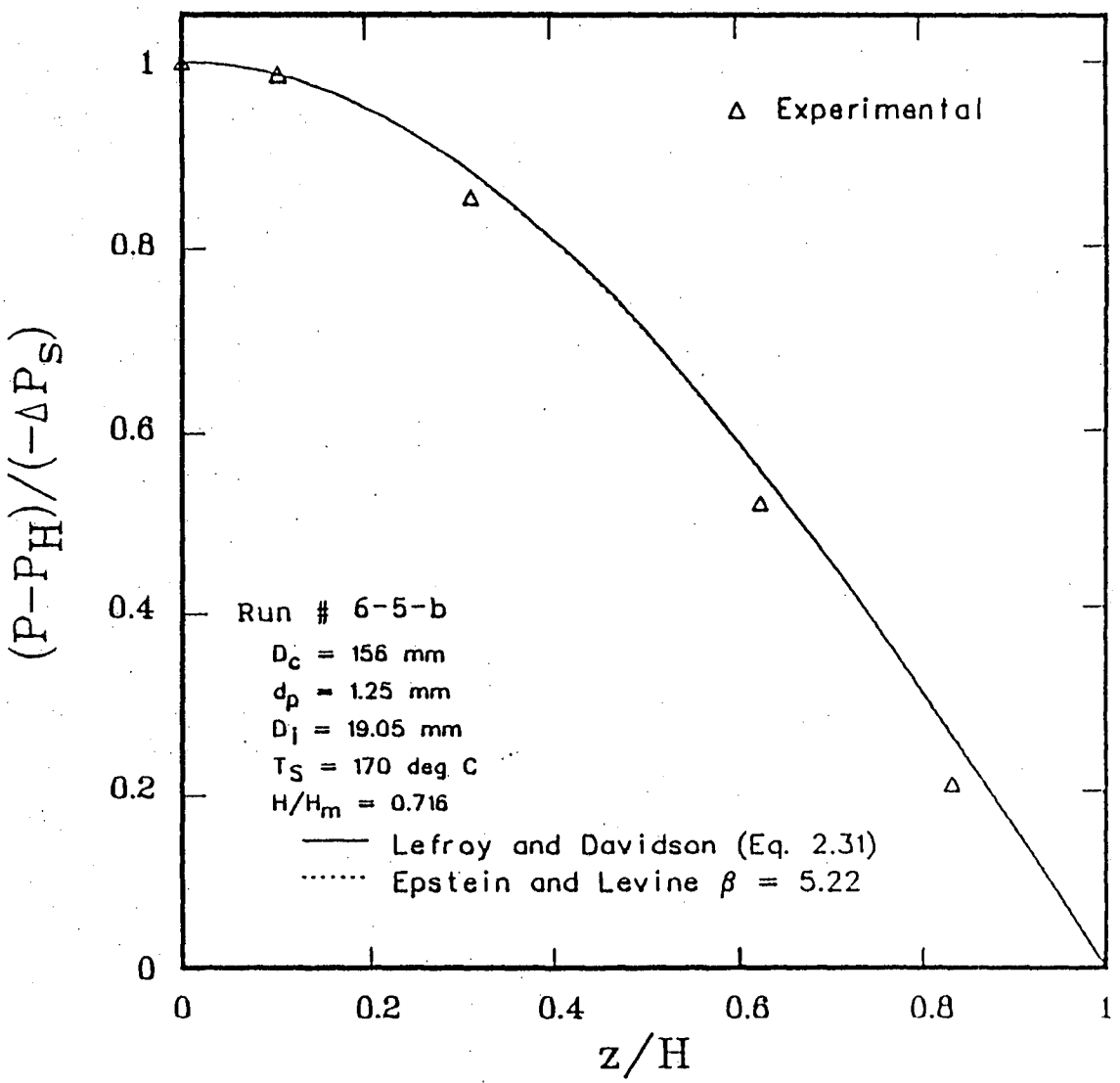

Figure 7.2b Longitudinal pressure profiles, experimental versus predicted (T_S = 170 °C)

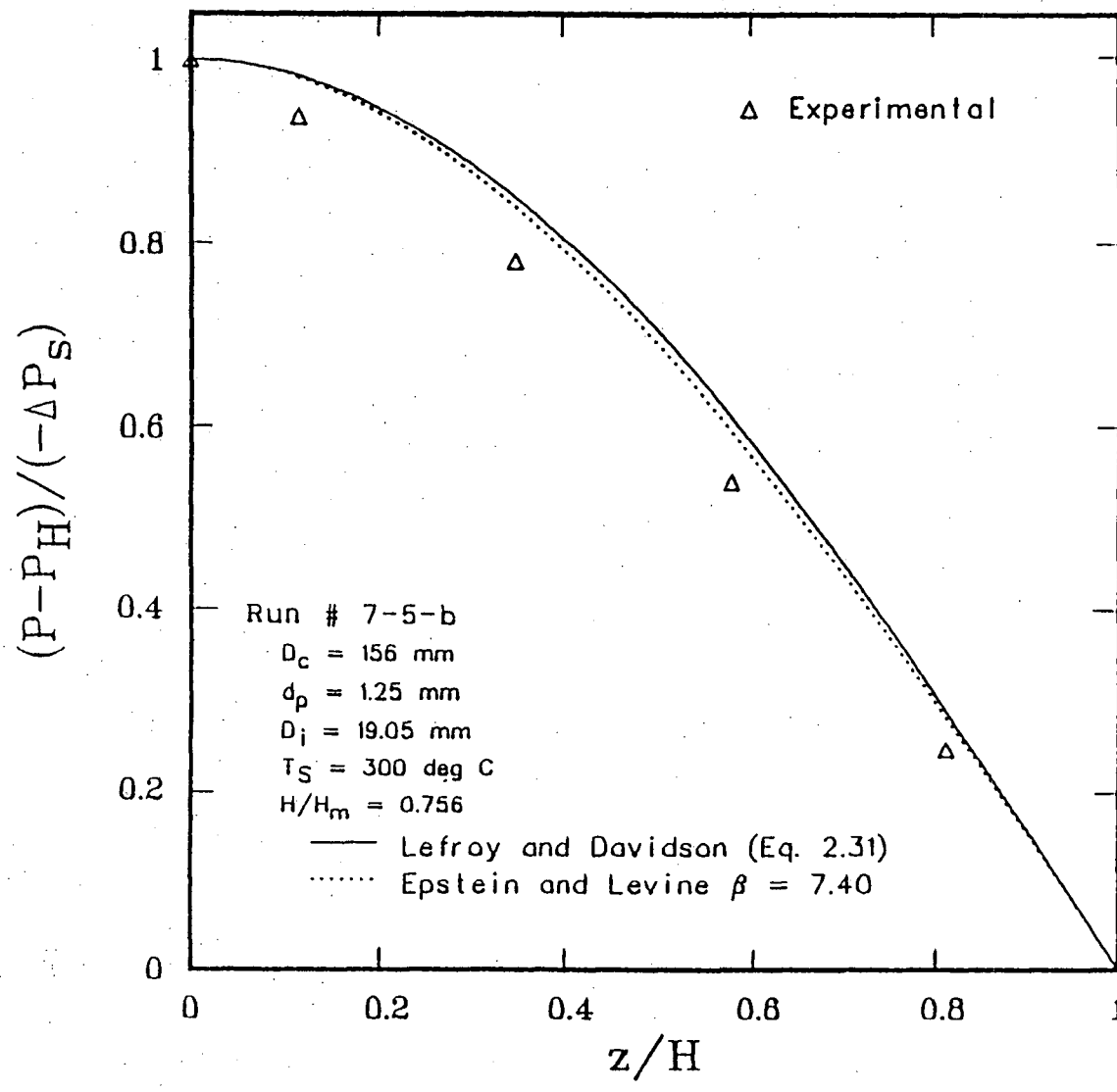

Figure 7.2c Longitudinal pressure profiles, experimental versus predicted (T_S = 300 °C)

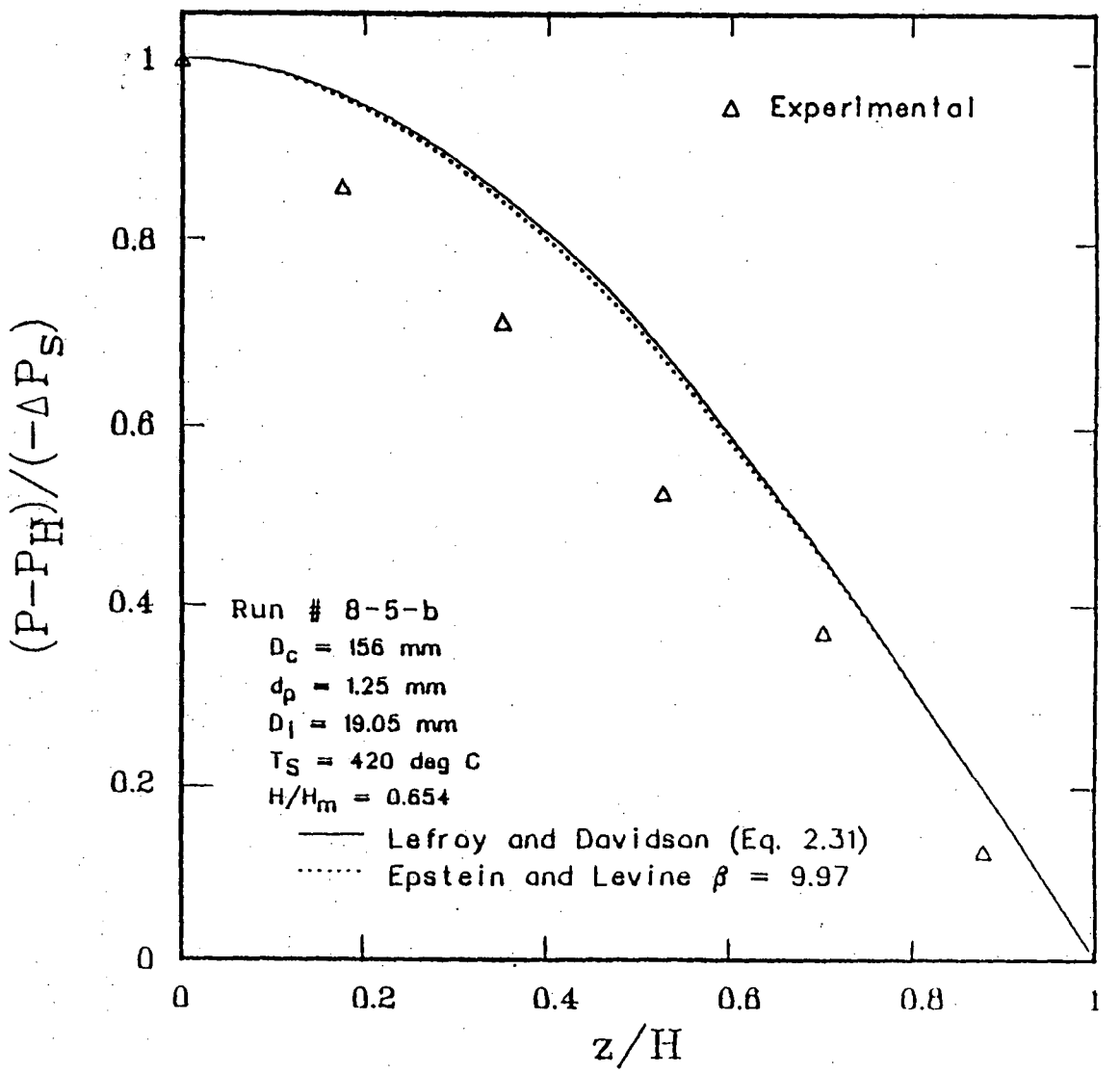

Figure 7.2d Longitudinal pressure profiles, experimental versus predicted (T_S = 420 °C)

Equation 2.31 does not predict any effect with bed temperature and yields the same profile for all four experimental conditions. For Equation 7.1, the effect of bed temperature is expressed through β (and partially through H_m implicitly). The (individual) effect of β can be seen from Figures 7.2a and 7.2c, using the Lefroy-Davidson line as reference. With H/H_m fixed, higher β yields lower $(P-P_H)/(-\Delta P_s)$ for any given values of z/H. Since β increases with increasing bed temperature, therefore Equation 7.1 predicts that if H/H_m is fixed, a higher bed temperature will produce lower $(P-P_H)/(-\Delta P_s)$. The experimental results (from Runs # 5-6-b and # 7-5-b) show a similar qualitative trend, that is, $(P-P_H)/(-\Delta P_s)$ decreases with increasing bed temperature. However, Equation 7.1 is still somewhat unsatisfactory because quantitatively its predicted values do not compare well with experimental values at higher temperatures. Improvement of Equation 7.1 can be made by replacing U_{mf} of Equation 2.27c with the measured value of U_{aH_m}. As indicated in Table 7.2 of the next sub-section, at room temperature, U_{aH_m} was approximately equal to U_{mf}; at higher temperatures, it was slightly smaller and the difference increased with temperature. Hence using U_{aH_m} instead of U_{mf} in Equation 2.27c generally produces higher values of β and hence lower values of $(P-P_H)/(-\Delta P_s)$ by Equation 7.1. However, $(P-P_H)/(-\Delta P_s)$ is not very sensitive to β, as shown in Figures 7.2a and 7.2c. Hence this improvement was too small to account for the measured

differences observed at high temperatures.

7.3 LONGITUDINAL FLUID VELOCITY

Section 3.7.5 described how the fluid velocities in the annulus (U_a) were determined. All measurements of U_a were made at a fixed radial position and the data are presented in Figure 7.3. There is no obvious trend regarding the effect of bed temperature and it is also clear that all data points do not fall on the same curve. In order to interpret the data on U_a and compare them with existing equations, it is important to determine U_{aH_m}, which was not measured experimentally. However, Lim (1975) has shown that under any fixed conditions of D_c, D_i, U/U_{ms}, bed material and spouting fluid, U_a at any given z is independent of bed height. In addition, U_a rises rapidly with z and levels off to a constant value. These two unique features make it possible to extrapolate to U_{aH_m} from data obtained at bed heights below H_m. Table 7.2 lists the experimental results of U_a versus z together with the values of U_{aH_m} obtained by extrapolation. These final results are then plotted in Figure 7.4 where they are compared to Equation 2.22 with U_{aH_m} replacing U_{mf} (Mamuro and Hattori, 1968), Equation 2.23 (Lefroy and Davidson, 1969) and Equation 2.24 with n = 2 (modified L-D). Equation 2.23 consistently underpredicted whereas the modified version, Equation 2.24, showed better agreement. Equation 2.22 did not work perfectly either, but

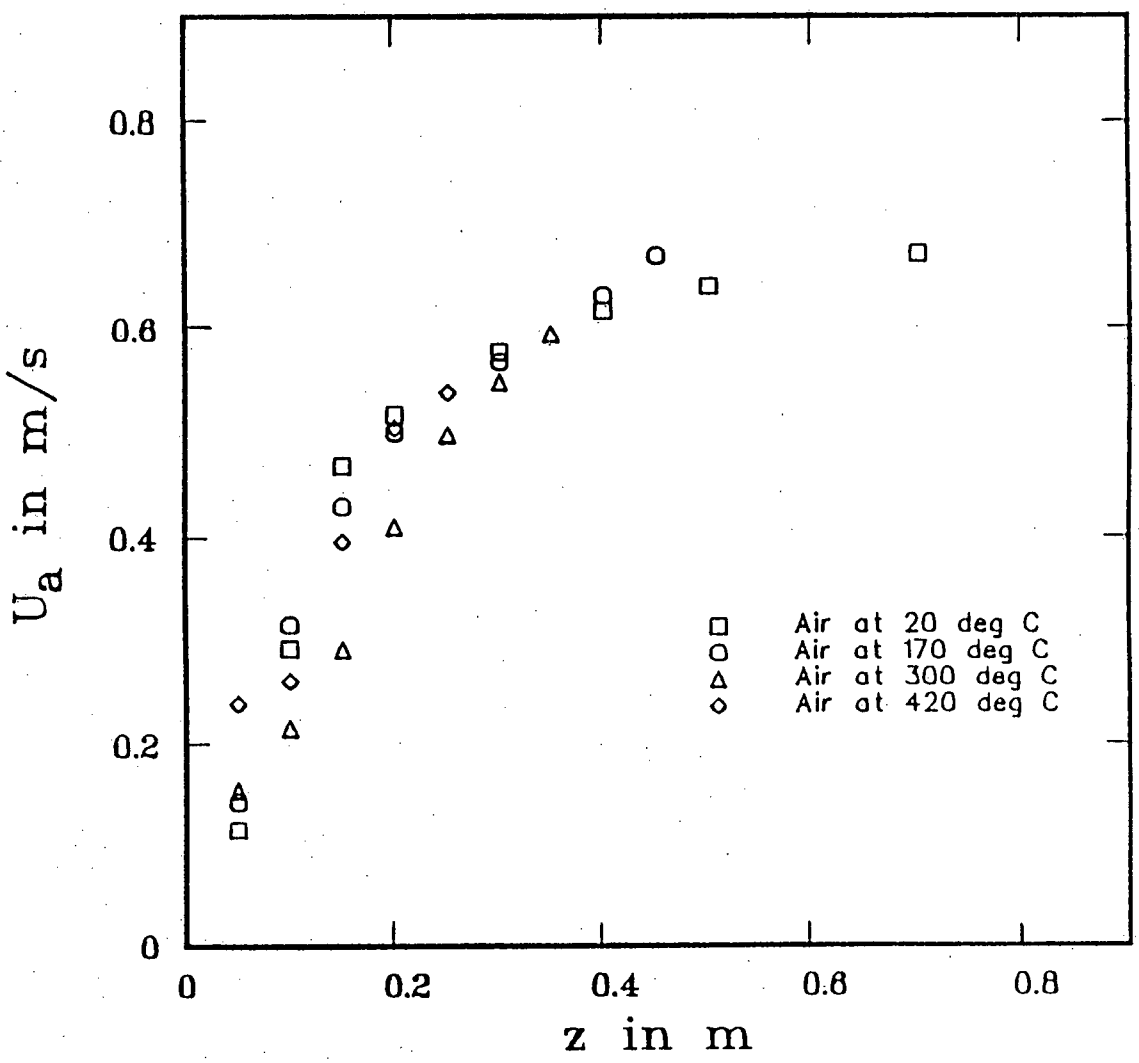

Figure 7.3 Effect of bed temperature on the longitudinal fluid velocity. d_p = 1.25 mm, D_i = 19.05 mm

Table 7.2 Experimental values of annular fluid velocity. d_p = 1.25 mm. D_t = 19.05 mm

Run #	Temp (°C)	H (m)	H_a (m)	U/U_{ms}	z (m)	U_a (m/s)	U_{aH_m} (m/s)	U_{mf} (m/s)
5-6-b	20	0.813	0.840	1.128	0.70	0.6742	0.7000	0.7000
					0.50	0.6427		
					0.40	0.6180		
					0.30	0.5771		
					0.20	0.5171		
					0.15	0.4690		
					0.10	0.2929		
					0.05	0.1177		
6-5-b	170	0.464	0.480	1.162	0.45	0.6726	0.6900	0.7100
					0.40	0.6340		
					0.30	0.5674		
					0.20	0.5002		
					0.15	0.4302		
					0.10	0.3160		
					0.05	0.1445		
7-5-b	300	0.413	0.430	1.112	0.35	0.5952	0.6500	0.6700
					0.30	0.5479		
					0.25	0.4984		
					0.20	0.4103		
					0.15	0.2921		
					0.10	0.2160		
					0.05	0.1559		
8-5-b	420	0.270	0.285	1.094	0.25	0.5384	0.5700	0.6300
					0.20	0.5084		
					0.15	0.3963		
					0.10	0.2616		
					0.05	0.2394		

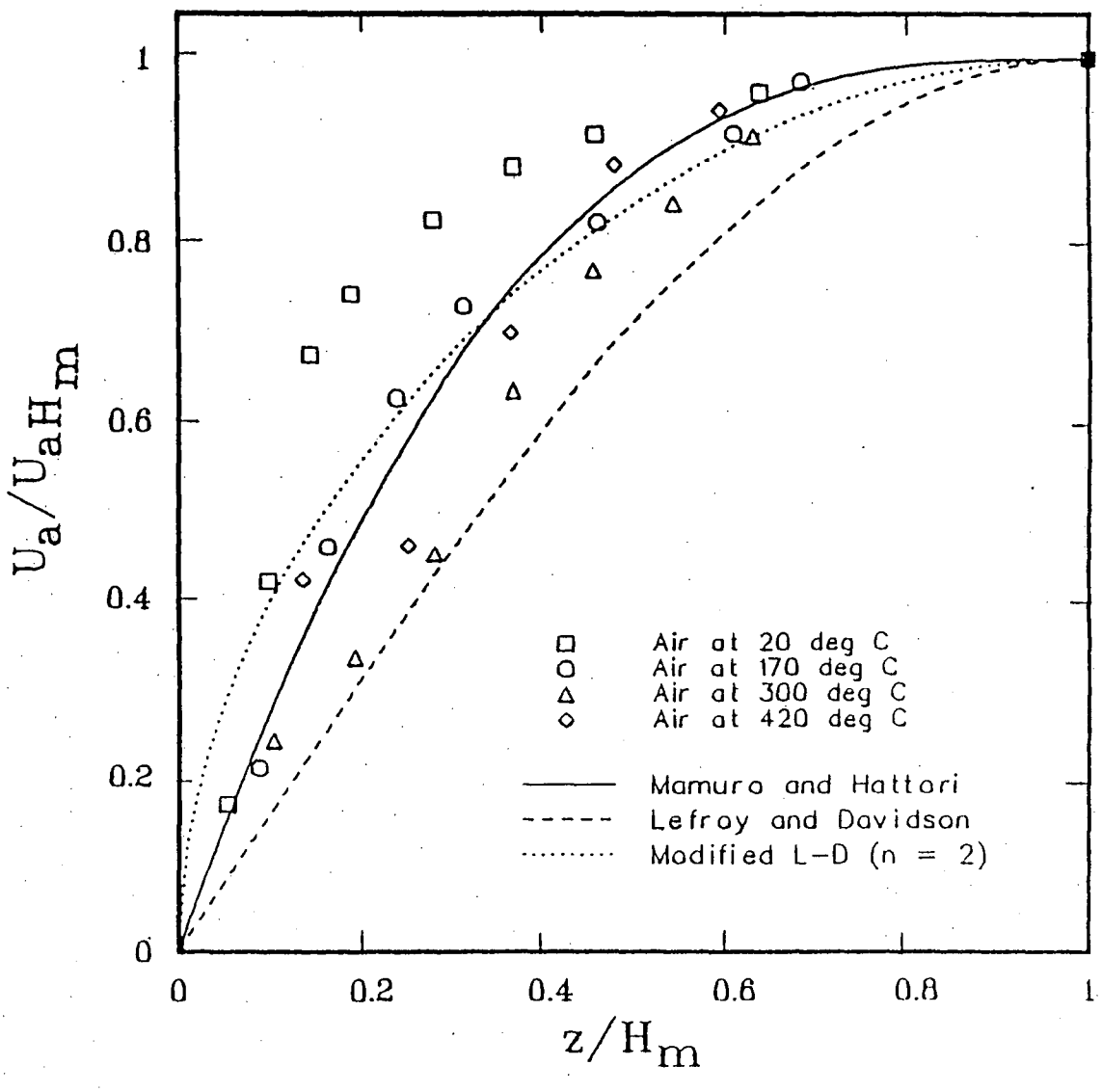

Figure 7.4 Longitudinal annular fluid velocity distribution

it was not any worse than Equation 2.24. Similar scatter has been noted by Epstein et al., 1978.

7.4 LONGITUDINAL PARTICLE VELOCITY

Rovero et al. (1986) have pointed out that the flat wall in a half column causes particles to slow down due to friction. This effect becomes very dominant at the corner between the flat and round walls. The particle velocity measured at the flat wall of a half column is therefore lower than that at the same radial position in a full column. Hence, the procedure described in Section 3.7.5 would not give very accurate results. However, for purposes of comparison and qualitative analysis, this method is probably adequate.

Table 7.3 lists all the measured results and Figure 7.5 shows a set of typical results. The particle velocity generally increased with bed level but decreased with increasing radius. The only exception was near the fluid inlet (i.e., in the conical section) where the velocity next to the spout wall was somewhat higher than that at the upper bed levels. This phenomenon is the result of reducing cross-sectional area in the cone.

The effect of bed temperature on V_p is shown in Figures 7.6a, 7.6b and 7.6c which compare the particle velocities at

Table 7.3 Experimental values of particle velocity, d_p = 1.25 mm, D_i = 19.05 mm

Run #	Temp (°C)	H (m)	H_a (m)	U/U_{ms}	z (m)	$V_p(r_1)$ (cm/s)	$V_p(r_2)$ (cm/s)	$V_p(r_3)$ (cm/s)	$V_p(r_4)$ (cm/s)	$V_p(r_5)$ (cm/s)	$\bar{V}_p$* (cm/s)
5-6-a	20	0.813	0.840	1.128	0.80	4.969	4.776	4.598	4.329	3.002	4.315
					0.70	4.040	3.883	3.578	3.436	2.222	3.411
					0.60	3.195	2.789	2.304	1.959	1.199	2.129
					0.50	2.532	2.448	2.103	1.944	0.742	1.929
					0.40	1.779	1.720	1.491	1.114	0.289	1.213
					0.30	1.626	1.339	1.034	0.750	0.190	0.872
					0.20	1.064	1.053	0.669	0.287	0.068	0.512
					0.10	1.704	1.166	0.142	0.0	0.0	0.341
					0.05	3.717	1.211	0.0	0.0	0.0	0.815
6-5-b	170	0.464	0.480	1.162	0.45	2.597	2.513	1.871	1.467	0.657	1.700
					0.40	1.878	1.594	1.429	1.199	0.360	1.230
					0.30	1.855	1.331	1.011	0.811	0.182	0.893
					0.20	1.236	0.886	0.696	0.370	0.117	0.521
					0.10	2.120	2.044	0.559	0.100	0.0	0.667
					0.05	4.211	0.612	0.0	0.0	0.0	0.551
7-5-b	300	0.413	0.430	1.112	0.40	2.143	1.668	1.486	1.325	0.405	1.323
					0.30	1.617	1.182	0.946	0.830	0.190	0.857
					0.20	1.345	0.765	0.557	0.363	0.090	0.469
					0.10	2.661	1.073	0.213	0.0	0.0	0.351
					0.05	4.878	0.797	0.0	0.0	0.0	0.656
8-5-b	420	0.270	0.285	1.094	0.25	3.315	1.289	0.841	0.384	0.109	0.692
					0.20	1.980	1.188	0.765	0.325	0.069	0.592
					0.15	1.928	1.059	0.424	0.238	0.0	0.457
					0.10	2.525	2.176	0.270	0.0	0.0	0.613
					0.05	4.115	0.838	0.0	0.0	0.0	0.610

* Definec by Equation 3.9

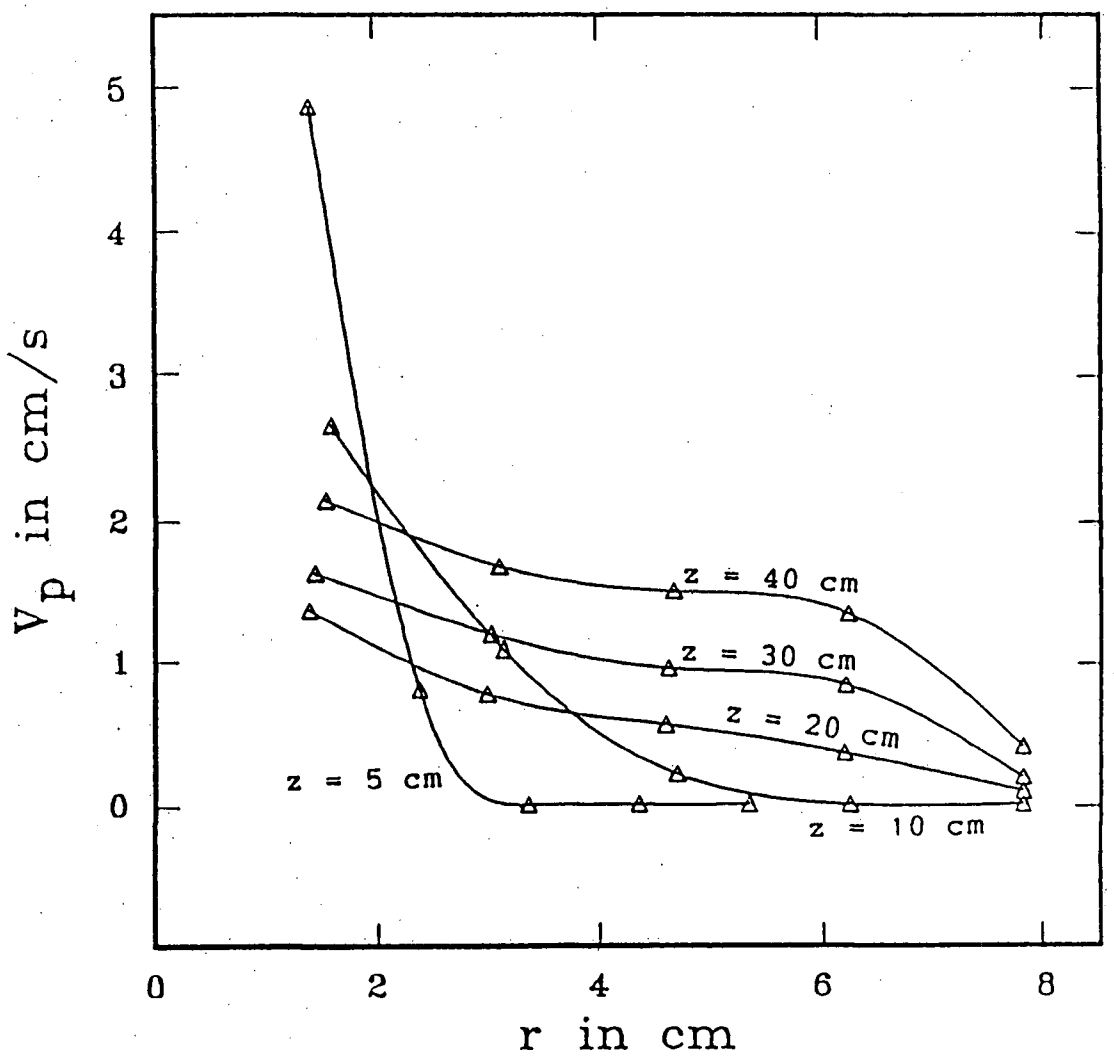

Figure 7.5 Particle velocity in the annulus (Run # 7-5-b)

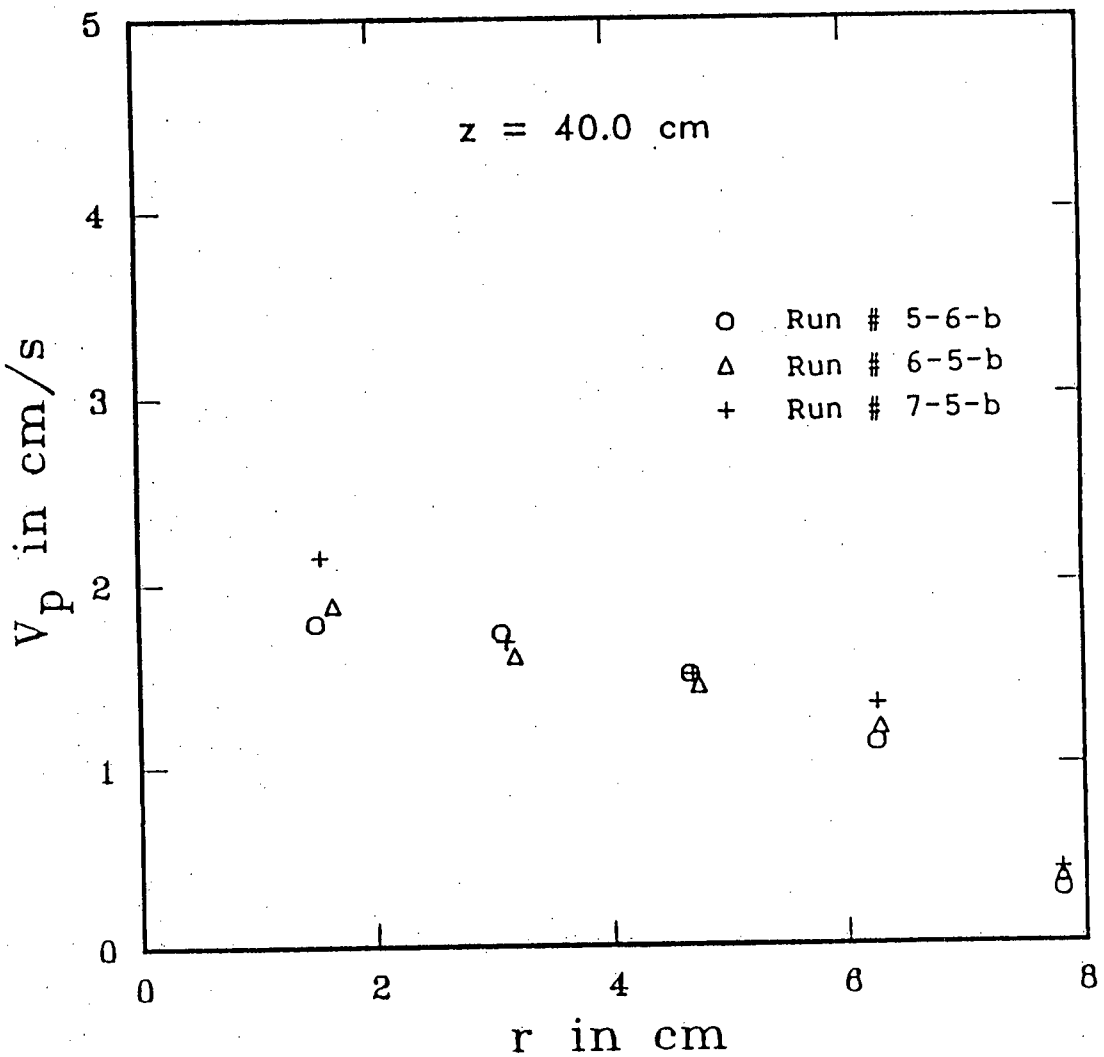

Figure 7.6a Effect of bed temperature and bed height on the radial profiles of V_p (z = 40 cm)

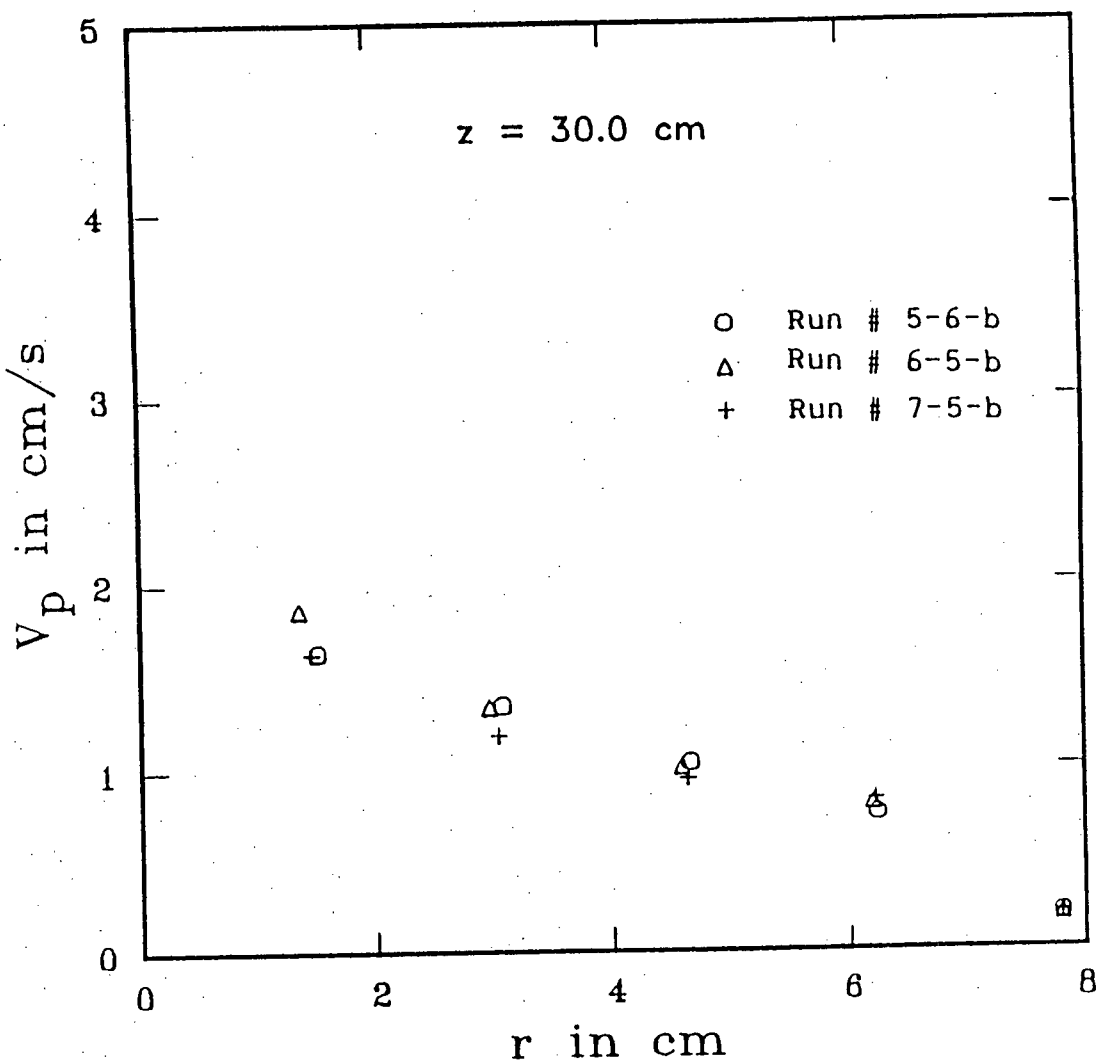

Figure 7.6b Effect of bed temperature and bed height on the radial profiles of V_p (z = 30 cm)

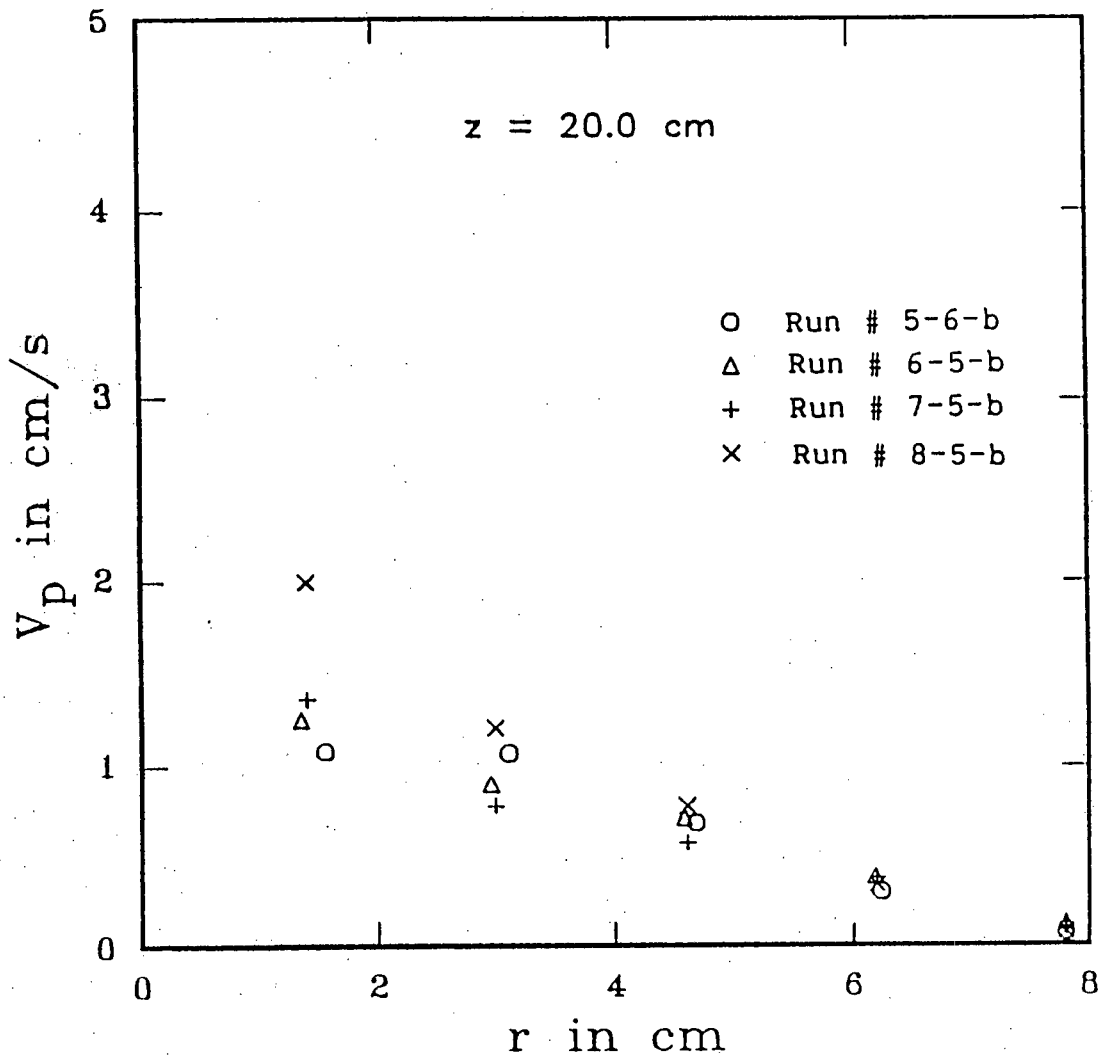

Figure 7.6c Effect of bed temperature and bed height on the radial profiles of V_p (z = 20 cm)

the same bed levels but for different bed heights and temperatures. Other parameters, such as d_p, D_i, D_c and U/U_{ms} were fixed. There were no significant differences in the particle velocities under these conditions, indicating that for any given bed level, $V_p(r)$ was independent of bed height and temperature. With this assumption, the radial-averaged particle velocity for all four runs was determined using Equation 3.9 and the final results are plotted on a single graph (Figure 7.7). Although there was some scatter, most of the points seemed to lie on one curve. This average particle velocity, $\overline{V}_p$ generally increased with bed level, except in the conical section, where it decreased with increasing bed level.

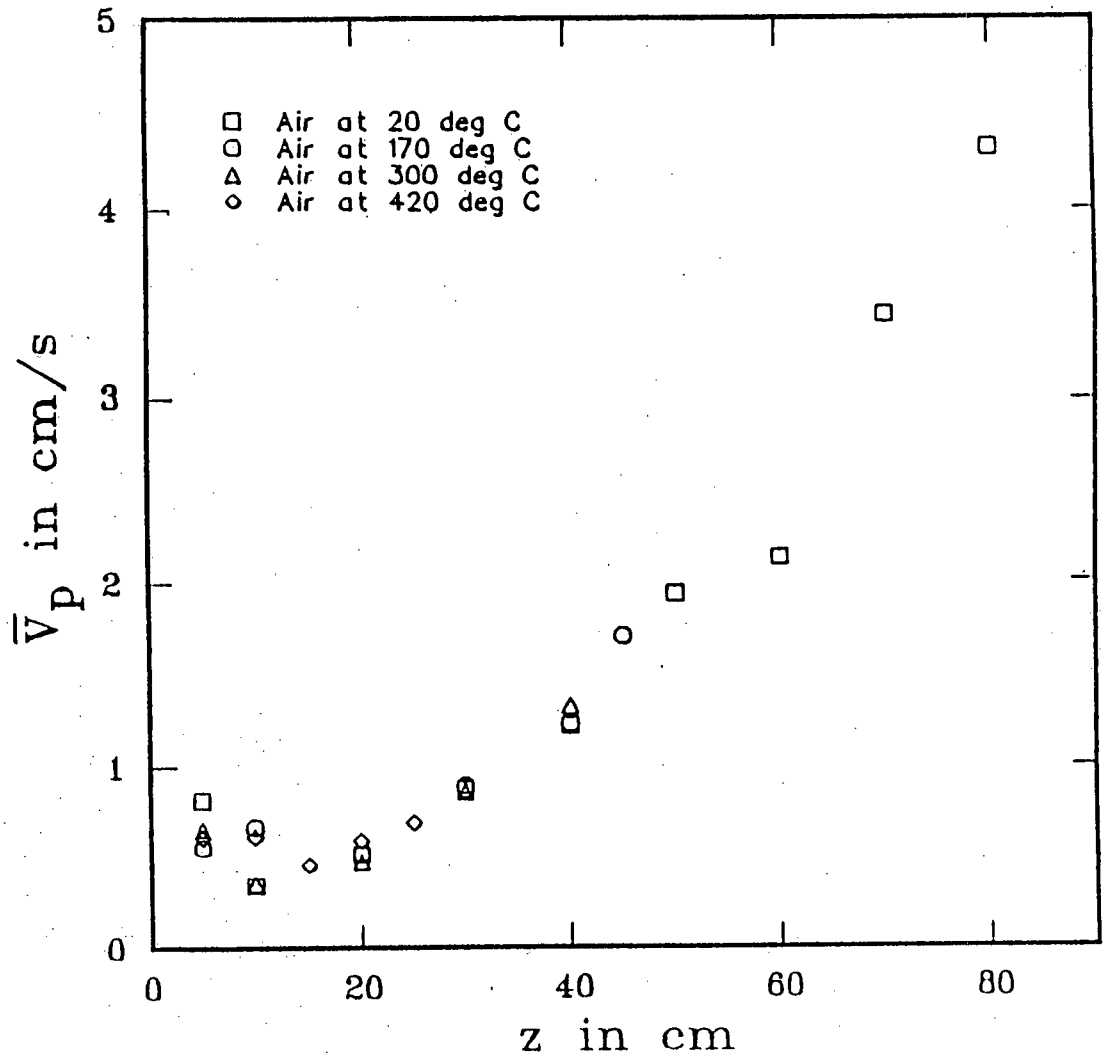

Figure 7.7 Effect of bed level on the radial-averaged particle velocity

8. CONCLUSIONS AND RECOMMENDATIONS

8.1 CONCLUSIONS

1. Experimental values of U_{ms} were compared to the Mathur and Gishler equation (i.e., Equation 2.1), which worked reasonably well at high temperature conditions but consistently underpredicted at room temperature, with deviations up to 30%. Applying statistical analysis to all the data from this work produced exponents which are somewhat different from those of the Mathur-Gishler equation, but the magnitude of corresponding exponents were roughly of the same order. Although the Mathur and Gishler equation was found to be unsatisfactory over the entire range of temperatures, it did manage to predict correctly the qualitative variation of U_{ms} with each variable.

2. The equation of Epstein and Levine (i.e., Equation 2.28) gave good prediction of bed pressure drop for room conditions but it overestimated the effect of temperature. It is important to note that this expression is based on the assumption of annular fluidization at H_m. Experimental results, however, indicated that the spout termination mechanism at high temperature might be due to choking of the spout or instability of the spout-annulus interface, rather than fluidization of the "entire" annulus surface. This would explain the discrepancy.

3. The spout diameter data for air at room conditions were in good agreement with those calculated by the McNab equation (i.e., Equation 2.16). The same equation was, however, found to be unreliable for air spouting at higher temperatures and for helium at room temperature; it failed to include fluid viscosity as a variable and also appeared to overestimate the effect of fluid density. A semi-empirical expression has been developed, by including both density and viscosity as parameters, and it seems to work much better than the McNab equation.

4. Experimental values of H_m were compared to the McNab and Bridgwater expression (i.e., Equation 2.8). Although it consistently gives low estimates of H_m, it correctly predicts the observed trend. For air spouting, H_m decreased with increasing temperature, indicating that steady spouting became more difficult. All other established equations for H_m which fail to include the effect of temperature or predict the opposite trend of H_m with temperature will not be applicable for design purposes at high temperatures.

5. H_m increased with increasing ρ_f but decreased with increasing μ (see Table 4.2). This is consistent with the observed effect of temperature on H_m.

6. The longitudinal fluid velocity in the annulus was reasonably well described by the Mamuro and Hattori equation

(i.e., Equation 2.22) and the modified Lefroy and Davidson equation (i.e., Equation 2.24 with n = 2), provided that U_{mf} was replaced by U_{aH_m}. This is significant since U_{aH_m} becomes smaller than U_{mf} as the temperature increases. This observation further suggested that at high temperature, annular fluidization might not be the spout terminating mechanism.

7. The longitudinal pressure profiles in the annulus could be represented by the Lefroy and Davidson equation (i.e., Equation 2.31). The more complicated expression of Epstein and Levine (i.e., Equation 7.1) worked well also, but did not produce better prediction.

8. The temperature did not have any significant effect on the particle circulation rate in the annulus. The radial-average particle velocity was found to increase with bed level, except at the conical section, where the cross-sectional area was smaller.

8.2 RECOMMENDATIONS

1. One particular area of interest is the effect of viscosity and density on the spoutability of particles. Based on the results for H_m, these two variables cannot be ignored. Future study in this area should also include D_i and d_p since they too have been found to be important

factors.

2. The effect of pressure on the hydrodynamics is also important. In addition, by operating the spouted bed under selected conditions of pressure and temperature, it becomes feasible to investigate the individual effect of viscosity under the condition of constant density. This is possible because the gas viscosity increases with temperature but is not very sensitive to change in pressure, whereas the density can be kept roughly constant by fixing the ratio of P/T.

3. Data from a fully cylindrical column should be obtained for comparison.

NOTATION

a_s	A_s/Ac	
A	$\rho_f U_{mf} U_t/[(\rho_p-\rho_f)gD_i]$	
Ar	$d_p^3(\rho_p-\rho_f)\rho_f g/\mu^2$	
A_c	Column cross-sectional area	(m^2)
A_s	Spout cross-sectional area	(m^2)
b	U_m/U_{mf}	
d_p	Average particle diameter	(m)
d_{pi}	Mean diameter of adjacent screen apertures	(m)
d_{pj}	Reciprocal mean diameter from sieve analysis	(m)
D_c	Column diameter	(m)
D_i	Orifice diameter	(m)
$D_s(z)$	Spout diameter at z	(m)
D_s	Area-averaged spout diameter	(m)
D_s^*	D_s at $H = H_m$ and $U = U_{ms}$	(m)
D_{sH}	D_s at $z = H$	(m)
D_{sH_m}	D_s at $z = H_m$	(m)
f	Friction factor	
g	Acceleration due to gravity	(m/s^2)
G	$\rho_f U$	(kg/m^2s)
G_a	Volumetric flowrate of solids	(m^3/s)
h	H/H_m	
H	Loosely packed bed height	(m)
H_a	Annulus height	(m)
H_F	Fountain height	(m)
H_m	Maximum spoutable bed height	(m)

k	Constant in Equation 6.1	
k_1, k_2, k_3 and k_4	Constants in Equation 6.2	
K, σ, τ, ω and ξ	Parameters in Equation 5.1	
K_1	Coefficient in Ergun equation	(kg/m^3s)
K_2	Coefficient in Ergun equation	(kg/m^4)
M	Number of particle size measurements or of data points	
n	Flow regime index	
N	Richardson-Zaki index	
P	Pressure	(N/m^2)
P_{ATM}	Atmospheric pressure	(N/m^2)
P_B	Absolute pressure measured upstream with the solids in the bed	(N/m^2)
P_E	Absolute pressure measured upstream without the solids in the bed	(N/m^2)
P_H	Absolute pressure at z = H	(N/m^2)
P_S	Absolute pressure in the bed	(N/m^2)
P_z	Absolute pressure in the bed at z	(N/m^2)
$-\Delta P$	Pressure drop across the bed	(N/m^2)
$-\Delta P_a$	Pressure drop measured above the orifice	(N/m^2)
$-\Delta P_f$	Minimum fluidization pressure drop	(N/m^2)
$-\Delta P_s$	Minimum spouting pressure drop	(N/m^2)
Q_s	Volumetric flowrate in the spout	(m^3/s)
Q_t	Total volumetric flowrate of fluid	(m^3/s)
r	Radial distance from the spout axis	(m)

Re_{mf}	$U_{mf}\rho_f d_p/\mu$	
Re_t	$U_t\rho_f d_p/\mu$	
R_c	Column radius	(m)
R_s	Spout radius	(m)
t	Defined in Equation 5.2	(m)
T_S	Average bed temperature	(°C, °K)
U	Superficial fluid velocity	(m/s)
$U_a(z)$	Superficial annulus fluid velocity at z	(m/s)
U_{aH}	U_a at z = H	(m/s)
U_{aH_m}	U_a at z = H_m	(m/s)
U_c	Choking velocity	(m/s)
U_m	U_{ms} at H = H_m	(m/s)
U_{mf}	Superficial minimum fluidization velocity	(m/s)
U_{ms}	Superficial minimum spouting velocity	(m/s)
$U_s(z)$	Superficial fluid velocity in the spout	(m/s)
U_{sH}	U_s at z = H	(m/s)
U_{sH_m}	U_s at z = H_m	(m/s)
U_t	Terminal velocity of a particle	(m/s)
$V_p(r)$	Annular particle velocity at r (downward)	(cm/s)
$\overline{V}_p$	Radial-averaged annular particle velocity	(cm/s)
V_{sH}	Particle velocity in the spout at z = H	(cm/s)
x	z/H_m	
x_i	Weight fraction of particles having an aperture mean diameter of d_{pi}	
z, Z	Vertical distance from the fluid inlet	(m)
α	Index in Equation 6.1	
ρ_b	Bulk solids density	(kg/m^3)

ρ_f	Fluid density	(kg/m^3)
ρ_p	True particle density	(kg/m^3)
ϵ_a	Annulus voidage	
ϵ_c	Voidage at choking	
ϵ_{mf}	Voidage at minimum fluidization	
ϕ	Shape factor of the particles = sphericity	
β	$2 + (3K_1/2K_2U_{mf})$	
ψ	Net downwards force per unit volume exerted by the solids	(kg/m^2s^2)
μ	Fluid viscosity	($kg/m \cdot s$)
κ, η	Parameters in Equation 2.2	
λ	Spoutability parameter	
θ	Angle of internal friction	(°)
δ	Angle of repose	(°)
γ	Defined by Equation 2.36	

REFERENCES

Arbib, H. A., Sawyer, R. F. and Weinberg, F. J., "The Combustion Characteristics of Spouted Beds", Proc. of Eighteenth Symposium (International) on Combustion. The Combustion Institute (1981).

Arbib. H. A. and Levy, A., "Combustion of Low Heating Value Fuels and Wastes in the Spouted Bed", Can. J. Chem. Eng., **60**, 528 (1982).

Arbib, H. A. and Levy, A., "The Reverse-Flow Spouted Bed Combustor", Combustion Science and Technology, **29**, 83 (1982).

Barton, R. K. and Ratcliffe, J. S., "The Rates of Devolatilation of Coal under Spouted Bed Conditions", Mechanical and Chemical Trans., May 1969.

Barton, R. K., Rigby, G. R. and Ratcliffe, J. S., "The Use of Spouted Bed for the Low Temperature Carbonization of Coal", Mechanical and Chemical Eng. Trans., May 1968.

Bridgwater, J., "Spouted beds", Chapter 6 in 'Fluidization', Ed. by Davidson, J. F., Cliff, R. and Harrison, D., Academic Press, London, 1985.

Bridgwater, J. and Mathur, K. B., "Prediction of Spout Diameter in a Spouted Bed - A Theoretical Model", Powder Technol., **6**, 183 (1972).

Chandnani, P. P., "Gas Spouting of Fine Particles", M.A.Sc. Thesis, University of British Columbia, Vancouver (1984).

Chandnani, P. P. and Epstein, N., "Spoutability and Spouting Destabilization of Fines Particles with a Gas", Proc. Fifth Engineering Foundation on **Fluidization**, pp 233-240, Engineering Foundation, May 1986.

Epstein, N., Lim, C. J. and Mathur, K. B., "Data and Models for Flow Distribution and Pressure Drop in Spouted Beds", Can. J. Chem. Eng., **56**, 436 (1978).

Epstein, N. and Levine, S., "Non-Darcy Flow and Pressure Distribution in a Spouted Bed", Proc. Second Engineering Foundation Conference on **Fluidization**, pp 98-103, Cambridge Univ. Press, April 1978.

Epstein, N. and Grace, J. R., "Spouting of Particulate Solids", Chapter 11 in 'Handbook of Powder Science and Technology', Ed. by Fayed, M.E. and Otten, L., Van Nostrand Reinhold Co., New Yory, 1984.

Ergun, S., "Fluid Flow through Packed Columns", Chem. Eng. Progr., **48(2)**, 89 (1952).

Foong, S. K., Lim, C. J. and Watkinson, A. P., "Coal Gasification in a Spouted Bed", Can. J. Chem. Eng., **58**, 84 (1980).

Foong, S. K., Cheng, G. and Watkinson, A. P., "Spouted Bed Gasification of Western Canadian Coals", Can. J. Chem. Eng., **59**, 625 (1981).

Geldart, D., Hemsworth, A., Sundavadra, R. and Whiting, K. J., "A Comparison of Spouting and Jetting in Round and Half-round Fluidized Beds", Can. J. Chem. Eng., **59**, 638 (1981).

Ghosh, B., "A Study on the Spouted Bed, Part I - A Theoretical Analysis", Indian Chem. Eng., 7, 16 (1965).

Grace, J. R. and Mathur, K. B., "Height and Structure of the Fountain Region above Spouted Beds", Can. J. Chem. Eng., **56**, 533 (1978).

Grbavcic, Z. B., Vukovic, D. V. Zdanski, F. K. and Littman, H., "Fluid Flow Pattern, Minimum Spouting Velocity and Pressure Drop in Spouted Beds", Can. J. Chem. Eng., **54**, 332 (1976).

Ingle, A. N. and Sarkar, S., "Gasification of Coal in Spouted-Bed", Indian J. Technol., **14**, 515 (1976).

Jarallah, A. and Watkinson, A. P., "Pyrolysis of Western Canadian Coals in a Spouted Bed", Can. J. Chem. Eng., **63**, 227 (1985).

Khoe, G. K. and Weve, D., "Visual Observations of Spouted Bed Gas Combustion Modes and Their Flow Regimes", Can. J. Chem. Eng., **61**, 460 (1983).

Khoshnoodi, M. and Weinberg, F. J., "Combustions in Spouted Beds", Combustion and Flame, The Combustion Institute, **33**, 11 (1978).

Lefroy, G. A. and Davidson, J. F., "The Mechanics of Spouted Beds", Trans. Instn. Chem. Engrs, **47**, T120, 1969.

Leung, L. S., "The Ups and Downs of Gas-Solids Flow : A Review", in '<u>Fluidization</u>', Ed. by Grace, J. R. and Masten, J. M., Plenum Press, New York, 1980.

Lim, C. J., "Gas Residence Time Distribution and Related Flow Patterns in Spouted Beds", Ph.D. Thesis, University of British Columbia, Vancouver (1975).

Lim, C. J., Barua, S. K., Epstein, N., Grace, J. R. and

Watkinson, A. P., "Spouted Bed and Spout-Fluid Bed Combustion of Solid Fuels", Proc. Inst. Energy Symp. on Fluidized Combustion, **1**, DISC/10/72, 1984.

Littman, H., "The Measurement and Prediction of the Maximum Spoutable Height, Spout Diameter, Minimum Spouting Velocity and Pressure Drop at Minimum Spouting in Spouted Beds", Lecture Notes for C.S.Ch.E. Continuing Education Course on Spouted Beds, Vancouver, 1982.

Littman, H., Morgan, M. H. III, Narayanan, P. V., Kim, S. J., Day, J. and Lazarek, G.M., "An Axisymmetric Model of Flow in the Annulus of a Spouted Bed of Coarse Particles. Model, Experimental Verification and Residence Time Distribution", Can. J. Chem. Eng., **63**, 188 (1985).

Littman, H., Morgan, M. H. III, Vukovic, D. V., Zdanski, F. K. and Grbavcic, Z. B., "A Theory for Predicting the Maximum Spoutable Height in a Spouted Bed", Can. J. Chem. Eng., **55**, 499 (1977).

Littman, H., Morgan, M. H. III, Vukovic, D. V., Zdanski, F. K. and Grbavcic, Z. B., "Prediction of the Maximum Spoutable Height and the Average Spout to Inlet Tube Diameter Ratio in Spouted Beds of Spherical Particles", Can. J. Chem. Eng., **57**, 684 (1979).

McNab, G. S., "Prediction of Spout Diameter", Brit. Chem. Eng. & Proc. Tech., **17**, 532 (1972).

McNab, G. S. and Bridgwater, J., "The Application of Soil Mechanics to Spouted Bed Design", Can. J. Chem. Eng., **52**, 162 (1974).

McNab, G. S. and Bridgwater, J., "Spouted Beds - Estimation of Spouted Pressure Drop and the Particle Size for Deepest Bed", Proc. European Congress on Particle Technology, Nuremberg (1977).

Malek, M. A. and Lu, B. C. Y., "Pressure Drop and Spoutable Bed Height in Spouted Beds", Ind. Eng. Chem. Process Des. Develop., **4**, 123 (1965).

Mamuro, T. and Hattori, H., "Flow Pattern of Fluid in Spouted Beds", J. Chem. Eng. Jap., **1**, 1 (1968)/Correction, J. Chem Eng. Jap., **3**, 119 (1970).

Manurung, F., "Studies in the Spouted Bed Technique with Particular Reference to Low Temperature Coal Carbonization", Ph.D Thesis, Univ. of New South Wales, Kensington, Australia, 1964.

Mathur, K. B. and Epstein, N., '<u>Spouted Beds</u>', Academic

Press, N.Y. (1974).

Mathur, K. B. and Gishler, P. E., "A Technique for Contacting Gases with Solid Particles", A.I.Ch.E. J., **1**, 157 (1955).

Morgan, M. H. III and Littman, H., "Predicting the Maximum Height in Spouted Beds of Irregularly Shaped Particles", Ind. Eng. Chem. Fundam., **21**, 23 (1982).

Nicol, T., "UBC INTEGRATION", UBC Computing Centre, May 1982.

Oman, A. O. and Watson, K. M., Refinery Management and Petroleum Chem. Tech., **36**, R-795 (1944).

Pallai, I. and Nemeth, J., "Analysis of Flow Forms in a Spouted Bed Apparatus by the So-called Phase Diagram", Int. Congr. Chem. Eng. (CHISA), 3rd, Prague, September 1969, Paper No. C2.4. Czechosslovak Society for Industrial Chemistry.

Ratcliff, J. S. and Rigby, B. E., "Low Temperature Carbonization of Coal in a Spouted Bed", "Prediction of Exit Char Volatile Matter", Mechanical annd Chemical Eng. Trans., May 1969.

Ray, T. B. and Sarkar, S., "Kinetics of Coal Pyrolysis in Spouted Bed", Indian Chemical Engineer, **18(2)**, 11 (1976).

Rovero, G., Brereton, C. M. H., Epstein, N., Grace, J. R. and Piccinini, N., "Gas Flow Distribution in Conical-Base Spouted Beds", Can. J. Chem. Eng., **61**, 289 (1983).

Rovero, G., Piccinini, N. and Lupo, A., "Solids Velocities in Full and Half-sectional Spouted Beds", Entropie, **124**, 13 (1985).

Wen, C. Y. and Yu, Y. H., "A Generalized Method for Predicting the Minimum Fluidization Velocity", A.I.Ch.E. J., **12**, 610 (1966).

Smith, T. N., "Limiting Volume Fraction in Vertical Pneumatic Transport", Chem. Eng. Sci., **33**, 745 (1978).

Whiting, K. J. and Geldart, D., "A Comparison of Cylindrical and Semi-cylindrical Spouted Beds of Coarse Particles", Chem. Eng. Sci., **35**, 1499 (1980).

Zhao, J., "Coal Combustion in Spouted and Spout-Fluid Beds", M.A.Sc. Thesis, University of British Columbia, Vancouver (1986).

APPENDIX A - MAXIMUM SPOUTABLE BED HEIGHT

A.1 DERIVATION OF H_m

At the minimum fluidization condition, the Ergun (1955) equation becomes:

$$\left(-\frac{dP}{dz}\right)_{mf} = (\rho_p-\rho_f)(1-\epsilon_{mf})g = K_1U_{mf} + K_2U_{mf}^2 \qquad A.1$$

where

$$K_1 = \frac{150\mu(1-\epsilon_{mf})^2}{(\phi d_p)^2\epsilon_{mf}^3} \qquad A.2a$$

$$K_2 = \frac{1.75\rho_f(1-\epsilon_{mf})}{\phi d_p\epsilon_{mf}^3} \qquad A.2b$$

Multiplying Equation A.1 by

$$\frac{\rho_f d_p^3\phi\epsilon_{mf}^3}{1.75\mu^2(1-\epsilon_{mf})}$$

it can be shown that

$$Re_{mf}^2 + 85.71\left[\frac{1-\epsilon_{mf}}{\phi}Re_{mf}\right] - 0.571\epsilon_{mf}^3\phi Ar = 0 \qquad A.3$$

where

$$Ar = \frac{d_p^3(\rho_p-\rho_f)g\rho_f}{\mu^2} \qquad A.4a$$

$$Re_{mf} = \frac{\rho_f U_{mf} d_p}{\mu} \qquad A.4b$$

Equation A.3 can be solved to yield

$$Re_{mf} = \frac{\rho_f U_{mf} d_p}{\mu} = 42.86\left[\frac{1-\epsilon_{mf}}{\phi}\right] \left[\sqrt{1+311X10^{-6}\left[\frac{\epsilon_{mf}^3}{(1-\epsilon_{mf})^2}\right]\phi^3 Ar} - 1\right] \quad A.5$$

An expression for H_m is obtained by combining Equations 2.5, 2.1a and A.5 to eliminate U_m and U_{mf}:

$$H_m = \left[\frac{D_c^2}{d_p}\right]\left[\frac{D_c}{D_i}\right]^{2/3}\left[\frac{918b^2}{Ar}\right]\left[\frac{1-\epsilon_{mf}}{\phi}\right]^2 \left[\sqrt{1+311X10^{-6}\left[\frac{\epsilon_{mf}^3}{(1-\epsilon_{mf})^2}\right]\phi^3 Ar} - 1\right]^2 \quad A.6$$

This expression is reduced by substituting ϕ and ϵ_{mf} with 0.6689 and 0.4744, respectively:

$$H_m = \left[\frac{D_c^2}{d_p}\right]\left[\frac{D_c}{D_i}\right]^{2/3}\left[\frac{568b^2}{Ar}\right][\sqrt{1+35.9X10^{-6}Ar} - 1]^2 \quad A.7$$

A.2 EFFECT OF TEMPERATURE ON H_m

When temperature increases, fluid density decreases while viscosity increases, which results in a lower value of Ar if d_p is fixed. Hence, the effect of temperature can be related to the effect of Ar. Equation A.7 is rewritten as

$$H_m = C_1[\sqrt{1/Ar+35.9X10^{-6}} - \sqrt{1/Ar}]^2 \quad A.8$$

and

$$\frac{dH_m}{dAr} = C_1\left[\sqrt{1/Ar+35.9X10^{-6}} - \sqrt{1/Ar}\right]$$

$$\left[\sqrt{\frac{1}{Ar^3}} - \sqrt{\frac{1}{Ar^3+35.9X10^{-6}Ar^4}}\right] \qquad A.9$$

$$> 0 \text{ for } Ar > 0$$

implying that H_m increases with Ar and thus decreases with increasing temperature.

A.3 CRITICAL PARTICLE DIAMETER

Substituting Equation A.4a into Equation A.7, the result can be rewritten as

$$H_m = \frac{C_2}{d_p{}^4}\left[\sqrt{1+C_3 d_p{}^3} - 1\right]^2 \qquad A.10$$

$$= C_2\left[\sqrt{\frac{1}{d_p{}^4}+\frac{C_3}{d_p}} - \left[\frac{1}{d_p{}^2}\right]\right]^2$$

and

$$\frac{dH_m}{dd_p} = 2C_2\left[\sqrt{\frac{1}{d_p{}^4}+\frac{C_3}{d_p}} - \left[\frac{1}{d_p{}^2}\right]\right]$$

$$\left[\frac{1}{2}\sqrt{\frac{d_p{}^4}{1+C_3 d_p{}^3}}\left[\frac{-4}{d_p{}^5}+\frac{-C_3}{d_p{}^2}\right] + \left[\frac{2}{d_p{}^3}\right]\right] \qquad A.11$$

$(d_p)_{crit}$ is found by setting $d(H_m)/d(d_p)$ equal to zero. The solution is then

$$(d_p)_{crit}^3 = 8/C_3 \qquad A.12$$

It can be shown from Equations A.4a and A.7 that

$$C_3 = 35.9X10^{-6}\left[\frac{(\rho_p-\rho_f)g\rho_f}{\mu^2}\right] \qquad A.13$$

Therefore

$$(d_p)_{crit} = 60.6\left[\frac{\mu^2}{(\rho_p-\rho_f)g\rho_f}\right]^{1/3} \qquad A.14$$

A.4 EFFECT OF ϕ AND ϵ_{mf} ON $(d_p)_{crit}$

If Equation A.6 is used instead of Equation A.7 when deriving $(d_p)_{crit}$, C_3 of Equation A.11 will be defined by

$$C_3 = 311X10^{-6}\left[\frac{\epsilon_{mf}^3}{(1-\epsilon_{mf})^2}\right]\phi^3\left[\frac{(\rho_p-\rho_f)g\rho_f}{\mu^2}\right] \qquad A.15$$

and

$$(d_p)_{crit} = 29.52\left[\frac{(1-\epsilon_{mf})^2}{\epsilon_{mf}^3\phi^3}\right]^{1/3}\left[\frac{\mu^2}{g(\rho_p-\rho_f)\rho_f}\right]^{1/3} \qquad A.16$$

which clearly shows how $(d_p)_{crit}$ varies with ϕ. The effect of ϵ_{mf} can be illustrated by differentiating $(d_p)_{crit}$ with respect to ϵ_{mf}. In fact, it is easier to differentiate $(d_p)_{crit}^3$. First, Equation A.16 is rewritten as

$$(d_p)_{crit}^3 = C_4\left[\frac{1}{\epsilon_{mf}^3} - \frac{2}{\epsilon_{mf}^2} + \frac{1}{\epsilon_{mf}}\right] \qquad A.17$$

and

$$\frac{d(d_p)_{crit}^3}{d\epsilon_{mf}} = C_4\left[\frac{-3}{\epsilon_{mf}^4} - \frac{-4}{\epsilon_{mf}^3} + \frac{-1}{\epsilon_{mf}^2}\right]$$

$$= -C_4[(\epsilon_{mf}-1)(\epsilon_{mf}-3)]/\epsilon_{mf}^4 \qquad \text{A.18}$$

$$< 0 \text{ for } 0 < \epsilon_{mf} < 1$$

which means that $(d_p)_{crit}^3$ and hence $(d_p)_{crit}$ decreases with increasing ϵ_{mf}.

Table B.1 Particle size distributions

Size Range (mm)	BEFORE EXPERIMENTS Weight friction for sample # 1	2	3	4	AFTER EXPERIMENTS Weight friction for sample # 1	2	3	4
**** SMALL ****								
1.41 - 1.19	0.0059	0.0030	0.0044	0.0053	0.0054	0.0035	0.0032	0.0037
1.19 - 1.00	0.5170	0.3957	0.4287	0.5735	0.4830	0.3370	0.3888	0.5190
1.00 - 0.841	0.3863	0.3686	0.3920	0.3258	0.3553	0.4019	0.3913	0.3445
0.841 - 0.595	0.0906	0.2092	0.1605	0.0944	0.1448	0.2139	0.1972	0.1256
0.595 - 0.354	0.0001	0.0235	0.0145	0.0010	0.0115	0.0438	0.0195	0.0071
**** MEDIUM ****								
2.00 - 1.68	0.0021	0.0015	0.0024	0.0062	0.0024	0.0030	0.0018	0.0111
1.68 - 1.41	0.2280	0.2684	0.1996	0.1836	0.1556	0.2142	0.1308	0.1898
1.41 - 1.19	0.5246	0.5257	0.4905	0.5438	0.4928	0.5387	0.5018	0.5114
1.19 - 1.00	0.2276	0.1920	0.2538	0.2326	0.2855	0.2180	0.2881	0.2485
1.00 - 0.841	0.0136	0.0090	0.0256	0.0179	0.0336	0.0153	0.0436	0.0259
0.841 - 0.595	0.0040	0.0031	0.0207	0.0125	0.0214	0.0076	0.0237	0.0114
0.595 - 0.354	0.0002	0.0003	0.0075	0.0034	0.0086	0.0032	0.0103	0.0020
**** LARGE ****								
2.38 - 2.00	0.1270	0.1213	0.1038	0.1144	0.1052	0.1014	0.0838	0.1077
2.00 - 1.68	0.5126	0.5288	0.5078	0.4877	0.4600	0.4748	0.3870	0.5348
1.68 - 1.41	0.3147	0.3064	0.3046	0.3005	0.3412	0.3140	0.3133	0.2560
1.41 - 1.19	0.0307	0.0315	0.0450	0.0649	0.0674	0.0659	0.1049	0.0585
1.19 - 1.00	0.0087	0.0072	0.0147	0.0227	0.0158	0.0201	0.0429	0.0243
1.00 - 0.841	0.0027	0.0026	0.0056	0.0056	0.0054	0.0085	0.0183	0.0086
0.841 - 0.595	0.0037	0.0023	0.0186	0.0043	0.0050	0.0153	0.0498	0.0101

APPENDIX C - CALIBRATION CURVES

C.1 FLOWMETER CALIBRATION FOR GASES

For a rotameter, the governing equation is

$$G = C_D A_2 \left[\frac{2gV_F(\rho_F - \rho_f)\rho_f}{A_F[1-(A_2/A_1)^2]} \right]^{1/2} \qquad C.1$$

where

V_F = volume of the float

ρ_F = density of the float (usually >> ρ_f)

ρ_f = density of the gas

A_1 = cross-sectional area of the tube

A_2 = area of annulus between the float and tube

A_F = maximum cross-sectional area of the float

C_D = drag coefficient

G = mass flowrate of gas

The coefficient C_D depends on the shape of the float and the Reynolds number for the flow through the annular space of area A_2. If the float is kept at a fixed vertical position, C_D can be assumed constant. Equation C.1 then becomes

$$G = B_1\sqrt{\rho_f} \qquad C.2$$

Figure C.1 illustrates the schematic set-up for the rotameter calibration. If the ideal gas law is assumed, and

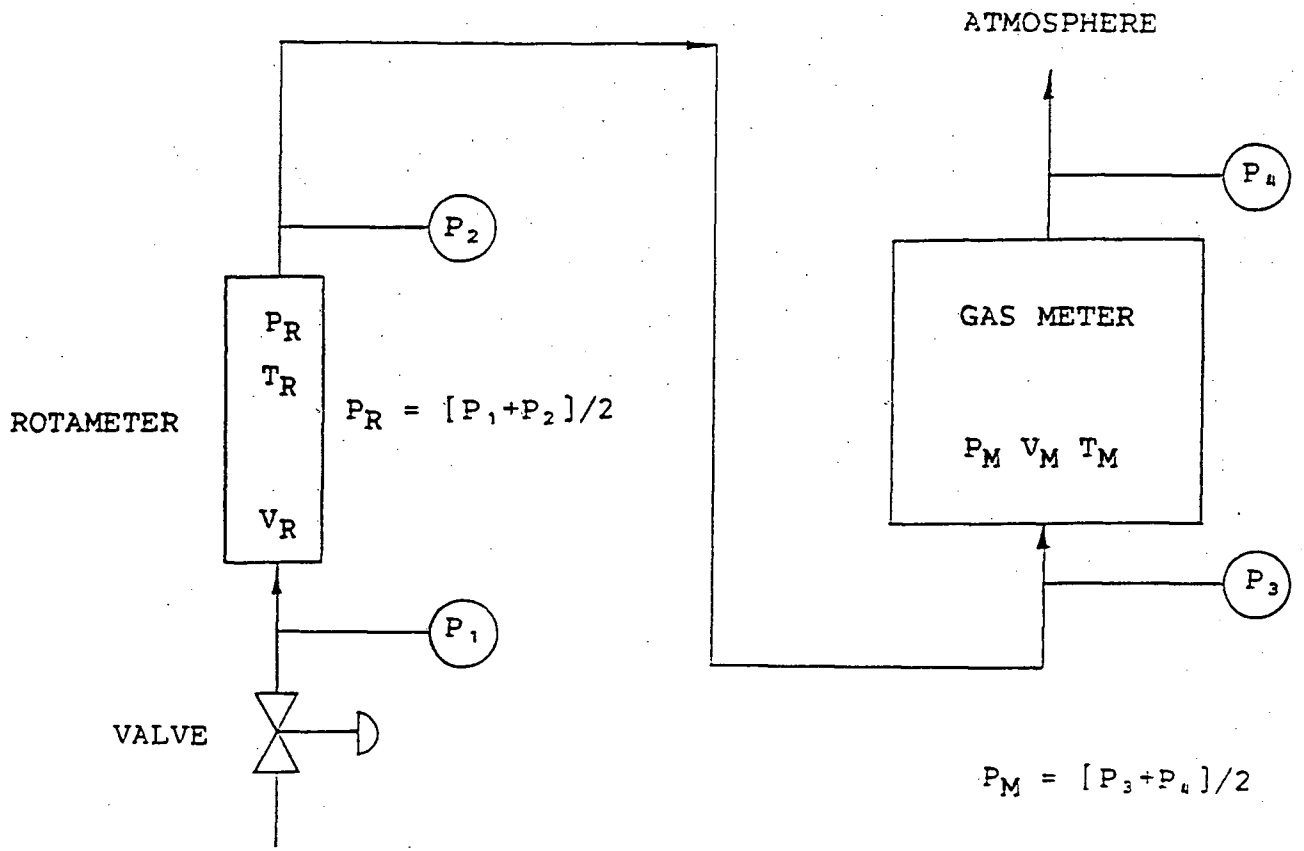

Figure C.1 Schematic set-up for rotameter calibration

$T_M = T_R = 20\ ^\circ C$, then

$$V_R = V_M\left[\frac{P_M}{P_R}\right] \qquad C.3$$

and

$$G_R = \rho_R V_R = \rho_R V_M\left[\frac{P_M}{P_R}\right] \qquad C.4$$

where ρ_R = fluid density in rotameter. Combining Equations C.2 and C.4 yields

$$B_1 = V_M\left[\frac{P_M}{P_R}\right]\sqrt{\rho_R} \qquad C.5$$

A standard condition of P = 1 atm and T = 20 °C was chosen. Substituting Equation C.5 into Equation C.2 gives

$$G_{STD} = \left[V_M\left[\frac{P_M}{P_R}\right]\sqrt{\rho_R}\right]\sqrt{\rho_{STD}} \qquad C.6$$

and

$$V_{STD} = \frac{G_{STD}}{\rho_{STD}} = V_M\left[\frac{P_M}{P_R}\right]\sqrt{\frac{\rho_R}{\rho_{STD}}} \qquad C.7$$

For ideal gas

$$\frac{\rho_R}{\rho_{STD}} = \frac{P_R}{P_{STD}} \qquad C.8$$

Substituting this relation into Equation C.7 gives

$$V_{STD} = V_M\left[\frac{P_M}{\sqrt{P_R P_{STD}}}\right] \qquad C.9$$

where

P_M = absolute pressure of the gas meter

P_R = absolute pressure of the rotameter

P_{STD} = 1 atm

V_M = measured volumetric flowrate (gas meter)

V_{STD} = corresponding volumetric flowrate for 1 atm and 20 °C

Using Equation C.9, two calibration curves were produced (Figures C.2 and C.3).

C.2 FLOWRATE IN THE SPOUTED BED

Figure C.4 is a simplified flow diagram of the experimental apparatus. Applying the ideal gas law,

$$V_S = V_R\left[\frac{P_R T_S}{P_S T_R}\right] \qquad C.10$$

From the rotameter reading, V_{STD} was determined from the calibration curves (i.e., Figures C.2 and C.3). This value is not equal to the actual volumetric flowrate (V_R) through the rotameter. However, it has been shown that for a gas rotameter that

$$V_R = B_1/\sqrt{\rho_R} \qquad C.11$$

Therefore

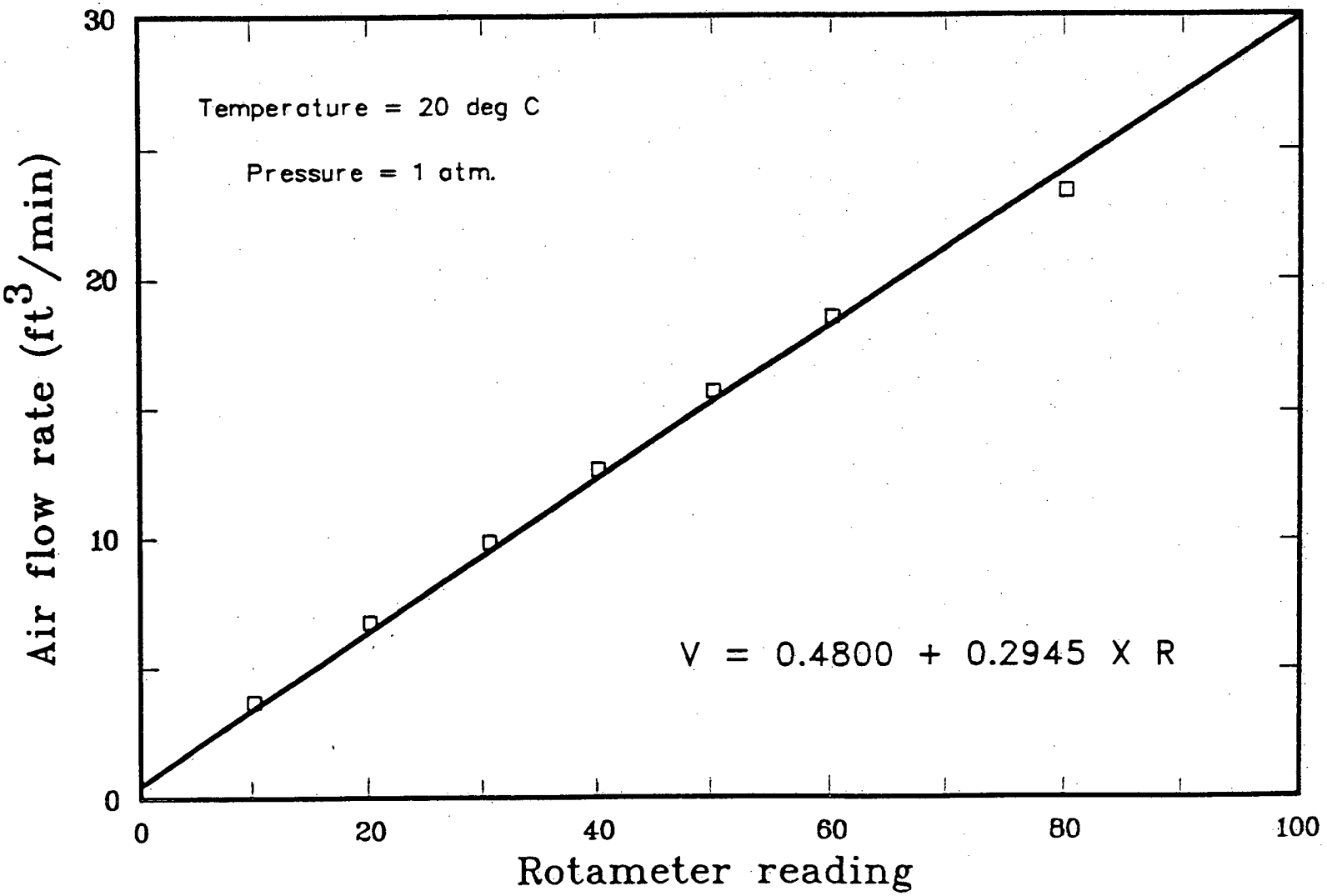

Figure C.2 Calibration curve (large rotameter)

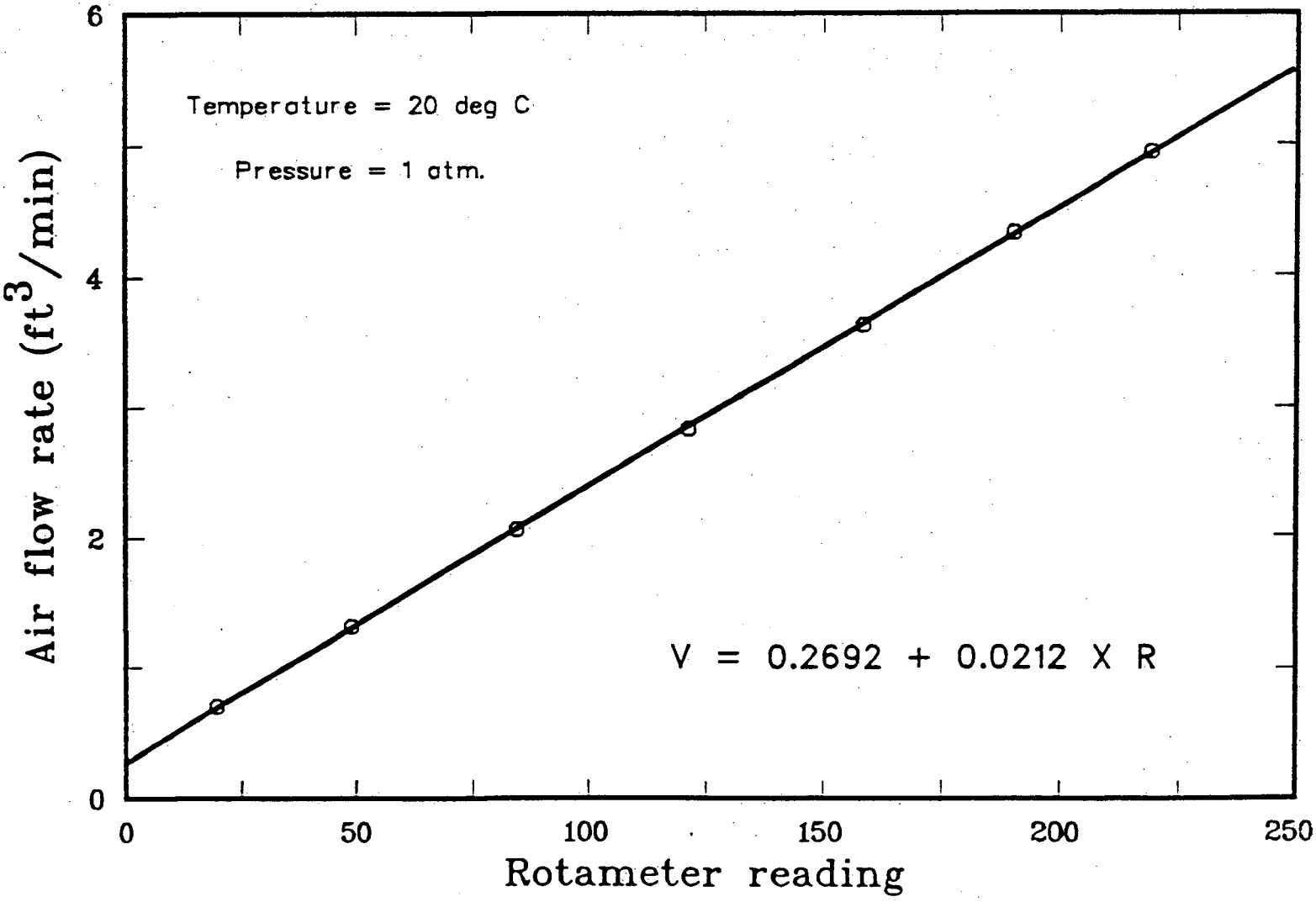

Figure C.3 Calibration curve (small rotameter)

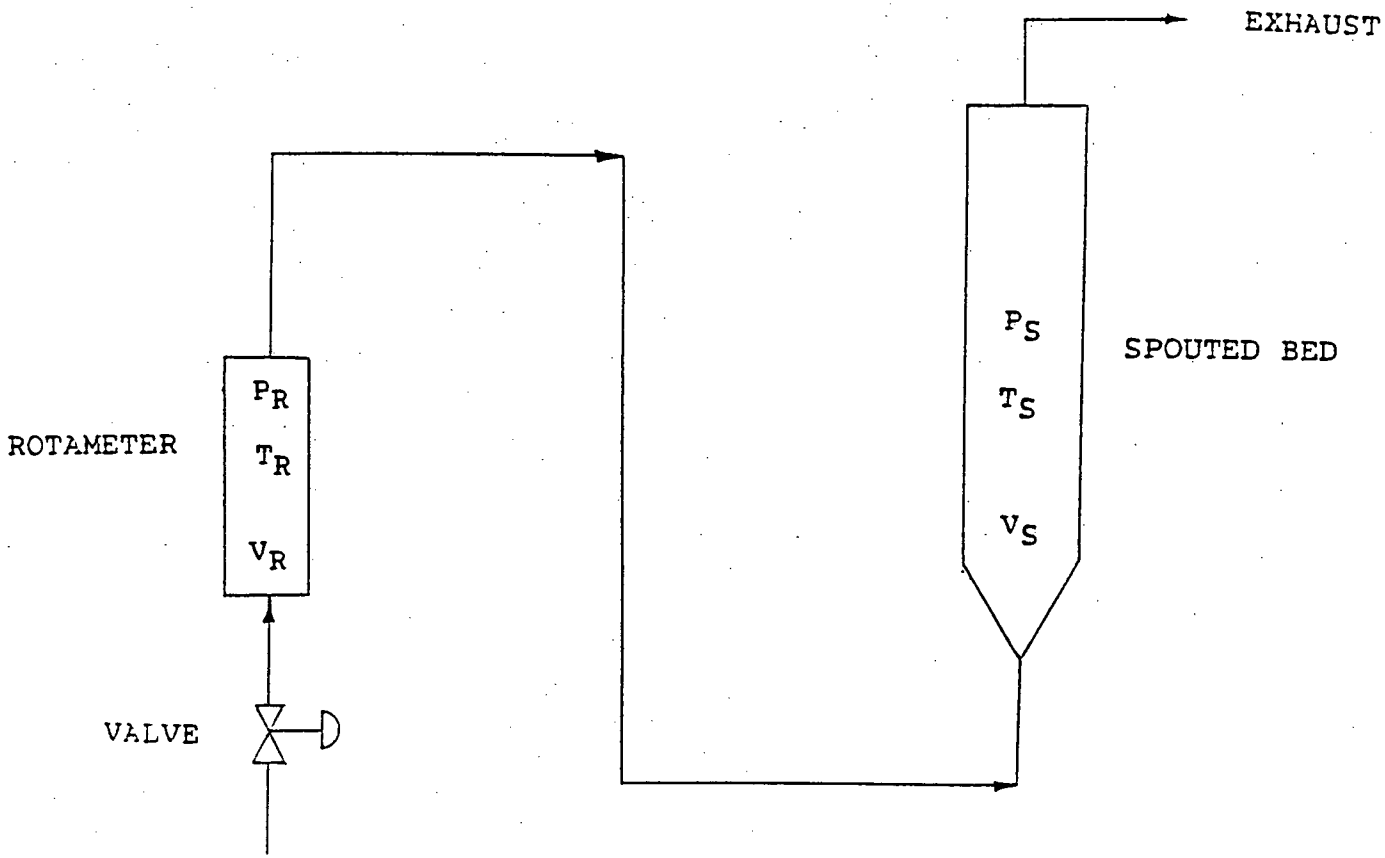

Figure C.4 Simplified flow diagram of the apparatus

$$\frac{V_R}{V_{STD}} = \sqrt{\frac{\rho_{STD}}{\rho_R}} \qquad C.12$$

and

$$V_R = V_{STD}\sqrt{\frac{\rho_{STD}}{\rho_R}} = V_{STD}\sqrt{\frac{P_{STD}}{P_R}} \qquad C.13$$

Substituting Equation C.13 into Equation C.10 gives

$$V_S = V_{STD}\sqrt{\frac{P_{STD}}{P_R}}\left[\frac{P_R T_S}{P_S T_R}\right] = V_{STD}\left[\frac{T_S}{T_R}\right]\frac{\sqrt{P_{STD}P_R}}{P_S} \qquad C.14$$

where

V_S = volumetric flowrate through the spouted bed

V_{STD} = volumetric flowrate taken from the calibration curve(s)

P_{STD} = 1 atm

P_R = absolute pressure of the rotameter

P_S = absolute pressure of the spouted bed

T_R = temperature of the rotameter(°K)

T_S = temperature of the spouted bed(°K)

The same calibration curves (i.e., Figures C.2 and C.3) could be used for different gases by making appropriate corrections, i.e., replacing ρ_{STD}/ρ_R in Equation C.12 by

$$\left[\frac{M_{STD}P_{STD}}{T_{STD}}\right] \Big/ \left[\frac{M_R P_R}{T_R}\right]$$

in which M_R and M_{STD} are molecular weights. Note that for the same gas at the same temperature, the above ratio would

be reduced to (P_{STD}/P_R).

C.3 CALIBRATION CURVE FOR $-\Delta P_s$ VERSUS $-\Delta P_a$

Data and the resulting curve are shown in Table C.1 and Figure C.5.

C.4 CALIBRATION FOR THE STATIC PRESSURE PROBE

The calibration data of pressure drop versus U_a were fitted to a second order polynomial, i.e.,

$$-\Delta P = d_1 U_a + d_2 U_a^2 \qquad \text{C.15}$$

with U_a in m/s and $-\Delta P$ in inches of butanol. The results are summarized in Table C.2.

Table C.1 Calibration data of $(-\Delta P_s)$ versus $(-\Delta P_a)$

$(-\Delta P_s)$ (cm of Hg)	$(-\Delta P_a)$ (cm of Hg)
0.64	0.49
1.24	1.10
2.22	2.08
3.17	3.06
3.97	3.90
4.96	4.91

Table C.2 Fitting parameters of Equation C.15
d_p = 1.25 mm, ρ_p = 2600 kg/m^3
and air at atmospheric pressure.

Run #	Temp (C)	d_1	d_2
5	20	0.99232	0.71996
6	170	1.05510	0.60319
7	300	1.05856	0.42582
8	420	1.08820	0.39660

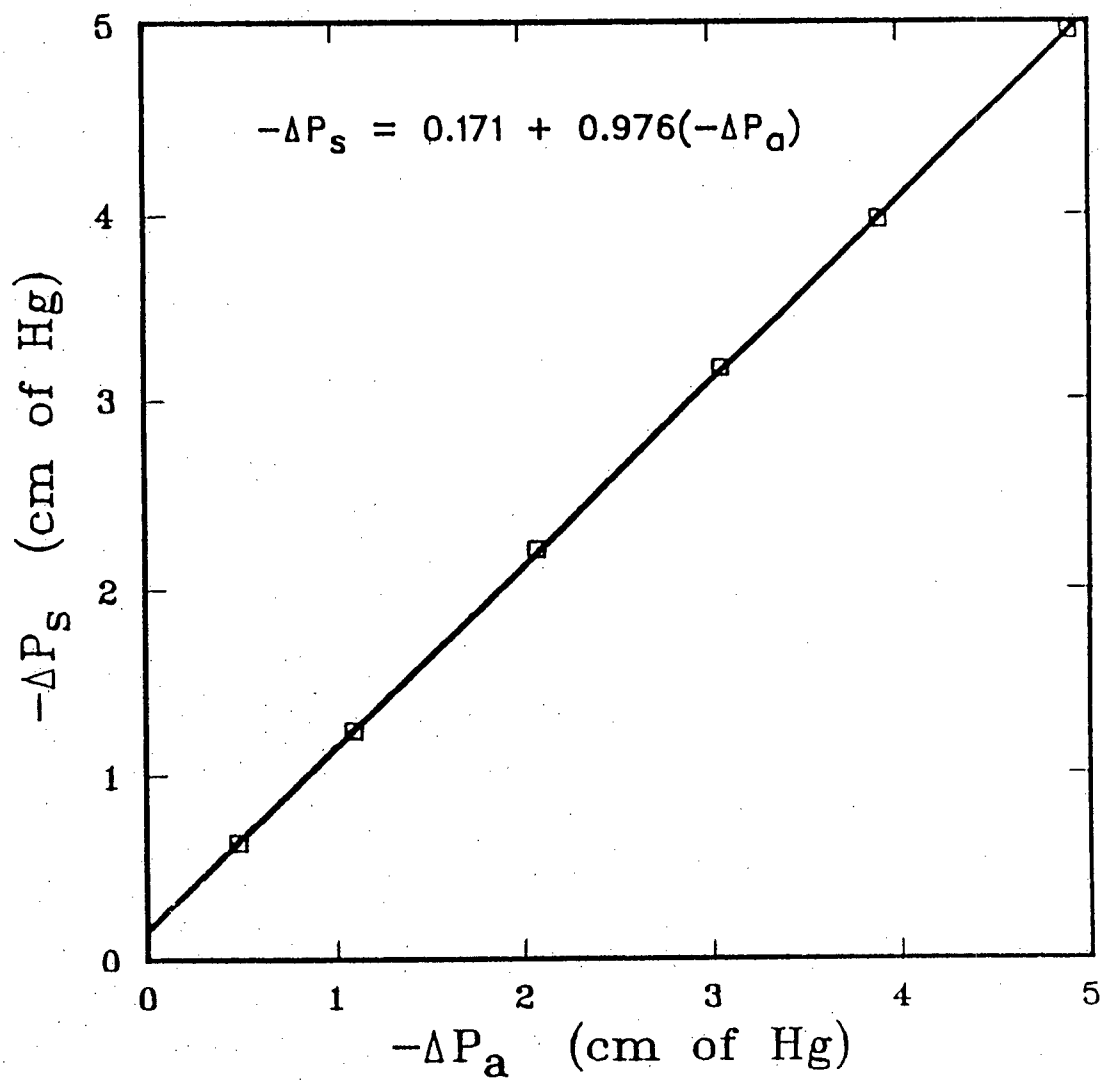

Figure C.5 $-\Delta P_s$ versus $-\Delta P_a$

APPENDIX D - EXPERIMENTAL CONDITIONS

Ottawa Sand, ρ_p = 2600 kg/m^3

Run #	Gas	Temp (°C)	d_p (mm)	D_i (mm)	H (m)	H/H_m	U/U_{ms}
1-1	AIR	20	0.945	19.05	1.168	1.000	1.000
1-1-a	AIR	20	0.945	19.05	1.168	1.000	1.075
1-2	AIR	20	0.945	19.05	1.168	0.761	1.000
1-2-a	AIR	20	0.945	19.05	1.168	0.761	1.095
1-3	AIR	20	0.945	19.05	1.168	0.495	1.000
1-3-a	AIR	20	0.945	19.05	1.168	0.495	1.124
2-1	AIR	170	0.945	19.05	0.419	1.000	1.000
2-1-a	AIR	170	0.945	19.05	0.419	1.000	1.101
2-2	AIR	170	0.945	19.05	0.419	0.697	1.000
2-2-a	AIR	170	0.945	19.05	0.419	0.697	1.104
2-3	AIR	170	0.945	19.05	0.419	0.484	1.000
2-3-a	AIR	170	0.945	19.05	0.419	0.484	1.099
5-1	AIR	20	1.250	19.05	1.067	1.000	1.000
5-1-a	AIR	20	1.250	19.05	1.067	1.000	1.085
5-2	AIR	20	1.250	19.05	1.067	0.753	1.000
5-2-a	AIR	20	1.250	19.05	1.067	0.753	1.121
5-3	AIR	20	1.250	19.05	1.067	0.485	1.000
5-3-a	AIR	20	1.250	19.05	1.067	0.485	1.110
6-1	AIR	170	1.250	19.05	0.648	1.000	1.000
6-1-a	AIR	170	1.250	19.05	0.648	1.000	1.089
6-2	AIR	170	1.250	19.05	0.648	0.696	1.000
6-2-a	AIR	170	1.250	19.05	0.648	0.696	1.114
6-3	AIR	170	1.250	19.05	0.648	0.451	1.000
6-3-a	AIR	170	1.250	19.05	0.648	0.451	1.100
7-1	AIR	300	1.250	19.05	0.546	1.000	1.000
7-1-a	AIR	300	1.250	19.05	0.546	1.000	1.105
7-2	AIR	300	1.250	19.05	0.546	0.756	1.000
7-2-a	AIR	300	1.250	19.05	0.546	0.756	1.113
7-3	AIR	300	1.250	19.05	0.546	0.510	1.000
7-3-a	AIR	300	1.250	19.05	0.546	0.510	1.106
8-1	AIR	420	1.250	19.05	0.413	1.000	1.000
8-1-a	AIR	420	1.250	19.05	0.413	1.000	1.101
8-2	AIR	420	1.250	19.05	0.413	0.646	1.000
8-2-a	AIR	420	1.250	19.05	0.413	0.646	1.105
8-3	AIR	420	1.250	19.05	0.413	0.499	1.000
8-3-a	AIR	420	1.250	19.05	0.413	0.499	1.100

CONTINUED

Run #	Gas	Temp (°C)	d_p (mm)	D_i (mm)	H (m)	H/H_m	U/U_{ms}
9-1	AIR	20	1.665	19.05	1.010	1.000	1.000
9-1-a	AIR	20	1.665	19.05	1.010	1.000	1.053
9-2	AIR	20	1.665	19.05	1.010	0.723	1.000
9-2-a	AIR	20	1.665	19.05	1.010	0.723	1.044
9-3	AIR	20	1.665	19.05	1.010	0.497	1.000
9-3-a	AIR	20	1.665	19.05	1.010	0.497	1.123
10-1	AIR	170	1.665	19.05	0.800	1.000	1.000
10-1-a	AIR	170	1.665	19.05	0.800	1.000	1.071
10-2	AIR	170	1.665	19.05	0.800	0.746	1.000
10-2-a	AIR	170	1.665	19.05	0.800	0.746	1.115
10-3	AIR	170	1.665	19.05	0.800	0.500	1.000
10-3-a	AIR	170	1.665	19.05	0.800	0.500	1.092
11-1	AIR	300	1.665	19.05	0.721	1.000	1.000
11-1-a	AIR	300	1.665	19.05	0.721	1.000	1.064
11-2	AIR	300	1.665	19.05	0.721	0.723	1.000
11-2-a	AIR	300	1.665	19.05	0.721	0.723	1.179
11-3	AIR	300	1.665	19.05	0.721	0.498	1.000
11-3-a	AIR	300	1.665	19.05	0.721	0.498	1.126
12-1	AIR	420	1.665	19.05	0.629	1.000	1.000
12-1-a	AIR	420	1.665	19.05	0.629	1.000	1.103
12-2	AIR	420	1.665	19.05	0.629	0.727	1.000
12-2-a	AIR	420	1.665	19.05	0.629	0.727	1.127
12-3	AIR	420	1.665	19.05	0.629	0.485	1.000
12-3-a	AIR	420	1.665	19.05	0.629	0.485	1.120
17-1	AIR	20	1.250	26.64	1.026	1.000	1.000
17-1-a	AIR	20	1.250	26.64	1.026	1.000	1.026
17-2	AIR	20	1.250	26.64	1.026	0.811	1.000
17-2-a	AIR	20	1.250	26.64	1.026	0.811	1.119
17-3	AIR	20	1.250	26.64	1.026	0.508	1.000
17-3-a	AIR	20	1.250	26.64	1.026	0.508	1.122
18-1	AIR	170	1.250	26.64	0.705	1.000	1.000
18-1-a	AIR	170	1.250	26.64	0.705	1.000	1.098
18-2	AIR	170	1.250	26.64	0.705	0.806	1.000
18-2-a	AIR	170	1.250	26.64	0.705	0.806	1.134
18-3	AIR	170	1.250	26.64	0.705	0.505	1.000
18-3-a	AIR	170	1.250	26.64	0.705	0.505	1.117

CONTINUED

Run #	Gas	Temp (°C)	d_p (mm)	D_i (mm)	H (m)	H/H_m	U/U_{ms}
19-1	AIR	300	1.250	26.64	0.419	1.000	1.000
19-1-a	AIR	300	1.250	26.64	0.419	1.000	1.093
19-2	AIR	300	1.250	26.64	0.419	0.773	1.000
19-2-a	AIR	300	1.250	26.64	0.419	0.773	1.090
19-3	AIR	300	1.250	26.64	0.419	0.523	1.000
19-3-a	AIR	300	1.250	26.64	0.419	0.523	1.106
20-1	AIR	420	1.250	26.64	0.343	1.000	1.000
20-1-a	AIR	420	1.250	26.64	0.343	1.000	1.027
20-2	AIR	420	1.250	26.64	0.343	0.703	1.000
20-2-a	AIR	420	1.250	26.64	0.343	0.703	1.106
20-3	AIR	420	1.250	26.64	0.343	0.490	1.000
20-3-a	AIR	420	1.250	26.64	0.343	0.490	1.114
21-1	AIR	20	1.665	26.64	0.978	1.000	1.000
21-1-a	AIR	20	1.665	26.64	0.978	1.000	1.011
21-2	AIR	20	1.665	26.64	0.978	0.850	1.000
21-2-a	AIR	20	1.665	26.64	0.978	0.850	1.109
21-3	AIR	20	1.665	26.64	0.978	0.572	1.000
21-3-a	AIR	20	1.665	26.64	0.978	0.572	1.148
22-1	AIR	170	1.665	26.64	0.838	1.000	1.000
22-1-a	AIR	170	1.665	26.64	0.838	1.000	1.050
22-2	AIR	170	1.665	26.64	0.838	0.746	1.000
22-2-a	AIR	170	1.665	26.64	0.838	0.746	1.123
22-3	AIR	170	1.665	26.64	0.838	0.504	1.000
22-3-a	AIR	170	1.665	26.64	0.838	0.504	1.131
23-1	AIR	300	1.665	26.64	0.679	1.000	1.000
23-1-a	AIR	300	1.665	26.64	0.679	1.000	1.080
23-2	AIR	300	1.665	26.64	0.679	0.748	1.000
23-2-a	AIR	300	1.665	26.64	0.679	0.748	1.113
23-3	AIR	300	1.665	26.64	0.679	0.505	1.000
23-3-a	AIR	300	1.665	26.64	0.679	0.505	1.124
24-1	AIR	420	1.665	26.64	0.540	1.000	1.000
24-1-a	AIR	420	1.665	26.64	0.540	1.000	1.124
24-2	AIR	420	1.665	26.64	0.540	0.752	1.000
24-2-a	AIR	420	1.665	26.64	0.540	0.752	1.124
24-3	AIR	420	1.665	26.64	0.540	0.470	1.000
24-3-a	AIR	420	1.665	26.64	0.540	0.470	1.112

CONTINUED

Run #	Gas	Temp (°C)	d_p (mm)	D_i (mm)	H (m)	H/H_m	U/U_{ms}
25-1	AIR	20	0.945	12.70	1.372	1.000	1.000
25-1-a	AIR	20	0.945	12.70	1.372	1.000	1.029
25-2	AIR	20	0.945	12.70	1.372	0.815	1.000
25-2-a	AIR	20	0.945	12.70	1.372	0.815	1.110
25-3	AIR	20	0.945	12.70	1.372	0.530	1.000
25-3-a	AIR	20	0.945	12.70	1.372	0.530	1.124
26-1	AIR	170	0.945	12.70	0.724	1.000	1.000
26-1-a	AIR	170	0.945	12.70	0.724	1.000	1.108
26-2	AIR	170	0.945	12.70	0.724	0.758	1.000
26-2-a	AIR	170	0.945	12.70	0.724	0.758	1.102
26-3	AIR	170	0.945	12.70	0.724	0.492	1.000
26-3-a	AIR	170	0.945	12.70	0.724	0.492	1.091
27-1	AIR	300	0.945	12.70	0.635	1.000	1.000
27-1-a	AIR	300	0.945	12.70	0.635	1.000	1.046
27-2	AIR	300	0.945	12.70	0.635	0.750	1.000
27-2-a	AIR	300	0.945	12.70	0.635	0.750	1.083
27-3	AIR	300	0.945	12.70	0.635	0.490	1.000
27-3-a	AIR	300	0.945	12.70	0.635	0.490	1.100
28-1	AIR	420	0.945	12.70	0.486	1.000	1.000
28-1-a	AIR	420	0.945	12.70	0.486	1.000	1.101
28-2	AIR	420	0.945	12.70	0.486	0.745	1.000
28-2-a	AIR	420	0.945	12.70	0.486	0.745	1.077
28-3	AIR	420	0.945	12.70	0.486	0.471	1.000
28-3-a	AIR	420	0.945	12.70	0.486	0.471	1.126
29-1	AIR	20	1.250	12.70	1.276	1.000	1.000
29-1-a	AIR	20	1.250	12.70	1.276	1.000	1.047
29-2	AIR	20	1.250	12.70	1.276	0.741	1.000
29-2-a	AIR	20	1.250	12.70	1.276	0.741	1.081
29-3	AIR	20	1.250	12.70	1.276	0.498	1.000
29-3-a	AIR	20	1.250	12.70	1.276	0.498	1.124
30-1	AIR	170	1.250	12.70	0.781	1.000	1.000
30-1-a	AIR	170	1.250	12.70	0.781	1.000	1.086
30-2	AIR	170	1.250	12.70	0.781	0.723	1.000
30-2-a	AIR	170	1.250	12.70	0.781	0.723	1.099
30-3	AIR	170	1.250	12.70	0.781	0.496	1.000
30-3-a	AIR	170	1.250	12.70	0.781	0.496	1.104

CONTINUED

Run #	Gas	Temp (°C)	d_p (mm)	D_i (mm)	H (m)	H/H_m	U/U_{ms}
31-1	AIR	300	1.250	12.70	0.654	1.000	1.000
31-1-a	AIR	300	1.250	12.70	0.654	1.000	1.105
31-2	AIR	300	1.250	12.70	0.654	0.757	1.000
31-2-a	AIR	300	1.250	12.70	0.654	0.757	1.096
31-3	AIR	300	1.250	12.70	0.654	0.476	1.000
31-3-a	AIR	300	1.250	12.70	0.654	0.476	1.103
32-1	AIR	420	1.250	12.70	0.533	1.000	1.000
32-1-a	AIR	420	1.250	12.70	0.533	1.000	1.095
32-2	AIR	420	1.250	12.70	0.533	0.750	1.000
32-2-a	AIR	420	1.250	12.70	0.533	0.750	1.103
32-3	AIR	420	1.250	12.70	0.533	0.435	1.000
32-3-a	AIR	420	1.250	12.70	0.533	0.435	1.104
33-1	AIR	20	1.665	12.70	1.029	1.000	1.000
33-1-a	AIR	20	1.665	12.70	1.029	1.000	1.045
33-2	AIR	20	1.665	12.70	1.029	0.741	1.000
33-2-a	AIR	20	1.665	12.70	1.029	0.741	1.108
33-3	AIR	20	1.665	12.70	1.029	0.518	1.000
33-3-a	AIR	20	1.665	12.70	1.029	0.518	1.110
34-1	AIR	170	1.665	12.70	0.832	1.000	1.000
34-1-a	AIR	170	1.665	12.70	0.832	1.000	1.052
34-2	AIR	170	1.665	12.70	0.832	0.744	1.000
34-2-a	AIR	170	1.665	12.70	0.832	0.744	1.088
34-3	AIR	170	1.665	12.70	0.832	0.488	1.000
34-3-a	AIR	170	1.665	12.70	0.832	0.488	1.093
35-1	AIR	300	1.665	12.70	0.743	1.000	1.000
35-1-a	AIR	300	1.665	12.70	0.743	1.000	1.071
35-2	AIR	300	1.665	12.70	0.743	0.730	1.000
35-2-a	AIR	300	1.665	12.70	0.743	0.730	1.117
35-3	AIR	300	1.665	12.70	0.743	0.491	1.000
35-3-a	AIR	300	1.665	12.70	0.743	0.491	1.104
36-1	AIR	420	1.665	12.70	0.654	1.000	1.000
36-1-a	AIR	420	1.665	12.70	0.654	1.000	1.086
36-2	AIR	420	1.665	12.70	0.654	0.743	1.000
36-2-a	AIR	420	1.665	12.70	0.654	0.743	1.108
36-3	AIR	420	1.665	12.70	0.654	0.476	1.000
36-3-a	AIR	420	1.665	12.70	0.654	0.476	1.108

CONTINUED

Run #	Gas	Temp (°C)	d_p (mm)	D_i (mm)	H (m)	H/H_m	U/U_{ms}
37-1	METHANE	20	1.250	19.05	1.380	1.000	1.000
37-1-a	METHANE	20	1.250	19.05	1.380	1.000	1.064
37-2	METHANE	20	1.250	19.05	1.380	0.773	1.000
37-2-a	METHANE	20	1.250	19.05	1.380	0.773	1.075
37-3	METHANE	20	1.250	19.05	1.380	0.511	1.000
37-3-a	METHANE	20	1.250	19.05	1.380	0.511	1.093
37-4	METHANE	20	1.250	19.05	1.380	0.184	1.000
37-4-a	METHANE	20	1.250	19.05	1.380	0.184	1.075
37-4-b	METHANE	20	1.250	19.05	1.380	0.184	1.117
37-4-c	METHANE	20	1.250	19.05	1.380	0.184	1.170
38-1	HELIUM	20	1.250	19.05	0.533	1.000	1.000
38-1-a	HELIUM	20	1.250	19.05	0.533	1.000	1.129
38-2	HELIUM	20	1.250	19.05	0.533	0.756	1.000
38-2-a	HELIUM	20	1.250	19.05	0.533	0.756	1.068
38-2-b	HELIUM	20	1.250	19.05	0.533	0.756	1.112
38-2-c	HELIUM	20	1.250	19.05	0.533	0.756	1.174
38-3	HELIUM	20	1.250	19.05	0.533	0.512	1.000
38-3-a	HELIUM	20	1.250	19.05	0.533	0.512	1.050
38-3-b	HELIUM	20	1.250	19.05	0.533	0.512	1.095
38-3-c	HELIUM	20	1.250	19.05	0.533	0.512	1.178

CONTINUED

Run #	Gas	Temp (°C)	d_p (mm)	D_i (mm)	H (m)	H/H_m	U/U_{ms}
5-4	AIR	20	1.250	19.05	1.073	1.000	1.000
5-5	AIR	20	1.250	19.05	1.073	0.941	1.000
5-6	AIR	20	1.250	19.05	1.073	0.758	1.000
5-6-a	AIR	20	1.250	19.05	1.073	0.758	1.075
5-6-b	AIR	20	1.250	19.05	1.073	0.758	1.128
5-6-c	AIR	20	1.250	19.05	1.073	0.758	1.190
5-7	AIR	20	1.250	19.05	1.073	0.556	1.000
5-8	AIR	20	1.250	19.05	1.073	0.414	1.000
5-9	AIR	20	1.250	19.05	1.073	0.260	1.000
5-9-a	AIR	20	1.250	19.05	1.073	0.260	1.058
5-9-b	AIR	20	1.250	19.05	1.073	0.260	1.118
5-9-c	AIR	20	1.250	19.05	1.073	0.260	1.179
6-4	AIR	170	1.665	19.05	0.648	1.000	1.000
6-5	AIR	170	1.250	19.05	0.648	0.716	1.000
6-5-a	AIR	170	1.250	19.05	0.648	0.716	1.079
6-5-b	AIR	170	1.250	19.05	0.648	0.716	1.162
6-5-c	AIR	170	1.250	19.05	0.648	0.716	1.208
6-6	AIR	170	1.250	19.05	0.648	0.412	1.000
6-6-a	AIR	170	1.250	19.05	0.648	0.412	1.039
6-6-b	AIR	170	1.250	19.05	0.648	0.412	1.122
6-6-c	AIR	170	1.250	19.05	0.648	0.412	1.180
7-4	AIR	300	1.250	19.05	0.546	1.000	1.000
7-5	AIR	300	1.250	19.05	0.546	0.756	1.000
7-5-a	AIR	300	1.250	19.05	0.546	0.756	1.055
7-5-b	AIR	300	1.250	19.05	0.546	0.756	1.112
7-5-c	AIR	300	1.250	19.05	0.546	0.756	1.160
7-6	AIR	300	1.250	19.05	0.546	0.570	1.000
7-7	AIR	300	1.250	19.05	0.546	0.489	1.000
7-7-a	AIR	300	1.250	19.05	0.546	0.489	1.049
7-7-b	AIR	300	1.250	19.05	0.546	0.489	1.111
7-7-c	AIR	300	1.250	19.05	0.546	0.489	1.162
8-4	AIR	420	1.250	19.05	0.413	1.000	1.000
8-5	AIR	420	1.250	19.05	0.413	0.654	1.000
8-5-a	AIR	420	1.250	19.05	0.413	0.654	1.041
8-5-b	AIR	420	1.250	19.05	0.413	0.654	1.094
8-5-c	AIR	420	1.250	19.05	0.413	0.654	1.191

APPENDIX E - VARIATIONS OF SPOUT DIAMETERS WITH BED LEVEL

Run # 1-1-a

z(cm)	Ds(cm)
0	1.9
5	3.2
10	3.6
15	3.0
20	3.0
30	2.9
40	2.9
50	2.9
60	2.9
70	3.1
80	3.1
90	3.2
100	3.5
110	3.7
121	4.0

Run # 1-2-a

z(cm)	Ds(cm)
0	1.9
5	2.9
10	3.5
15	3.2
20	3.0
30	2.7
40	2.7
50	2.7
60	2.7
70	2.8
80	2.9
91	3.6

Run # 1-3-a

z(cm)	Ds(cm)
0	1.9
5	2.7
10	3.2
15	3.0
20	2.8
30	2.7
40	2.7
50	2.9
60	3.3

Run # 2-1-a

z(cm)	Ds(cm)
0	1.9
5	2.6
10	3.0
15	2.8
20	2.9
30	3.1
40	3.3
43	3.9

Run # 2-2-a

z(cm)	Ds(cm)
0	1.9
5	2.5
10	2.8
15	2.6
20	2.4
25	2.4
30	2.5

Run # 2-3-a

z(cm)	Ds(cm)
0	1.9
2.5	2.4
5	2.7
7.5	2.9
10	2.7
12.5	2.6
15	2.4
17.5	2.1
20	2.1
22	2.3

Run # 5-1-a

z(cm)	Ds(cm)
0	1.9
5	3.1
10	3.4
15	3.2
20	3.0
30	3.0
40	3.0
50	3.1
60	3.3
70	3.5
80	3.7
90	3.9
100	4.1
108	4.5

Run # 5-2-a

z(cm)	Ds(cm)
0	1.9
5	3.0
10	3.4
15	3.0
20	3.1
30	3.0
40	3.0
50	3.0
60	3.1
70	3.2
80	3.3
82	3.6

Run # 5-3-a

z(cm)	Ds(cm)
0	1.9
5	2.9
10	3.3
15	3.1
20	2.8
30	2.8
40	2.9
50	3.2
52	3.4

Run # 6-1-a

z(cm)	Ds(cm)
0	1.9
5	3.0
10	3.4
15	3.2
20	3.0
30	3.0
40	3.0
50	3.0
60	3.3
66	4.2

Run # 6-2-a

z(cm)	Ds(cm)
0	1.9
5	3.0
10	3.4
15	3.2
20	2.7
30	2.7
40	3.1
49	3.8

Run # 6-3-a

z(cm)	Ds(cm)
0	1.9
5	2.8
10	3.3
15	3.0
20	2.7
25	2.7
30	2.8

Run # 7-1-a

z(cm)	Ds(cm)
0	1.9
5	2.8
10	3.3
15	3.0
20	2.8
30	2.8
40	2.9
50	3.3
55	3.7

Run # 7-2-a

z(cm)	Ds(cm)
0	1.9
5	2.8
10	3.2
15	2.8
20	2.8
30	2.8
40	2.8
44	3.2

Run # 7-3-a

z(cm)	Ds(cm)
0	1.9
5	2.8
10	3.2
15	2.8
20	2.8
25	2.7
29.5	2.9

Run # 8-1-a

z(cm)	Ds(cm)
0	1.9
5	2.8
10	3.3
15	2.8
20	2.8
25	2.8
30	2.8
35	2.8
40	2.9
42	3.3

Run # 8-2-a

z(cm)	Ds(cm)
0	1.9
5	2.7
10	3.2
15	2.8
20	2.8
25	2.8
29	2.8

Run # 8-3-a

z(cm)	Ds(cm)
0	1.9
5	2.6
10	3.1
15	2.5
20	2.5
22	2.5

Run # 9-1-a

z(cm)	Ds(cm)
0	1.9
5	3.3
10	3.9
15	3.7
20	3.3
30	3.4
40	3.5
50	3.5
60	3.6
70	3.7
80	3.8
90	4.0
110	4.2
115	4.2

Run # 9-2-a

z(cm)	Ds(cm)
0	1.9
5	3.3
10	3.8
15	3.2
20	3.2
30	3.3
40	3.4
50	3.5
60	3.6
72	4.2

Run # 9-3-a

z(cm)	Ds(cm)
0	1.9
5	3.3
10	3.8
15	3.5
20	3.2
30	3.2
40	3.2
45	3.2
51	3.8

Run # 10-1-a

z(cm)	Ds(cm)
0	1.9
5	3.3
10	3.8
15	3.6
20	3.4
30	3.3
40	3.3
50	3.3
60	3.6
70	3.8
80	4.0
83	4.3

Run # 10-2-a

z(cm)	Ds(cm)
0	1.9
5	3.2
10	3.8
15	3.4
20	3.2
30	3.2
40	3.2
50	3.3
62	3.7

Run # 10-3-a

z(cm)	Ds(cm)
0	1.9
5	3.0
10	3.7
15	3.3
20	3.2
30	3.2
41	3.5

Run # 11-1-a

z(cm)	Ds(cm)
0	1.9
5	3.3
10	3.8
15	3.5
20	3.3
30	3.3
40	3.3
50	3.4
60	3.5
76	4.1

Run # 11-2-a

z(cm)	Ds(cm)
0	1.9
5	3.2
10	3.8
15	3.4
20	3.2
30	3.2
40	3.2
50	3.3
55	3.8

Run # 11-3-a

z(cm)	Ds(cm)
0	1.9
5	3.1
10	3.5
15	3.1
20	3.0
30	3.0
35	3.2

Run # 12-1-a

z(cm)	Ds(cm)
0	1.9
5	3.0
10	3.5
15	3.3
20	3.2
30	3.3
40	3.6
50	3.8
67	4.2

Run # 12-2-a

z(cm)	Ds(cm)
0	1.9
5	3.0
10	3.4
15	3.3
20	3.2
30	3.2
40	3.4
47	3.7

Run # 12-3-a

z(cm)	Ds(cm)
0	1.9
5	3.0
10	3.2
15	3.0
20	2.9
25	2.9
31	3.2

Run # 17-1-a

z(cm)	Ds(cm)
0	2.7
5	3.4
10	3.8
15	3.6
20	3.2
30	3.1
40	3.2
50	3.2
60	3.2
70	3.2
80	3.4
90	3.6
100	3.8
110	4.2
115	4.6

Run # 17-2-a

z(cm)	Ds(cm)
0	2.7
5	3.4
10	3.8
15	3.5
20	3.1
30	3.1
40	3.1
50	3.1
60	3.2
70	3.3
80	3.5
87	3.8

Run # 17-3-a

z(cm)	Ds(cm)
0	2.7
5	3.3
10	3.4
15	3.2
20	2.8
30	2.8
40	3.0
50	3.2
53.5	3.4

Run # 18-1-a

z(cm)	Ds(cm)
0	2.7
5	3.4
10	3.7
15	3.4
20	2.9
30	3.0
40	3.1
50	3.1
60	3.3
70	4.2
75	4.6

Run # 18-2-a

z(cm)	Ds(cm)
0	2.7
5	3.2
10	3.6
15	3.4
20	2.8
30	2.8
40	2.9
50	3.4
58	4.3

Run # 18-3-a

z(cm)	Ds(cm)
0	2.7
5	3.0
10	3.4
15	3.0
20	2.4
25	2.6
30	3.1
40	3.7

Run # 19-1-a

z(cm)	Ds(cm)
0	2.7
5	3.0
10	3.4
15	3.1
20	2.8
30	2.9
40	3.2
43	3.7

Run # 19-2-a

z(cm)	Ds(cm)
0	2.7
5	3.0
10	3.2
15	3.0
20	2.6
25	2.7
30	3.2
32.5	3.4

Run # 19-3-a

z(cm)	Ds(cm)
0	2.7
2.5	2.8
5	3.0
7.5	3.1
10	3.2
12.5	2.8
15	2.7
17.5	2.6
20	2.5
22	2.6

Run # 20-1-a

z(cm)	Ds(cm)
0	2.7
5	2.9
10	3.3
15	2.9
20	2.7
25	2.7
30	2.7
35.5	3.3

Run # 20-2-a

z(cm)	Ds(cm)
0	2.7
2.5	2.7
5	2.8
7.5	3.0
10	3.2
12.5	3.0
15	2.8
17.5	2.6
20	2.6
22.5	2.6
25	2.9

Run # 20-3-a

z(cm)	Ds(cm)
0	2.7
2.5	2.7
5	2.8
7.5	3.1
10	2.6
12.5	2.6
15	2.6
18	2.9

Run # 21-1-a

z(cm)	Ds(cm)
0	2.7
5	3.7
10	3.9
15	3.7
20	3.4
30	3.5
40	3.6
50	3.6
60	3.9
70	3.9
80	4.0
90	4.0
100	4.1
110	4.4
117	4.7

Run # 21-2-a

z(cm)	Ds(cm)
0	2.7
5	3.5
10	3.8
15	3.6
20	3.3
30	3.4
40	3.4
50	3.7
60	3.8
70	4.0
80	4.3
88	4.5

Run # 21-3-a

z(cm)	Ds(cm)
0	2.7
5	3.4
10	3.7
15	3.5
20	3.2
30	3.3
40	3.4
50	3.6
57	3.8

Run # 22-1-a

z(cm)	Ds(cm)
0	2.7
5	3.4
10	3.8
15	3.6
20	3.4
30	3.4
40	3.4
50	3.5
60	3.5
70	3.5
80	3.7
92	4.2

Run # 22-2-a

z(cm)	Ds(cm)
0	2.7
5	3.4
10	3.8
15	3.6
20	3.3
30	3.3
40	3.3
50	3.4
60	3.5
65	3.7

Run # 22-3-a

z(cm)	Ds(cm)
0	2.7
5	3.2
10	3.7
15	3.5
20	3.2
30	3.3
40	3.3
43.5	3.6

Run # 23-1-a

z(cm)	Ds(cm)
0	2.7
5	3.4
10	3.8
15	3.6
20	3.3
30	3.4
40	3.4
50	3.4
60	3.6
74	4.0

Run # 23-2-a

z(cm)	Ds(cm)
0	2.7
5	3.3
10	3.8
15	3.5
20	3.1
30	3.2
40	3.1
50	3.5
53	3.9

Run # 23-3-a

z(cm)	Ds(cm)
0	2.7
5	3.1
10	3.5
15	3.3
20	3.2
25	3.2
30	3.2
35	3.7

Run # 24-1-a

z(cm)	Ds(cm)
0	2.7
5	3.2
10	3.6
15	3.4
20	3.3
30	3.4
40	3.5
50	3.6
58	4.1

Run # 24-2-a

z(cm)	Ds(cm)
0	2.7
5	3.1
10	3.6
15	3.4
20	3.2
25	3.3
30	3.4
35	3.6
40	3.8
42	4.0

Run # 24-3-a

z(cm)	Ds(cm)
0	2.7
5	3.0
10	3.4
12.5	3.3
15	3.2
17.5	2.8
20	2.9
23	2.9
26	3.4

Run # 25-1-a

z(cm)	Ds(cm)
0	1.3
5	3.0
10	3.2
20	3.1
30	2.7
40	2.7
50	2.7
60	2.8
70	2.8
80	2.8
90	2.9
100	3.0
110	3.1
120	3.2
130	3.3
140	3.5
150	3.7
155	4.1

Run # 25-2-a

z(cm)	Ds(cm)
0	1.3
5	2.6
10	3.1
20	2.9
30	2.8
40	2.7
50	2.7
60	2.7
70	2.7
80	2.8
90	2.9
100	3.1
110	3.2
116	3.8

Run # 25-3-a

z(cm)	Ds(cm)
0	1.3
5	2.6
10	2.9
20	2.6
30	2.6
40	2.6
50	2.6
60	2.6
70	2.7
74	3.3

Run # 26-1-a

z(cm)	Ds(cm)
0	1.3
5	2.5
10	2.7
20	2.4
30	2.5
40	2.6
50	2.6
60	2.6
70	3.2
74.5	3.6

Run # 26-2-a

z(cm)	Ds(cm)
0	1.3
5	2.5
10	2.6
15	2.4
20	2.4
30	2.4
40	2.4
50	2.4
55.5	2.4

Run # 26-3-a

z(cm)	Ds(cm)
0	1.3
5	2.4
10	2.4
15	2.3
20	2.3
25	2.3
30	2.3
35	2.3

Run # 27-1-a

z(cm)	Ds(cm)
0	1.3
5	2.4
10	2.6
15	2.4
20	2.3
30	2.4
40	2.5
50	2.5
60	2.7
65	3.3

Run # 27-2-a

z(cm)	Ds(cm)
0	1.3
5	2.4
10	2.5
15	2.3
20	2.2
25	2.2
30	2.2
35	2.3
40	2.3
49	2.4

Run # 27-3-a

z(cm)	Ds(cm)
0	1.3
5	2.1
10	2.3
15	2.0
20	2.0
25	2.0
30	2.0
31.5	2.1

Run # 28-1-a

z(cm)	Ds(cm)
0	1.3
5	2.3
10	2.5
15	2.3
20	2.2
25	2.3
30	2.3
35	2.3
40	2.3
45	3.1
50.5	3.8

Run # 28-2-a

z(cm)	Ds(cm)
0	1.3
5	2.2
10	2.4
15	2.0
20	2.0
25	2.0
30	2.0
37	2.0

Run # 28-3-a

z(cm)	Ds(cm)
0	1.3
2.5	1.6
5	2.2
7.5	2.4
10	2.1
12.5	1.9
15	1.8
20	1.9
23.5	1.9

Run # 29-1-a

z(cm)	Ds(cm)
0	1.3
5	3.0
10	3.4
20	2.9
30	3.0
40	3.0
50	3.1
60	3.1
70	3.1
80	3.2
90	3.3
100	3.5
110	3.7
120	3.9
134	4.1

Run # 29-2-a

z(cm)	Ds(cm)
0	1.3
5	2.6
10	3.2
15	3.0
20	2.9
30	2.9
40	2.9
50	2.9
60	3.0
70	3.2
80	3.4
90	3.6
99	3.9

Run # 29-3-a

z(cm)	Ds(cm)
0	1.3
5	2.6
10	3.2
15	3.0
20	2.8
30	2.8
40	2.8
50	2.9
60	3.0
65	3.2

Run # 30-1-a

z(cm)	Ds(cm)
0	1.3
5	2.7
10	3.4
15	3.1
20	2.6
30	2.7
40	2.8
50	2.8
60	2.9
70	3.3
80	3.8
82	4.0

Run # 30-2-a

z(cm)	Ds(cm)
0	1.3
5	2.6
10	3.2
15	2.9
20	2.6
30	2.6
40	2.6
50	2.9
59	3.4

Run # 30-3-a

z(cm)	Ds(cm)
0	1.3
5	2.6
10	3.2
15	2.8
20	2.5
25	2.5
30	2.5
35	2.8
40	3.1

Run # 31-1-a

z(cm)	Ds(cm)
0	1.3
5	2.6
10	3.3
15	3.1
20	2.7
30	2.7
40	2.7
50	2.9
60	3.3
69	3.7

Run # 31-2-a

z(cm)	Ds(cm)
0	1.3
5	2.6
10	3.2
15	2.8
20	2.6
25	2.6
30	2.6
40	2.7
51	2.8

Run # 31-3-a

z(cm)	Ds(cm)
0	1.3
5	2.6
10	3.1
15	2.7
20	2.5
25	2.5
30	2.5
31	2.5

Run # 32-1-a

z(cm)	Ds(cm)
0	1.3
5	2.6
10	3.3
15	2.8
20	2.7
30	2.7
40	2.8
50	3.0
55	3.4

Run # 32-2-a

z(cm)	Ds(cm)
0	1.3
5	2.6
10	3.2
15	2.7
20	2.5
25	2.5
30	2.5
35	2.5
40.5	2.6

Run # 32-3-a

z(cm)	Ds(cm)
0	1.3
5	2.6
10	3.1
15	2.5
20	2.4
23	2.4

Run # 33-1-a

z(cm)	Ds(cm)
0	1.3
5	3.8
10	4.0
15	3.7
20	3.2
30	3.2
40	3.3
50	3.3
60	3.3
70	3.5
80	3.7
90	3.9
100	4.1
110	4.3

Run # 33-2-a

z(cm)	Ds(cm)
0	1.3
5	3.6
10	4.0
15	3.6
20	3.2
30	3.0
40	3.0
50	3.1
60	3.3
70	3.5
80	4.0

Run # 33-3-a

z(cm)	Ds(cm)
0	1.3
5	3.4
10	3.9
15	3.3
20	2.9
30	2.9
40	3.0
50	3.3
53	3.8

Run # 34-1-a

z(cm)	Ds(cm)
0	1.3
5	3.7
10	4.0
15	3.7
20	3.2
30	3.2
40	3.2
50	3.2
60	3.3
70	3.5
80	3.8
91	4.2

Run # 34-2-a

z(cm)	Ds(cm)
0	1.3
5	3.7
10	4.0
15	3.4
20	3.1
30	2.8
40	3.0
50	3.3
60	3.7
66	4.0

Run # 34-3-a

z(cm)	Ds(cm)
0	1.3
5	3.4
10	3.9
15	3.4
20	2.7
25	2.7
30	2.7
35	3.1
41	3.8

Run # 35-1-a

z(cm)	Ds(cm)
0	1.3
5	3.6
10	3.8
15	3.7
20	3.4
30	3.2
40	3.2
50	3.2
60	3.4
70	3.6
77	4.0

Run # 35-2-a

z(cm)	Ds(cm)
0	1.3
5	3.1
10	3.5
15	3.2
20	3.2
30	3.2
40	3.3
50	3.4
58	3.7

Run # 35-3-a

z(cm)	Ds(cm)
0	1.3
5	3.2
10	3.4
15	2.8
20	2.8
25	2.8
30	2.8
37	2.8

Run # 36-1-a

z(cm)	Ds(cm)
0	1.3
5	3.1
10	3.7
15	3.2
20	3.2
30	3.2
40	3.3
50	3.4
60	3.5
68	3.9

Run # 36-2-a

z(cm)	Ds(cm)
0	1.3
5	3.1
10	3.5
15	3.2
20	3.2
30	3.2
40	3.2
45	3.4
50	3.8

Run # 36-3-a

z(cm)	Ds(cm)
0	1.3
5	3.0
10	3.2
15	3.0
20	2.7
25	2.8
31	3.0

Run # 37-1-a

z(cm)	Ds(cm)
0	1.9
10	3.8
20	3.3
30	3.2
40	3.2
50	3.2
80	3.4
100	4.0
120	4.2
140	4.6

Run # 37-2-a

z(cm)	Ds(cm)
0	1.9
10	3.5
20	3.2
30	3.1
50	3.2
60	3.1
90	3.6
110	4.5

Run # 37-3-a

z(cm)	Ds(cm)
0	1.9
10	3.5
20	2.9
30	2.9
40	3.0
50	3.0
60	3.3
65	3.5
71	4.0

Run # 37-4-a

z(cm)	Ds(cm)
0	1.9
5	2.9
10	2.7
15	2.4
20	2.3
28.5	2.2

Run # 37-4-b

z(cm)	Ds(cm)
0	1.9
5	2.9
10	2.7
15	2.5
20	2.4
28.5	2.3

Run # 37-4-c

z(cm)	Ds(cm)
0	1.9
5	3.0
10	2.8
15	2.6
20	2.5
28.5	2.4

Run # 38-1-a

z(cm)	Ds(cm)
0	1.9
5	3.2
10	2.8
15	2.6
20	2.6
30	2.6
40	2.6
50	2.9
54.5	3.2

Run # 38-2-a

z(cm)	Ds(cm)
0	1.9
5	2.9
10	2.7
15	2.5
20	2.5
30	2.5
41	2.7

Run # 38-2-b

z(cm)	Ds(cm)
0	1.9
5	2.9
10	2.7
15	2.5
20	2.5
30	2.6
41	2.8

Run # 38-2-c

z(cm)	Ds(cm)
0	1.9
5	2.9
10	2.7
15	2.6
20	2.6
30	2.6
41	2.9

Run # 38-3-a

z(cm)	Ds(cm)
0	1.9
5	2.8
10	2.6
15	2.3
20	2.3
28.5	2.3

Run # 38-3-b

z(cm)	Ds(cm)
0	1.9
5	2.9
10	2.9
15	2.5
20	2.4
28.5	2.4

Run # 38-3-c

z(cm)	Ds(cm)
0	1.9
5	2.9
10	2.9
15	2.5
20	2.5
28.5	2.5

Run # 5-6-a

z(cm)	Ds(cm)
0	1.9
5	3.0
10	3.3
15	2.8
20	2.9
30	2.9
40	2.9
50	3.0
60	3.0
70	3.1
80	3.3
81.5	3.5

Run # 5-6-b

z(cm)	Ds(cm)
0	1.9
5	3.0
10	3.5
15	3.1
20	3.1
30	3.0
40	3.0
50	3.0
60	3.1
70	3.3
80	3.5
81.5	3.8

Run # 5-6-c

z(cm)	Ds(cm)
0	1.9
5	3.0
10	3.5
15	3.2
20	3.1
30	3.0
40	3.0
50	3.0
60	3.1
70	3.3
80	3.7
81.5	3.9

Run # 5-9-a

z(cm)	Ds(cm)
0	1.9
5	2.7
10	3.5
15	3.1
20	2.7
25	2.7
28.5	2.9

Run # 5-9-b

z(cm)	Ds(cm)
0	1.9
5	2.8
10	3.5
15	3.1
20	2.8
25	2.8
28.5	2.9

Run # 5-9-c

z(cm)	Ds(cm)
0	1.9
5	2.9
10	3.6
15	3.1
20	2.9
25	2.9
28.5	3.0

Run # 6-5-a

z(cm)	Ds(cm)
0	1.9
5	3.0
10	3.5
15	3.2
20	2.6
30	2.6
40	3.2
48	3.6

Run # 6-5-b

z(cm)	Ds(cm)
0	1.9
5	3.0
10	3.5
15	3.2
20	2.7
30	2.7
40	3.3
48	3.8

Run # 6-5-c

z(cm)	Ds(cm)
0	1.9
5	3.1
10	3.6
15	3.2
20	2.8
30	2.8
40	3.5
48	4.1

Run # 6-6-a

z(cm)	Ds(cm)
0	1.9
5	2.8
10	3.2
15	2.8
20	2.7
25	2.7
28.5	2.7

Run # 6-6-b

z(cm)	Ds(cm)
0	1.9
5	2.8
10	3.3
15	2.9
20	2.7
25	2.8
28.5	2.8

Run # 6-6-c

z(cm)	Ds(cm)
0	1.9
5	2.8
10	3.4
15	3.0
20	2.8
25	2.8
28.5	2.8

Run # 7-5-a

z(cm)	Ds(cm)
0	1.9
5	2.8
10	3.2
15	2.7
20	2.7
25	2.7
30	2.9
35	2.9
43	3.2

Run # 7-5-b

z(cm)	Ds(cm)
0	1.9
5	2.8
10	3.2
15	2.8
20	2.8
25	2.8
30	2.9
35	2.9
43	3.3

Run # 7-5-c

z(cm)	Ds(cm)
0	1.9
5	2.8
10	3.2
15	3.1
20	2.9
25	2.9
30	3.0
35	3.0
43	3.5

Run # 7-7-a

z(cm)	Ds(cm)
0	1.9
5	2.7
10	3.3
15	2.7
20	2.7
25	2.7
28.5	2.7

Run # 7-7-b

z(cm)	Ds(cm)
0	1.9
5	2.8
10	3.3
15	2.7
20	2.7
25	2.8
28.5	2.9

Run # 7-7-c

z(cm)	Ds(cm)
0	1.9
5	2.8
10	3.4
15	2.7
20	2.7
25	2.9
28.5	3.1

Run # 8-5-a

z(cm)	Ds(cm)
0	1.9
5	2.5
10	3.3
15	2.7
20	2.7
25	2.7
28.5	2.7

Run # 8-5-b

z(cm)	Ds(cm)
0	1.9
5	2.6
10	3.4
15	2.8
20	2.8
25	2.8
28.5	2.8

Run # 8-5-c

z(cm)	Ds(cm)
0	1.9
5	2.7
10	3.5
15	2.9
20	2.9
25	2.9
28.5	3.0